VOLUME 112 NUMBER 2

THE ASTROPHYSICAL JOURNAL

AN INTERNATIONAL REVIEW OF SPECTROSCOPY AND ASTRONOMICAL PHYSICS

SEPTEMBER 1950

THE UNIVERSITY OF CHICAGO PRESS
CHICAGO, ILLINOIS, U.S.A.

September 1950 Vol. 112, No. 2

THE ASTROPHYSICAL JOURNAL

AN INTERNATIONAL REVIEW OF SPECTROSCOPY AND ASTRONOMICAL PHYSICS

The Astrophysical Journal is published bimonthly by the University of Chicago at the University of Chicago Press, 5750 Ellis Avenue, Chicago 37, Illinois, during July, September, November, January, March, and May. ¶Two volumes are published per year, one beginning with the January issue and the other beginning with the July issue. The subscription price is $6.00 per volume or $12.00 per year; the price of single copies is $3.00. (Orders for service of less than a volume will be charged at the single copy rate.) ¶Postage is prepaid by the publishers on all orders from the United States and its possessions. No extra charge is made for postage to countries in the Pan American Postal Union. ¶Postage is charged extra as follows: for Canada, 20 cents per volume, 40 cents per year (total $6.20 per volume, $12.40 per year); on single copies 5 cents (total $3.05); for all other countries in the Postal Union, 50 cents per volume, $1.00 per year (total $6.50 per volume, $13.00 per year), on single copies 10 cents (total $3.10). ¶Subscriptions are payable in advance. Please make all remittances payable to The University of Chicago Press, in United States currency or its equivalent by postal or express money orders or bank drafts.

The following is an authorized agent:

For the British Empire, except North America and Australasia: The Cambridge University Press, Bentley House, 200 Euston Road, London, N.W. 1, England. Prices of yearly subscriptions and of single copies may be had on application.

Claims for missing numbers should be made within the month following the regular month of publication. The publishers expect to supply missing numbers free only when losses have been sustained in transit, and when the reserve stock will permit.

Business correspondence should be addressed to The University of Chicago Press, Chicago 37, Illinois.

Communications for the editors and manuscripts should be addressed to: W. W. Morgan, Editor of The Astrophysical Journal, Yerkes Observatory, Williams Bay, Wisconsin.

Line drawings and photographs should be made by the author, and all marginal notes such as co-ordinates, wave lengths, etc., should be included in the cuts. It will not be possible to set up such material in type.

One copy of the corrected galley proof should be returned as soon as possible to the editor, Yerkes Observatory, Williams Bay, Wisconsin. Authors should take notice that the manuscript will not be sent to them with the proof.

The cable address is "Observatory, Williamsbay, Wisconsin."

The articles in this journal are indexed in the *International Index to Periodicals*, New York, N.Y.

Applications for permission to quote from this journal should be addressed to The University of Chicago Press, and will be freely granted.

Microfilms of complete journal volumes are available to regular subscribers only and may be obtained at the end of the year. Orders and inquiries should be addressed to University Microfilms, 313 North First Street, Ann Arbor, Michigan.

Notice to subscribers: If you change your address, please notify us and your local postmaster immediately. The Post-Office does not forward second-class mail.

Entered as second-class matter, July 31, 1930, at the Post-Office at Chicago, Ill., under the Act of March 3, 1879.
Acceptance for mailing at special rate of postage provided for in United States Postal Act of October 3, 1917, Section 1103, amended February 28, 1925.

[PRINTED IN U.S.A.]

THE ASTROPHYSICAL JOURNAL

AN INTERNATIONAL REVIEW OF SPECTROSCOPY AND ASTRONOMICAL PHYSICS

VOLUME 112 SEPTEMBER 1950 NUMBER 2

ON THE DETERMINATION OF THE CONVERGENT POINT OF A MOVING CLUSTER FROM PROPER MOTIONS

ARCHIBALD BROWN*
Yerkes Observatory
Received July 1, 1950

ABSTRACT

The paper discusses several methods which have been used to determine the convergent point of a moving cluster from the proper motion of the stars which are members of the cluster. These methods represent, in the main, different ways of utilizing the position angle, θ, as observed for each star, and it is desirable to see if they would be affected by the form of the frequency distribution expected for θ. With reasonable assumptions as to the distribution of the errors of the observed quantities, namely, the components of proper motion, it is possible to derive the frequency distribution of θ, and this suggests an alternative method of solution which would appear to have some advantages over the existing methods.

As an illustration of the method, its application to the nucleus stars of the Ursa Major cluster is considered. Because of a geometrical peculiarity of this particular case, the *directions* of the proper motions are insufficient in themselves to define the convergent point accurately; they define a curve on which the convergent point should lie, but additional information is required to fix the position of the convergent point on this curve with any precision. Using the *amount* of the proper motion in right ascension for each star helps to locate the position of the convergent point on the curve and leads to a solution which gives good agreement with the radial-velocity observations. However, it is emphasized that there is still an appreciable uncertainty associated with the determination.

I

Ten years ago the problem of determining the convergent point of a moving cluster from the proper motions of the members of the cluster appeared to have been settled satisfactorily. Charlier and Bohlin had each derived an equation of condition which was applicable to any star in the cluster, and by combining these equations the position of the convergent point on the celestial sphere could be derived.[1] Basically, the equations of condition were equivalent, so there was nothing to choose between the two methods. The first hint of trouble came in 1945, when Seares[2] pointed out that Charlier's method would lead to an incorrect solution and showed that the effect was appreciable for the Taurus cluster. Charlier had derived a linear equation of condition in order that the equations from different stars could be combined by the method of least squares. Unfortunately, all the coefficients of the unknowns in his equation of condition involved quantities subject

* Commonwealth Fund Fellow.

[1] Details of these methods are given by W. M. Smart, *Stellar Dynamics* (Cambridge: At the University Press, 1938), pp. 284–286.

[2] *Ap. J.*, **102**, 366, 1945; *Mt. W. Contr.*, No. 716.

to appreciable errors of observation, and this introduces a systematic error in the solution. (As might be expected from the equivalence of the two methods, this objection applies to the Bohlin method also.)

Later, Petrie[3] and Miss Roman[4] independently turned to the method of "differential corrections" in working on the Ursa Major cluster. In this method an approximate position of the convergent point is assumed, and a linear equation is derived for the corrections required to get from the assumed position to the true position. One could proceed by successive approximations in this way; in practice, both authors were satisfied that, after applying the method once, the data did not warrant further approximations. In one respect, Miss Roman's equation is preferable to Petrie's, in that the effect of errors in the observed quantities enters into only one coefficient in her equation. Thus it is free from the criticism which Seares had made against the Charlier and Bohlin methods. However, there are other objections which can be raised against the method of differential corrections in this application, and these will be mentioned below (Sec. III).

Section II gives the basic formulae required in the investigation, together with some remarks on matters arising from the Charlier method of solution. Section III discusses the method of differential corrections. Section IV starts with some general considerations. By a suitable change in the co-ordinate system, it is possible to isolate two elements of the problem more completely, namely, finding the direction of the convergent point from the cluster and finding the distance of the convergent point from the cluster. A possible method of attack is to derive the frequency distribution of the position angle, θ, for the proper motion of any star and then apply the method of maximum likelihood to find the convergent point. In this way one can take the form of the distribution of θ into account and so provide a sounder theoretical basis for the solution. The discussion brings out the relation of the existing methods to the maximum-likelihood solution, since they bear a close resemblance to a limiting case of the latter method.

Finally, the application of the maximum-likelihood solution to the Ursa Major cluster is considered in Section V.

II

Following the notation used by Smart,[1] let the space motion of the cluster relative to the sun be V km/sec and the convergent point be in the direction (A, D), using equatorial co-ordinates. Then the components of the space velocity of each star, relative to the sun, are

$$X = V \cos A \cos D\,, \qquad Y = V \sin A \cos D\,, \qquad Z = V \sin D\,,$$

referred to the usual system of orthogonal axes. If ξ and η, in seconds of arc per annum, are the true components of proper motion of any star in the cluster in right ascension and declination, respectively, then

$$-X \sin \alpha + Y \cos \alpha = \frac{\kappa \xi}{p}\,, \tag{1}$$

$$-X \cos \alpha \sin \delta - Y \sin \alpha \sin \delta + Z \cos \delta = \frac{\kappa \eta}{p}\,, \tag{2}$$

where (α, δ) is the position of the star on the celestial sphere, p is its parallax, and $\kappa = 4.74$ is the constant required to adjust the units on either side of the equations. Let θ_0 be the (true) position angle of the star's proper motion; then, by eliminating p from equations (1) and (2), we get

$$\cot \theta_0 = \frac{\eta}{\xi} = \frac{-X \cos \alpha \sin \delta - Y \sin \alpha \sin \delta + Z \cos \delta}{-X \sin \alpha + Y \cos \alpha}\,. \tag{3}$$

[3] *Pub. Dom. Ap. Obs. Victoria*, Vol. **8**, No. 2, 1949; *M.N.*, **109**, 693, 1949.

[4] *Ap. J.*, **110**, 205, 1949.

In Charlier's method the equation of condition is obtained by rewriting equation (3) in the form

$$X(\eta \sin \alpha - \xi \cos \alpha \sin \delta) - Y(\eta \cos \alpha + \xi \sin \alpha \sin \delta) + Z\xi \cos \delta = 0 . \quad (4)$$

Now if we use x and y to denote the *observed* components of proper motion, in right ascension and declination respectively, then the solution is performed by substituting x for ξ and y for η in equation (4) and combining the equations from the different stars by the method of least squares. This gives the ratios $X:Y:Z$, and these ratios are, of course, sufficient to define A and D. It will be seen that the effect of errors in the observed quantities enters into each of the coefficients in equation (4), and, as Seares pointed out, this has a systematic effect on the solution.

It might be advisable to explain more explicitly what this "systematic effect" implies. It does not mean that solving from a particular set of data is bound to lead to the wrong result. One might compare the situation to measuring some quantity on a scale which had a zero error. If the errors of measurement were of the same order of magnitude as the zero error, then a single observation might easily give a reading smaller than the true value, greater than the true value, or exactly correct, despite the zero error. But if the observation were repeated a large number of times, then the average value would show the effects of the zero error, and one would deduce that a correction ought to be applied to all the observations. In the same way the systematic effect in the Charlier method of solution arises when we consider the average values obtained for the ratios $X:Y:Z$ from all the possible solutions which are consistent with the errors in the observed quantities. On the average, the ratios would not have their correct values, and therefore it is advisable to correct the results obtained in any particular solution for the effects of this systematic error.

Seares has discussed this matter in two papers,[5] but his treatment has been criticized subsequently. A more satisfactory discussion is given by Lindley.[6] Without going into detail as to the corrections required, it might appear from what has been said above that one could find the convergent point in a satisfactory manner by solving for the ratios $X:Y:Z$ by Charlier's method and then correcting for the effects of bias in the solution. Now it is possible that in some cases this method would be satisfactory, but there is no guaranty that the conditions required for its application would be fulfilled in every case. The equation of condition used to solve for X/Z and Y/Z can be written:

$$x \cos \delta = \frac{X}{Z}\{x \cos \alpha \sin \delta - y \sin \alpha\} + \frac{Y}{Z}\{x \sin \alpha \sin \delta + y \cos \alpha\}. \quad (5)$$

In using this equation of condition, we are assuming that the regression of $x \cos \delta$ on the other two observed quantities $x \cos \alpha \sin \delta - y \sin \alpha$ and $x \sin \alpha \sin \delta + y \cos \alpha$ is linear, i.e., that the average value of $x \cos \delta$, for given values of $x \cos \alpha \sin \delta - y \sin \alpha$ and $x \sin \alpha \sin \delta + y \cos \alpha$, is a linear function of these independent variables. Although equation (4) holds exactly, when one changes from the true values (ξ, η) to the observed values (x, y) the analogous regression relation need not hold, i.e., it does not follow automatically that $x \cos \delta$ is a linear function of $x \cos \alpha \sin \delta - y \sin \alpha$ and $x \sin \alpha \sin \delta + y \cos \alpha$. The required conditions have been given by Fix;[7] in this case they would depend on the positions of the members of the cluster on the celestial sphere. It seems unlikely that the conditions would be rigidly fulfilled, although they might be fulfilled approximately in a few cases.

[5] *Ap. J.*, **100**, 255, 1944, and **102**, 366, 1945; *Mt. W. Contr.*, Nos. 698 and 716.

[6] *Suppl. J. R. Stat. Soc.*, 9 218, 1947.

[7] "Distributions Which Lead to Linear Regressions," *Proc. Berkeley Symp. Mathematical Statistics and Probability* (University of California, 1949), p. 49.

The discussion in this section has dealt only with the Charlier method of solution but the same arguments apply to Bohlin's method.

III

The method of differential corrections.—If we assume an approximate position for the convergent point (A_1, D_1), we can compute the position angle, θ_1, in which the proper motion of each star should be directed. If θ is the observed position angle and

$$\Delta\theta = \theta - \theta_1 , \qquad \Delta A_1 = A - A_1 ,$$

$$\Delta \cot\theta = \cot\theta - \cot\theta_1 , \qquad \Delta D_1 = D - D_1 ,$$

then, by differentiating equation (3), we can derive a relation of the form

$$\Delta \cot\theta = -\Delta\theta \operatorname{cosec}^2\theta = l\Delta A_1 + m\Delta D_1 , \tag{6}$$

where l and m are functions of A_1, D_1, α, and δ, provided that we can neglect higher-order terms in ΔA_1 and ΔD_1. Miss Roman[4] used equation (6) as it stands as her equation of condition; Petrie[3] multiplied equation (6) by $\sin^2\theta$ and used, instead,

$$\Delta\theta = -l\sin^2\theta\Delta A_1 - m\sin^2\theta\Delta D_1 . \tag{7}$$

The most obvious criticism of this treatment is that if there is a relation between ΔA_1 and ΔD_1, e.g., if the solution tends to lie on a curve so that changing A automatically entails a change in D, then it is incorrect to treat ΔA_1 and ΔD_1 as independent variables in the equation of condition. A second objection arises from the nature of the residuals to be expected in the equation of condition. If we use equation (6) and write

$$w = l\Delta A_1 + m\Delta D_1 - \Delta \cot\theta ,$$

then, if we are to apply the method of least squares, it is essential that the expectation value of w should be zero for each star. For an individual observation, we should not expect w to be zero, but, to avoid any systematic errors, we must have $\bar{w} = 0$, where the average is taken over all permissible combinations of the errors of observation. Effectively, this means that the expectation value of $\cot\theta$, written $E(\cot\theta)$, should be equal to $\cot\theta_0$, i.e., $E(y/x) = E(\cot\theta)$ should equal $\eta/\xi = \cot\theta_0$.

To examine this point, we require some assumption as to the frequency distribution of the errors involved in x and y. If we assume

a) that the errors in x and y are independent,

b) that $E(x) = \xi$ and $E(y) = \eta$,

then it can be shown that, in general, $E(y/x) \neq (\eta/\xi)$. Let us denote the frequency distribution of x by $f_1(x)$ and the frequency distribution of y by $f_2(y)$. Then we have

$$\begin{aligned} E\left(\frac{y}{x}\right) &= \int\int\left(\frac{y}{x}\right) f_1(x)\, f_2(y)\, dx\, dy \qquad \text{over all possible values of } x \text{ and } y \\ &= \int\left(\frac{1}{x}\right) f_1(x)\, dx \times \int y\, f_2(y)\, dy \\ &= \left\{E\left(\frac{1}{x}\right)\right\}\{E(y)\} \\ &= \eta E\left(\frac{1}{x}\right). \end{aligned} \tag{8}$$

Now, in general,

$$E\left(\frac{1}{x}\right) \neq \frac{1}{E(x)} = \frac{1}{\xi}.$$

Hence, in general,

$$E\left(\frac{y}{x}\right) \neq \frac{\eta}{\xi}.$$

From equation (8), one exceptional case is when $\eta = 0$; but, as it is unlikely that η would be zero for all the members of the cluster, the special case of strict equality is not of much interest. However, it is useful to notice that if $|\eta| \ll |\xi|$, the bias in $\bar{w}$ will be small. Another exceptional case is when $f_1(x)$ has zero dispersion; for in that case there is no error involved in the determination of ξ. Consequently, $E(1/x) = (1/\xi)$. Once again, this is an unlikely case, but it corresponds to something which is readily understandable: that the more accurately x is determined, the less we need worry about the bias in $\bar{w}$.

The assumptions used in evaluating $E(y/x)$ need little defense. The measurement and reduction of the two components of the proper motion is usually independent; hence it seems likely that the distribution of the errors is independent. The second assumption, that $E(x) = \xi$ and $E(y) = \eta$, also seems reasonable; it simply means that the observed components of proper motion are assumed to be free from systematic errors.

As a final comment on the method of differential corrections, there is a danger of obtaining incorrect probable errors in the solution when this method is applied.[8]

It is perhaps worth noting that the difficulties mentioned above arise because the authors tried to find a procedure in which the data from different stars could be combined by a least-squares solution. For example, Petrie concluded that the best criterion to use in determining the convergent point would be to have

$$\Sigma (\Delta\theta)^2 = \Sigma (\theta - \theta_1)^2$$

a minimum at the convergent point. If this criterion had been applied in a less sophisticated manner, namely, by computing the value of $\Sigma(\theta - \theta_1)^2$ for a network of assumed convergent points, the restrictions of a least-squares solution would have been avoided, and the only point at issue would have been whether or not the best criterion had been adopted. The latter question will be discussed in more detail in Section IV.

IV

It is easy enough to be critical of the existing methods of solution; it is more difficult to find anything better to replace them. One method of attack might be to separate the solution into two parts as far as possible, i.e., to determine separately the *distance* of the convergent point from the cluster and the *direction* of the convergent point from the cluster. Suppose we refer the stars to a new system of co-ordinates on the celestial sphere, a system whose origin is approximately the center of the cluster and whose "equatorial" plane is defined by drawing a great circle through the origin and in the direction defined by the mean proper motion of the cluster. Then the convergent point will lie close to this equatorial plane, although it may be slightly above or below it. If we resolve the proper motion of each star into a component r parallel to this equatorial plane and a component s perpendicular to r, then most of the motion will be in r, which would be expected to have the same sign for all the stars involved and to be large relative to the errors of measurement (otherwise there would be little point in attempting a solution). Denoting co-ordinates parallel to the equatorial plane by ρ and co-ordinates perpendicular to the equatorial plane by σ, we expect the s-component of the proper motion to be small compared with r and to change sign as we move across the cluster in the σ-direction. Essentially, this component will define the distance of the convergent point above or below the equatorial plane, while the distance of the convergent point from the cluster will be

[8] S. L. Piotrowski, *Proc. Nat. Acad. Sci.*, **34**, 23, 1948.

defined by the change in the r-component of proper motion on moving across the cluster parallel to the equatorial plane. Thus the determination of the two co-ordinates of the convergent point will be practically independent, and it will be possible to see more clearly where the uncertainties in the solution arise. It is probable that in most cases the σ co-ordinate of the convergent point will be fairly well determined and that most of the uncertainty in the determination will be in the ρ co-ordinate, i.e., in the distance of the convergent point from the cluster. If radial velocities are available for the members of the cluster, then the change in radial velocity with the ρ co-ordinate of the stars might be used to strengthen the determination of the distance of the convergent point. However, the probable errors of the determination will usually be too large to show the change with ρ clearly. Proceeding in this way, we would bring out more clearly such difficulties as the fact that, if the convergent point is about 90° from the cluster, it will be practically impossible to determine the distance of the convergent point from the cluster by using the proper motions alone.

This change in the co-ordinate system gives more favorable conditions than usual for applying the method of differential corrections. The determination of the two co-ordinates of the convergent point becomes practically independent, the ratio of r to its probable error is large and the ratio of s to r small. (Taking s to correspond to y of Sec. III and r to correspond to x, one could easily obtain an equation analogous to eq. [6] in terms of the new co-ordinate system.) Hence the conditions for applying the method of differential corrections will be as favorable as possible.

It will be observed that the method of differential corrections, as applied by Petrie and Miss Roman, uses the directions of the proper motions only. In Charlier's method the equation of condition is homogeneous in x and y; by dividing throughout by x in equation (5), we could change the equation of condition to one in which only the direction of the proper motion appears and the amount of the motion is irrelevant. In fact, when using equation (5) as it stands, we may, in general, expect the direction of the motion to be the dominant factor; although the amount of the motion appears as a factor in the equation, it will not change greatly from star to star, and we might regard it as a kind of weighting factor which modifies slightly the dominant effect of the change in θ from star to star. Similarly, in Bohlin's method the dominant effect will be the change in θ. Thus all four methods represent, to a first approximation, different ways of utilizing the observed values of θ to define the convergent point. It would appear advisable, therefore, to examine the frequency distribution to be expected for θ and see if this suggests any method of combining the different θ's which would be an improvement on the existing methods.

Let us assume that for any member of the cluster the observed component of proper motion in right ascension, x, has a Gaussian distribution about the true value, ξ, with a standard deviation denoted by σ_x and, similarly, that the observed component of proper motion in declination, y, has a Gaussian distribution about its true value, η, with standard deviation σ_y. Then, in the notation of Section III,

$$f_1(x) = \frac{1}{\sqrt{2\pi}\sigma_x} \exp\left\{-\frac{(x-\xi)^2}{2\sigma_x^2}\right\},$$

$$f_2(y) = \frac{1}{\sqrt{2\pi}\sigma_y} \exp\left\{-\frac{(y-\eta)^2}{2\sigma_y^2}\right\}.$$

From what we know about the errors of measurement involved in determining x and y, these assumptions seem reasonable approximations to the truth. Let

$$v = \cot\theta = \frac{y}{x}. \tag{9}$$

Then the form of the distribution of v is known[9] and can be written down immediately in terms of the ratios $\xi:\eta:\sigma_x:\sigma_y$. Let

$$a = \frac{\eta}{\xi} = \cot\theta_0, \qquad b = \frac{\xi}{\sigma_x}, \qquad c = \frac{\sigma_y}{\sigma_x}. \tag{10}$$

Then the probability of occurrence of a value of v in the interval v to $v + dv$ is given by

$$g(v)\,dv = \frac{dv}{\pi}\left[\left(\frac{c}{v^2+c^2}\right)e^{-b^2(1+a^2/c^2)/2} + \frac{b(av+c^2)}{(v^2+c^2)^{3/2}}\,e^{-[b^2(v-a)^2]/[2(v^2+c^2)]}\int_0^q e^{-t^2/2}dt\right], \tag{11}$$

where

$$q = \frac{b(av+c^2)}{c(v^2+c^2)^{1/2}}. \tag{12}$$

This gives the distribution of $v = \cot\theta$, and it would be a straightforward matter to write down the frequency distribution of θ or of any desired function of θ from the known form of $g(v)$. However, $\cot\theta$ is such a simple function of the observed quantities x and y that there are advantages in working with it rather than with θ. There is one special case in which the distribution of θ takes a relatively simple form, namely, when $c = \sigma_y/\sigma_x = 1$. (In general, the mean-square error in the determination of x and y will be about the same, and c will be close to unity. The assumption that $c = 1$ throughout would not be too drastic, but, as it happens, there is no need to make it.) When $c = 1$, then the frequency distribution of θ is given by

$$g_1(\theta)\,d\theta = \text{Probability of occurrence of a value of } \theta \text{ in the interval } \theta \text{ to } \theta + d\theta$$
$$= \frac{d\theta}{\pi}\left[e^{-k^2/2} + k\cos(\theta-\theta_0)\,e^{-[k^2\sin^2(\theta-\theta_0)]/2}\int_0^{k\cos(\theta-\theta_0)} e^{-t^2/2}dt\right], \tag{13}$$

where

$$k = b\,\operatorname{cosec}\theta_0 = \frac{\mu_0}{\sigma_x}. \tag{14}$$

(We shall denote by μ_0 the true value of the total proper motion of any star, with μ as the corresponding observed value.)

The frequency distribution given by equation (11) is reasonably well behaved, provided that x is not likely to be small compared with y. If it were, one could, of course, use $\tan\theta$ instead of $\cot\theta$ and obtain an analogous distribution. It will be evident that the change of co-ordinate system suggested at the beginning of this section can again be used with advantage; for, by throwing most of the proper motion into the r-component, we can insure that the ratio s/r is small and accordingly that its frequency distribution is well behaved. It has been mentioned that c will usually be close to unity, and we have seen that a, or an analogous constant, can be made small. As for b, to insure that x will not be likely to take the value zero, it is desirable to have $|b| \geqslant 4$. This condition is almost certain to be fulfilled in practice, either for b or for the analogous constant obtained on changing to the r- and s-components of the proper motion, since it is an essential requirement if the position of the convergent point is going to be determined with any precision.

Thus for any star in the cluster we have an observed value, v, and we can write down the frequency distribution of v for that star in terms of the three ratios a, b, and c. These ratios will vary from star to star, and account must be taken of this in the method of solution. One method of taking into account the form of $g(v)$ and its change from star to

[9] It is given by E. C. Fieller, *Biometrika*, **24**, 428, 1932, for a more general case.

star is to apply the method of maximum likelihood,[10] a method which has not been used widely in astronomy, although it is of much more general application than the method of least squares. Suppose there are n stars in the cluster and let v_i be the observed value of v for the ith star. Then the probability of occurrence of a value of v_i between v_i and $v_i + dv_i$ is $g_i(v_i)$, where $g_i(v)$ denotes the frequency distribution of v for the ith star. The probability of obtaining a set of values in the element of volume $(v_1, v_2, \ldots, v_n)$ to $(v_1 + dv_1, v_2 + dv_2, \ldots, v_n + dv_n)$ is

$$\prod_{i=1}^{n} g_i(v_i)\, dv_i .$$

Let

$$L = \prod_{i=1}^{n} g_i(v_i) .$$

Then the combined probability of the set of values $v_1, v_2, \ldots, v_n$ is $L dv_1\, dv_2 \ldots dv_n$, and the method of maximum likelihood consists in choosing the available parameters, in this case A and D, to make L a maximum. L is called the *likelihood*, and one way to evaluate A and D is to solve the *likelihood equations*,

$$\frac{\partial L}{\partial A} = 0 , \qquad \frac{\partial L}{\partial D} = 0 , \tag{15}$$

since these are necessary conditions for a maximum in L. However, with $g(v)$ as given by equation (11), the likelihood equations are very cumbersome. They could be solved by trial and error, but it appeared simpler to determine L, or, in practice, $\log L$, for a number of trial positions of the convergent point and to see where the maximum value of L occurred. This treatment has the advantage that one can see how L behaves in the neighborhood of the convergent point and hence recognize how well the convergent point is defined. Details of a numerical application are given below in Section V.

In general, the values obtained for A and D by the method of maximum likelihood will be, in a sense, "best" values. More explicitly, suppose we have a formula of some kind or a method of solution which can be used to determine A. Let A' be a value obtained for A by applying this method of solution to a particular set of data. If we repeat the observations independently and apply the method of solution again, we will usually get a different value of A'. Repeating this process a number of times, we can build up a frequency distribution of A' whose mean value and dispersion are partly determined by the method of solution as well as by the data of the problem. There will be similar frequency distributions of the computed values corresponding to other methods of solution. Clearly, one essential property of any method of solution which is to be used is that the average value obtained by applying the method a large number of times should tend toward the true value, i.e., that

$$E(A') = A ,$$

where A is the true value we are trying to determine. Another desirable property is that the dispersion in the computed values should be as small as possible, i.e., that

$$E\{(A' - A)^2\}$$

should be a minimum. This condition allows us to choose between different methods of solution which satisfy the first criterion. Now, in general, if a formula for evaluating A

[10] For a description of this method and a justification of its use see H. Cramer, *Mathematical Methods of Statistics* (Princeton: Princeton University Press, 1946), p. 498. The method is originally due to R. A. Fisher.

exists which has this property of giving minimum dispersion in the computed values, then the method of maximum likelihood gives a unique solution which is the required formula. In more technical language, if an efficient statistic for A exists, then the method of maximum likelihood gives this statistic and the solution is unique. This property of the method of maximum likelihood has been the main justification for its use. More recently, Neyman and Miss Scott[11] have shown that exceptions to the above rule can be found. In the present case it has not been possible to decide whether the method of maximum likelihood will give an optimum solution or not, but, from the objections to the existing methods in Sections II and III and from further considerations below, it appears that its use should at least represent an improvement.

Before turning to the numerical application, there is one further point of interest which arises from the distribution of v. Taking equation (5) as the equation of condition in Charlier's method of solution, we can rewrite it as

$$\frac{x}{Z}(X\cos\alpha\sin\delta + Y\sin\alpha\sin\delta - Z\cos\delta) + \frac{y}{Z}(Y\cos\alpha - X\sin\alpha) = 0,$$

$$\text{i.e.,}\left(\frac{\kappa}{\rho Z}\right)(\xi y - x\eta) = 0 \qquad \left(\text{from equations [1] and [2]}\right);$$

this reduces to

$$\left(\frac{\kappa}{\rho Z}\right)\mu\mu_0\sin(\theta_0 - \theta) = 0.$$

Thus, in the Charlier method, $\Sigma\{(\mu\mu_0/\rho)\sin(\theta_0 - \theta)\}^2$ is minimized; or, if we take $\sigma_x = \sigma_y$ and assume that the equations would be weighted proportionally to $1/\sigma_x^2$, then we can say that $M_1 = \Sigma\{(\mu\mu_0/\rho\sigma_x)\sin(\theta_0 - \theta)\}^2$ is minimized. In Bohlin's method, as given by Smart,[12] the equation of condition for each star is

$$\frac{X}{Z}\cos A'' + \frac{Y}{Z}\sin A'' + \tan D'' = 0, \tag{16}$$

where (A'', D'') is the pole of the great circle to which the proper motion of the star is tangential and which passes through the star's position (α, δ). With this equation of condition and the same assumption as before about weighting the observations, combining the observations by the method of least squares makes

$$M_2 = \Sigma\left\{\frac{\mu_0}{\rho\sigma_x}\sin(\theta_0 - \theta)\right\}^2\{\cos^2\theta + \sin^2\delta\sin^2\theta\}^{-1}$$

a minimum. However, if we multiply by $\cos D''$ in equation (16) and take as our equation of condition,

$$\frac{X}{Z}\cos A''\cos D'' + \frac{Y}{Z}\sin A''\cos D'' + \sin D'' = 0,$$

then the quantity minimized would be

$$M_3 = \Sigma\left\{\frac{\mu_0}{\rho\sigma_x}\sin(\theta_0 - \theta)\right\}^2.$$

On comparing the expressions M_1, M_2, and M_3, we observe that basically the Charlier and Bohlin methods determine the convergent point in such a way that $\Sigma\sin^2(\theta_0 - \theta)$ is minimized, although the solution is affected by slightly different methods of weighting

[11] *Econometrica*, Vol. 16, No. 1, 1948.

[12] *Op. cit.*, p. 285.

the equations from individual stars. It will be evident, too, that we could take as our equation of condition,

$$\phi \sin (\theta_0 - \theta) = 0 ,$$

where ϕ is an arbitrary function of α, δ, μ, θ, and p, and in this way we could obtain an infinite variety of systems of weighting. The question arises whether the weighting functions used in M_1, M_2, or M_3 have any special validity which would justify their use.

To examine this problem, we turn to the distribution found for $v = \cot \theta$. From the form of $g(v)$ in equation (11), it can be shown[13] that when $|b|$ is large, then

$$t = \frac{b\,(v - a)}{(v^2 + c^2)^{1/2}} = \frac{\mu_0 \sin (\theta_0 - \theta)}{\{\sigma_x^2 \cos^2\theta + \sigma_y^2 \sin^2\theta\}^{1/2}}$$

has approximately a Gaussian distribution with mean zero and unit standard deviation. Applying the method of maximum likelihood to this case, we require that

$$L = \prod_{i=1}^{n} e^{-t_i^2/2}$$

should be a maximum for the set of observed values of t. The condition for this is simply that

$$M_4 = \Sigma t^2 = \Sigma \frac{\{\mu_0 \sin (\theta_0 - \theta)\}^2}{(\sigma_x^2 \cos^2\theta + \sigma_y^2 \sin^2\theta)}$$

should be a minimum. We can compare M_1, M_2, and M_3 with M_4, and it will be seen that M_3 is the closest approximation. However, M_4 was obtained by a limiting process, by making $|b| \to \infty$, and in practice it would seem better to make a maximum-likelihood solution from $g(v)$ as it stands rather than through the approximate distribution for t.

V

To find how a maximum-likelihood solution would work in practice, it was applied to the nucleus stars of the Ursa Major cluster. The three fainter stars found by Miss Roman[4] were excluded, since the errors attached to their proper motions are much larger than for the brighter stars. For the latter, the *General Catalogue* proper motions[14] were used, after they had been corrected for systematic errors according to the table of corrections given by Blaauw and Delhaye.[15] Table 1 lists the stars used, their GC number, position, and corrected proper motion, together with the catalogue value of the probable errors in the components of proper motion. The last two columns show the values of b and c used for each star.

The ratio c was obtained by arranging the stars in groups according to their probable errors, i.e., 78 UMa and ζ UMa B were grouped together, and the mean value of their probable errors was used to compute c. Similarly, HR 4867 and HD 115043 were grouped together, and the remaining stars were taken as a single group with $c = 1$ and probable error $0''.0009$ per annum in each co-ordinate. In accordance with a suggestion by Schlesinger and Miss Barney,[16] who found that the probable errors of the GC proper motions had

[13] See R. C. Geary, *J. R. Stat. Soc.*, **93**, 442, 1930.

[14] *General Catalogue of 33,342 Stars for the Epoch 1950* (Washington: Carnegie Institution of Washington, 1937).

[15] *B.A.N.*, No. 400, 1949.

[16] *A.J.*, **48**, 51, 1939.

been underestimated, the catalogue values were multiplied by 1.35. Thus for any star,

$$\sigma_x = \frac{1.35}{0.6745} \times \text{(published p.e. in right ascension)}$$

$$= 2.0 \times \text{(published p.e. in right ascension)}.$$

Then the observed values x/σ_x were used as an approximation to $b = \xi/\sigma_x$ for each star. The remaining constant in the distribution of v, namely, a, can be evaluated for any assumed position for the convergent point. For each star,

$$a = \cot\theta_0 = \tan D \cos\delta \operatorname{cosec}(A - \alpha) - \sin\delta \cot(A - \alpha),$$

where (A, D) are the co-ordinates of the assumed convergent point. Inserting a, b, and c in equations (11) and (12), we can evaluate $g(v)$ for each star and hence find the value of L corresponding to the assumed convergent point. It will be observed from Table 1 that most of the proper motion is in right ascension and that b is satisfactorily large, so there is no need to change the co-ordinate system in this case.

TABLE 1

POSITIONS AND PROPER MOTIONS OF STARS USED IN SOLUTION

No.	Name	GC No.	1950 Positions		Corrected Proper Motions and Probable Errors (in Seconds of Arc p.a.)				b	c
			α	δ	x	p.e.	y	p.e.		
1	37 UMa	14527	10^h32^m0	57°20′	0.066	0.0013	+0.039	0.0011	36.7	1.00
2	β UMa	15145	10 57.8	56 39	.083	.0008	+ .035	.0008	46.1	1.00
3	γ UMa	16268	11 51.2	53 58	.095	.0006	+ .012	.0006	52.8	1.00
4	δ UMa	16736	12 13.0	57 19	.107	.0008	+ .010	.0008	59.4	1.00
5	HR 4867	17404	12 46.5	60 36	.109	.0035	+ .002	.0025	14.9	0.79
6	ϵ UMa	17518	12 51.8	56 14	.115	.0008	− .003	.0008	63.9	1.00
7	78 UMa	17664	12 58.6	56 38	.116	.0020	− .008	.0016	30.5	0.87
8	HD 115043	17919	13 11.6	56 58	.113	.0038	− .027	.0033	15.5	0.79
9	ζ UMa A	18133	13 21.9	55 11	.126	.0008	− .019	.0008	70.0	1.00
10	ζ UMa B	18134	13 21.9	55 11	.120	.0018	− .027	.0017	31.6	0.87
11	80 UMa	18155	13 23.2	55 15	0.121	0.0013	−0.015	0.0013	67.2	1.00

With such large values of b, the computation of L is simplified considerably. If we consider the first term in $g(v)$, then $c/(v^2 + c^2)$ is of order unity and

$$\exp\left\{-\tfrac{1}{2}b^2\left(1 + \frac{a^2}{c^2}\right)\right\} \leq \exp\left(-\frac{b^2}{2}\right).$$

Now, for $b = 12$, $e^{-b^2/2} = e^{-72} = 10^{-31}$. Hence we can safely neglect the first term in equation (11). Now consider the integral in the second term. The upper limit of the integral is approximately equal to b, or greater, since

$$\frac{(a v + c^2)}{\{c (v^2 + c^2)^{1/2}\}} \sim \frac{(v^2 + c^2)^{1/2}}{c} \geq 1$$

Now

$$\int_b^\infty e^{-t^2/2} dt = \left[-\frac{1}{t} e^{-t^2/2}\right]_{t=b}^{t=\infty} - \int_b^\infty \frac{1}{t^2} e^{-t^2/2} dt < \frac{1}{b} e^{-b^2/2}$$

Hence, for $b > 12$,

$$\int_b^\infty e^{-t^2/2}dt < 10^{-32}.$$

Thus, for the values of b in Table 1, the integral in the second term of $g(v)$ differs from $\int_0^\infty e^{-t^2/2}dt = \sqrt{(\pi/2)}$ by less than 10^{-32}. Hence we can replace the integral by $\sqrt{(\pi/2)}$. Finally, since b and c do not change when we assume different convergent points, we can write

$$\log L = \Sigma\left\{\log (a v + c^2) - \tfrac{1}{2} (\log e)\, b^2 \frac{(v-a)^2}{(v^2+c^2)}\right\} + \text{a constant},$$

when considering the effect of different convergent points on the value of L. It is therefore sufficient to find where

$$\log L' = \Sigma\left\{\log (a v + c^2) - \tfrac{1}{2} (\log e)\, b^2 \frac{(v-a)^2}{(v^2+c^2)}\right\}$$

has a maximum value. In the computations it was evident that the second term was the dominant one. For points in the neighborhood of the convergent point, $av + c^2$ is approximately equal to $v^2 + c^2$, and, accordingly, $\Sigma \log (av + c^2)$ does not change much from one test position of the convergent point to another. Table 2 shows values of $-\log L'$ for various assumed positions of the convergent point; over the range of positions shown in this table $\Sigma \log (av + c^2)$ ranged from -0.38 to -0.35 only. Hence its contribution has a negligible effect on the results. For each value of D, the value of A at which $\log L'$ had its maximum was determined, and this is shown at the foot of the table, together with the corresponding value of $-\log L'$. It will be evident that if a curve is drawn through these points, $\log L'$ changes rapidly if one moves away from the curve but changes very slowly along the curve.

This can be explained from the geometry of the problem. Although the Ursa Major cluster extends over about 20° in one direction on the celestial sphere, the extension at right angles to this, i.e., in declination, is only about 6°. Unfortunately, the proper motions are mainly in right ascension, i.e., parallel to the direction along which the cluster is elongated; hence in the neighborhood of the convergent point, about 135° away, shifting the assumed convergent point toward or away from the cluster has hardly any effect on the computed values of the position angles. This can be seen from Table 3, which shows the observed values of θ, together with the values computed for three assumed positions of the convergent point. Although the declinations of these assumed positions range over 10°, the computed position angles agree about as well with the observed values for all three points. Roughly, the points which give turning values of L for a fixed D will lie on a great circle passing through the convergent point and through the middle of the cluster. We can say in this case that the directions of the proper motions define a curve Q on the celestial sphere on which the convergent point lies but do not define the distance of the convergent point from the cluster. This seems a plausible explanation of the divergence in the solutions found for this cluster when different methods of combining the data were applied.[3] In all these methods the directions of the proper motions provided the dominant factor in the solution, and thus the solution is practically indeterminate along the curve Q.

Is there any way out of this impasse? One easy way would be to accept the curve Q as giving a locus for the convergent point and then choose that point on the curve which gives best agreement between the observed radial velocities, parallaxes, and proper motions. However, the relatively large errors of measurement associated with the parallaxes and the radial velocities make it desirable to avoid them as far as possible, or at least to make use of them only as a last resort. As regards the radial velocities, some of

TABLE 2

VALUES OF $-\log L'$ FOR DIFFERENT TEST POSITIONS OF THE CONVERGENT POINT

A	D								
	$-16°$	$-18°$	$-20°$	$-22°$	$-24°$	$-26°$	$-28°$	$-30°$	$-33°$
290°	6.86								
291	5.58	8.25							
292	6.85	5.72	10.34						
293		5.94	6.66						
294		8.85	5.47	8.31					
295			7.10	5.79	11.10				
296				5.89	6.98				
297				8.85	5.57	9.43			
298					6.88	6.27			
299					11.14	5.86	8.58		
300						8.28	6.15		
301							6.54	8.31	
302								6.36	
303								7.45	12.82
304									8.68
305									7.27
306									8.91
Minimum value	5.55	5.45	5.43	5.48	5.62	5.67	6.15	6.35	7.24
Corresponding value of A	290°9	292°4	293°9	295°4	297°2	298°7	300°1	301°9	304°9

TABLE 3

COMPARISON OF OBSERVED AND COMPUTED POSITION ANGLES FOR DIFFERENT TEST POSITIONS OF THE CONVERGENT POINT

Star No.	Values of Position Angle				Star No.	Values of Position Angle			
	Observed	Computed Values				Observed	Computed Values		
		$A=294°$, $D=-20°$	$A=297°$, $D=-24°$	$A=302°$, $D=-30°$			$A=294°$, $D=-20°$	$A=297°$, $D=-24°$	$A=302°$, $D=-30°$
1	59°4	59°5	59°0	57°9	7	93°9	93°7	93°9	94°1
2	67.1	66.7	66.5	66.1	8	103.4	96.3	96.3	96.5
3	82.8	81.0	81.4	82.1	9	98.6	99.0	99.2	99.6
4	84.7	83.8	83.8	84.0	10	102.7	99.0	99.2	99.6
5	89.0	89.5	89.3	88.8	11	97.1	99.2	99.4	99.8
6	91.5	92.5	92.7	93.0					

the stars have diffuse lines which make it difficult to measure their radial velocity, while for the parallaxes the probable errors range from about 20 to 50 per cent of the actual value. Under these circumstances, one can readily understand the reluctance of the earlier investigators to find a convergent point simply by forcing agreement between radial velocities, parallaxes, and proper motions.

It turns out that we can extract some additional information from the amount of the proper motion in right ascension, and this helps to define the position of the convergent point on Q. In evaluating L', the dominant term was the term proportional to $(v - a)^2$, i.e., to $(\cot \theta - \cot \theta_0)^2$. Thus it was the *directions* of the motions which played the most important role in the solution. As mentioned above, they define the direction of the convergent point from the cluster, and, to find the distance of the convergent point, we can

TABLE 4

RATIO OF x TO SIN $(A - \alpha)$

STAR NO.	α	VALUES OF A							
		294°	296°	298°	300°	302°	304°	306°	308°
1	158° 0′	0.095	0.099	0.103	0.107	0.112	0.118	0.125	0.132
2	164 27	.108	.111	.115	.119	.123	.128	.133	.140
3	177 48	.106	.108	.110	.112	.115	.118	.121	.124
4	183 15	.114	.116	.118	.120	.122	.125	.127	.130
5	191 38	.112	.113	.114	.115	.116	.118	.120	.122
6	192 57	.117	.118	.119	.120	.122	.123	.125	.127
7	194 39	.118	.118	.119	.120	.122	.123	.125	.126
8	197 54	.114	.114	.115	.116	.117	.118	.119	.120
9	200 28	.126	.127	.127	.128	.129	.130	.131	.132
10	200 28	.120	.121	.121	.122	.122	.123	.125	.126
11	200 48	0.121	0.122	0.122	0.123	0.123	0.124	0.125	0.127

examine the change in the proper motion component in right ascension along the length of the cluster. From equation (1), this component is given by

$$\begin{aligned}\frac{\kappa\xi}{p} &= -X \sin \alpha + Y \cos \alpha \\ &= -V \cos A \cos D \sin \alpha + V \sin A \cos D \cos \alpha \\ &= V \cos D \sin (A - \alpha) .\end{aligned}$$

Therefore, if we assume as a first approximation that the stars are all at the same distance, ξ should be proportional to sin $(A - \alpha)$, independent of the declination of the convergent point. Table 4 shows the values of the ratio $x/[\sin (A - \alpha)]$ for each star for a number of values of A. It will be seen that for $A = 294°$ there is a systematic increase in the ratio with right ascension. As the value of A is increased, this systematic effect tends to decrease and finally reverses itself, so that for $A = 308°$ the ratio is tending to decrease with right ascension. We are interested in the value of A for which the systematic effect disappears, and this would appear to be about $A = 304°$. Reading off the corresponding declination from the curve Q, we get the position of the convergent point as $A = 304°$, $D = -32°$. From Table 4, A appears to be defined within about 4° by the amounts of the proper motions in right ascension; from the rapid change in L perpendicular to the curve Q (Table 2), this would imply that the solution must lie within an area about 4° long and 3° wide, along and on either side of the curve Q.

The mean value of the ratio $x/[\sin(A - a)]$ for $A = 304°$ is 0.123, and, if we take the mean parallax of the cluster as 0".040, this would give a space motion $V = 17.2$ km/sec. Table 5 shows the radial velocities to be expected with the above space motion and convergent point and compares them with the observed values. For the latter, Miss Roman's values were used.[17] The agreement is good, but it should be emphasized that there are still appreciable uncertainties inherent in the result. For example, adopting a different mean parallax would change the value of V obtained from the ratio of x to sin $(A - a)$ in Table 4. Taking the mean parallax as 0".038 would make $V = 18.1$ km/sec;

TABLE 5

COMPARISON OF OBSERVED AND COMPUTED VALUES OF RADIAL VELOCITY, IN KM/SEC

Star No.	Observed	Mean-Square Error	Computed	O−C		Star No.	Observed	Mean-Square Error	Computed	O−C	
				+	−					+	−
1	12.5	1.0	14.2	.....	1.7	8	8.5	0.6	9.9	.....	1.4
2	11.5	0.6	13.7	.....	2.2	9	9.3	0.5	9.4	.....	0.1
3	13.5	1.0	12.5	1.0	.....	10	11.2	0.8	9.4	1.8	.....
4	16.1	1.5	11.7	4.4	.....	11	9.2	1.5	9.4	.....	0.2
5	13.8	1.0	10.7	3.1	.....						
6	6.7	1.0	10.5	.....	3.8	Mean value	.....	.....	.....	+0.1	
7	11.0	1.0	10.3	0.7	.....						

taking it as 0".042 would make $V = 16.4$ km/sec. Either of these values would be compatible with the errors in the published parallaxes, and they would lead to a slight disagreement between the observed and the computed radial velocities.

This work has been carried out in fits and starts during the past year, and I am grateful to the Commonwealth Fund, whose financial assistance made it possible for me to work at the Yerkes Observatory during that time. I should like to acknowledge the benefit I have received from correspondence with Miss Elizabeth L. Scott, University of California, on some of the statistical problems involved. Last summer I had the opportunity of discussing the problem with Dr. R. M. Petrie, of the Dominion Astrophysical Observatory, and I should like to thank him also. I am especially indebted to Miss Nancy G. Roman, whose work on the Ursa Major cluster stimulated this research and with whom I have had many helpful discussions both on the contents and on the presentation of this paper.

[17] *Op. cit.*, p. 221, Table 15.

THE COLOR-MAGNITUDE ARRAY FOR THE GALACTIC CLUSTER NGC 2362*

HAROLD L. JOHNSON
Washburn Observatory, University of Wisconsin
Received June 17, 1950

ABSTRACT

Photoelectrically determined colors and magnitudes have been obtained for stars in the galactic cluster NGC 2362. A comparison of the color-magnitude array with those obtained by Eggen for the Hyades and Pleiades clusters gives a distance modulus for NGC 2362 of 10.75 mag., corresponding to a distance of 1410 parsecs. If τ Canis Majoris is a member of the cluster, its absolute magnitude is -7.0.

The present photometric work on the galactic cluster NGC 2362 ($\alpha_{1950} = 7^h16^m6$; $\delta_{1950} = -24°52'$) was suggested by Dr. W. Baade, who pointed out that the cluster stars are almost exclusively of early type and that there is no discernible nebulosity associated with the cluster. The observations were made during November, 1949, with the 100-inch and 60-inch telescopes of the Mount Wilson Observatory. For the brightest stars, the 60-inch telescope, diaphragmed down to 18 inches aperture, was used. The light-sensitive device was a type 1P21 photomultiplier refrigerated with dry ice. The glass color filters, used to isolate the three spectral bands, are discussed in detail at the end of this paper. The magnitudes were derived from measures made with the "clear" filter, while the colors were derived from the measures with the "yellow" and "blue" filters.

A photograph of the cluster, taken by Dr. Baade with the 100-inch telescope, is shown in Figure 1. A chart showing the positions of the observed stars in the cluster is given in Figure 2. The magnitudes and colors for the individual stars are given in Table 1 and Figure 3. In Table 1, column 1 contains the number of the star; columns 2 and 3 contain the photographic magnitudes and colors, referred to the North Polar Sequence; and column 4 contains the absolute photographic magnitudes determined in a manner to be described. The colors and magnitudes given are the means of two or more observations; the probable errors of these means are as follows: C_p: ± 0.007 mag.; Pg_p: ± 0.010 mag.; $Pg_p < 14$. These probable errors indicate the precision with which the relative colors and magnitudes of the stars in the cluster are known. The zero points, however, are not so well known, owing principally to the fact that the maximum altitude of NGC 2362 at Mount Wilson is about 30° and that most of the observations were made at even lower altitudes. The estimated probable errors of the zero points of the scales are ± 0.025 mag. for both C_p and Pg_p.

The colors and magnitudes given in Table 1 are referred to the North Polar Sequence and are therefore on the International System over the range of colors available in the North Polar Sequence. Inasmuch as no NPS stars bluer than $C = +0.06$ were used in the comparison, most of the stars in NGC 2362 are outside the range of spectral types of the standard stars; therefore, since the wave-length bands covered by the filters[1] used in this investigation are not the same as those used for the determination of the International System, the colors and magnitudes of the bluer cluster stars are not exactly on that system. This fact makes desirable a calibration of the color system of this paper in terms of spectral type. Accordingly, the colors of several essentially unreddened stars of known spectral type on the Yerkes system[2] were observed, using the same filters and

* Report based on observations made at the Mount Wilson and Palomar Observatories.

[1] See the filter calibrations at the end of this paper.

[2] The spectral types were kindly supplied by Dr. W. W. Morgan.

FIG. 1.—NGC 2362 as photographed with 100-inch telescope. The center of the cluster was dodged in reproduction. North is at top.

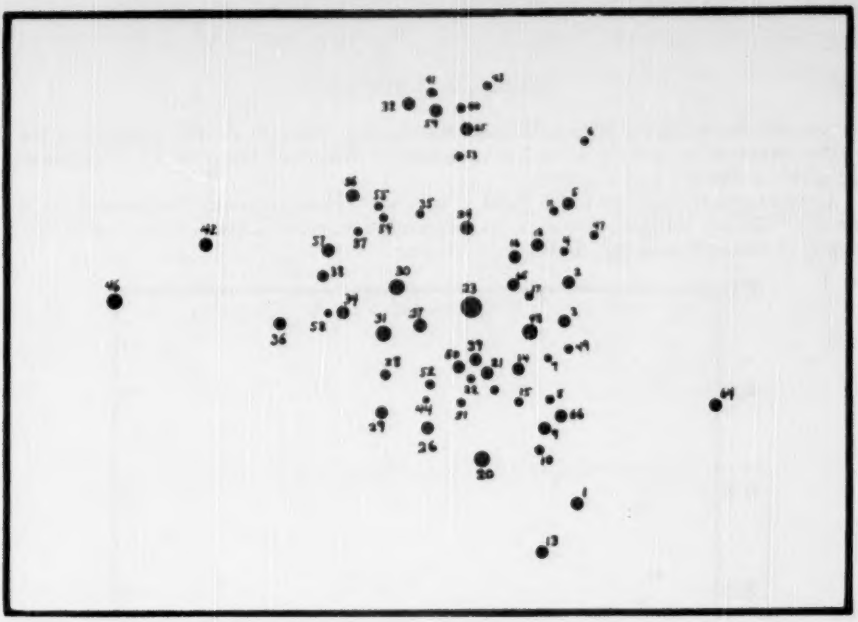

FIG. 2.—Star chart for NGC 2362

TABLE 1

COLORS AND MAGNITUDES OF STARS IN NGC 2362

Star (1)	P_{fp} (2)	C_p (3)	M_p (4)	Star (1)	P_{fp} (2)	C_p (3)	M_p (4)
1	11.12	−0.24	+0.37	32*	10.62	+0.15	−0.13
2	11.87	−0.26	+1.12		10.87		+0.12
3	10.90	−0.12	+0.15	34	10.59	− .26	−0.16
4	12.33	−0.09	+1.58	35	13.10	+ .15	+2.35†
5	10.39	−0.31	−0.36	36	10.48	− .24	−0.27
6	12.87	+0.02	+2.12	37	12.75	+ .22	+2.00
7	13.45	+0.04	+2.70†	38	12.69	− .04	+1.94
8	12.72	+0.24	+1.97	39	9.34	− .38	−1.41
9	9.42	−0.35	−1.33	40	12.99	+ .16	+2.24
10	12.27	+0.26	+1.52	41	13.52	+ .42	+2.77†
11	11.72	−0.17	+0.97	42	11.04	− .23	+0.29
12	9.63	−0.32	−1.12	43	15.09	+ .37	+4.34†
13	10.42	−0.06	−0.33	44	14.84	+ .06	+4.09†
14	9.11	−0.38	−1.64	46	6.33	− .44	−4.42†
15	11.54	−0.19	+0.79	47	14.04	+ .25	+3.29†
16	10.39	−0.13	−0.36	48	9.06	− .40	−1.69
17	13.33	+1.06	+2.58†	49	12.56	+ .24	+1.81
20	8.23	−0.45	−2.52	50	9.92	− .24	−0.83
21	10.08	−0.31	−0.67	51	12.49	+ .29	+1.74
22	11.72	−0.18	+0.97	52	11.76	− .14	+1.01
23	3.79	−0.48	−6.96	53	13.57	+ .02	+2.82
24	10.67	−0.28	−0.08	54	14.38	+ .28	+3.63†
25	10.50	−0.22	−0.25	55	14.82	+ .36	+4.07†
26	10.04	−0.34	−0.71	56	11.95	− .03	+1.20
27	9.76	−0.36	−0.99	57	11.93	− .16	+1.18
28	11.84	−0.18	+1.09	58	12.04	− .11	+1.29
29*	10.79	−0.24	+0.04	59	12.25	+ .07	+1.50
	11.04		+0.29	64	12.11	+ .34	+1.36
30	7.61	−0.48	−3.14	65	11.71	+ .07	+0.96
31	8.83	−0.41	−1.92	66	11.20	−0.21	+0.45

* The photometer sensitivity switch is calibrated in steps of exactly 0.25 mag. For stars Nos. 29 and 32, an error of one step was made in the recording for one of the two observations.

† These stars are likely not to be members of the cluster.

photomultiplier as in the Mount Wilson observations, with the 24-inch reflector of the Yerkes Observatory and the 15-inch refractor of the Washburn Observatory. The results are given in Table 2 and Figure 4.

According to the data given in Table 2, τ Canis Majoris is among the bluest stars in the sky.[3] We are justified, therefore, in assuming that there is little, if any, space reddening or absorption in the direction of this star.

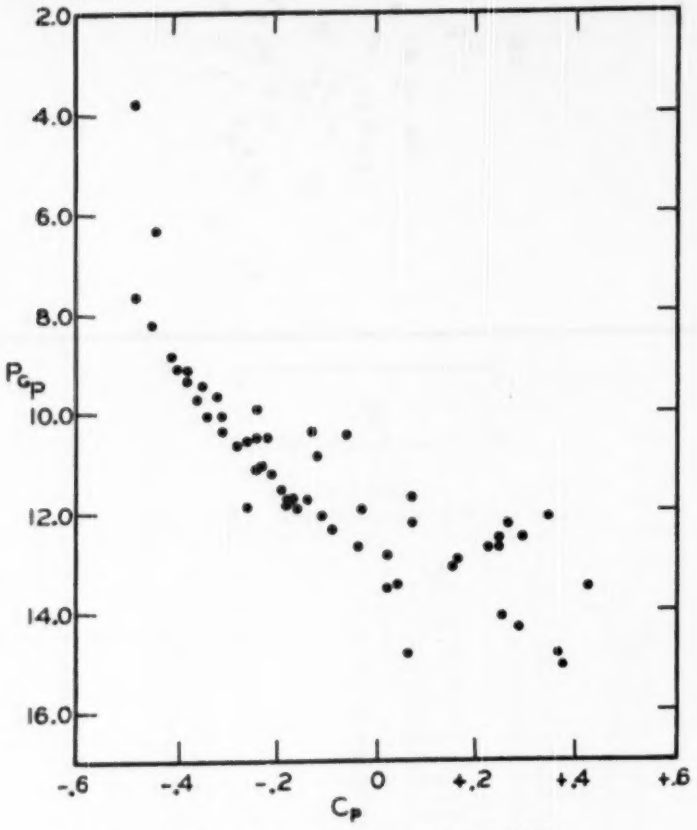

FIG. 3.—Color-magnitude array for NGC 2362

An examination of Figure 1 will show that there is little reason to suspect the existence of nebulosity in NGC 2362; an examination of the original negative likewise shows no nebulosity. The visual appearance with the 100-inch telescope is in agreement with the conclusion that the amount of nebulosity associated with the cluster is negligible.

It is interesting to make a comparison of these results on NGC 2362 with those obtained by Eggen[4] on the Hyades and Pleiades clusters. As soon as one attempts such a

[3] HD 14633 is the bluest star in the entire list of 1332 B stars observed by Stebbins, Huffer, and Whitford (*Ap. J.*, 91, 20, 1940).

[4] *Ap. J.*, 111, 65, 81, 1950.

TABLE 2

COLORS OF STANDARD STARS

Star HD	Name	Spectral Type	C_p	Star HD	Name	Spectral Type	C_p
14633	.....	O8	−0.46	100600	90 Leo	B5 V	−0.33
57061	τ CMa	O9 V	− .48	143807	ϵ CrB	A0 V	− .21
120315	η UMa	B3 V	− .39	109358	β CVn	G0 V	+ .50
74280	η Hya	B3 V	−0.38	145328	τ CrB	K0 III	+0.97

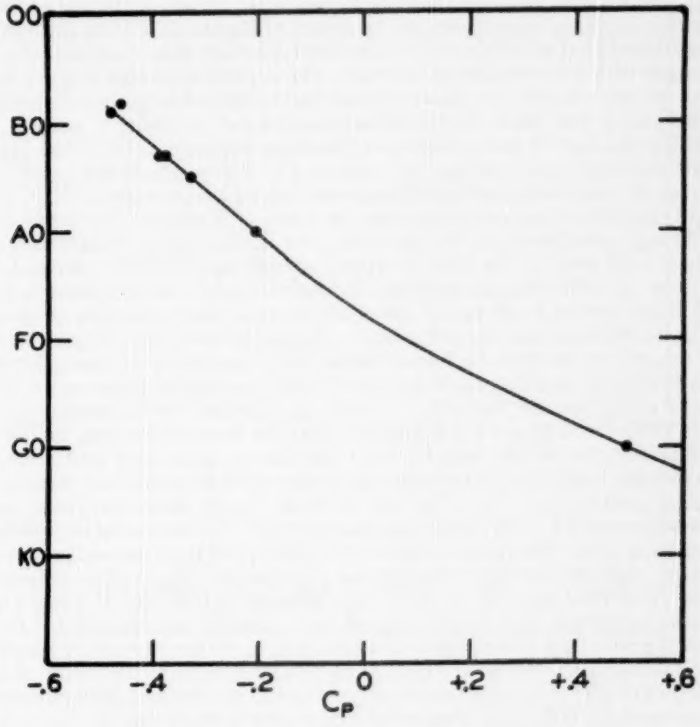

FIG. 4.—Color–spectral-type calibration-curve

comparison, however, one notices that the two color-magnitude systems are not exactly the same. The reason for this difference, as is discussed in more detail elsewhere,[5] is that the polar comparisons for the two photoelectric systems are based upon a different selection of NPS stars. We have observed four stars (NPS 6, NPS 10, NPS 4r, NPS 2r) in common; therefore, the equations relating the two photoelectric systems may be determined. These equations are:

$$C_p = -0.066 + 1.077 C_p^E \pm 0.002 \pm 0.002 \text{ (p.e.)},$$

$$Pg_p = Pg_p^E - 0.004 - 0.004 C_p^E \pm 0.024 \pm 0.026 \text{ (p.e.)},$$

where C_p and Pg_p are the colors and magnitudes on the system of this paper and C_p^E and Pg_p^E are the colors and magnitudes on the system of Eggen. As is to be expected for two well-determined photoelectric systems, the transformations from one system to the other can be made with a high degree of accuracy. The various sequences as given by Eggen[4] may now be converted to the present system and compared with the colors and magnitudes in Table 1. The result of this comparison is shown in Figure 5, where it has been *assumed* that the best fit is obtained for a distance modulus for NGC 2362 of 10.75 mag. The solid lines are Eggen's sequences, converted to the system of this paper, while the dotted line is a suggested additional sequence defined by the stars in NGC 2362. The spectral-type calibrations are taken from the curve of Figure 4. The distance modulus of 10.75 mag. corresponds, on the assumption of no absorption of light in space, to a distance of 1410 parsecs. The absolute magnitudes given in Table 1, column 4, were obtained from Pg_p on the assumption that the distance modulus of the cluster is 10.75 mag.

R. J. Trumpler[6] points out that the nearly vertical rise in absolute magnitude that occurs in the Pleiades, starting at spectral type approximately B8, is a general characteristic of the galactic clusters. He further states that, "in different clusters, this rise is not associated with any particular spectral type."[6] The color-magnitude array for NGC 2362, showing a nearly vertical rise at $C_p = -0.47$, is, therefore, not unreasonable.

From Table 2 and Figure 4 it is apparent that the B-type stars used for the spectral-type calibration are not the same kind as those that occur in the Pleiades, for the color indices of these bright field stars are considerably more negative than those of the corresponding spectral type there. The stars in Table 2 were chosen as typical, essentially unreddened, examples of the particular spectral types. Discussions of the mean absolute magnitudes of early-type general field stars[6, 7] have yielded values not greatly different from those obtained for stars lying on the principal sequence of the color-magnitude array for NGC 2362 ($m - M = 10.75$). The absolute magnitudes of Table 1 are in approximate agreement with recent unpublished magnitudes obtained by Dr. W. W. Morgan[8] for early-type general field stars belonging to the main sequence (Class V on the Yerkes *Atlas* system). While such data as are available indicate that many of the O and B stars found in the vicinity of the sun may be similar in color and absolute magnitude to the stars found in NGC 2362, it seems unwise to assume that they are identical, in view of Trumpler's work indicating the existence of sequences not yet observed photoelectrically.

[5] Stebbins, Whitford, and Johnson, "Photoelectric Magnitudes and Colors of Stars in Selected Areas 57, 61, and 68," *Ap. J.*, in press.

[6] *Lick Obs. Bull.*, **14**, No. 420, 154, 1930.

[7] Stebbins, Huffer, and Whitford, *Ap. J.*, **90**, 209, 1939.

[8] Private communication, April, 1950.

Very little can be said about the brightest stars ($P_{g_p} < 8$) in NGC 2362 regarding membership in the cluster, since published radial velocities[9] of the individual stars and proper motions[10] are available for the brightest star (τ Canis Majoris) only. Trumpler[11] has interpreted the difference between the radial velocity of τ Canis Majoris and the

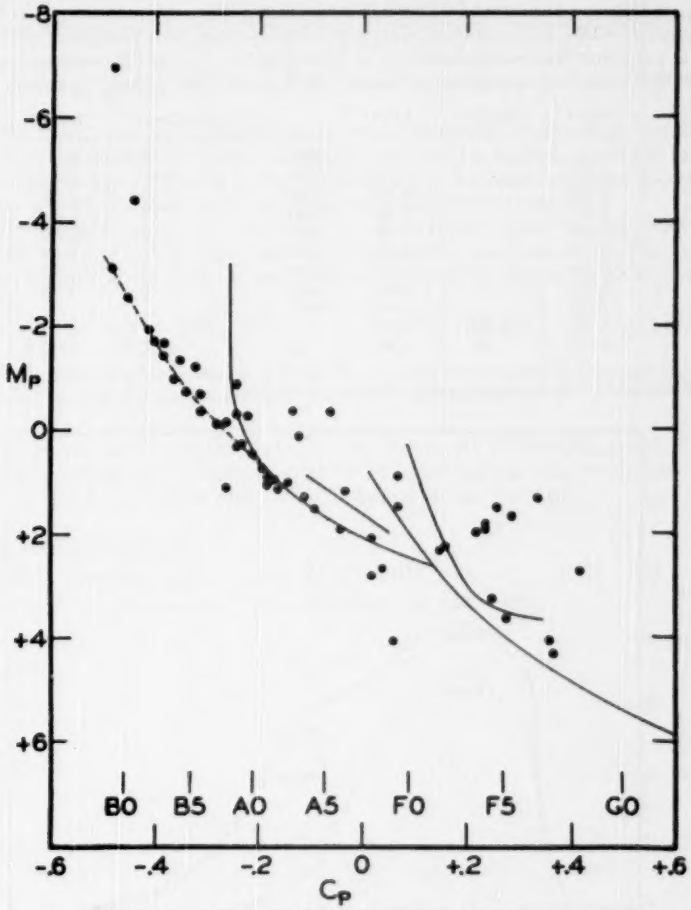

FIG. 5.—Color–absolute-magnitude array for NGC 2362

mean radial velocity of seven fainter cluster stars as an Einstein red-shift corresponding to a mass of 300 suns. If τ Canis Majoris is a member of the cluster, as would seem likely from its apparent position in the center of the cluster (see Fig. 1), its absolute photo-

[9] Struve and Pogo, *Ap. J.*, **68**, 335, 1928.

[10] B. J. Boss, *General Catalog of 33,342 Stars for the Epoch 1950* (Washington: Carnegie Institution of Washington, 1937).

[11] *Pub. A.S.P.*, **47**, 249, 1935.

graphic magnitude, $M_g = -7.0$, is a not unreasonable value for a supergiant. The published proper motion (".01) is not decisive. Morgan's classification of τ Canis Majoris as O9 V[12] does, however, create some doubt as to its membership in the cluster. The second

TABLE 3

FILTER-BAND CALIBRATIONS

Wave Length A	Relative Response			Wave Length A	Relative Response		
	Clear*	Yellow*	Blue*		Clear*	Yellow*	Blue*
3400			0.80	5000	7.82	5.24	1.05
3500	1.00		2.80	5200	4.60	4.35	0.44
3600	3.50		5.43	5400	2.90	2.86	0.13
3700	7.05		6.00	5600	1.68	1.65	
3800	7.50		6.59	5800	0.92	0.90	
3900	8.10		7.07	6000	0.50	0.49	
4000	8.39		6.80	6200	0.25	0.25	
4200	8.35		5.94	6400	0.10	0.10	
4400	7.78		4.55	6600			
4600	6.90	0.20	2.80	λ_{eff}	4500 A	5240 A	4215 A
4800	6.35	1.60					

* The filter glasses used are described in Stebbins, Whitford, and Johnson. In press.

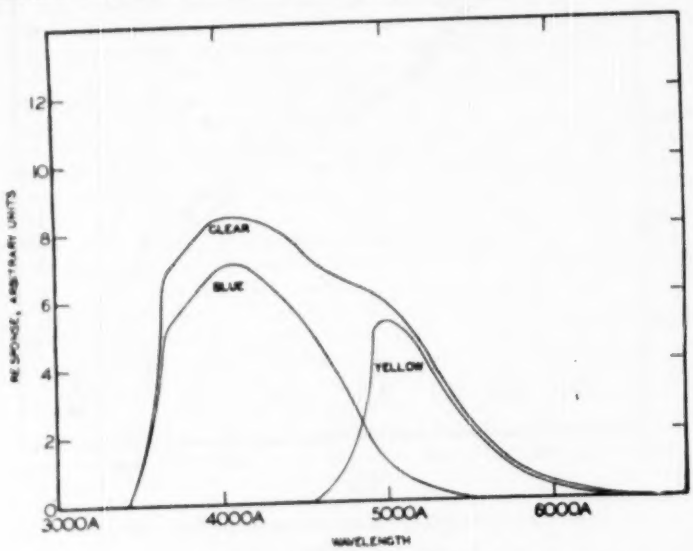

FIG. 6.—Filter-band calibrations

brightest star, No. 46, is quite far from the center of the cluster and may not be a member. τ Canis Majoris is a single-line spectroscopic binary.[9] Nothing can be said, from presently available data, regarding possible binaries among the other members of the cluster.

[12] Private communication; see Table 2.

With regard to cluster membership for stars for which $Pg_p > 8$, a statistical argument can be made. According to van Rhijn,[13] the average number of stars brighter than $m_{pg} = 12$ in the part of the sky near NGC 2362 is 100 per square degree. Since the area of the cluster covered in the present investigation is about 0.02 square degree, the expectation is two field stars brighter than $m_{pg} = 12$ in the area of the cluster. The corresponding figures for $m_{pg} = 13$ are: 306 stars per square degree and 6 stars in the area of the cluster. These numbers indicate that practically all the stars brighter than $Pg_p = 12$ are cluster members; that many of the stars between $Pg_p = 12$ and $Pg_p = 13$ are members; and that little, or nothing, can be said regarding cluster membership for stars fainter than $Pg_p = 13$.

The filter bands used in this investigation were calibrated on the monochromator of the Washburn Observatory. These calibrations, reduced for equal intensity of radiation at all wave lengths, are given in Table 3 and Figure 6. As has been noted above, these filter bands are not the same as those of the International System.[14]

In computing the values of C_p and Pg_p given in Table 1 from the observed photoelectric color index, C_{pe}, and the observed photoelectric magnitude, P_e, the following equations, determined by means of certain selected stars[15] in the North Polar Sequence, were used:

$$C_p = 1.12C_{pe} + 1.08\,, \qquad Pg_p = P_e + 0.20C_p\,.$$

The observed photoelectric colors and magnitudes may be computed through these relations. C_{pe} and P_e are the values outside the earth's atmosphere.

I wish to express my sincere thanks to Drs. W. Baade, W. W. Morgan, and A. E. Whitford for many stimulating discussions. The development of the photometer used in this investigation was supported in part by the Office of Naval Research.

[13] *Groningen Pub.*, No. 43, 1929.

[14] Frederick H. Seares and Mary C. Joyner, *Ap. J.*, **98**, 312, 1943.

[15] See n. 5 for a list and the adopted colors and magnitudes of these stars.

A SPECTROSCOPIC COMPARISON BETWEEN HIGH- AND LOW-VELOCITY F DWARFS*

MARTIN AND BARBARA SCHWARZSCHILD
Princeton University Observatory
Received June 6, 1950

ABSTRACT

High-dispersion spectrograms were obtained with the coudé spectrograph of the 100-inch telescope at Mount Wilson for nine F stars, including three high-velocity and three low-velocity dwarfs. On the spectrograms, depths were measured for seventy-eight lines, equivalent widths for thirteen lines, and profiles for four lines. The relative temperatures and pressures of the nine stars were analyzed with the help of the photoelectric color indices determined by Dr. Eggen and the degrees of ionization derived from the line depths, and the various measurements were discussed as functions of temperature and pressure. The final data showed no difference between the high-velocity and the low-velocity F dwarfs, with the following exceptions: The *CH* features were found somewhat stronger relative to the *Fe* I lines in the high-velocity dwarfs than in the low-velocity dwarfs, indicating that the abundance ratio of *C* to *Fe* is probably approximately 2.5 times higher in the high-velocity dwarfs than in the low-velocity dwarfs. A second, though extremely uncertain, difference appeared in the equivalent widths of the *Fe* I lines, which indicated that possibly the abundance ratio of *H* to *Fe* might be larger in the high-velocity dwarfs by about a factor of 2 as compared with the low-velocity dwarfs.

I. INTRODUCTION

The stellar populations I and II differ greatly from each other in their kinematic behavior within a galactic system. In addition, they appear to differ also in their astrophysical characteristics.[1] This is indicated, first, by the existence of several types of stars which occur only, or nearly only, in one of the two stellar populations and, second, by such specific astrophysical differences as the observed abnormal weakness of the *CN* bands in high-velocity giants or the abnormal light-curves of high-velocity cepheids. Thus the question arises: Does there exist a general astrophysical difference between all stars of population I, on the one side, and all stars of population II, on the other side, and, if such a general difference exists, is it the basic chemical composition which distinguishes the two populations?

The purpose of the program here reported was to investigate, with the help of high-dispersion spectrograms of high- and low-velocity stars, whether the two stellar populations might differ basically in their chemical composition. To insure a very direct comparison of high- and low-velocity stars, the program stars were selected to be as similar as possible in spectral type and absolute magnitude. For the spectral type, F was chosen, since in this type an appreciable number of elements are represented by measurable lines in a limited spectral region, while, on the other hand, the crowding of the lines is not yet so large as to make the measurements unreliable. Regarding absolute magnitudes, dwarfs were chosen, since the atmospheres of dwarf stars seem to be theoretically well enough understood to assure that the observed data could be interpreted with fair certainty. The limitation to one spectral type and one absolute magnitude seemed appropriate for the present program, since every high-velocity star should contain abnormal chemical abundances if the two stellar populations have indeed a general difference in chemical composition.

* This investigation was made possible by a co-operative arrangement between the Mount Wilson and Palomar Observatories and the Princeton University Observatory.

[1] W. Baade, *Ap. J.*, **100**, 137, 1944.

II. OBSERVATIONS

The nine stars chosen for this program are listed in Table 1. The apparent magnitudes and color indices shown in this table were determined photoelectrically by Dr. Eggen. The great value of these accurate color indices for the present investigation will be apparent from the discussion in Section VI. The trigonometric parallaxes given in Table 1 are mainly based on the Yale parallax catalogue.[2] More recent parallax measurements, however, to which Miss Jenkins kindly provided the references, have also been taken into account. For star E the published values of the parallax are extremely discrepant. The value here used is based on new measurements made at the Yale University Observatory and at the Cape Observatory. These new measurements were made available most generously by Miss Jenkins and Dr. Jackson. If the trigonometric parallax determination of star H had been available at the beginning of this program, this star would not have been included; the spectroscopic parallax used as a guide indicated a much lower absolute magnitude for star H than now seems likely.

The proper motions and radial velocities were taken from the Yale bright-star catalogue.[3] From these data the space velocities, reduced for the solar motion, were computed. These velocities, listed in the last column of Table 1, show that stars B, D, F, and G are high-velocity stars, while the remaining five stars have low velocities.

For the nine stars spectrograms were obtained with the coudé spectrograph of the 100-inch telescope at Mount Wilson. Altogether, thirty plates were taken; twelve of these, however, could not be used because of over- or underexposure. The eighteen plates, two for each star, which showed a density appropriate for photometry are listed in Table 2. This table also contains two plates taken of the sky in the zenith just before sunset, for comparison purposes. All plates were taken with the 32-inch camera of the coudé spectrograph, giving a dispersion of 10.36 A/mm. The width of the spectrograph slit was chosen to correspond to 0.015 mm on the plate. The spectra were widened by trailing, so that they had uniform density over a width of 0.3 mm on the plate. Eastman IIa-O plates were used throughout.

Through generous advice and much active help from Dr. Olin Wilson, it was possible during this program to keep the auxiliary optics providing the calibration-step spectra in such adjustment that no arbitrary corrections to the step intensities had to be applied in the subsequent photometric reductions. The exposure times of the calibration spectra were chosen sufficiently long that in the majority of cases they differed by less than a factor of 3 from the effective exposure times of the stellar spectra (which, because of the trailing, were appreciably shorter than the total stellar exposure times).

III. MEASUREMENTS

The twenty spectra of Table 2 were registered with the Mount Wilson microphotometer from λ 4220 to λ 4680. A hundred fold enlargement was used for the recording. The width of the photometer slit was chosen to correspond to 0.005 mm on the plate. The calibration spectra were registered at two wave lengths, λ 4550 and λ 4300; one of these two registrations was made immediately before the recording of the star spectrum and one immediately afterward. The two calibration registrations were found to give calibration-curves so nearly alike that only one mean calibration-curve was used for each plate for the entire wave-length region in question.

On the registrations of the stellar spectra three types of measurements were made: First, line depths were measured for all the lines between λ 4240 and λ 4660 for which the centers appeared to be essentially unblended. A total of seventy-eight lines, representing

[2] Schlesinger and Jenkins, *General Catalogue of Stellar Parallaxes* (New Haven: Yale University Observatory, 1935).

[3] Schlesinger and Jenkins, *Catalogue of Bright Stars* (2d ed.; New Haven: Yale University Observatory, 1940).

TABLE I. DATA FOR THE NINE STARS OBSERVED

	Name	α 1900	δ 1900	Sp.T. Mt.W.	M_{ph} Eggen	CI Eggen
A	74 Ori	$6^h10.^m8$	+12° 18′	F5	5.38	+0.34
B	-	8 54.0	-15 45	F5	6.18	+0.42
C	40 Leo	10 14.3	+19 59	F5	5.14	+0.37
D	-	12 10.0	- 9 44	F3	6.46	+0.35
E	53 Vir	13 6.7	-15 40	F5	5.33	+0.37
F	-	14 31.7	-11 53	F5	6.53	+0.35
G	5 Ser	15 14.2	+ 2 9	F6	5.46	+0.47
H	20 Oph	16 44.3	-10 36	F5	5.00	+0.40
K	99 Her	18 3.2	+30 33	F5	5.42	+0.43

TABLE I--Continued

	π (trig.)	M_{ph} (trig.)	μ_α	μ_δ	R.V.	V $\frac{km}{sec}$
A	.042± 7	3.5±0.3	+0.082	+0.188	+ 9	35
B	.026±10	3.3±0.7	+0.239	+0.216	+122	130
C	.051±11	3.7±0.4	-0.233	-0.221	+ 6	15
D	.031± 6	3.9±0.4	+0.031	-1.024	+ 6	150
E	.029± 6	2.6±0.4	+0.095	-0.293	- 14	50
F	.036± 4	4.3±0.2	-0.876	+0.359	- 70	130
G	.038± 6	3.4±0.3	+0.369	-0.521	+ 53	105
H	.014± 8	0.7±1.0	+0.090	-0.100	0	45
K	.065± 4	4.5±0.1	-0.098	+0.067	+ 1	20

TABLE 2. DATA FOR THE TWENTY PLATES USED

Star	Coude' Plate	Date 1948	Expos. Middle (P.S.T.)	Expos. time (min.)	Seeing
A	5103	Feb 24	7^h44^m	81	<1
"	5113	Mar 20	7 20	40	<1
B	5107	Feb 25	10 10	210	1-2
"	5119	Mar 21	8 43	80	2
C	5105	Feb 24	13 50	80	<<1
"	5114	Mar 20	8 35	70	<1
D	5108	Feb 25	14 38	300	<1
"	5120	Mar 21	10 33	120	2
E	5121	Mar 21	12 05	50	2
"	5172	May 13	8 41	60	1-2
F	5116	Mar 20	13 59	270	<1
"	5179	May 14	8 58	120	2
G	5125	Mar 21	16 16	25	2-3
"	5126	Mar 21	16 46	25	2-3
H	5117	Mar 20	16 48	45	1
"	5181	May 14	11 04	47	2
K	5176	May 13	14 16	25	2-3
"	5177	May 13	14 48	25	2-3
Sky	5171a	May 13	6 24	3	-
"	5178a	May 14	6 42	15	-

nine different elements, was included. Second, equivalent widths were measured for thirteen unblended lines of *Fe* I. Third, profiles were determined for four *Fe* I lines which were selected to be free from blending and to be sufficiently weak that complications from damping and from radiation-transfer problems would be largely avoided.

As a basis for the three types of measurement, the continuum in each of the twenty spectra was derived in the following way. The entire wave-length range was divided into twenty sections, each 23 A long, and in each section the mean height of the continuum was measured. The twenty measurements were plotted against wave lengths, and a smooth curve was drawn through the twenty points. Readings from this curve were then taken to represent the actual continuum. It appears likely that smoother and hence more consistent data are obtained from the continuum by this procedure than by drawing the continuum directly into the tracings.

Table 3 gives the results for the line depths in terms of the logarithm of the intensity of the continuum divided by the intensity in the line center. Each entry in Table 3 represents the mean of measurements on two plates. The accuracy of the line-depth measurements could be determined from the differences found between the two plates of each star. Thus the probable error of a line depth as given in Table 3 was found to be ± 0.008, or, in terms of magnitudes, ± 0.020 mag. At the bottom of Table 3 are added measurements at three points in $H\gamma$. The measurements of equivalent widths are given in Table 4. As before, each value is based on two plates. The probable error of one entry of Table 4, again derived from the differences between two plates of the same star, is, on the average, ± 0.007 A. The measurements of line profiles are given in Table 5. The profiles were derived from four *Fe* I lines at λλ 4447.72, 4547.85, 4602.94, and 4625.05. For each star one profile is given which represents the mean of the four individual lines measured. To obtain this mean, despite the different equivalent widths of the four lines, the individual measurements were expressed in terms of the quantity i, defined by

$$i = \frac{I_C - I_L}{I_C}/W .$$

In terms of i the area of the profile is normalized to 1, a procedure which makes possible the averaging of line profiles with somewhat different equivalent widths. Each entry in Table 5 is based on eight measurements from four lines on two plates.

IV. ROTATIONAL VELOCITIES

Before taking up the analysis of the line-intensity measurements, the differences in the line profiles of the nine stars may be discussed. Since the program stars, with the exception of star H, lie on or near the main sequence, it appears probable that, for the relatively weak lines measured, the broadening produced by turbulence or atomic processes will be inappreciable in comparison with the width of the instrumental profile. Correspondingly, the instrumental profile and rotational broadening should be the main determining factors.

The instrumental profile was determined by measuring three iron-arc comparison lines, differing appreciably in strength, on two plates (Nos. 5107 and 5177), differing greatly in exposure time. All these measurements agreed well with one another and gave the instrumental profile tabulated in the second column of Table 7.

The lines used for profile measurements have an average equivalent width of 0.09 A. Since they lie on the flat portion of the curve of growth, their true width will be about equal to their equivalent width. Hence, this true line width (without rotation) is small but not negligible in comparison with the instrumental profile. To take account at least approximately of the effect of the true line width, the instrumental profile was convoluted with a rectangular profile having a width of 0.09 A. The result is given in the fourth column of Table 7. This i_0 profile should give the measured line profiles for nonrotating

TABLE 3. MEASUREMENTS OF LINE DEPTHS, LOG I_C/I_L

No.	λ	El.	EP	A	B	C	D	E	F	G	H	K	Sky
1	4246.83	ScII	0.31	.14	.24	.16	.20	.24	.19	.30	.32	.28	.28
2	4250.12	FeI	2.46	.14	.22	.18	.20	.24	.18	.30	.28	.28	.39
3	4250.79	FeI	1.55	.18	.28	.21	.23	.26	.20	.34	.32	.32	.45
4	4254.35	CrI	0.00	.16	.25	.18	.20	.21	.18	.33	.28	.31	.43
5	4260.48	FeI	2.39	.24	.29	.28	.27	.30	.26	.42	.34	.38	.52
6	4264.21	FeI	3.33	.05	.06	.08	.06	.08	.08	.14	.10	.10	.16
7	4266.97	FeI	2.72	.06	.08	.08	.06	.10	.09	.15	.12	.10	.16
8	4281.96	CH	-	.03	.09	.04	.05	.05	.06	.08	.06	.07	.14
9	4282.41	FeI	2.17	.14	.17	.15	.17	.18	.16	.28	.22	.26	.30
10	4283.01	CaI	1.88	.12	.18	.14	.16	.16	.14	.24	.19	.22	.31
11	4303.88	CH	-	.08	.22	.11	.13	.12	.14	.22	.12	.22	.31
12	4311.57	CH	-	.08	.16	.10	.12	.12	.14	.19	.10	.20	.32
13	4312.21	CH	-	.06	.15	.10	.10	.10	.10	.18	.10	.16	.28
14	4323.14	CH	-	.08	.14	.09	.12	.12	.12	.20	.10	.15	.28
15	4323.90	CH	-	.08	.13	.10	.12	.12	.12	.18	.11	.15	.28
16	4375.93	FeI	0.00	.12	.16	.12	.15	.17	.13	.24	.20	.22	.28
17	4379.24	VI	0.30	.06	.10	.09	.09	.09	.08	.19	.13	.12	.20
18	4383.55	FeI	1.48	.32	.45	.38	.38	.40	.34	.54	.47	.50	.58
19	4387.90	FeI	3.06	.08	.08	.10	.06	.08	.08	.14	.14	.10	.14
20	4388.41	FeI	3.59	.08	.08	.13	.10	.11	.10	.20	.14	.12	.19
21	4395.85	TiII	1.24	.08	.10	.10	.08	.12	.09	.16	.14	.10	.14
22	4404.75	FeI	1.55	.24	.36	.31	.32	.32	.30	.50	.38	.42	.53
23	4415.12	FeI	1.60	.20	.24	.24	.26	.28	.24	.39	.34	.32	.47
24	4416.82	FeII	2.77	.10	.10	.13	.10	.14	.10	.23	.19	.14	.14
25	4417.72	TiII	1.16	.12	.15	.12	.18	.17	.12	.24	.21	.18	.18
26	4433.22	FeI	3.64	.08	.10	.09	.06	.12	.09	.18	.12	.12	.18
27	4435.69	CaI	1.88	.12	.18	.12	.14	.15	.14	.22	.20	.18	.22
28	4442.34	FeI	2.19	.11	.16	.13	.16	.17	.14	.27	.20	.18	.30
29	4443.80	TiII	1.08	.13	.18	.16	.20	.22	.18	.31	.29	.23	.24
30	4444.56	TiII	1.11	.06	.08	.08	.08	.10	.09	.16	.13	.09	.11
31	4447.72	FeI	2.21	.10	.16	.14	.12	.16	.14	.28	.20	.20	.28
32	4453.31	TiI	1.42	.04	.06	.08	.04	.05	.06	.10	.08	.06	.11
33	4461.65	FeI	0.09	.13	.16	.14	.14	.17	.16	.24	.22	.20	.22
34	4468.49	TiII	1.13	.12	.20	.17	.20	.23	.18	.30	.29	.24	.22
35	4470.48	NiI	3.38	.06	.06	.10	.06	.10	.10	.14	.10	.09	.12
36	4470.86	TiII	1.16	.07	.08	.10	.10	.11	.09	.16	.15	.10	.10
37	4484.23	FeI	3.59	.09	.10	.10	.08	.12	.09	.19	.14	.12	.18
38	4485.68	FeI	3.67	.06	.07	.08	.05	.07	.06	.15	.10	.08	.12
39	4489.74	FeI	0.12	.07	.10	.09	.08	.11	.09	.18	.13	.13	.15
40	4490.77	FeI	3.93	.07	.06	.08	.06	.09	.07	.15	.10	.07	.13

TABLE 3. --Continued

No.	λ	El.	EP	A	B	C	D	E	F	G	H	K	Sky
41	4491.40	FeII	2.84	.09	.09	.10	.08	.14	.10	.20	.20	.12	.12
42	4494.57	FeI	2.19	.10	.16	.16	.16	.18	.15	.26	.22	.20	.26
43	4508.28	FeII	2.84	.08	.12	.10	.14	.15	.13	.21	.21	.14	.14
44	4512.73	TiI	0.83	.04	.06	.02	.07	.05	.07	.10	.06	.06	.10
45	4515.34	FeII	2.83	.10	.10	.12	.10	.18	.12	.16	.22	.13	.16
46	4526.94	CaI	2.70	.08	.07	.08	.08	.08	.10	.16	.10	.10	.15
47	4534.78	TiI	0.83	.06	.10	.08	.10	.11	.08	.17	.11	.12	.15
48	4545.96	CrI	0.94	.05	.09	.08	.07	.09	.08	.14	.11	.10	.12
49	4547.85	FeI	3.53	.08	.08	.08	.10	.08	.08	.14	.12	.10	.12
50	4548.76	TiI	0.82	.05	.08	.06	.07	.06	.06	.08	.07	.07	.10
51	4554.03	BaII	0.00	.18	.20	.19	.21	.26	.18	.32	.29	.24	.27
52	4555.49	TiI	0.84	.08	.06	.05	.06	.06	.06	.10	.07	.06	.09
53	4558.66	CrII	4.06	.11	.09	.10	.10	.16	.10	.19	.22	.10	.12
54	4563.76	TiII	1.22	.14	.18	.16	.16	.21	.15	.28	.28	.20	.20
55	4568.31	TiII	1.22	.04	.04	.04	.04	.05	.05	.08	.06	.04	.04
56	4571.97	TiII	1.56	.17	.21	.18	.20	.24	.18	.30	.30	.22	.24
57	4574.72	FeI	2.27	.04	.04	.06	.05	.06	.05	.10	.09	.03	.09
58	4576.33	FeII	2.83	.09	.06	.08	.06	.12	.08	.13	.16	.08	.10
59	4578.56	CaI	2.51	.07	.08	.08	.08	.10	.06	.14	.12	.09	.14
60	4582.84	FeII	2.83	.10	.04	.08	.06	.12	.08	.14	.14	.06	.08
61	4588.22	CrII	4.05	.09	.07	.10	.09	.10	.11	.16	.17	.10	.08
62	4589.96	TiII	1.23	.08	.12	.12	.11	.14	.12	.18	.18	.12	.12
63	4602.00	FeI	1.60	.05	.06	.05	.06	.06	.04	.12	.09	.09	.12
64	4602.94	FeI	1.48	.08	.12	.10	.11	.13	.10	.19	.16	.14	.20
65	4616.14	CrI	0.98	.06	.07	.08	.06	.09	.08	.13	.12	.09	.14
66	4619.29	FeI	3.59	.08	.07	.08	.08	.10	.10	.14	.12	.10	.13
67	4620.51	FeII	2.82	.06	.06	.06	.04	.08	.07	.12	.12	.06	.06
68	4625.05	FeI	3.23	.06	.08	.08	.07	.12	.07	.16	.09	.10	.14
69	4630.12	FeI	2.27	.06	.05	.06	.06	.08	.05	.09	.09	.06	.12
70	4634.11	CrII	4.05	.08	.04	.07	.07	.12	.07	.12	.12	.05	.08
71	4635.33	FeII	5.93	.02	.02	.06	.04	.04	.04	.04	.06	.02	.04
72	4637.51	FeI	3.27	.08	.06	.10	.09	.10	.10	.14	.12	.10	.13
73	4638.02	FeI	3.59	.06	.06	.08	.08	.09	.08	.13	.14	.10	.13
74	4643.47	FeI	3.64	.08	.04	.08	.06	.08	.08	.12	.10	.06	.11
75	4646.17	CrI	1.03	.10	.11	.11	.10	.12	.12	.20	.16	.12	.17
76	4648.66	NiI	3.40	.10	.06	.10	.09	.10	.09	.14	.16	.10	.13
77	4651.28	CrI	0.98	.06	.05	.07	.07	.08	.07	.12	.10	.08	.12
78	4652.16	CrI	1.00	.06	.08	.07	.08	.08	.08	.14	.12	.12	.15
H_γ	4340.47	center		.52	.54	.58	.56	.68	.56	.65	.66	.58	.44
"	4339.10	interm.		.20	.14	.22	.18	.22	.21	.18	.18	.14	.14
"	4342.64	wing		.12	.08	.14	.11	.14	.14	.10	.12	.09	.06

TABLE 4. MEASUREMENTS OF EQUIVALENT WIDTHS, IN 0.001Å

Line No.	A	B	C	D	E	F	G	H	K	Sky	Sun
18	312	352	352	272	328	358	434	362	365	951	1070
22	258	268	314	224	262	284	363	282	276	629	749
26	70	57	70	32	82	90	103	77	65	104	96
31	98	91	106	86	132	115	132	133	105	164	152
38	53	48	64	42	60	55	82	80	48	72	81
42	118	96	130	108	142	134	153	148	102	165	176
49	76	60	75	66	65	85	74	92	66	70	85
57	68	31	46	28	52	54	52	75	22	60	56
63	62	36	48	34	35	35	56	70	47	56	74
64	91	75	86	74	102	96	106	108	88	114	119
68	78	46	70	47	85	61	73	79	62	85	92
69	66	24	62	48	63	42	58	77	37	71	74
74	92	35	65	34	76	84	92	81	44	86	74

TABLE 5. MEASUREMENTS OF LINE PROFILES

A		B		C		D		E	
Δλ	i	Δλ	i	Δλ	i	Δλ	i	Δλ	i
-0.330	0.55	-0.240	0.50	-0.278	1.02	-0.259	0.52	-0.259	0.71
-0.227	1.11	-0.136	1.54	-0.175	1.71	-0.155	1.60	-0.155	1.71
-0.123	1.73	-0.032	3.38	-0.071	2.27	-0.052	2.55	-0.052	2.59
-0.019	1.95	+0.071	2.91	+0.032	2.22	+0.052	2.67	+0.052	2.45
+0.084	1.86	+0.175	1.24	+0.136	1.50	+0.155	1.63	+0.155	1.43
+0.188	1.42	+0.278	0.12	+0.240	1.02	+0.259	0.70	+0.259	0.54
+0.291	0.82								
+0.395	0.27								

TABLE 5.--Continued

F		G		H		K		Sky	
Δλ	i	Δλ	i	Δλ	i	Δλ	i	Δλ	i
-0.220	1.22	-0.220	0.68	-0.240	0.79	-0.240	0.42	-0.291	0.46
-0.117	1.96	-0.117	2.42	-0.136	1.69	-0.136	1.51	-0.188	1.11
-0.013	2.19	-0.013	3.50	-0.032	2.52	-0.032	3.09	-0.084	2.49
+0.091	1.97	+0.091	2.19	+0.071	2.45	+0.071	2.85	+0.019	3.06
+0.194	1.40	+0.194	0.72	+0.175	1.48	+0.175	1.26	+0.123	1.65
+0.298	0.77			+0.278	0.58	+0.278	0.55	+0.227	0.71

stars. This expectation is verified by the fact that the narrowest profiles actually measured, i.e., those of stars B and G, agree well with the i_0.

Finally, the i_0 profile was convoluted with three rotation profiles corresponding to projected equatorial velocities ($v \sin i$) of 8, 16, and 25 km/sec, respectively. The resulting profiles i_0 to i_s are shown in Figure 1, together with the measurements for stars A and B, which happen to represent the widest and the narrowest of the measured profiles.

The rotational velocity was determined for each star by graphically comparing the measured profile from the stellar spectrum with the computed rotation profiles. The results are given in the fourth column of the summarizing Table 10. Each value given there is estimated to have a probable error of less than ± 5 km/sec. The rotational velocities thus found show an appreciable dependence on the color index. The five bluest stars have an average $v \sin i$ of 14 km/sec for an average color index of 0.36, corresponding approximately to F5 in the Yerkes scale. On the other hand, the three reddest stars (excluding the sun and the giant H) have a mean $v \sin i$ of 2 km/sec for an average color index of 0.44, corresponding approximately to F8. Thus the sample of stars here investigated seems to represent the tail end of the fast-rotating, early-type stars.

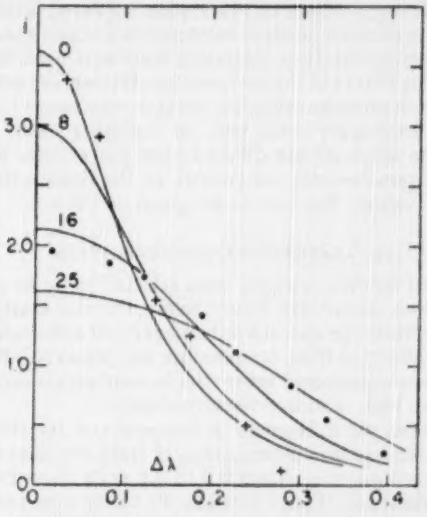

FIG. 1.—Line profiles. *Curves:* computed profiles for various speeds of rotation (numbers on the curves give $v \sin i$ in km/sec); *dots:* measurements for star A; *crosses:* measurements for star B.

The results of the profile measurements do not indicate a significant difference in rotational velocity between the high-velocity and the low-velocity stars.

V. PSEUDO-CURVES OF GROWTH

The purpose of the line-depth measurements was to obtain relative abundances. For this purpose it is necessary to derive for each star the pseudo-curve of growth which relates the line depths with the relative atom numbers characterized by log X values. To derive these curves it is necessary either to rely on known f values or to use log X values of a particular star for which the curve of growth has already been determined. Here solar log X values were used in the following manner.

From Allen's equivalent widths[4] and K. O. Wright's solar curve of growth,[5] log X values for the sun were derived for all the lines listed in Table 3. The results are shown in the last column of Table 6. Of all the lines listed, only the thirty-one lines of *Fe* I were used for the determination of the pseudo-curves of growth. These thirty-one lines were combined according to their strength into seven groups, and for each group the mean solar log X value was determined. For the same seven groups of lines, mean line depths were computed for each star (here not log $[I_C/I_L]$ but log $[I_C/(I_C - I_L)]$ was used for the line depth to obtain curves of growth of the typical shape). Finally, the mean line depths were plotted against the mean solar log X values for each star, and a smooth curve was drawn through the seven normal points. Thus the pseudo-curve of growth was obtained for each star.

The direct use of solar log X values for the F stars appeared justified for the following reasons: The difference in electron pressure between the sun and the F stars had no effect, since only lines of one element and one ionization state were used for the construction of the curves of growth. The effects of the temperature differences between the sun and the F stars were sufficiently small to be negligible because, on the one hand, the temperature differences themselves were fairly small and, on the other hand, the mean excitation potential for each of the seven groups differed from the average by at most 1.1 volts.

With the help of the pseudo-curves of growth, all the line-depth measurements were transformed into log X values. The results are given in Table 6.

VI. TEMPERATURES AND PRESSURES

The nine stars chosen for this problem were selected to be as similar as possible in spectral type and absolute magnitude. Nevertheless, the nine stars will differ somewhat from one another in spectral type and absolute magnitude and consequently in temperature and pressure. The effects of these temperature and pressure differences on the measured quantities have to be determined before the measurements can be analyzed for possible differences between high- and low-velocity stars.

It had been hoped that the differences in temperatures for the nine stars could be found by determining the excitation temperatures from the lines of *Fe* I. Accordingly, eighteen *Fe* I lines, covering a range from 0.0 to 3.6 volts in excitation potential, were selected (the seven weakest and the six strongest *Fe* I lines were not used, since they are based on the uncertain ends of the pseudo-curves of growth). For each of the eighteen lines the mean log X value was formed from the nine stars, and this mean was subtracted from the individual values. Then for each star the residual log X values were considered as a function of the excitation potential; and the excitation temperature, in terms of $\Delta\theta = (5040/\theta) - (5040/\theta)$, was determined with the help of a least-squares solution. The results are given in the fifth column of Table 10. The probable error of one $\Delta\theta$ value was found to be, on the average, ± 0.022. Since none of the $\Delta\theta$ values exceed the probable error by an appreciable factor, the $\Delta\theta$ values determined from *Fe* I cannot be considered significant. Since, further, no other element covers a larger range in excitation potential with a sufficient number of measured lines than that covered by *Fe* I, it had to be concluded that the temperature differences between the nine stars could not be determined with the help of the excitation temperatures.

There remain two quantities from which the temperature differences may be determined. The first quantity is Dr. Eggen's photoelectric color index, given in the seventh column of Table 1. The second quantity is the degree of ionization which is derived by first forming the mean log X value from all the measured lines of a neutral element, then forming the corresponding mean from the ionized lines of the same element, and, finally,

[4] *Mt. Stromlo Commonwealth Solar Obs.*, Mem. No. 5, Part II, 1934.

[5] *Ap. J.*, 99, 249, 1944.

TABLE 6. LOG X VALUES DERIVED FROM LINE DEPTHS

No.	A	B	C	D	E	F	G	H	K	Sky	Sun
1	2.73	3.12	2.58	2.95	3.10	2.92	2.69	3.32	2.97	2.35	2.40
2	2.73	2.94	2.82	2.95	3.10	2.78	2.69	3.03	2.97	2.96	3.25
3	3.25	3.41	3.12	3.17	3.23	3.05	3.09	3.32	3.24	3.30	3.25
4	3.04	3.19	2.82	2.95	2.76	2.78	2.99	3.03	3.17	3.21	3.19
5	3.68	3.46	3.62	3.50	3.54	3.55	3.57	3.45	3.59	3.60	3.58
6	0.68	0.97	1.08	0.92	0.97	1.17	1.06	0.93	1.19	1.38	1.36
7	0.92	1.27	1.08	0.92	1.23	1.31	1.18	1.20	1.19	1.38	1.43
8	-	1.38	-	0.73	0.52:	0.86	-	-	0.86	1.16	0.31
9	2.73	2.40	2.45	2.61	2.42	2.51	2.50	2.46	2.77	2.48	2.24
10	2.34	2.51	2.26	2.51	2.17	2.18	2.09	2.12	2.45	2.54	2.24
11	1.46	2.94	1.71	2.09	1.54	2.18	1.88	1.20	2.45	2.54	2.50
12	1.46	2.29	1.48	1.95	1.54	2.18	1.58	0.93	2.27	2.61	2.82
13	0.92	2.19	1.48	1.64	1.23	1.48	1.47	0.93	1.86	2.35	2.54
14	1.46	2.05	1.27	1.95	1.54	1.83	1.69	0.93	1.77	2.35	2.66
15	1.46	1.90	1.48	1.95	1.54	1.83	1.47	1.08	1.77	2.35	2.49
16	2.34	2.29	1.88	2.41	2.29	2.00	2.09	2.26	2.45	2.35	2.18
17	0.92	1.51	1.27	1.48	1.10	1.17	1.58	1.34	1.42	1.77	1.92
18	3.98	3.98	3.98	3.98	3.98	3.98	3.98	3.98	3.98	3.98	3.98
19	1.46	1.27	1.48	0.92	0.97	1.17	1.06	1.48	1.19	1.16	1.02
20	1.46	1.27	2.08	1.64	1.40	1.48	1.69	1.48	1.42	1.67	1.47
21	1.46	1.51	1.48	1.32	1.54	1.31	1.27	1.48	1.19	1.16	0.54
22	3.68	3.74	3.75	3.76	3.66	3.80	3.87	3.66	3.73	3.72	3.66
23	3.44	3.12	3.38	3.40	3.42	3.44	3.39	3.45	3.24	3.39	3.11
24	1.91	1.51	2.08	1.64	1.87	1.48	1.94	2.12	1.64	1.16	0.90
25	2.34	2.19	1.88	2.73	2.29	1.83	2.09	2.32	2.06	1.57	1.53
26	1.46	1.51	1.27	0.92	1.54	1.31	1.47	1.20	1.42	1.57	1.42
27	2.34	2.51	1.88	2.25	2.05	2.18	1.88	2.26	2.06	1.92	1.97
28	2.15	2.29	2.08	2.51	2.29	2.18	2.41	2.26	2.06	2.48	2.28
29	2.53	2.51	2.58	2.95	2.90	2.78	2.78	3.10	2.51	2.07	2.00
30	0.92	1.27	1.08	1.32	1.23	1.31	1.27	1.34	1.08	0.78	0.49
31	1.91	2.29	2.26	1.95	2.17	2.18	2.50	2.26	2.27	2.35	2.23
32	0.43:	0.97	1.08	0.54:	0.52:	0.86	0.65	0.68	0.75	0.78	0.62
33	2.53	2.29	2.26	2.25	2.29	2.51	2.09	2.46	2.27	1.92	2.12
34	2.34	2.76	2.70	2.95	2.96	2.78	2.69	3.10	2.63	1.92	2.06
35	0.92	0.97	1.48	0.92	1.23	1.48	1.06	0.93	1.08	0.89	1.03
36	1.17	1.27	1.48	1.64	1.40	1.31	1.27	1.64	1.19	0.65	0.54
37	1.68	1.51	1.48	1.32	1.54	1.31	1.58	1.48	1.42	1.57	1.40
38	0.92	1.11	1.08	0.73	0.81	0.86	1.18	0.93	0.98	0.89	1.02
39	1.17	1.51	1.27	1.32	1.40	1.31	1.47	1.34	1.53	1.29	1.79
40	1.17	0.97	1.08	0.92	1.10	1.00	1.18	0.93	0.86	1.02	0.68

TABLE 6.--Continued

No.	A	B	C	D	E	F	G	H	K	Sky	Sun
41	1.68	1.38	1.48	1.32	1.87	1.48	1.69	2.26	1.42	0.89	0.71
42	1.91	2.29	2.58	2.51	2.42	2.38	2.24	2.46	2.27	2.18	2.38
43	1.46	1.78	1.48	2.25	2.05	2.00	1.75	2.32	1.64	1.16	1.17
44	0.43:	0.97	-	1.11	0.52:	1.00	0.65	-	0.75	0.65	0.70
45	1.91	1.91	1.88	1.64	2.42	1.83	1.27	2.46	1.53	1.38	0.99
46	1.46	1.11	1.08	1.32	0.97	1.48	1.27	0.93	1.19	1.29	0.93
47	0.92	1.51	1.08	1.64	1.40	1.17	1.36	1.08	1.42	1.29	1.66
48	0.68	1.38	1.08	1.11	1.10	1.17	1.06	1.08	1.19	0.89	1.20
49	1.46	1.27	1.08	1.64	0.97	1.17	1.06	1.20	1.19	0.89	1.10
50	0.68	1.27	0.66	1.11	0.66	0.86	0.44:	0.51:	0.86	0.65	0.81
51	3.25	2.76	2.95	3.00	3.23	2.78	2.89	3.10	2.63	2.30	2.35
52	1.46	0.97	0.49:	0.92	0.66	0.86	0.65	0.51:	0.75	0.53:	0.61
53	2.15	1.38	1.48	1.64	2.17	1.48	1.58	2.46	1.19	0.89	0.76
54	2.73	2.51	2.58	2.51	2.76	2.38	2.50	3.03	2.27	1.77	1.94
55	0.43:	0.66:	-	0.54:	0.52:	0.75	-	-	-	-	-
56	3.15	2.81	2.82	2.95	3.10	2.78	2.69	3.18	2.45	2.07	2.14
57	0.43:	0.66:	0.66	0.73	0.66	0.75	0.65	0.80	0.38::	0.53:	0.59
58	1.68	0.97	1.08	0.92	1.54	1.17	0.96	1.75	0.98	0.65	0.42
59	1.17	1.27	1.08	1.32	1.23	0.86	1.06	1.20	1.08	1.16	0.91
60	1.91	0.66:	1.08	0.92	1.54	1.17	1.06	1.48	0.75	0.42::	0.25
61	1.68	1.11	1.48	1.48	1.23	1.67	1.27	1.86	1.19	0.42::	0.60
62	1.46	1.78	1.88	1.82	1.87	1.83	1.47	1.99	1.42	0.89	0.93
63	0.68	0.97	0.49:	0.92	0.66	0.64:	0.85	0.80	1.08	0.89	0.79
64	1.46	1.78	1.48	1.82	1.70	1.48	1.58	1.75	1.64	1.77	1.79
65	0.92	1.11	1.08	0.92	1.10	1.17	0.96	1.20	1.08	1.16	1.33
66	1.46	1.11	1.08	1.32	1.23	1.48	1.06	1.20	1.19	1.02	1.04
67	0.92	0.97	0.66	0.54:	0.97	1.00	0.85	1.20	0.75	0.17::	0.22
68	0.92	1.27	1.08	1.11	1.54	1.00	1.27	0.80	1.19	1.16	1.22
69	0.92	0.82	0.66	0.92	0.97	0.75	0.54:	0.80	0.75	0.89	0.78
70	1.46	0.66:	0.86	1.11	1.54	1.00	0.85	1.20	0.63:	0.42::	0.25
71	-	-	0.66	0.54:	-	0.64:	-	-	-	-	-
72	1.46	0.97	1.48	1.48	1.23	1.48	1.06	1.20	1.19	1.02	1.16
73	0.92	0.97	1.08	1.32	1.10	1.17	0.96	1.48	1.19	1.02	1.06
74	1.46	0.66:	1.08	0.92	0.97	1.17	0.85	0.93	0.75	0.78	0.78
75	1.91	1.65	1.71	1.64	1.54	1.83	1.69	1.75	1.42	1.48	1.81
76	1.91	0.97	1.48	1.48	1.23	1.31	1.06	1.75	1.19	1.29	1.10
77	0.92	0.82	0.86	1.11	0.97	1.00	0.85	0.93	0.98	0.89	1.01
78	0.92	1.27	0.86	1.32	0.97	1.17	1.06	1.20	1.42	1.29	1.41

TABLE 7. INSTRUMENTAL AND ROTATIONAL LINE PROFILES

Instrumental Profile		Line=0.09Å Rot.=0 km/sec		Line=0.09Å Rot.=8 km/sec		Line=0.09Å Rot.=16 km/sec		Line=0.09Å Rot.=25 km/sec	
$\Delta\lambda$	i_i	$\Delta\lambda$	i_0	$\Delta\lambda$	i_1	$\Delta\lambda$	i_2	$\Delta\lambda$	i_3
0.00	3.80	0.00	3.62	0.00	3.00	0.00	2.14	0.00	1.61
.03	3.58	.05	3.09	.04	2.81	.04	2.09	.06	1.58
.06	2.93	.10	2.00	.08	2.38	.08	1.97	.12	1.48
.09	2.19	.15	1.18	.12	1.82	.12	1.77	.18	1.31
.12	1.57	.20	0.72	.16	1.28	.16	1.50	.24	1.08
.15	1.16	.25	0.44	.20	0.86	.20	1.20	.30	0.80
.18	0.87	.30	0.27	.24	0.58	.24	0.89	.36	0.52
.21	0.64	.35	0.17	.28	0.38	.28	0.62	.42	0.30
.24	0.48	.40	0.11	.32	0.27	.32	0.42		
.27	0.35			.36	0.18	.36	0.28		
.30	0.27			.40	0.12	.40	0.19		

TABLE 8. EFFECT OF LINES ON COLORS

Star	$\lambda\lambda$	Δm	ΔCI
αPer F5Ib Supergiant	4225-4675 4000-5000 5000-6000	0.33 0.29 0.11	0.18
αCanMi F5IV Subgiant	4225-4675 4000-5000 5000-6000	0.21 0.20 0.06	0.14
40 Leo F7+V dwarf	4225-4675	0.13	(0.09)

TABLE 9. RELATIVE ABUNDANCES, $\overline{\log X}$

Element	Fe I	Fe II	Ti I	Ti II	Cr I	Cr II
No. of Lines Mean EP	18 2.46	7 2.82	4 0.98	9 1.21	6 0.82	3 4.05
A	1.63	1.64	0.87	2.01	1.40	1.76
B	1.64	1.25	1.18	2.07	1.57	1.05
C	1.64	1.39	0.83	2.05	1.40	1.27
D	1.66	1.32	1.05	2.24	1.51	1.41
E	1.65	1.75	0.81	2.23	1.41	1.65
F	1.63	1.45	0.94	2.03	1.52	1.38
G	1.63	1.36	0.78	2.00	1.44	1.23
H	1.66	1.94	0.70	2.35	1.53	1.84
K	1.66	1.24	0.95	1.87	1.54	1.00
Sky	1.63	0.83	0.81	1.43	1.49	0.58
Sun	1.63	0.67	0.93	1.35	1.66	0.54

TABLE 9.--Continued

Element	Ca I	V I	Ni I	Sc II	Ba II	CH
No. of Lines Mean EP	4 2.24	1 0.30	2 3.39	1 0.31	1 0.00	5 -
A	1.83	0.92	1.42	2.73	3.25	1.35
B	1.85	1.31	0.97	3.12	2.76	2.27
C	1.58	1.27	1.48	2.58	2.95	1.48
D	1.85	1.48	1.20	2.95	3.00	1.92
E	1.61	1.10	1.23	3.10	3.23	1.48
F	1.68	1.17	1.40	2.92	2.78	1.90
G	1.58	1.38	1.06	2.69	2.89	1.62
H	1.63	1.34	1.34	3.32	3.10	1.01
K	1.70	1.42	1.14	2.97	2.63	2.02
Sky	1.73	1.77	1.09	2.35	2.30	2.44
Sun	1.51	1.92	1.07	2.40	2.35	2.60

TABLE 10. SUMMARY OF CHARACTERISTICS

Star	Veloc.	Class	Rotat. v sin i (km/sec)	Excit. temp. $\Delta\theta$	Ioniz. $\log \frac{X_{II}}{X_I}$	Reduc. Color C_T	CH $\log \frac{X_{CH}}{X_{FeI}}$	Fe $\overline{\log w_{FeI}}$
A	low	dwarf	20	+0.022	+0.50	+0.34	-0.28	-1.03
B	high	dwarf	0	-0.035	-0.01	+0.42	+0.63	-1.18
C	low	dwarf	15	+0.063	+0.28	+0.37	-0.16	-1.04
D	high	dwarf	10	-0.012	+0.25	+0.35	+0.26	-1.20
E	low	subg.	10	-0.009	+0.59	+0.32	-0.17	-1.03
F	high	dwarf	15	+0.016	+0.26	+0.35	+0.27	-1.04
G	high	subg.	0	+0.011	+0.25	+0.42	-0.01	-0.97
H	low	giant	10	-0.020	+0.75	+0.33	-0.65	-0.96
K	low	dwarf	5	-0.036	-0.01	+0.43	+0.36	-1.13
Sky	low	dwarf	5	+0.010	-0.36	+0.49*	+0.81	-0.90
Sun	low	dwarf	(2)	-0.039	-0.55	+0.49*	+0.97	-0.88

* Measurement of Stebbins quoted by Eggen, Publ. ASP, 61, 258

taking the difference between these two means. From the present material the degree of ionization could be determined for *Fe*, *Ti*, and *Cr*. The final values given in the sixth column of Table 10 represent for each star the average degree of ionization from the three elements. (The mean log X values on which the degree of ionization was based are given in detail in the upper half of Table 9.)

The two quantities—the color index and the degree of ionization—both depend mainly on the temperature but are also affected by the pressure. Hence each alone cannot be used as a unique indicator of the temperature. The two quantities together, however, may be expected to give the temperature and the pressure simultaneously. In Figure 2 the degree of ionization is plotted against the color index. Most of the points in this figure are seen to fall close to one curve, as should be expected for main-sequence stars for

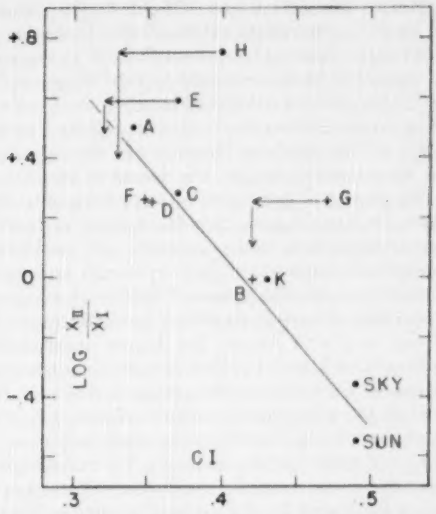

FIG. 2.—Degree of ionization versus color index. *Dots:* low-velocity stars; *crosses:* high-velocity stars; *sky:* data from sky spectra; *sun:* data from solar measurements of Allen.

which pressure and temperature are uniquely correlated. For the stars E, G, and H, however, the points do not lie on the curve, indicating that these three stars should not belong to the main sequence. The trigonometric absolute magnitudes given in Table 1, in conjunction with the color indices, indicate that star H might be a giant and stars E and G subgiants. To substantiate this tentative conclusion, it is necessary to investigate the expected pressure effect for both the color index and the degree of ionization.

The color of the continuum of the later F stars is rather little affected by pressure, i.e., absolute magnitude, since the continuous absorption processes are dominated by H^-, even for the giants, and since the wave-length dependence of H^- is independent of pressure. The measured color indices, however, are determined not only by the color of the continuum but also by the total absorption of the lines, and this absorption does vary with the absolute magnitude. The effect of the absorption lines on the measured color indices was estimated in the following way. Spectrum tracings are available from the Williams-Hiltner *Atlas*[6] for one F5 supergiant (α Per) and one F5 subgiant (α CMi).

[6] *Photometric Atlas of Stellar Spectra* (Ann Arbor: University of Michigan Press, 1946).

In addition, for a limited wave-length range there are available the spectrum tracings of the present program from which 40 Leo, star C, was chosen to represent F dwarfs. For the range of λλ 4225–4675 the total line absorption was determined in each of the three spectra with the help of a planimeter. The results are given in the third column of Table 8, in terms of the mean depression of the continuum by the absorption lines, expressed in magnitudes. The three numbers show a large increase with absolute brightness, corresponding to the increasing strength of absorption lines from dwarfs to supergiants. For the two F stars in the Williams-Hiltner *Atlas*, corresponding measurements were also made in the ranges from λ 4000 to λ 5000 and from λ 5000 to λ 6000. Since these two ranges should correspond approximately to those used in the color-index determinations, the difference of the average depression of the continuum by the lines in the two ranges should give directly the reddening effect of the absorption lines on the measured color indices. The results are given in the last column of Table 8. The value listed there for the dwarf star was obtained by an approximate extrapolation based on the line strength in the available wave-length range. The final numbers show that the measured color index of a subgiant should be corrected by approximately 0.05 mag. and that of a giant by approximately 0.07 mag. if the reduced color indices are to be used as pure temperature criteria. The corresponding corrections are indicated in Figure 2 by the three horizontal arrows. The reduced color indices are also listed in the seventh column of Table 10.

The pressure effect on the second quantity, the degree of ionization, is given directly by the Saha equation: The degree of ionization is proportional to the reciprocal of the electron pressure. For the later F stars, for which the opacity is provided by H^- and the free electrons by H, the electron pressure varies proportionally to the cube root of the gravity.[7] Since, for a given effective temperature, gravity varies approximately proportionally to the reciprocal of the three-fourths power of the luminosity, one finds altogether that the degree of ionization should vary proportionally to the fourth root of the luminosity. Correspondingly, if one wants to correct the degree of ionization of subgiants or giants for the pressure effect, one has to apply a correction just equal to one-tenth the absolute-magnitude difference. According to the assignment of stars E and G to the subgiant sequence and star H to the giant sequence and according to their respective color indices, one may estimate[8] that star E lies above the main sequence by 1.0 mag., star G by 1.5 mag., and star H by 3.5 mag. Correspondingly, the corrections (in logarithms) to the degree of ionization for the pressure are 0.1, 0.15, and 0.35, respectively, for the three stars. These corrections are indicated by the vertical arrows in Figure 2.

As shown by Figure 2, after appropriate corrections for the pressure effects were applied, all the stars fall satisfactorily close to one line, correlating the degree of ionization with the color index.

From the discussion in this section one may conclude that: (*a*) star H is probably a giant, stars E and G probably subgiants, and the remaining stars of this program dwarfs; (*b*) the measured color indices, after being corrected for line-absorption effect, may be used as a pure temperature criterion; and (*c*) the three high-velocity dwarfs—F, D, and B—do not show a significant difference from the three low-velocity dwarfs—A, C, and K—in the relation between the degree of ionization and the color index.

VII. RELATIVE ABUNDANCES

The results of the previous section make it possible now to analyze the measurements for possible abundance differences without disturbances from pressure or temperature differences. To avoid possible difficulties with pressure effects, the discussion will be limited to main-sequence stars; hence stars E, G, and H will be excluded from present con-

[7] B. Strömgren, *Pub. Copenhagen Obs.*, No. 138, esp. p. 33, 1944.

[8] O. Eggen, *Ap. J.*, **112**, 141, 1950.

siderations. To take account properly of temperature effects, all quantities will be considered as functions of the reduced color C_T.

The log X values obtained from the line-depth measurements are summarized in Table 9. In this table a mean log X value is given for every element, from all the available lines, for each star. (The last line in this table contains the values obtained for the sun from Allen's equivalent widths.) For each element the mean log X values were plotted against C_T. None of these plots, with the exception of that for *CH*, showed any significant difference between the three high-velocity dwarfs—B, D, and F—and the three low-velocity dwarfs—A, C, and K. Hence it appears that any possible differences between high- and low-velocity F dwarfs in the relative abundances of *Fe*, *Ti*, *Cr*, *Ca*, *V*, *Ni*, *Sc*, and *Ba* must be small, probably appreciably less than a factor of 2.

The plot for *CH* is given in Figure 3. It shows that *CH* is relatively stronger in the high-velocity dwarfs as compared with the low-velocity dwarfs. Comparing each high-velocity dwarf with a low-velocity dwarf of similar color (F with A, D with C, B with K), one obtains, for the logarithmic difference, 0.55, 0.44, and 0.25, respectively, or, in the mean, 0.41. Since all the log X values were derived from pseudo-curves of growth based on *Fe* I, the abundances here discussed are relative to the abundance of *Fe* I. To indicate this explicitly, values of log $(X_{CH}/X_{Fe\,I})$ were shown in Figure 3; the same values are also given in the eighth column of the summarizing Table 10. The X value of *CH* is proportional to the product of the pressure of *C* and the pressure of *H*, while the X value of *Fe* I is proportional to the pressure of *Fe* and the electron pressure (since *Fe* is mostly ionized). Further, since in F stars hydrogen provides both the opacity and the free electrons, the pressure of *H* and the electron pressure at a given depth are independent of any abundance ratios. The quantity $X_{CH}/X_{Fe\,I}$, therefore, is a direct measure of the abundance of *C* relative to *Fe*. Thus Figure 3 indicates that the abundance of *C* as compared with that of *Fe* may be about 2.5 times higher in the high-velocity F dwarfs than in the low-velocity F dwarfs.

The measurements made in $H\gamma$, which are listed at the bottom of Table 3, were plotted against C_T, in the same manner as were the log X values. These plots did not show any significant differences between the high- and the low-velocity dwarfs. This is in agreement with expectation, since any hydrogen phenomenon in an F spectrum should be independent of all possible differences in relative abundances.

The last data to be considered are the equivalent widths of *Fe* I lines listed in Table 4. The logarithms of these equivalent widths were plotted for each star against the solar log X values. These plots showed that the linear portions of the curves of growth were not covered with these measurements. Therefore, if an attempt had been made to fit theoretical curves of growth through the plotted points, a unique fit could not have been obtained, since, within limits, any sidewise shift corresponding to a change in *Fe* abundance could have been compensated by a vertical shift corresponding to a change in turbulent velocity. Instead, simple averages were formed from the log W values for each star. These averages are listed in the last column of Table 10 and are plotted against C_T in Figure 4 (again exclusive of the three nonmain-sequence stars, E, G, and H). A comparison of the solar points in this diagram with the mean of the F-star points shows an increase of the equivalent widths of the *Fe* I lines with decreasing temperature, as was to be expected. Further, the measurements indicate a correlation with rotational broadening; thus star A with strong rotation has large equivalent widths, while star B with slow rotation has relatively small ones. In addition to these two effects, Figure 4 shows some tendency for the high-velocity points to lie lower than the low-velocity points. On the average, for the three high-velocity dwarfs ($\overline{C_T} = 0.37$, $\overline{v \sin i} = 8$) as against the three low-velocity F dwarfs ($\overline{C_T} = 0.38$, $\overline{v \sin i} = 13$), the difference amounts to 0.07 in log W. This value is so uncertain, however, that, rather than establishing the existence of a difference, it only indicates that such a difference may exist.

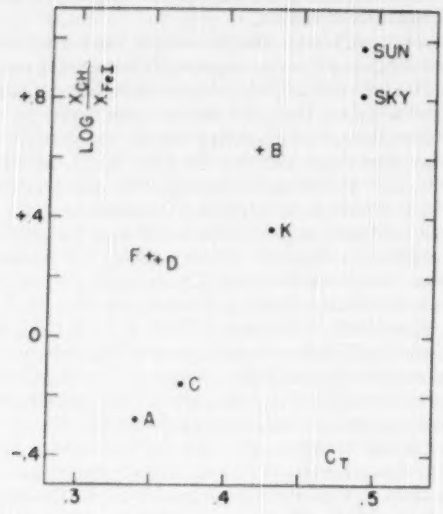

FIG. 3.—Relative strength of *CH* versus reduced color index. Symbols as in Fig. 2

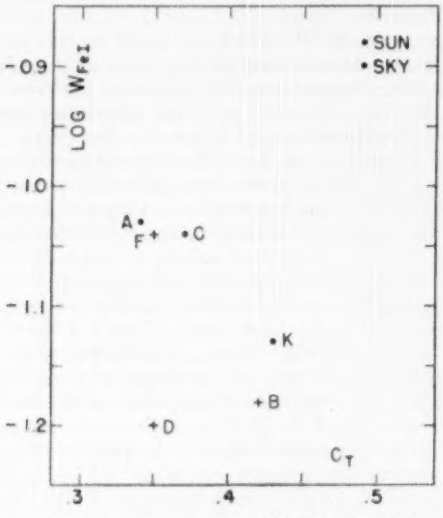

FIG. 4.—Strength of *Fe* I versus reduced color indices. Symbols as in Fig. 2

If one assumes that this difference in log W is real and if one further assumes that main-sequence stars of the same spectral type do not differ significantly in turbulent velocity, then a difference between high- and low-velocity stars in the *Fe* abundance could be determined. Since the average slope of the flat portion of the curve of growth was here found to be approximately one-fourth, the above difference in log W gives a difference in log $X_{Fe\,I}$ of 0.3. Since the $X_{Fe\,I}$ values are proportional to the pressure of *Fe* divided by the pressure of *H* (as *Fe* is mostly ionized and H^- provides most of the opacity), one would conclude that the relative abundance of *Fe* compared with *H* is smaller by a factor of 2 for the high-velocity dwarfs than for the low-velocity dwarfs. This conclusion, however, can be considered only a possibility, not a secure result.

VIII. CONCLUSIONS

The discussions of the preceding section may be summarized as follows: The only difference between the high-velocity and low-velocity dwarfs found from the present observational material with fair certainty is shown by the *CH* features, which indicate that the abundance of *C* relative to the metals is probably about 2.5 times larger in the high-velocity F dwarfs than in the low-velocity dwarfs. This difference runs parallel to that found in the *CH* features of the N stars[9] but runs opposite to the behavior of *CN* in the K giants.[10]

Second, a possible difference is shown, though with little certainty, by the absolute strength of the *Fe* I lines, which indicate that the abundance ratio of *Fe* to *H* might be lower in the high-velocity dwarfs by a factor of approximately 2 as compared with the low-velocity dwarfs.

If the second difference should actually prove right, one might suspect from these two differences that the high-velocity dwarfs are similar to the low-velocity dwarfs in ratio of hydrogen to the elements of the oxygen group (represented in the present material only by *C*) but that they differ from the low-velocity dwarfs in having a smaller relative abundance of the elements of the iron group.

We acknowledge with much gratitude the active co-operation of the Mount Wilson Observatory in obtaining the observations here reported; the persistent help of Dr. Olin Wilson in the handling of the 100-inch coudé spectrograph and the calibration equipment; the essential contribution of Dr. Olin Eggen, in determining the photoelectric color indices; the kind help of Miss Jenkins and Dr. Jackson in assembling the parallax data; and the assistance of Mr. Savedoff in measuring and reducing the tracings.

[9] N. W. McLeod, *Ap. J.*, **105**, 390, 1947.

[10] W. W. Morgan, P. C. Keenan, and Edith Kellman, *An Atlas of Stellar Spectra* ("Astrophysical Monographs" [Chicago: University of Chicago Press, 1943]).

A SPECTROGRAPHIC STUDY OF HD 193576*

GUIDO MÜNCH
Yerkes and McDonald Observatories
Received June 12, 1950

ABSTRACT

A series of 93 spectrograms of the eclipsing system HD 193576, obtained during the summer of 1949, has been used to study the variations in radial velocity and intensity of various spectral features. The velocity-curve of the O component was determined from measures of *H*8, *H*9, and *H*10, which give $\gamma = +10$ km/sec and $K = 120$ km/sec. The radial-velocity-curves for the WR spectrum have an amplitude $K = 305$ km/sec, but the γ-axis of the *N* V lines is shifted 60 km/sec to the red with respect to the systematic velocity of the *H* lines, while the γ-axis for *N* IV λ 4058 is shifted to the blue by 50 km/sec. The observations provide new evidence confirming the plausibility of explaining the shifts of emission lines as a result of self-absorption processes in the WR envelope.

The absorption lines of the O star, during primary minimum, have been observed to become shallower and broader than at other phases. This variation has been accounted for in terms of the noncoherent scattering of the O-star radiation by free electrons in the WR envelope and in the outer layers of the O star itself. The problem of the illumination of the envelope by radiation of the O star is briefly considered. It is shown that, at conjunctions, the light of the O star, scattered in the line of sight by the envelope, amounts to at least 10 per cent of the continuous radiation attributed to the WR component.

In the last section of the paper an attempt is made to analyze the general characteristics of the WR spectrum. It is shown how some of the observed features can be interpreted in terms of an envelope with radially decelerated motions. In this model the kinetic energy of mass motion at the lower base of the envelope, supplied by a hypothetical impulsive mechanism from the parent-nucleus, is partly used to support the matter against gravity of the core and partly dissipated into heat of atomic motion, as matter moves outward. It is also suggested that the radiation of the O star in the far ultraviolet is an important factor in determining the physical and dynamical state of the matter in the outer parts of the observed envelope. There seems to be some observational evidence indicating that the state of ionization of the envelope is higher in the hemisphere facing the O star, but no conclusive test of the hypothesis is provided by the available observations.

I. INTRODUCTION

Since O. C. Wilson[1] discovered the binary nature of HD 193576 = V 444 Cyg,[2] this system has been the subject of a number of investigations. Spectroscopic studies have been carried out by O. C. Wilson,[3] C. S. Beals,[4] and E. S. Keeping.[5] Following the recognition of the object as a spectroscopic double with large amplitude, S. Gaposchkin[6] announced its eclipsing nature from previous photographic observations, and G. E. Kron and K. C. Gordon[7] obtained photoelectrically a light-curve of the system. For an account of the extensive work carried out by several authors on the interpretation of the light-curve, we refer to the recently published paper by Kron and Gordon.[8] Here we only recall that the unconventional features of the light-curve have revealed the existence of a large, semitransparent envelope, surrounding the fainter and smaller component, with which the WR spectrum is associated. From the analysis of the primary minimum observed at λ 4500, Z. Kopal and M. B. Shapley[9] derived the conclusion that the opacity in the

* *Contributions from the McDonald Observatory, University of Texas*, No. 194.

[1] *Pub. A.S.P.*, **51**, 55, 1939.

[2] HV 11111 = BD+38°4010, $\alpha = 20^h15^m8$, $\delta = +38°25'$ (1900).

[3] *Ap. J.*, **91**, 379, 1940, and **95**, 402, 1942.

[4] *M.N.*, **104**, 205, 1944.

[5] *Pub. Dom. Ap. Obs., Victoria*, **7**, 349, 1947.

[6] *Pub. A.A.S.*, **10**, 52, 1940; *Ap. J.*, **93**, 202, 1941.

[7] *Ap. J.*, **97**, 311, 1943.

[8] *Ibid.*, **111**, 454, 1950.

[9] *Ap. J.*, **104**, 160, 1946.

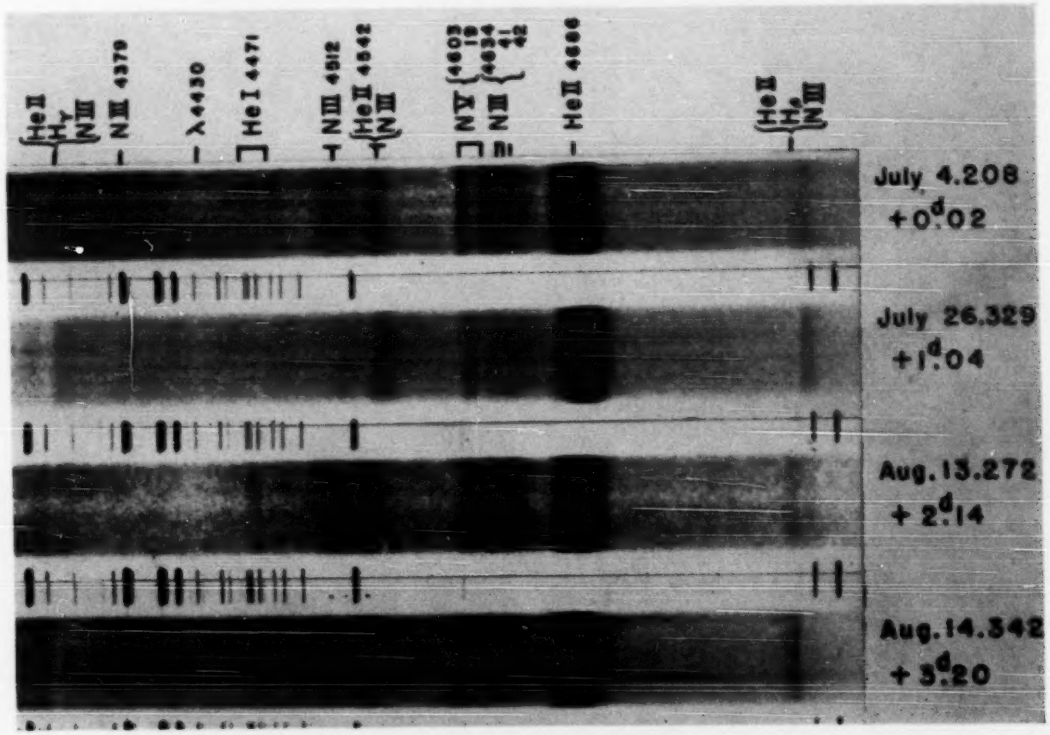

FIG. 1.—The spectrum of HD 193576 in the region $H\gamma$–$H\beta$

envelope was probably due to electron scattering. Later observations by W. A. Hiltner[10] and Kron and Gordon[8] have verified that the shape of the primary minimum is practically the same over the wave-length interval λλ 3300–7200, an observational fact which confirmed the hypothesis advanced by Kopal and Mrs. Shapley.

The work presented in this paper was originally planned with a view to establishing the effects of the scattering properties of the WR envelope on the observed spectral characteristics. The inspection of the first few spectrograms secured for that purpose revealed the exceedingly complex nature of the phenomena involved. Following the advice of Dr. O. Struve, it was decided to extend the observing program in order to obtain additional information in regard to the radial-velocity-curves and to variations of the line intensities through the orbital period.

II. THE OBSERVATIONS

Between July 4 and August 15, 1949, 93 spectrograms were obtained by Dr. Struve and the writer with the Cassegrain quartz spectrograph of the McDonald Observatory, in a dispersion of 40 A/mm at λ 3933. The exposures were made alternately on emulsions 103*a*-O and II*a*-O, keeping the slit-width constant at 0.05 mm. The length of the slit was changed in order to obtain, with an exposure time of about 40 minutes, spectra 0.4 mm wide in the former plates, while in the latter the spectra are twice as wide and have an optimum density around $H\gamma$. All plates were calibrated immediately after exposure with a spot sensitometer and filters giving effective wave lengths at 4100 and 4600 A. In order to derive the phases of the observations, we have computed the times of primary minimum, T_0, from the elements given by Kron and Gordon,[8] as follows:

$$T_0 = \text{JD } 2428771.379 + 4.21238n,$$

corrected by the departures from this formula found by the same authors on July 24 and September 23, 1949. Between these two dates the observed time of conjunction changed by 0.04 day, and for this reason we give the phases of our spectra only to 0.01 day.

III. THE RADIAL VELOCITIES

Our narrow plates are well suited for a redetermination of the orbit of the absorption component of the system, if the higher members of the Balmer series are selected for that purpose. These lines are relatively free of blends, in comparison with those in the blue region of the spectrum used by earlier investigators. The heliocentric radial velocities given in Table 1 for the absorption star of the binary are the straight averages of the velocities derived from *H*8, *H*9, and *H*10, using laboratory wave lengths. The fact that we did not find any systematic difference between the velocities of *H*8 and those of the other lines indicates that the blending of *H*8 with *He* I 3888.65 does not produce an error larger than the observational uncertainty. From the internal agreement of velocities derived from plates taken in succession and from the same plate measured twice, we estimate that the accidental errors of measurement are of the order of 15 km/sec. For this reason all velocities given in Table 1 have been rounded off to the nearest multiple of 5 km/sec. For the emission spectrum, only the velocities of *N* IV 4057.80 and the average of the velocities of the *N* V lines at λ 4603.2 and λ 4619.4 are given. The line λ 4619.4 becomes almost indistinguishable at phases near secondary minimum (see Fig. 1), and consequently only λ 4603.2 was measured at those phases. No systematic difference was detected between the two *N* V lines. In Figure 2 we have plotted the individual velocities for the two components of the binary. It is seen that the points define, without much ambiguity, the run of the velocity-curves. Assuming that they represent circular motion, we derive the set of elements given in Table 2. For comparison purposes we have repro-

[10] *Ap. J.*, **110**, 95, 1949.

TABLE 1

RADIAL VELOCITIES OF HD 193576

Plate (CQ)	Date 1949	Phase (Days)	Velocities (Km/Sec)					
			H	N IV 4058	N V 4603–19	He I		
						3889	3889	4471
7611	July 4.208	0.02	− 10	+ 65	+130	−1360	.....	.....
7612	4.242	0.06	− 45	− 35	+165	−1390	.....	.....
7614	4.413	0.23	− 30	+ 50	+150	−1365	.....	.....
7615	4.448	0.26	− 40	+ 95	+150	−1380	.....	.....
7621	5.249	1.06	− 95	+315	+415	−1385	.....	.....
7622	5.283	1.10	− 90	+300	+340	−1410	.....	.....
7623	5.425	1.24	− 80	+265	+305	−1450	.....	.....
7624	5.455	1.27	−125	+210	+370	−1420	.....	.....
7636	10.342	1.94	+ 20	− 45	+170	−1315	.....	.....
7637	10.405	2.01	− 5	+ 40	+190	−1345	.....	−1190
7639	11.202	2.80	+110	−240	−125	−1305	.....	.....
7640	11.325	2.84	+135	−345	−200	−1470	.....	.....
7642	12.155	3.76	+ 80	−310	.....	−1345	.....	.....
7645	13.199	0.59	− 90	+140	+260	−1450	.....	.....
7646	13.242	0.63	− 50	+125	+325	−1430	.....	.....
7647	15.460	2.85	+100	−380	−195	−1355	.....	.....
7649	16.174	3.56	+ 95	−335	−205	−1400	.....	.....
7650	16.201	3.59	+100	−370	−170	−1475	.....	.....
7651	16.347	3.74	+130	−300	−140	−1410	.....	.....
7652	16.382	3.77	+ 60	−320	−145	−1515	.....	.....
7653	16.414	3.80	+105	−275	−155	−1430	.....	.....
7656	17.154	0.33	− 65	+125	+150	−1595	.....	.....
7657	17.190	0.37	− 75	+160	+190	−1560	.....	.....
7658	17.225	0.40	− 30	+215	+280	−1520	.....	.....
7659	17.417	0.59	.....	.....	+300	.....	.....	.....
7660	17.452	0.63	.....	.....	+305	.....	.....	.....
7662	18.167	1.34	− 70	+215	+315	.....	.....	.....
7663	18.204	1.38	− 90	+225	+340	.....	.....	.....
7664	18.242	1.42	.....	.....	+330	.....	.....	.....
7665	18.259	1.44	−130	+210	+320	−1405	.....	− 845
7666	18.291	1.47	− 95	+150	+335	.....	.....	.....
7667	18.342	1.52	− 75	+130	+290	−1560	.....	− 940
7668	18.378	1.56	−100	+195	+310	−1535	−1100	− 905
7669	18.415	1.59	− 75	+180	+250	−1315	− 795	− 755
7671	19.117	2.29	+ 25	−145	− 15	−1160	.....	−1005
7672	19.147	2.32	+ 50	−205	− 30	−1175	.....	−1120
7673	19.171	2.35	.....	−160	− 25	.....	.....	− 920
7674	19.197	2.38	+ 80	−110	− 50	−1150	.....	−1015
7675	19.229	2.41	+ 85	−215	− 25	−1340	.....	−1165
7676	19.260	2.44	+ 45	−130	− 75	−1175	−1620	−1040
7677	19.294	2.47	.....	.....	− 75	.....	.....	.....
7678	19.319	2.50	+ 70	− 75	−100	.....	−1185	−1220
7681	19.408	2.58	+ 55	−175	−140	.....	−1260	−1015
7682	19.448	2.62	+ 80	−225	−160	.....	−1400	−1215
7683	26.239	1.04	−110	+225	+370	−1530	.....	.....
7684	26.377	1.09	−105	+210	+395	−1805	−1420	.....
7685	26.416	1.13	−155	+190	+390	−1670	−1145	.....
7702	30.282	0.78	−105	+235	+340	−1405	.....	.....
7703	30.318	0.82	−110	+220	+350	−1240	.....	.....
7704	30.346	0.85	−125	+290	+355	−1405	.....	.....
7707	30.415	0.92	−115	+225	+340	−1490	.....	.....
7708	30.444	0.95	−110	+305	+410	−1500	.....	.....
7709	30.467	0.97	.....	+360	.....	.....	.....	.....
7720	31.331	1.83	− 10	+ 50	+120	−1185	.....	.....

TABLE 1—*Continued*

Plate (CQ)	Date 1949	Phase (Days)	Velocities (Km/Sec)					
			H	*N* IV 4058	*N* V 4603–19	*He* I		
						3889	3889	4471
7721	July 31.360	1.86	− 15	+ 15	+160	−1315	.....	.....
7722	31.387	1.89	− 45	− 30	+120	−1290	.....	.....
7723	31.413	1.91	− 10	+ 50	+150	−1205	.....	.....
7724	31.442	1.94	− 20	+ 25	+135	−1300	.....	.....
7725	31.470	1.97	.....	− 5	+155	−1305	.....	−1155
7735	Aug. 1.417	2.92	+110	−265	−235	−1315	.....	−1160
7736	1.441	2.94	+115	−435	−245	−1350	− 805	− 995
7737	1.474	2.98	+120	−190	−250	−1295	.....	.....
7773	2.452	3.97	+ 55	−220	− 65	−1430	.....	.....
7774	2.474	3.99	− 25	−170	− 30	−1430	.....	.....
7775	10.137	3.21	+140	−350	−230	−1330	.....	−1275
7777	10.219	3.29	+135	−300	−250	−1325	.....	−1275
7779	10.353	3.43	+ 90	−350	−260	−1390	.....	.....
7780	11.191	0.05	+ 15	+ 20	+ 80	−1450	.....	.....
7782	11.380	0.24	− 45	− 50	+180	−1580	.....	.....
7783	13.160	2.02	− 15	+ 15	+155	−1620	−1095	.....
7784	13.188	2.05	+ 20	− 50	+165	−1590	−1125	− 975
7785	13.217	2.08	+ 30	− 30	+115	.....	−1060	.....
7787	13.272	2.14	+ 20	− 30	+120	.....	−1050	−1055
7788	13.304	2.17	+ 30	− 75	+ 55	−1585	−1090	− 995
7789	13.338	2.20	+ 15	− 50	+ 50	.....	.....	−1015
7790	13.366	2.23	+ 60	− 25	+ 90	.....	−1045	−1080
7792	14.139	3.00	+130	−390	−180	−1535	−1055	− 995
7793	14.170	3.03	+105	−400	−210	−1495	−1055	− 965
7795	14.242	3.10	+110	−385	−230	−1500	−1110	− 915
7796	14.274	3.14	+120	−370	−235	−1600	− 990	− 985
7797	14.308	3.17	+110	−415	−240	−1535	−1210	.....
7798	14.342	3.20	+125	−340	−230	−1590	−1255	.....
7799	14.378	3.24	+ 85	−345	−235	−1620	.....	.....
7800	14.413	3.28	+130	−325	−235	−1420	.....	.....
7801	14.449	3.31	+ 75	−320	−210	−1400	.....	.....
7802	15.104	3.97	+ 5	−145	− 45	−1510	.....	.....
7803	15.137	4.00	− 20	−170	− 55	−1530	.....	.....
7804	15.174	4.04	+ 40	−130	− 20	−1580	.....	.....
7805	15.212	4.08	+ 35	−115	+ 50	−1525	.....	.....
7806	15.253	4.12	+ 50	−110	− 10	−1510	.....	.....
7808	15.341	4.21	+ 30	−105	+ 65	−1520	.....	.....
7809	15.390	0.04	+ 15	− 10	+110	−1495	.....	.....
7810	15.432	0.08	.....	.....	+105	.....	.....	.....

duced in Table 2 the elements derived earlier by O. C. Wilson[3] and E. S. Keeping.[5] Disregarding for a moment our values for *N* IV 4058, we see that the only significant difference between O. C. Wilson's elements and ours is the one involved in the γ-velocities for the absorption component. With respect to this point, it should be remarked that the possibility of a systematic difference between the velocities obtained at McDonald and those at Mount Wilson is ruled out by the agreement of the measured velocities of interstellar *Ca* II for this star. We derive, from 83 spectrograms, $V = -8.8 \pm 3.3$ (p.e.) km/sec, while O. C. Wilson obtained $V = -8.6$ km/sec from 11 spectra. The discrepancy we find, therefore, is most likely to have originated in the distortion produced by the emission of *N* III and *He* II on the contour of *H*γ in absorption, on which Wilson's

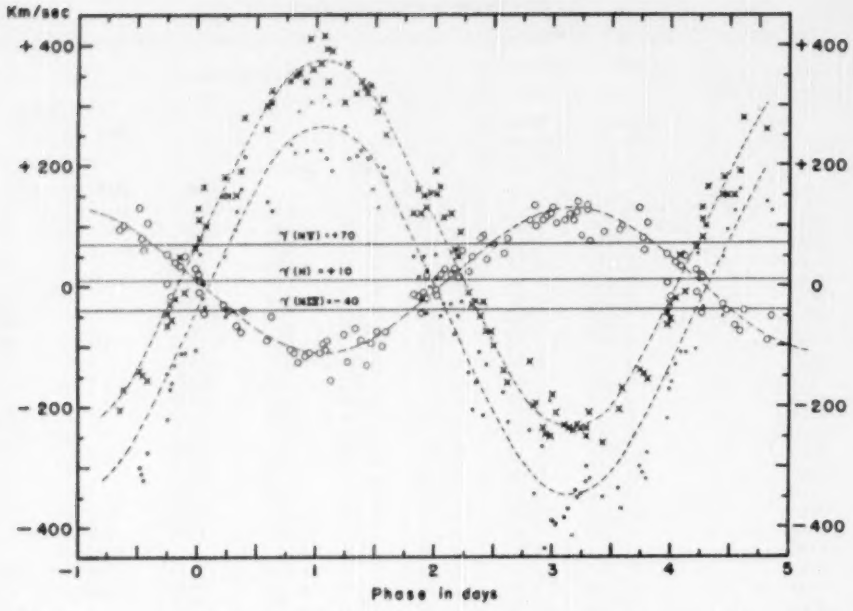

FIG. 2.—The radial-velocity-curves of HD 193576. The circles represent the average of the velocities derived from *H*8, *H*9, and *H*10. The crosses and dots represent the velocities given by the *N* V lines at λ 4603 and λ 4619 and by the *N* IV line at λ 4058, respectively.

TABLE 2

ELEMENTS OF THE SPECTROSCOPIC ORBITS

		O. C. Wilson	E. S. Keeping	Present Work
	(Km/Sec)			
Emission	γ	+ 56.4±4.4	*N* V: +55 *N* IV: + 8	*N* V: +70 *N* IV: −40
	K	308.6±6	301.5±3.9	305
Absorption	γ	− 33.6±4.4	+ 32.8±1.5	+ 10
	K	120.7±5.8	177.2±3.9	120
$m_o \sin^3 i$ $(M_\odot)$		24.8	30.8	24.1
$m_w \sin^3 i$ $(M_\odot)$		9.74	17.3	9.5
$a_o \sin i$ $(R_\odot)$		10.1	14.4	10.0
$a_w \sin i$ $(R_\odot)$		25.7	25.5	25.4
$(a_o+a_w) \sin i$		35.8	39.9	35.4

orbit is based. This distortion is undoubtedly more serious than the blending with the line of *He* II in absorption, a blend which E. S. Keeping thought could be accounted for by adopting the average of the laboratory positions of *Hγ* and *He* II 4338.71 as standard wave length. Such a procedure does not seem to be justified. When comparing the various elements for the emission lines, we should keep in mind that the procedure followed by Keeping of averaging the velocities of all emission lines to find the "motion" of the WR star is incorrect. Recent measures by O. Struve[11] and W. A. Hiltner[12] in the spectra of WR systems have established beyond any doubt that different emission lines are shifted by different amounts with respect to the velocity of their center of mass. If we assume that the γ-axis of our velocity-curve for the hydrogen lines represents the motion of the center of mass of the system, we see that, in our measures, the *N* V lines are shifted 60 km/sec to the red, while the *N* IV line is shifted 50 km/sec to the blue. With respect to the apparent blue shift of *N* IV λ 4057.80, it should be said that the line at the elonga-

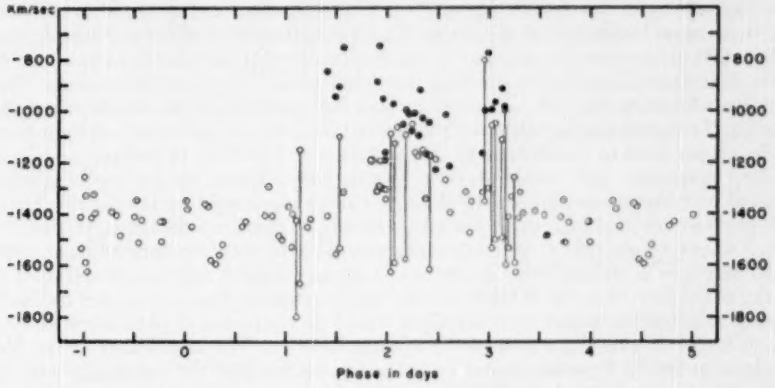

FIG. 3.—The radial velocities of the violet absorption edges of the emission lines of *He* I at λ 3888.65 (*empty circles*) and λ 4471.48 (*filled circles*). The circles joined by a line represent the velocities of the two apparent components at times when the line is double.

tions is often distorted on the red side, in the manner described in the next paragraph. This distortion explains the greater scatter of the representative velocities around the elongations. For the same reason, the center of the emission feature, as estimated visually on the plate, does not necessarily coincide with the center estimated in a microphotometer tracing. Hence the difference between our γ-velocity and the one derived by Keeping is probably not physically significant.

The violet absorption edges of the emission lines of *He* I at λ 3888.65 and λ 4471.48 have also been measured whenever possible. The λ 4471 edge, as Beals[13] first pointed out, is visible only in the neighborhood of secondary minimum. Around this conjunction the λ 3889 edge can often be seen clearly as double, and the velocities derived for the two apparent components are given in Table 1. The plot of the radial velocities of the two lines, given in Figure 3, does not show any definite tendency to follow the general run of the curve found previously for the velocities of the emission lines. In regard to the absorption edge of λ 3889, it should be said that it becomes very shallow and difficult to

[11] *Ap. J.*, **100**, 188, 1944.

[12] *Ap. J.*, **101**, 356, 1945.

[13] *Op. cit.*, Fig. 5. The displacement measured by Beals for the edge of λ 4471 was −400 km/sec, a value which is less than half the average velocity which we derived. This discrepancy raises the question of a possible intrinsic change in the spectrum from the time that the star was observed at Victoria.

measure around the first quadrature, when the associated emission is strongest and extends farther to the violet. We have noticed also that there is a rough correlation between the intensity of the emission line and the measured displacements of its absorption edge. For these reasons it is believed that the measured wave-length displacements do not reflect the mass motion of the absorbing atoms in a straightforward fashion.

IV. DESCRIPTION OF THE WOLF-RAYET SPECTRUM

The WR spectrum of HD 193576 displays conspicuous changes not only throughout the orbital period but also from cycle to cycle. On account of the general relevance of such changes for a proper understanding of the physical state of the matter producing the spectral lines, in this section we describe in detail the variations observed in their intensities and shapes.

He II

The asymmetry of the λ 4686 line of *He* II at phases near conjunctions[3] is easily detected in a casual inspection of the plates. The measurement of its total strength, however, is a difficult problem, on account of the overexposure of the central parts of the line and the uncertainty involved in drawing the "continuum" between two regions "free" of emission which are over 100 A apart and where the sensitivity of the emulsion is falling off rapidly. The average equivalent widths derived from the measurement of eight plates with the proper level of density are 88, 83, and 74 A at the times of primary minimum, secondary minimum, and outside eclipse, respectively. These results are in essential agreement with the values obtained by Wilson. Taking into consideration the effect of the eclipse on the continuum to which the measures are referred, we obtain an intrinsic decrease of about 12 per cent at primary minimum. The information derived from photographic measures is certainly not accurate enough to establish any eclipse effect on the intensity of the line when the Wolf-Rayet nucleus is eclipsed. The only proper method of obtaining information about such an effect would be observing it photoelectrically, as W. A. Hiltner[14] has recently done in the system CQ Cep. The appearance of the *He* II 4542 emission line in Figures 1 and 4 gives the impression that the line is narrower and slightly stronger near the elongations than at conjunctions. This effect, however, is certainly not real but is caused by the distortion produced by the same line in absorption in the spectrum of the companion star. It is believed that at the present time it is impossible to say whether or not the line is effectively stronger at the conjunctions, because of the blending with some lines of *N* III, which are stronger at these phases. Similar situations are encountered when attempting to ascertain the behavior of other emission lines of the Pickering series.

N III

The emission spectrum shows a number of broad features identified with groups of *N* III lines, which cannot be easily measured; nevertheless, they undergo rather remarkable changes. Thus, in Figures 1 and 4 the difference of the feature centered around λ 4542 at conjunctions and at the elongations is conspicuous. It appears stronger in the plates at primary minimum than at the secondary, being weakest at elongations. The same behavior probably is shown by the line at λ 4379 and the group of lines which appears blended with *He* II λ 4542. Unlike the lines just mentioned, the members of the multiplet $3p^2P - 3d^2D$ around λ 4640 are stronger at secondary minimum than at the primary. The increase in the intensity of the lines at phases near secondary minimum takes place very rapidly and is accompanied by a marked change in the intensity distribution within the emission feature, as the tracings reproduced in the right half of Figure 4 illustrate. The appearance of the feature as a whole in the plates of best quality suggests evidence for an inner structure. It is also believed that the feature extends too

[14] *Ap. J.*, in press.

far into the red at primary minimum to be due only to the three *N* III lines and that possibly there is a further contributor around λ 4650.[15]

N IV

The members of the $3s^3S-3p^3P$ multiplet of *N* IV at λλ 3479, 3483, and 3485 are blended together, forming the strongest feature in the ultraviolet emission spectrum. It appears only in our narrow spectra, overexposed in the blue region. The most remarkable change shown by this feature is the appearance, at primary minimum, of a strong absorption component, displaced to the violet by 4 A (= −340 km/sec) with respect to the apparent center of the emission (λ = 3482.8 A). This violet absorption edge is not present at all when the absorption star is out of eclipse, as can be seen in the tracings

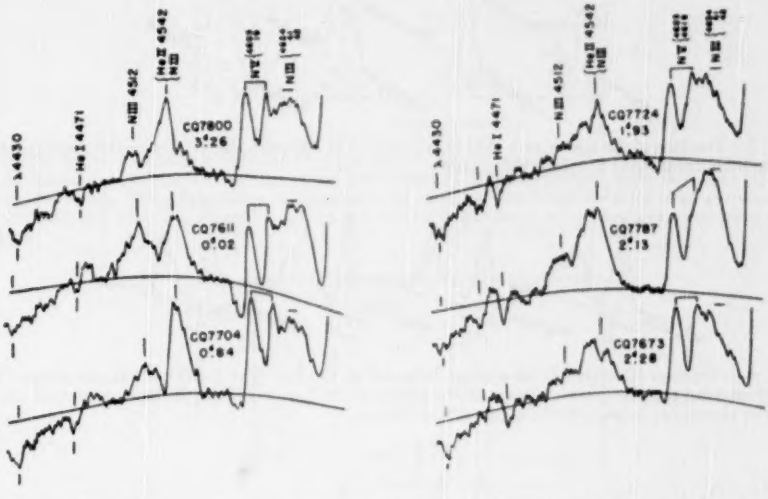

FIG. 4.—Microphotometer tracings of the spectrum of HD 193576 over the wave-length region λλ 4430–4660.

reproduced in Figure 5. The measures of the intensity at the center of the emission, marked in the figure, were made on the characteristic curve for λ 4100 and are given only to show the considerable decrease of the apparent strength of the feature at primary minimum. The other strong line of *N* IV at λ 4057.8 does not show a displaced absorption component at primary minimum, and, on the contrary, it looks strongest at these phases. In Figure 6 we give representative contours of the line at times when it appears to the eye nearly symmetrical. In some plates, however, it appears more or less distorted in a manner which suggests the presence of a superimposed narrow absorption line on the red wing of the emission. In extreme cases it is possible to see clearly a narrow absorption line overlying the emission, as is illustrated in Figure 7, where the tracings of two plates at the same phase, but at different epochs, are reproduced. The reality of the absorption feature in the plate CQ 7684 is unquestionable, as it runs clearly across the whole spectrum and appears nearly in the same position (λ = 4061.9 A) in four plates taken in

[15] P. Swings (*Ap. J.*, **95**, 112, 1942) has suggested that the broad emission feature observed around λ 4638 in the spectrum of HD 192163 extends too far to the red to be attributed to *N* III only and that there may be some blending effect by *C* III and *C* IV around λ 4652 A.

succession. Only on another occasion did four successive plates, CQ 7720–23, covering the phases 1.83–1.91, show the same absorption line nearly as strong as it appears in CQ 7684. The appearance of this absorption line is not periodical, and we have not been able to find out whether it is correlated to some other varying feature of the WR spectrum.[18] On the basis of the material now available, it appears that the emission line under consideration is more often distorted when the WR star is farther away from, than when it is nearer to, the observer and that the presence of the absorption feature does not persist longer than about 6 hours. It is certain that the large scattering shown

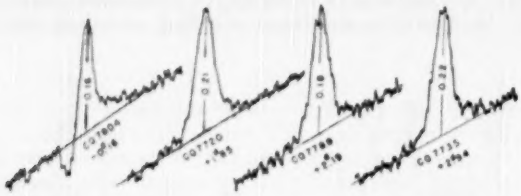

FIG. 5.—Tracings of the line *N* IV λ 3483 in HD 193576 at different phases. Notice the appearance of the absorption component at primary minimum.

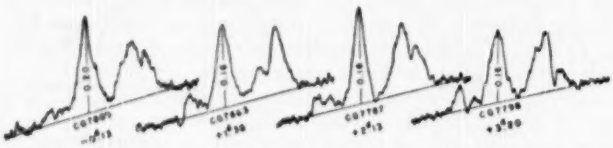

FIG. 6.—Tracings illustrating the average behavior of the line *N* IV λ 4058 at various phases. The number marking the maximum ordinate in the profile of the line considered is the logarithm of the intensity at that point in units of the apparent continuum.

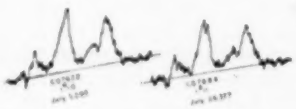

FIG. 7.—Comparison of the profiles of the *N* IV λ 4058 line at the same phase and different epochs.

by the radial velocities of λ 4057.80 is due to the distortion of its profile. To study the variations in intensity of the line through the orbital period, we have selected for measurement the wide plates which appear free of noticeable distortion. As an indicator of the strength of the line, we have taken the height of the emission line in units of the continuum. The results of the measurements are given graphically in Figure 8, where we have plotted the logarithm of the ratio of the maximum intensity in the profile to the intensity in the continuum as a function of phase. The increase of the values of this ratio at the times of conjunction is well marked. If all the measures are referred to the continuum outside eclipse, the figure shows that the apparent increase in the intensity of the emission at primary minimum is due to the decrease in the continuum. It may be intrinsically stronger at secondary minimum than at other phases.

[18] C. S. Beals (*op. cit.*, Fig. 4) has observed a narrow absorption core on the contour of *Hα*, which possibly might have the same nature as the one we have observed in *N* IV λ 4058.

N v

The weakening of the *N* v lines at λ 4603.2 and λ 4619.4 at the times of conjunctions is noticeable in Figure 1. This visual impression is confirmed by the measurements, as can be seen in Figure 9, where we have plotted the logarithm of the ratio of the maximum intensity in the λ 4603.2 line to the intensity in the continuum as a function of phase. The representative points show considerable scatter, but it is apparent that the general run of the points is opposite to that shown by the measures of *N* IV 4057.8 in Figure 8.

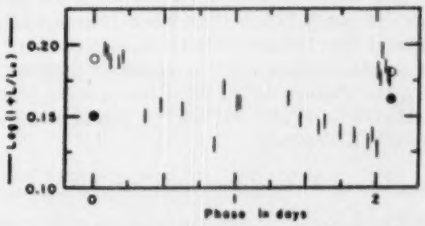

FIG. 8.—The dependence on phase of the height of the emission line *N* IV λ 4058, measured in units of the apparent continuum. The vertical bars represent individual measures, reflected about each minimum. The empty circles denote the values adopted at central eclipses, and the filled circles represent the values obtained when the height at the time of eclipse is measured in units of the continuum outside eclipse.

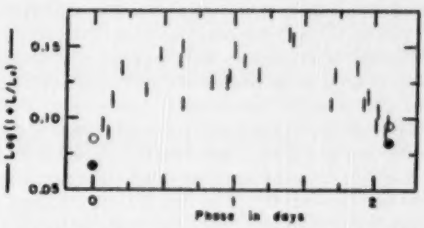

FIG. 9.—The dependence on phase of the height of the emission line *N* v λ 4603 measured in units of the apparent continuum. The vertical bars represent individual measures reflected about each minimum. The empty circles denote the values adopted at central eclipses, and the filled circles represent the values obtained when the height at the time of eclipse is measured in units of the continuum outside eclipse.

When the effect of the eclipses on the continuum is taken into account, we obtain a further decrease of the intensities at conjunctions. The absorption edges which border the emission lines in the violet also undergo conspicuous changes through the period. In Figure 4 they appear considerably deeper at primary minimum than near the elongations, while they become weaker in the neighborhood of secondary minimum, disappearing completely at central conjunction. The approximate values of the apparent central residual intensities, in units of the continuum, at primary minimum and at the elongations are, respectively, 0.88 and 0.96.

He I

The emission lines of *He* I are very broad and have low contrast with the continuum. For this reason it is difficult to estimate variations in their intensity. The violet absorption edges associated with the emission, however, vary in intensity and shape in a spectacular fashion. The violet edge of λ 3888.65 is narrowest and looks strongest around pri-

mary minimum, but it does not have the same intensity at different epochs. Thus, in the four plates obtained near the conjunction which took place on July 4.18, 1949, the line appears much stronger than in plates of corresponding phases at three other epochs observed (see upper part of Fig. 10). On plates taken the following night, however, the line in question has nearly the same strength as in corresponding phases of other cycles. Around secondary minimum the line appears to be considerably broader and sometimes even gives the impression of being double or, at least, of having a central reversal (see lower part of Figs. 10 and 11), but again in a manner which is not strictly periodical. In general, the line as a whole can be seen more clearly when the Wolf-Rayet nucleus is approaching the observer (phases 2.1–3.2) than when it is receding (phases 1.0–2.1). We have not found indications that the aperiodical changes of *He* I λ 3889 are accompanied by similar variations in other absorption or emission features of the WR spectrum. Since the variability of the absorption edges of the lines of *He* I has been observed by W. A. Hiltner in HD 214419[17] and HD 193928,[18] it is reasonable to consider it as a common characteristic of all WR systems.

V. ANALYSIS OF THE SPECTRUM OF THE ABSORPTION STAR

The standard intensity ratios of the absorption lines of *He* I and *He* II in HD 193576, according to C. S. Beals,[4] give for the absorption component of the system a type near O6. The same author, on the basis of the relative intensities of the absorption lines in HD 193576 and in standard stars of type O6, also estimated that the O component provides five-sixths of the continuous light observed in the whole system, out of eclipse, over the wave-length region λλ 4000–6000. The correct order of magnitude of this estimate was confirmed by Beals, who compared the emission-line intensities in the system and in other "typical" WN 5–6 stars. Our observations are not entirely consistent with all the conclusions derived by Beals. While there is no question that the emission-line intensities correspond to a ratio of the luminosities near 5, the appearance of the O spectrum in the near ultraviolet is not exactly that of a star of type O6. In Figure 11 we have reproduced tracings of the spectra of the system and of λ Cep, a standard star of type O6f. It is noticed that in λ Cep the ratio *He* II λ 3813/*He* I λ 3820 is about unity, while in HD 193576 it is appreciably smaller than unity and corresponds to a star of type O8 (ξ Per). It also can be seen that the line *H*10 is stronger and has more extended wings in the binary than in the standard star. The manner in which *H*10 and *H*11 overlap suggests that the Stark effect may be the cause of stronger lines in the O star of the system. A further indication of this possibility is provided by the sudden termination of the Balmer series at *H*14, while in λ Cep and in other O stars (θ′ Ori C, λ Ori) it ends with *H*16. This difference can hardly be explained by the presence of the λ 3750 group of emission lines, for neither is strong enough or extends sufficiently to the violet in "typical" WN 5–6 stars. It is therefore tempting to conclude that the end of the Balmer series at *H*14 is due to the higher Stark effect in the O component of the system.

On an earlier occasion[19] the writer called attention to the change suffered by the absorption lines of the O star when it is eclipsed. To the eye this change is striking, as can be seen in Figure 10 by comparing the appearance of *H*9 and *H*10 during primary minimum and out of eclipse. Figure 11 also shows that the contours of the same lines at minimum light are more shallow and have a different shape than when the O star is not eclipsed. In the note just mentioned there was suggested a tentative explanation of this phenomenon, based on the redistribution in frequency suffered by radiation of the O star when scattered by thermal free electrons in the WR envelope. It would be a difficult problem to attempt a critical test of this hypothesis, taking into proper consideration the actual circumstances of the eclipse. We should have to discuss the geometry of the WR envelope, the darkening toward the limb of the O spectrum, and the possible effects of

[17] *Ap. J.*, **99**, 273, 1944. [18] *Ap. J.*, **101**, 356, 1945. [19] *Ap. J.*, **108**, 540, 1948.

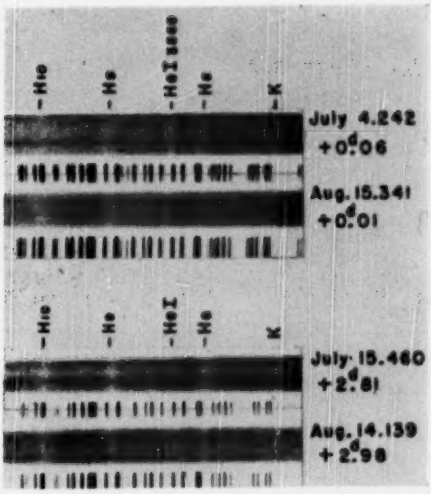

FIG. 10.—The spectrum of HD 193576 in the near ultraviolet. Notice the different intensity of the violet absorption edge of *He* I λ 3889 at the primary minima occurred on July 4.18 and August 15.34, 1949. Compare also the different appearance of *H*9 and *H*10 at primary minimum and at other phases.

rotation on the absorption lines of the partially eclipsed star. We restrict our considerations, therefore, to a simple situation which illustrates only the essential characteristics of the radiation scattered in the WR envelope. Imagine a plane surface, S, radiating in all directions the spectrum of the O star. We idealize the conditions of eclipse by superposing on S a plane-parallel layer of electrons of optical thickness τ and with a kinetic temperature T. This layer is also supposed to radiate a continuous spectrum equal to that of the WR component. We shall now show that the spectrum of the surface S, when observed through the electron layer, has some of the characteristic features of the O-star spectrum at minimum light.

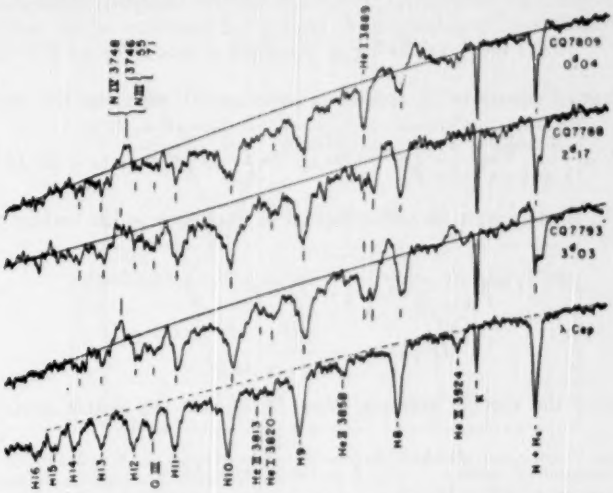

FIG. 11.—Tracings of the spectrum of HD 193576 in the near ultraviolet. Notice the different appearance of the $H10$ line and of the region between $H10$ and $H9$ at primary minimum and at other phases. The tracing of λ Cephei is included for comparison purposes.

Let $F_0(\lambda)$ and $F_1(\Delta\lambda)$ be the emergent fluxes from the surface S, respectively, at a wave length λ in the continuous spectrum and at a distance $\Delta\lambda$ from the center λ of an absorption line. We denote by $F_0'(\lambda)$ and $F_1'(\Delta\lambda)$ the corresponding quantities at minimum light. Then, if $F_W(\lambda)$ is the monochromatic flux of the WR spectrum radiated by the layer, the depths $D(\lambda)$ and $D'(\Delta\lambda)$ of the absorption line considered, respectively, when S is uneclipsed and eclipsed, are

$$D(\Delta\lambda) = F_0 - F_1(\Delta\lambda) \qquad \text{and} \qquad D'(\Delta\lambda) = \frac{F_0' - F_1'(\Delta\lambda)}{F_0' + F_W}, \tag{1}$$

where we express all fluxes in units of $F_0 + F_W$ and measure the depths from, and in units of, the continuum. In order to express $D'(\Delta\lambda)$ in terms of $D(\Delta\lambda)$ and the parameters τ and T of the electron layer, we use the approximate solution of the relevant Schuster problem given by the author.[20] Writing

$$a = \left(\frac{m c^2}{4kT}\right)^{1/2} \frac{\Delta\lambda}{\lambda} = 3.850 \times 10^4 \frac{\Delta\lambda}{\lambda\sqrt{T}}, \tag{2}$$

[20] *Ap. J.*, **108**, 116, eqs. (11) and (55), 1948. This paper will be referred to as "Paper I"; cf. also S. Chandrasekhar, *Radiative Transfer* (Oxford: Clarendon Press, 1950), eqs. (119) and (141), pp. 337 and 341.

we have

$$F_1'(a) = e^{-\tau\sqrt{3}}F_1(a) + \int_{-\infty}^{\infty} F_1(\beta)\Phi(\tau, a-\beta)\,d\beta, \tag{3}$$[21]

where $\Phi(\tau, a)$ is a certain function of its arguments known in numerical form and with the property

$$\int_{-\infty}^{\infty} \Phi(\tau, a)\,da = \frac{1}{1+\frac{1}{2}\tau\sqrt{3}} - e^{-\tau\sqrt{3}}. \tag{4}$$

Setting $F_1(a \to \infty) = F_0$ in equation (3), we obtain

$$F_0' = \frac{F_0}{1+\frac{1}{2}\tau\sqrt{3}}; \tag{5}$$

and, by substituting equations (3) and (5) in equation (1), we derive the required relation:

$$D'(a) = \frac{1+\frac{1}{2}\tau\sqrt{3}}{1+\frac{1}{2}\tau\sqrt{3}F_W}\left\{e^{-\tau\sqrt{3}}D(a) + \int_{-\infty}^{\infty} D(\beta)\Phi(\tau, a-\beta)\,d\beta\right\}. \tag{6}$$

For comparison, if there were no redistribution in frequency in the scattering process, we should have

$$\Phi(\tau, a-\beta) = \left(\frac{1}{1+\frac{1}{2}\tau\sqrt{3}} - e^{-\tau\sqrt{3}}\right)\delta(a-\beta) \tag{7}$$

and

$$D'(a) = \frac{D(a)}{1+\frac{1}{2}\tau\sqrt{3}F_W}. \tag{8}$$

We now consider the specific example when $D(\Delta\lambda)$ has the simple analytical form

$$D(\Delta\lambda) = \frac{0.25}{1+(0.286\Delta\lambda)^2}, \tag{9}$$

which roughly represents the observed contour of $H10$ in HD 193576 out of eclipse. Using equation (6) and the numerical values of $\Phi(\tau, a)$,[22] we have computed the resulting contours $D'(\Delta\lambda)$ for $\tau = 0.4$ and $\tau = 0.8$. The result of the calculations is given graphically in Figure 12, where we have plotted two contours of the form (9), with centers 38 Å apart, and the broadened contours $D'(\Delta\lambda)$. We can then compare the appearance of the profiles of $H9$ and $H10$ in the tracings of Figure 11 with the theoretical contours of Figure 12. In a general way, we see that the main features of the change suffered by the lines during eclipse are present in the contours broadened by electron scattering in a layer of optical thickness around $\tau = 0.5$. In order to estimate an upper limit for the value of τ compatible with the observed light-curve, we may substitute the values $F_0 = 0.83$ and $F_0' = 0.61$ in equation (5). In this manner we obtain $\tau \cong 0.3$, a value which

[21] In connection with the use of eq. (3) it is useful to give an approximate form for the function $\Phi(\tau, a)$,

$$\Phi_1(\tau, a) = \left(\frac{1}{1+\frac{1}{2}\tau\sqrt{3}} - e^{-\tau\sqrt{3}}\right)\left(\frac{3}{\pi}\right)^{1/2} e^{-3a^2}, \tag{3'}$$

which represents the spectral distribution of monochromatic light after being scattered once at an angle of $\cos^{-1}(\frac{1}{3})$. This function has been normalized in order to satisfy the flux condition of the Schuster problem in the first approximation. Numerically, it has been verified that, for contours narrow compared with $\lambda(4\,kT/mc^2)^{1/2}$, the use of $\Phi_1(\tau, a)$, as defined above, gives values for the scattered light which do not differ by more than 10 per cent from the values obtained from the more approximate function $\Phi(\tau, a)$ for $\tau \leq 0.5$.

[22] Paper I, Table 1 and eq. (62).

would seem not sufficiently large to explain the observed broadening of the lines. We should keep in mind, however, that in the actual eclipse the central parts of the disk of the O star are more occulted than are the regions near its limb. Under these conditions the effects of electron scattering in the outer layers of the atmosphere of the O star itself should be considered,[23] in accordance with a suggestion made earlier by the author.[24] It is also relevant to mention, in this context, that Kron and Gordon[25] in their analysis of the light-curve have considered the possibility of the existence of a "tenuous atmosphere surrounding the O component." Such an envelope would be so highly ionized as to be detectable only by means of its scattering properties. From these considerations we may conclude with confidence that the observed appearance of the absorption lines of the eclipsed O star can be explained in terms of the scattering of its radiation by free electrons in the WR envelope and in the outer layers of the O star itself.

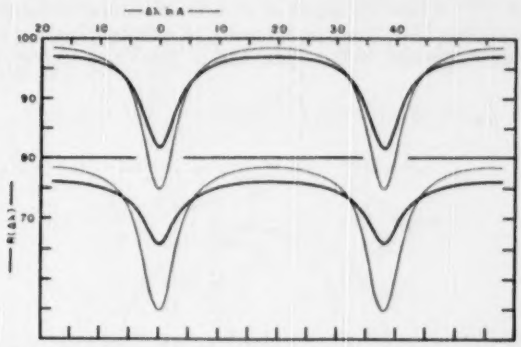

FIG. 12.—Comparison of the contours of two absorption lines (*thin lines*), nearly as strong as *H*10 in HD 193576 outside primary minimum, with the same profiles as modified by electron scattering (*thick lines*) in a layer of optical thickness τ and temperature $T = 80{,}000°$ K. The upper figure is obtained for $\tau = 0.4$ and the lower for $\tau = 0.8$.

VI. ILLUMINATION OF THE WOLF-RAYET ENVELOPE BY THE O STAR

The light of the O star scattered in the line of sight by the WR envelope plays a very important role in the analysis of the light-curve, for it may amount to an appreciable fraction of the continuous radiation observed in the WR component.[26] It is not our intention now to study the intricacies of the problem, as it would carry us into a complete analysis of the light-curve. Instead, we shall consider a model based on the simple geometry of the system, derived in previous analysis of the photometric orbit. Specifically, we shall evaluate the illumination of a spherical distribution of free electrons, with known density and dimensions, by parallel radiation of a net flux πF coming from a point *O*. We assume that a quantum of radiation is scattered isotropically by the electrons only once, the cross-section for scattering, σ, having the classical Thomson value. Let us take a system of co-ordinates (see Fig. 13) with origin at *W*, its *z*-axis in the direc-

[23] Recent calculations of model atmospheres of stars of early B types, by Miss A. B. Underhill (*Ap. J.*, 111, 203, 1950), have shown that the effective depth of the layers at which the wings of the strong absorption lines are formed may be as high as $\tau = 1.5$, the opacity in the outer layers being largely due to electron scattering.

[24] Paper I, § 7.

[25] *Ap. J.*, 111, 454, 1950.

[26] See the remarks made by Kopal and Mrs. Shapley, *op. cit.*, pp. 169–170.

tion of the observer, and its xz-plane containing O. Let ϵ be the phase angle of the illuminating radiation reckoned from the positive z-axis. Then, at a point $P = P(r, \vartheta, \phi)$ of the atmosphere, the specific intensity of the direct light (radiation which reaches P without having been scattered) is

$$\tfrac{1}{4}F \exp\{-\tau_P(\epsilon)\}, \tag{10}$$

where $\tau_P(\epsilon)$ is the optical depth of the point P, measured from the boundary in the direction of the incident radiation. Accordingly, the specific intensity of diffuse radiation which arrives at the point R of the boundary in the direction of the observer, after being scattered at the point P, will be

$$dI_R = \tfrac{1}{4}F \exp\{-\tau_P(\epsilon) - \tau_P\}\, d\tau_P, \tag{11}$$

where $\tau_P = \tau_P(\epsilon = 0)$ is now the depth of P in the direction of the observer. It follows, by integrating equation (11), that the intensity of diffuse radiation at R scattered in a column containing P, parallel to the z-axis and of unit cross-section, is

$$I_R(\vartheta_0, \phi, \epsilon) = \tfrac{1}{4}F \int_0^{\tau_T} \exp\{-\tau_P(\epsilon) - \tau_P\}\, d\tau_P. \tag{12}$$

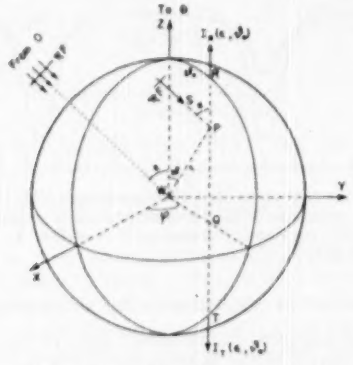

FIG. 13.—Co-ordinate system

Similarly, the specific intensity of diffuse radiation at the boundary point T, in a direction antiparallel to the observer, is

$$I_T(\vartheta_0, \phi, \epsilon) = \tfrac{1}{4}F \int_{\tau_T}^{0} \exp\{-\tau_P(\epsilon) - \tau_{P'}\}\, d\tau_{P'}, \tag{13}$$

where

$$\tau_{P'} = \tau_P(\epsilon = \pi) = \tau_T - \tau_P. \tag{14}$$

Obviously, by changing the phase angle from ϵ to $\pi - \epsilon$, the meanings of the points R and T are interchanged. The integrations involved in equations (13) and (14) can be carried out explicitly only at full phases, $\epsilon = 0$ or $\epsilon = \pi$. We then have

$$I_R(\vartheta_0, \phi) = \tfrac{1}{4}F(1 - e^{-2\tau_T}) \tag{15}$$

and

$$I_T(\vartheta_0, \phi) = \tfrac{1}{4}F\tau_T e^{-\tau_T}. \tag{16}$$

It is noticed that, as they should be, these values are identical with the reflected and transmitted diffuse intensities in a plane-parallel atmosphere of thickness τ_T, when the directions of illumination and observation coincide with the normal.[27]

To obtain the total diffuse radiation of the envelope, as observed from the earth at full phases, we integrate equations (15) and (16) over the visible hemisphere. The values r and t, of the radiations diffusely reflected and transmitted in the WR envelope, in units of the observed light of the WR component, L_W, are, therefore,

$$r = \frac{R_W^2}{L_W} \int_0^{2\pi} d\phi \int_0^{\pi/2} \tfrac{1}{4} F \left(1 - e^{-2\tau_T}\right) \cos \vartheta_0 \sin \vartheta_0 d\vartheta_0 \tag{17}$$

and

$$t = \frac{R_W^2}{L_W} \int_0^{2\pi} d\phi \int_0^{\pi/2} \tfrac{1}{4} F \tau_T e^{-\tau_T} \cos \vartheta_0 \sin \vartheta_0 d\vartheta_0 . \tag{18}$$

In terms of the radius a of the relative orbit of the O star, the flux incident on the envelope is approximately given by

$$\pi F = \frac{L_0}{a^2}; \tag{19}$$

and equations (17) and (18) become, after writing $x = \sin \vartheta_0$,

$$r = \frac{L_0}{L_W} \left(\frac{R_W}{a}\right)^2 \frac{1}{8} \left\{1 - 2 \int_0^1 e^{-2\tau(x)} x dx\right\} \tag{20}$$

and

$$t = \frac{L_0}{L_W} \left(\frac{R_W}{a}\right)^2 \frac{1}{2} \int_0^1 \tau(x)\, e^{-\tau(x)} x dx . \tag{21}$$

Now in Figure 13 it is readily seen that

$$\tau_T = \tau_T(\vartheta_0) = 2\sigma R_W \sin \vartheta_0 \int_{\vartheta_0}^{\pi/2} N_e \left(R_W \frac{\sin \vartheta_0}{\sin \vartheta}\right) \frac{d\vartheta}{\sin^2 \vartheta} . \tag{22}$$

This equation, in terms of the variable x and by the definition of R_W, can be written with sufficient accuracy in the form

$$\tau(x) = 2\sigma R_W x \int_1^\infty N_e (R_W x t)\, d\,(t^2 - 1)^{1/2} . \tag{23}$$

The electron densities derived by Kopal and Mrs. Shapley[28] can be represented with any desired accuracy by an interpolation formula of the type

$$N_e(r) = e^{-kr} \sum_{j=0}^{n} c_j r^j , \tag{24}$$

for which the integration in equation (23) can be carried out explicitly. For our purposes, it is sufficient to take a first-order expansion, with $k = 2.68 \times 10^{-12}$ cm^{-1} and $c_0 = 2.32 \times 10^{12}$ cm^{-3}. With $R_W = 1.85 \times 10^{12}$ cm ($= 0.75a$),[29] equation (24) takes the numerical form

$$\tau(x) = 5.73 \times K_1(4.96x) , \tag{25}$$

[27] Cf. Chandrasekhar, *op. cit.*, chap. viii, eqs. (108), (109), and (113), pp. 201–202.

[28] *Op. cit.*, Table 9.

[29] This value of R_W, taken from Kopal and Mrs. Shapley's work, is considerably larger than the value derived by Kron and Gordon. The final numerical values of r and t, however, are quite independent of the value of R_W adopted.

where $K_1(x)$ is the Bessel function of the second kind for an imaginary argument.[30] If the integrals of the functions of $\tau(x)$ indicated in equations (20) and (21) are then numerically carried out, we obtain

$$r = 0.031 \frac{L_0}{L_W}\left(\frac{R_W}{a}\right)^2 \quad \text{and} \quad t = 0.030 \frac{L_0}{L_W}\left(\frac{R_W}{a}\right)^2. \tag{26}$$

If the adopted values of L_0/L_W and R_W/a are inserted into equations (26), we obtain the result that the diffusely reflected and transmitted light at full phase, in our model, amounts to nearly 10 per cent[31] of the observed radiation in the WR component. This value represents only a rough lower limit for r and t, and the true values for the reflected and transmitted lights are probably much larger for the following reasons: In the first place, the contributions of higher-order scattering are certainly large in an atmosphere of diametral thickness of the order of unity. In the second place, the values of $N_e(r)$ derived by Kopal and Mrs. Shapley are minimum values. And, finally, if the illuminating radiation is considered conical instead of parallel, quite large additive corrections may be expected.[32]

We should keep in mind that the preceding estimate of the illumination of the WR envelope refers only to radiation of the O star scattered by free electrons. The intensity distribution of the diffuse continuous spectrum has nearly the same form as the incident radiation. There is, however, another process which may induce a true continuum in the envelope. As a consequence of the large cross-section of the material in the envelope for short wave-length radiation, it is reasonable to expect that a significant fraction of the light of the O star absorbed in the far ultraviolet will be re-emitted at longer wave lengths. The physical conditions in the envelope are, however, so far removed from thermodynamic equilibrium as to make invalid the use of the Kirchhoff-Planck equation for describing the induced radiation field. Consequently, a strict evaluation of the energy density in the outer envelope would be a very difficult problem. At the present time we cannot develop these considerations in a quantitative manner; we merely recognize the possibility that the continuous spectrum observed by Kron and Gordon in the inner parts of the WR envelope derives to some extent from the ultraviolet light of the companion.

It is appropriate here to make some general remarks on the interpretation of the light-curve of the system. The most striking characteristic of the light-curve is the difference in the duration of the two eclipses. In their work Kopal and Mrs. Shapley[33] advocate the view that a "great difference in width of the alternate minima discloses immediately that the conditions in the W envelope must depart widely from thermodynamic equilibrium." But this view does not seem to have much physical basis: if the opacity of the envelope in the accessible region is electron scattering, it must re-emit exactly as much as it absorbs; the lack of thermodynamic equilibrium in the envelope will not disturb this situation. The narrowness of the secondary minimum must, therefore, have a different explanation. It would be interesting to analyze in detail the possibility of explaining it in terms of a large reflection effect in the system. We do not observe a decrease in the total light when the outer parts of the envelope are being occulted by the disk of the O star, because the increase in brightness of the unocculted parts compensates for the effect of

[30] Cf. G. N. Watson, *Treatise on the Theory of Bessel Functions* (Cambridge: At the University Press, 1944), eq. (6.15.4), p. 172.

[31] In magnitudes, the reflected and transmitted radiations would be 0.02, a quantity which should be compared with the observed depth, 0.14 mag., of the secondary minimum.

[32] Cf. Z. Kopal, *An Introduction to the Study of Eclipsing Variables* ("Harvard Observatory Monographs," No. 6 [Cambridge, Mass., 1946]), § 64, p. 155.

[33] *Op. cit.*, pp. 160–161, also n. 5.

eclipse. When the O star is behind, there is no such compensation, because in a thick atmosphere the diffusely transmitted light will be smaller than the reflected.

VII. ON THE SHIFT OF WOLF-RAYET EMISSION LINES

Recent work by O. Struve[11] and W. A. Hiltner[12] has established the plausibility of explaining the red shift of certain emission lines in WR spectra in terms of self-absorption processes in the envelope. Our observations of V 444 Cyg provide new information related to the question, which will now be discussed. We have seen that all violet absorption edges, with the exception of *He* I 4471, become deeper at the time of primary minimum. This phenomenon cannot be explained in terms of the decrease in the intensity of the continuous spectrum, if the ratio of the lights of the two components is 5 to 1. It is undoubtedly due to the absorption of the direct continuous radiation of the O star by atoms in the WR envelope. This observational fact provides the most convincing proof for the relevance of absorption processes in the formation of the observed emission lines.

The clearest example of a red shift being produced by an absorption edge is provided by the observed behavior of the group of *N* v lines at λ 3483 A. At minimum light, when the absorption edge appears, the center of the emission is displaced to the red by 1.5 A (= +130 km/sec), with respect to the apparent center of the emission feature at secondary minimum. If this line could be measured for radial velocity, we should probably find a red shift only during primary minimum.

The strengthening of the absorption edges of the lines of *N* v at λ 4603 and λ 4619 does not produce a measurable increase in their red shift. This observational fact cannot be used as an argument against the explanation of the red shift in terms of self-absorption. The emission line λ 4603 is placed just in between the two absorption edges, in such a manner that the increased absorption produces only a decrease in the intensity of the emission, without appreciable shift. The line at λ 4619, on the other hand, is difficult to measure around primary minimum and, being badly blended with the *N* III lines, does not provide conclusive evidence. It is, nevertheless, not easy to understand why the disappearance of the absorption edge of λ 4603 at secondary minimum does not produce a shift to the blue in the measured radial velocities. If it is a geometrical effect of the eclipse, one would expect such a blue shift. But the possibility of blending with an emission feature increasing in intensity at secondary minimum cannot be definitely excluded.

VIII. INTERPRETATION OF THE WOLF-RAYET SPECTRUM

The main features shown by WR spectra have been described by C. S. Beals[34] and other investigators in terms of a hypothesis which postulates an ejection of material from a high-temperature nucleus. The ejected atoms are supposed to form a symmetrical extended envelope, in which the characteristic emission spectrum originates. The discussion of observational data related to HD 193576, however, led O. C. Wilson[35] to formulate serious doubts as to whether the ejection hypothesis could at all explain the observed phenomena. The main difficulty encountered by this author in accepting the existence of a large envelope in outward motion is that it necessarily implies a difference between the times of photometric and of spectroscopic conjunctions, which is definitely ruled out by the observations. In the original form of Beals's hypothesis, the motion in the envelope is accelerated outward, to such an extent that the presence of the O star cannot modify appreciably the trajectories of atoms moving with velocities several times as large as the velocity of escape from the whole system. The absence of a transit-time effect, therefore, could hardly be explained by the asymmetry of the envelope produced by tidal forces, as Beals suggested later.[36] This and other difficulties encountered in Beals's original hypoth-

[34] *M.N.*, **90**, 202, 1929.

[35] *Ap. J.*, **95**, 402, 1942.

[36] *M.N.*, **104**, 205, 1944.

esis, however, may be avoided by postulating that the ascending mass motions in the envelope are decelerated.[27] Such a situation is realized if matter leaves the nucleus by the action of an impulsive force: part of the kinetic energy supplied is used for support of the matter against the gravity of the nucleus, and the rest is dissipated into heat of atomic motion by turbulence.[28] We shall discuss, in the following paragraphs, the consequences of this alternative hypothesis, in the light of the observational evidence available at the present time. The nature of the physical processes determining the spectral characteristics will also be briefly considered.

STRATIFICATION IN THE ENVELOPE

In Beals's model for a WR envelope the ions are arranged outward in order of decreasing ionization potentials. This stratification is an immediate consequence of the postulate of a high-temperature core producing the ionization in the envelope. The recognition of HD 193576 as a binary with an O component, however, immediately throws doubt on the possibility that the observed *He* I lines could arise in the outermost layers of the envelope. Recalling that O stars radiate sufficient energy in the far ultraviolet to produce nebular luminosity and interstellar emission, we find it difficult to imagine the conditions under which *He* I could exist in a low-density envelope close to the O star without being completely ionized. In a decelerated envelope, on the contrary, the highest ionization comes from the highest levels, in such a way that the continuous radiation of the O star beyond the ionization limit of a given ion does not reach the layers in which the lines of that ion mostly originate. This remark does not imply that the state of ionization of the envelope depends only on the ultraviolet radiation of the O star. The physical conditions in the envelope will be determined primarily by the manner in which the energy of mass motion supplied by the core is dissipated in the higher layers. It would seem reasonable to expect, nevertheless, that the ultraviolet radiation of the O star would have an appreciable effect on the state of ionization of the outer envelope. Careful comparisons of line intensities in WR systems with different orbital radii could establish the magnitude of such an effect.

STATE OF MOTION IN THE ENVELOPE

The striking behavior of the displaced lines of *He* I immediately reveals the intrinsic variability of the conditions in which they are formed. We have observed erratic changes in their intensity in such short intervals of time as a few hours. On this account alone, it is tempting to describe the state of motion in the lower envelope in terms of a random flow of gas leaving the WR nucleus in all directions, with the same velocity on the average. The statistical fluctuations of the field, observed at the lower strata, are smoothed out as matter moves outward, in such a manner that lines originating in the higher layers do not undergo erratic changes. It would also be a simple matter to ascribe certain symmetry properties to the gas flow in order to explain the observed dependence on phase of the average intensity of the *He* I lines. Thus we could imagine that a greater amount of matter leaves the core from the advancing hemisphere than from the opposite one.[29] But, once this hypothesis is made, we should have to explain why lines originating at the

[27] In *M.N.*, **94**, 522, 1934, S. Chandrasekhar considered the possibility of decelerated radial ejection of atoms in WR stars.

[28] This mechanism is essentially the same as that considered by W. H. McCrea (*M.N.*, **89**, 718, 1929) to explain the support of the solar chromosphere. It also should be mentioned in this context that recently R. N. Thomas (*Ap. J.*, **109**, 500, 1949) constructed a model for a WR envelope based on a similar fundamental idea.

[29] An anisotropic pattern of this kind has been observed by O. Struve in the streams of gas flowing between the components of a number of close binaries. In the case of the eclipsing system UX Mon, such a flow has been described by the same author (*Ap. J.*, **106**, 253, 1947) in terms of a field of prominences subject to considerable random variations.

higher levels do not show any asymmetry between the advancing and receding sides of the envelope. This question leads us to the main difficulty encountered in attempting to explain the observed spectrum of V 444 Cyg and similar systems. In a close binary of this kind one would expect the existence of an envelope common to both components, formed by a system of currents between them. The dynamics of such an envelope have been studied by G. P. Kuiper,[40] and observations of a variety of eclipsing binaries by O. Struve[41] have established the properties and dimensions of the phenomena involved. In the case we are dealing with, the photometric observations can be interpreted in terms of a large envelope surrounding the fainter and smaller component. However, spectroscopically we find that the material giving origin to the observed emission lines is not subject to large-scale currents (within the observational uncertainty of the radial-velocity-curves) and has a spatial distribution nearly symmetrical around the line of centers.[42] Although it has not been possible to determine even approximately the linear dimensions of the emitting regions, there is no doubt that they must be comparable to the diameter of the primary star, which is about half the radius of the relative orbit. Nevertheless, the measured velocities of the emission lines originating in the higher strata are apparently unaffected by the gravitational field of the heaviest component. The solution to this paradoxical situation is undoubtedly related to the strong radiation pressure of the O star and the effectiveness of the mixing processes in the WR envelope. The ions directly exposed to the ultraviolet radiation of the O star are subject to a repulsive force, which tends to keep them bound to the WR star. It is difficult to foresee, without a careful analysis, whether the combined effect of the mixing agents in the WR envelope, the radiation pressure of the O star, and the general gravitational field could localize the emitting material to a region which, as a whole, would show the observed properties. It should also be added that it is not entirely unreasonable to think of an envelope extending so far as to inclose the O star. We have mentioned before that Kron and Gordon,[25] from the purely formal aspects of the light-curve, have suggested such a possibility. And, from the spectroscopic point of view, it could very well happen that it is not observed because its state of ionization is very high. In any case, before attempting to formulate these considerations in a less speculative manner, we should find some observational facts revealing the effects of the radiation of the O star on the high-level emission lines of the WR spectrum. Certain features we have observed in V 444 Cyg can be tentatively interpreted in terms of these effects, but they do not offer a conclusive test, mainly because of our lack of knowledge of the basic processes forming the lines.

NATURE OF THE EMISSION SPECTRUM

One of the unsolved problems is offered by the appearance of absorption edges only in certain emission lines and not in others. There is no doubt that a long life for the lower state of the transition involved is favorable for the appearance of the edges, but it is not a necessary condition. As examples we mention the lines *He* I 3889 and *N* IV 3483, which have violet absorption edges and arise from metastable levels, but the *N* V lines also have strong absorption edges and arise from short-lived states. Essentially the same problem is encountered in the selectivities shown by certain lines to appear in emission in Of stars. We recall that, in the spectrum of 9 Sge, Struve and Swings[43] observed the line $3p^1P^o - 3d^1D$ of *N* IV in emission, while the lines $3s^3S - 3p^3P^o$ occur only in absorption. In our case the former always appears in emission, while the latter develop an absorption edge at primary minimum. Another analogy between the spectra of 9 Sge and V 444

[40] *Ap. J.*, **93**, 133, 1941.

[41] *Stellar Evolution* (Princeton: Princeton University Press, 1950), p. 188.

[42] This remark is based on the apparently similar characteristics of the emission lines in systems with the same WR type but with different orbital inclinations.

[43] *Ap. J.*, **91**, 546, 1940.

Cyg is found in the behavior of the multiplet $3p^2P^0 - 3d^2D$ of *N* III. In the Of star it is the only one which appears in emission, while in the WR star it increases in intensity at secondary minimum much more than other lines of the same ion. Independently of the detailed mechanisms producing such selectivities, we may draw the definite conclusion that we are not dealing with a pure recombination spectrum. This conclusion invalidates the methods followed by C. S. Beals[44] and other authors[45] in deriving the excitation temperatures of emission lines.

It would be impossible to explain the detailed variations with phase of the intensity in the emission lines only in terms of the geometrical effects of the eclipses. Undoubtedly, there are unknown physical reasons for the strengthening of some lines at certain phases. We can notice, however, that most of the lines are intrinsically weaker at primary minimum than at secondary. Considering, also, that there are no appreciable eclipse effects on the lines (disregarding the lines of *N* v), we can conclude that the emission lines of the envelope are stronger over the hemisphere facing the O star than in the opposite one. This phenomenon could be interpreted by postulating an *ad hoc* geometrical form for the emitting regions. But it can also be explained less artificially as a phase effect of the ultraviolet radiation of the O component. At the present time, however, no critical choice can be made between these two points of view.

THE FORM OF THE EMISSION LINES

It is well known that the interpretation of the profiles of emission lines observed in WR spectra in terms of the expanding-envelope hypothesis has encountered serious difficulties.[46] We are not going to rediscuss every aspect of the problem, but it is appropriate to make some remarks about the absence of an "occultation effect." In the earlier work on the subject, the observed symmetry of the contours was taken as a proof that the nucleus was of negligible dimensions as compared with the envelope. The study of the eclipsing properties of the WR envelope of V 444 Cyg has revealed, however, that the envelope is far from transparent to its own radiation. The value $\tau = \frac{1}{2}$ found for the radial optical thickness of the envelope in electron scattering invalidates the afore-mentioned explanation for the absence of an occultation effect.[46] The nearly symmetrical form of the emission lines, therefore, must result from the processes of self-absorption, which tend to cancel the occultation effects, and from other broadening agents with a local character. One question of some interest in this context is to analyze the extent to which the observed broadening in an emission line can be attributed to the effect of electron scattering in the upper strata. We shall consider specific examples to illustrate this effect. Let us suppose that the whole line is formed at a certain level and that between this level and the observer there is a layer of free thermal electrons of optical thickness τ. The problem is to find the intensity distribution within an emission line, $R(\Delta\lambda)$, which, after being scattered in the electron layer, will look like the observed contour $R'(\Delta\lambda)$. Using equation (3), we have no difficulty in finding the solution by trial and error. For order-of-magnitude considerations it is sufficient to use the approximate equation (3′), and then we have simply

$$R'(\Delta\lambda) = kR(\Delta\lambda) + (1-k)\int_{-\infty}^{\infty} R(\Delta\lambda')\,\psi(\Delta\lambda - \Delta\lambda')\,d(\Delta\lambda'), \tag{27}$$

where

$$k = k(\tau) = (1 + \tfrac{1}{2}\tau\sqrt{3})\,e^{-\tau\sqrt{3}} \tag{28}$$

and

$$\psi(\Delta\lambda) = \frac{1}{\sigma\sqrt{\pi}}\,e^{-(\Delta\lambda/\sigma)^2}, \tag{29}$$

[44] *Pub. Dom. Ap. Obs., Victoria*, **4**, 271, 1930, and **6**, 95, 1934.

[45] In a recent paper (*B.A.N.*, **11**, 165, 1950), H. Zanstra and J. Weenen have investigated the problem of the abundances of the ions in a WR envelope under the hypothesis of pure recombination.

[46] R. N. Thomas (*Ap. J.*, **106**, 482, 1947) has also called attention to this circumstance.

with

$$\sigma = 1.50 \times 10^{-5} \lambda \sqrt{T} \qquad (\lambda \text{ in A}). \tag{30}$$

Let us now consider, as an example, a contour of the form

$$R(\Delta\lambda) = \frac{E}{m\sqrt{\pi}} e^{-(\Delta\lambda/m)^2}. \tag{31}$$

Equation (28) then becomes

$$R'(\Delta\lambda) = kR(\Delta\lambda) + \frac{(1-k)E}{[\pi(\sigma^2+m^2)]^{1/2}} e^{-(\Delta\lambda)^2/(\sigma^2+m^2)}. \tag{32}$$

For the case of the *He* II λ 4686 line, we have observed $E = 370$ A, in units of the intensity of the neighboring continuum of the WR star only. With $\tau = \frac{1}{2}$, $T = 80{,}000°$ K, and $m = 8$ A, we obtain the contours $R(\Delta\lambda)$ and $R'(\Delta\lambda)$ represented in Figure 14. We plot in a log scale observed points in the contour of λ 4686 to illustrate the rough agreement of the observed contour with $R'(\Delta\lambda)$. It is seen that the original contour $R(\Delta\lambda)$ is broadened considerably by electron scattering. Interpreting as a Doppler motion a dispersion of 8 A for the original contour, we find a spread in velocity of about 500 km/sec, a value which is less than half the range of representative velocities in the broadened contour. As another example we consider in Figure 15 the broadening of a line with about the

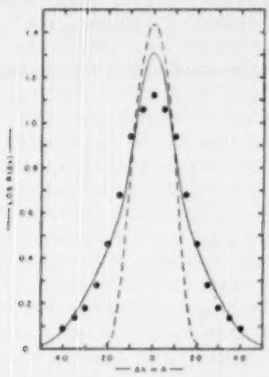

FIG. 14.—The effect of electron scattering on a strong emission line. The dashed-line contour is changed by scattering in an electron atmosphere of optical thickness $\tau = 0.5$ and temperature $T = 80{,}000°$ K into the full-line profile. The broadened contour was chosen so as to represent nearly the observed intensities (*dots*) of *He* II λ 4686 in HD 193576.

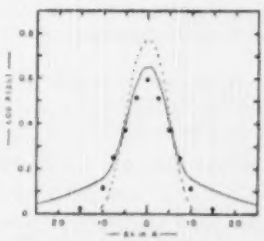

FIG. 15.—The effect of electron scattering on an emission line of moderate intensity. The dashed contour is modified by scattering in an electron atmosphere of thickness $\tau = 0.5$ and temperature $T = 80{,}000°$ K to the full-line profile. The broadened contour was chosen so as to represent roughly the observed intensities (*dots*) of *N* IV λ 4058 in HD 193576.

same intensity and shape as *N* IV λ 4058 (E = 44 A, m = 5 A) by a layer of electrons with the same optical thickness and kinetic temperature as before. It is seen that in this narrower line, with smaller total strength, the broadened contour has marked the extended wings more, reflecting the high Doppler velocities of the electrons. From these two examples it is seen that electron scattering produces an appreciable broadening in the emission lines formed at the deeper layers of the WR envelope. Nevertheless, the widths of the lines, after allowing for the broadening effects of electron scattering, are still very large. As further broadening agents we may invoke the large-scale turbulence of the envelope and the collisional broadening of ions and electrons. Earlier workers in the field have discarded the possibility of broadening by interatomic forces, on the grounds that the densities in a WR envelope are not sufficiently high. Since the study of V 444 Cyg has established electron densities of the order of 10^{12} cm^{-3}, it would seem that, at the high thermal velocities involved, the effects of particle perturbations on the atomic energy levels cannot be disregarded without a careful analysis. In conclusion, we may remark that local broadening agents, such as electron scattering, turbulence, and collisional broadening, necessarily require a stratification in the envelope in which the state of ionization increases outward.

It is a pleasure to express my gratitude to Professor O. Struve for his help in securing the observations studied in this paper and for many valuable discussions. I am indebted to Drs. G. E. Kron and K. C. Gordon for allowing me to read their investigation in advance of publication. My thanks are also due to Dr. S. Chandrasekhar, Dr. W. A. Hiltner, and Dr. O. C. Wilson for reading the manuscript and for their criticisms.

OBSERVATIONS OF SOLAR LIMB DARKENING BETWEEN 0.5 AND 10.2 μ*

A. K. PIERCE, R. R. MCMATH, LEO GOLDBERG, AND O. C. MOHLER
McMath-Hulbert Observatory, University of Michigan, Pontiac, Michigan
Received May 29, 1950

ABSTRACT

Measurements of solar limb darkening are tabulated for thirteen wave lengths between 0.5 and 10.2 μ. Observations in the wave-length region 0.5–2.2 μ were carried out with the McGregor Tower telescope and spectrometer for the interval $\cos\theta = 1.0$ to $\cos\theta = 0.16$. Measurements at three longer wave lengths were made with a Perkin-Elmer spectrometer attached to the 24-inch reflector and covered the interval $\cos\theta = 1.0$ to $\cos\theta = 0.2$.

At certain wave lengths the near infrared measurements agree with those of Abbot's to within 0.1 per cent; at other wave lengths the systematic differences are as large as 1 per cent. It is found that the degree of limb darkening decreases in the infrared from 3.5 to 10.2 μ. This result is qualitatively consistent with a systematic increase of the solar continuous opacity toward longer wave lengths in the infrared, as predicted by theoretical calculations of the absorption coefficient of the negative hydrogen ion.

INTRODUCTION

Observations of solar limb darkening are of fundamental importance in the determination of model solar atmospheres, which are, in turn, required for the interpretation of Fraunhofer intensities and for theoretical studies of line formation. As observations of Fraunhofer lines become more extensive and precise, new demands are placed upon the accuracy of the model atmospheres, especially when one considers the role of second-order effects like turbulence and blanketing in modifying the temperature and opacity gradients.

Since the continuous opacity varies with wave length, it is necessary that observations of solar limb darkening be made throughout the observable spectrum. Because the thickness of the solar atmosphere is small in comparison with the solar radius, it is also important that the observations be carried as close as possible to the extreme limb. The observational basis for existing model solar atmospheres has been provided by measures of limb darkening made by Abbot[1] and others.[2] Abbot's measures covered the spectral region from λ 3737 to λ 20,970 and extended over about 95 per cent of the solar radius. From an analysis of these observations, Chalonge and Kourganoff[3] have derived the observed variation of the solar continuous absorption coefficient with wave length. Chandrasekhar and Münch[4] have concluded that the observations are consistent with the theory that the negative hydrogen ion is the source of opacity between λ 4000 and λ 24,000. However, comparison of the observed and calculated opacity-curves reveals a pronounced discrepancy at wave lengths greater than about λ 16,000, the calculated opacity being systematically too high. It is therefore desirable that Abbot's observations be repeated and at the same time be extended closer to the limb.

The present paper describes the results of limb-darkening observations made at the McMath-Hulbert Observatory in the region 0.5–10.2 μ. Observations at 3.5, 8.3, and 10.2 μ have been carried out with the Francis C. McMath reflecting telescope and a Perkin-Elmer

* Work supported in part by contract N6onr 232-V with the Office of Naval Research.

[1] *Ann. Smithsonian Inst.*, **3**, 159, 1913; **4**, 220, 1922.

[2] Moll, Burger, and van der Bilt, *B.A.N.*, **3**, 83, 1925; Raudenbush, *A.N.*, **266**, 316, 1938; Chalonge and Canavaggia, *Ann. d'ap.*, **9**, 1943, 1946; Minnaert, van den Hoven van Genderen, and van Diggelen, *B.A.N.*, **11**, 55, 1949.

[3] *Ann. d'ap.*, **9**, 69, 1946.

[4] *Ap. J.*, **104**, 446, 1946.

recording spectrometer.[5] The observations between λ 5000 and λ 22,000 were made with the McGregor all-reflecting tower telescope and a high-dispersion spectrometer employing a Cashman *PbS* cell as energy detector.

OBSERVATIONS

Region 3.5–10.2 μ.—Limb-darkening observations in this region were carried out with a Perkin-Elmer spectrometer mounted at the Cassegrain focus of the 24-inch reflector. The

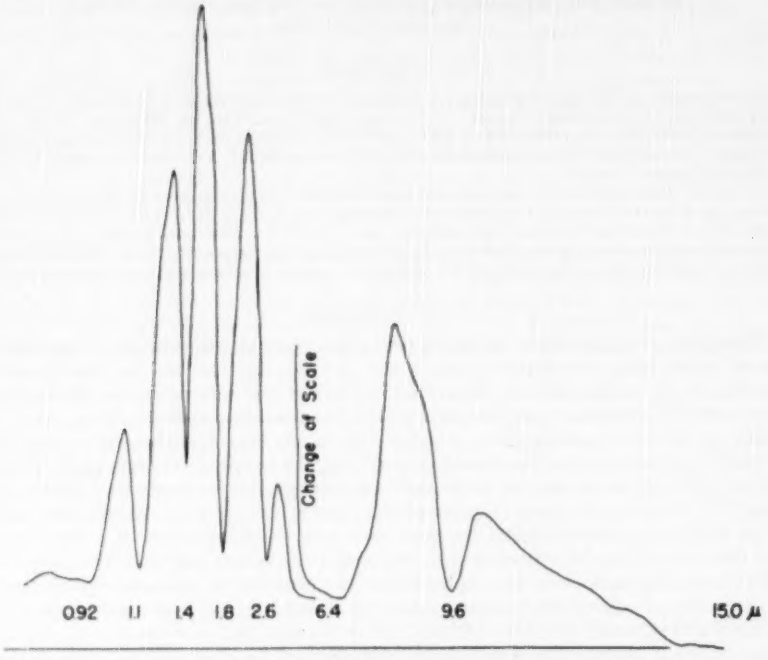

FIG. 1.—*KBr* prismatic solar spectrum

diameter of the solar image was 5″.4. The entrance slit of the spectrometer, 7 mm long and 0.30 mm wide, was oriented so that its length coincided with the east-west direction. The declination drive of the telescope was used to move the solar image across the slit in approximately 7 minutes. In this manner, drift-curves were made at the energy peaks in the atmospheric windows at 3.5, 8.3, and 10.2 μ (see Fig. 1).

Owing to the finite length and width of the entrance slit, each point on a given drift-curve represents an integration over a small area of the solar surface. The slit-length is so short in comparison with the diameter of the sun's image that the variation of the solar radius along its length is practically negligible. The rather large slit-width, which corresponds to 0.45 per cent of the radius of the solar image, was made necessary both by the weakness of the infrared solar energy and by the relative insensitivity of the thermocouple as an energy detector. The first and second slits of the spectrometer were interconnected. Therefore, the second slit was equal in width to the first and permitted a considerable por-

[5] A. K. Pierce, *Pub. A.S.P.*, **61**, 217, 1949.

tion of the spectrum, about 0.3 μ, to be integrated into each drift-curve. The dispersive medium was a 60° *KBr* prism.

The a.c. amplifier was used normally at about one-third full gain with an interruption frequency of 6 C.P.S.; the output of the amplifier was breaker-rectified and fed to a Brown recorder. The d.c. drift was sometimes troublesome, because the spectrometer was bolted to the tailpiece of the telescope and was therefore susceptible to the effects of wind disturbances, fluctuations in room temperature, and heating by the solar image. Thus there was considerable advantage in a.c. operation, which effectively re-established the zero point six times per second. Figure 2, *a*, shows an observed drift-curve obtained at 8.3 μ.

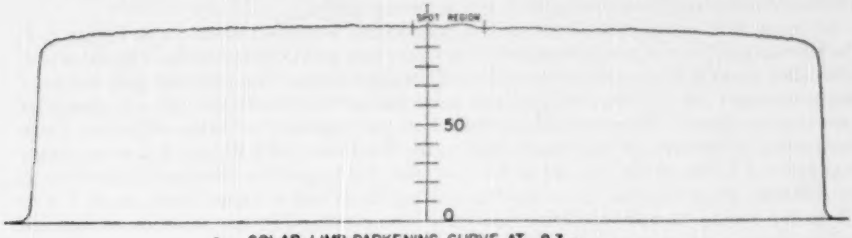

a. SOLAR LIMB-DARKENING CURVE AT 8.3 μ

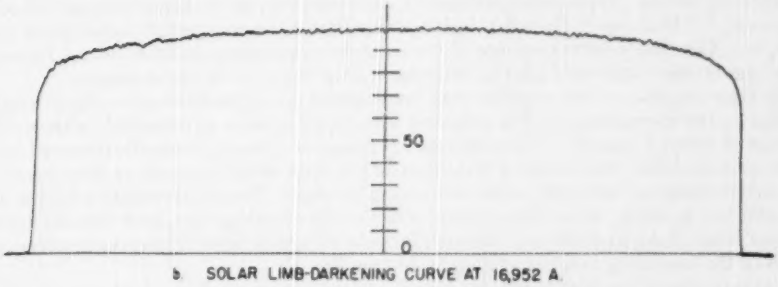

b. SOLAR LIMB-DARKENING CURVE AT 16,952 A

FIG. 2.—Typical drift-curves at λ 16,952 and at 8.3 μ

Region 0.5–2.2 μ.—A description of the McGregor Tower telescope and spectrometer has been given by McMath and Mohler.[6] Briefly, a coelostat and a 12-inch off-axis paraboloid form an achromatic image of the sun, about 5½ inches in diameter, on the entrance slit of a predispersing monochromator. The monochromator effectively eliminates the overlapping orders of the high-dispersion grating spectrometer and thus filters out a potential source of scattered light. A rotating sector, placed in front of the first slit of the spectrometer, modulates the radiation beam at 1080 C.P.S. The spectrometer employs a 15,000 g/inch plane reflection grating in a Pfund-type mounting; the equivalent focal length is 23½ feet. The energy receiver is a Cashman lead sulfide cell which possesses unusually high sensitivity in the 1–2 μ region and which has adequate response down to 0.5 μ. After amplification, the signal from the cell is recorded on a Leeds and Northrup Speedomax Recorder.

[6] *J. Opt. Soc. America*, **39**, 903, 1949.

The determination of solar limb darkening requires the measurement of monochromatic intensity along a solar radius. With the McGregor spectrometer the observational procedure was as follows: (1) the grating was oriented so that the desired wave length was centered on the second slit of the spectrometer; (2) the solar image was moved across the entrance slit of the monochromator at a uniform rate of speed and along a solar diameter by means of the right-ascension drive of the telescope. Owing to the relatively slow speed of response of the Speedomax Recorder (as compared, for example, with an insensitive, critically damped galvanometer system) a rather slow scanning rate was employed; each traversal of the sun's image required about 14 minutes. Inasmuch as the observations were made only on days of good transparency when the sun was close to the meridian, variations in atmospheric absorption during each run were negligible.

A typical drift-curve, traced out by the Speedomax Recorder, is shown in Figure 2, *b*. The entrance slit of the monochromator was 7 mm long and 0.10 mm wide. The slit-width subtended about 0.15 per cent of the radius of the solar image. The amplifier gain was kept nearly constant for all observations; the noise background from the cell and amplifier amounted to about 0.20 per cent of the deflection produced at the center of the sun. Since the opening of the first slit was maintained at the fixed value of 0.10 mm, it was necessary to adjust the width of the exit slit of the spectrometer to provide adequate deflections at the different wave lengths. Thus the transmitted band width varied from about 1 A to 3 A in the region λλ 5000–20,000. Great care was exercised in the selection of spectral regions that were entirely free of absorption lines.

REDUCTION OF OBSERVATIONS AND RESULTS

Region 3.5–10.2 μ.—The observed drift-curves show the variation of recorder deflection with time. Their reduction to true limb-darkening-curves requires that account be taken of the following factors: (1) possible nonlinearity and time delay in the amplifying and recording system; (2) blurring of the solar limb by scintillation, lack of perfect focus, finite slit-width, etc. The steady-state response of the recorder to radiation incident on the thermocouple was studied and was found to be linear within the error of measurement.

The time response of the recorder was investigated by application of a step-intensity function to the thermocouple. The response was approximately exponential, with a time constant of about 2 seconds. When the rate of change of intensity is small compared with the reciprocal of the time constant, the effect of the time delay is merely to displace each drift-curve along the time axis, without altering its shape. The observations with the 24-inch reflector, however, were carried out at a fairly high scanning rate, with the result that the time delay of the amplifier and recorder introduced appreciable differences between the shapes of the ascending and descending limbs (see Fig. 3).

The correction of the drift-curves for time delay may be accomplished with the aid of the superposition theorem.[7] Let the solar radiation incident on the energy receiver be $I(t')$, where the solar diameter is taken as a time axis with origin at the limb. Also let $x = 1 - r$ be the distance from the limb in units of the solar radius. Then $x = Vt'$, where V is the scanning rate in fractions of a solar radius per second. The observed quantity in the limb-darkening observations is the recorder deflection $\delta(t)$, which is related to $I(t')$ by the superposition theorem. Let the function $K(t)$ express the deflection of the recorder in response to a unit step in I at the receiver. Then,

$$\delta(t) = I(0)\,K(t) + \int_0^t K(t-t')\,I'(t')\,dt', \qquad (1)$$

where I' is the time rate of change of the energy incident on the receiver.

Equation (1) is an integral equation that is to be solved for $I'(t')$. In it, $\delta(t)$ is the observed limb profile and $K(t)$ is determined experimentally. In practice, $I(t')$ is most conveniently evaluated by numerical methods. In the present instance the quantities $\delta(t)$ and

[7] V. Bush, *Operational Circuit Analysis* (New York: John Wiley & Sons, 1929), p. 60.

$K(t)$ were expressed in tabular form and equation (1) was solved for $I'(t')$ by the method of Burger and van Cittert.[8] Finally $I(t')$ was obtained directly by numerical integration. The result of the correction for time delay is shown in Figure 3 for observations at 8.3 μ. The observed ascending and descending limbs are shown as dashed and solid lines, respectively, whereas the dotted line between them is the corrected limb profile.

The function $I(t')$ or $I(x)$ represents the true brightness distribution, modified by scintillation and instrumental imperfections. The correction for the diffusion of the sun's

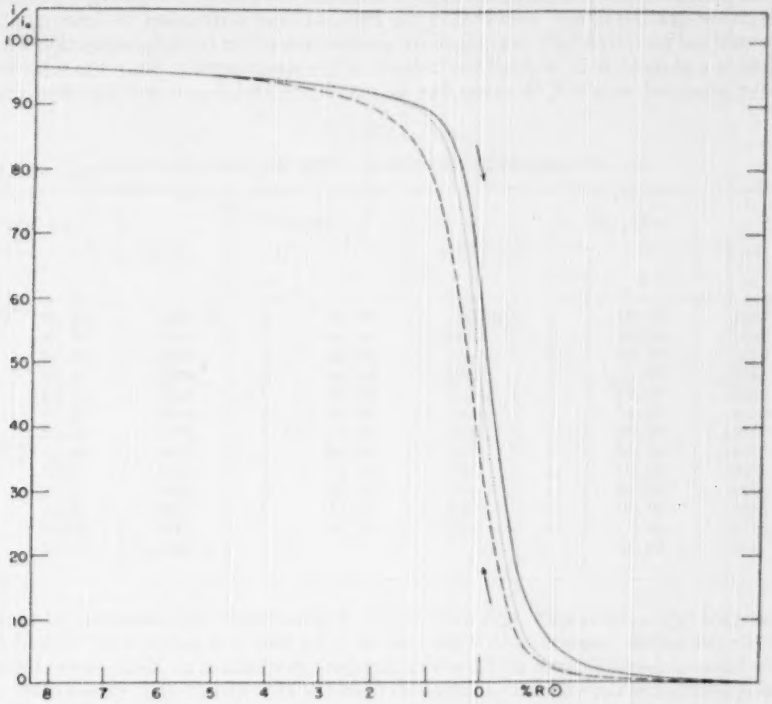

FIG. 3.—Solar limb profiles at 8.3 μ. The dashed and solid lines are the observed ascending and descending limbs, respectively. The dotted line represents the profile after correction for time delay.

limb was applied according to the method outlined by Minnaert, van den Hoven van Genderen, and van Diggelen[9] and employed by them for the reduction of photographic limb-darkening observations. Minnaert and his co-workers used the assumption of Wanders[10] that each point along a solar radius is blurred according to a Gaussian curve:

$$j = \frac{a}{\pi} e^{-a(\xi^2+\eta^2)}, \qquad (2)$$

where ξ and η are Cartesian co-ordinates, in units of a solar radius, measured in the direction of and normal to the solar radius. The quantity a is called the "scintillation constant" and is very large when the diffusion effects are very small. It was found that if the limb of the sun is taken as a straight edge, the effect of the diffusion process is to distort the intensity profile into an S-shaped curve similar to the dotted curve of Figure 3.

[8] *Zs. f. Phys.*, **79**, 722, 1932. [9] *Op. cit.* [10] *Zs. f. Ap.*, **8**, 108, 1934.

The position of the true limb is at the point of inflection. In practice, a family of theoretical curves with parameter a is computed. Comparison of the observed curve with the theoretical family yields an "observed" value for the scintillation constant, which may then be employed to derive the true intensity distribution. For the observations with the 24-inch reflector, the average value of a was 16,000, which means that for a distance of $1\frac{1}{2}\frac{1}{2}R_\odot$ the intensity has diminished by a factor of $1/e$.

Finally, the observed limb-darkening-curve is modified by the effect of scattered light in the spectroscope. The scattered light of different wave lengths is greatly minimized by the coarse-grating filters[11] provided in the Perkin-Elmer instrument. A determination of the residual scattered light was made by observation of the recorder deflection with and without a glass filter in front of the first slit of the spectrometer. Since the solar energy-curve observed with a *KBr* prism has its maximum at 1.6 μ, it was assumed that the

TABLE 1

SOLAR LIMB DARKENING FOR THE SPECTRAL REGION 3.5–10.2 μ

$\overline{\cos\theta}$	10.2 μ (Wt. 9)		$\overline{\cos\theta}$	8.3 μ (Wt. 17)		$\overline{\cos\theta}$	3.5 μ (Wt. 23)	
	I	Wt.		I	Wt.		I	Wt.
0.9963	99.90	3	0.9967	99.99	2	0.9960	99.85	2
.9692	99.88	3	.9786	99.79	3	.9708	99.78	2
.9105	99.62	3	.9409	99.81	3	.9298	99.34	2
.8437	99.28	2	.8808	99.24	3	.8514	98.59	3
.7469	98.94	2	.7931	98.95	3	.7480	97.34	2
.6634	98.47	1	.6609	98.16	3	.6631	96.09	1
.5780	97.98	3	.5519	97.34	3	.5797	95.25	2
.5271	97.51	3	.4847	96.56	3	.5198	94.29	3
.4680	96.93	3	.4475	96.17	3	.4650	93.32	2
.3975	96.19	3	.4022	95.58	3	.4003	92.03	3
.3255	95.40	3	.3301	94.47	3	.3290	90.56	3
.2713	94.93	3	0.2152	92.74	2	.2755	89.29	3
0.2153	94.55	2				0.2098	87.97	3

scattered light originated at this wave length. The scattered light, measured at the center of the sun's disk, amounted to 9 per cent at 3.5 μ and to 1 per cent at 8.3 and 10.2 μ. The limb-darkening-curve at 1.6 μ was therefore normalized to these percentages, and the quantities so derived were subtracted from the appropriate drift-curves after correction for time delay and scintillation.

To summarize, the observations with the 24-inch reflector consisted of a total of twenty-three runs on two separate days at 3.5 μ, seventeen runs on two days at 8.3 μ, and nine runs on one day at 10.2 μ. Each curve was measured at about forty points along the radius. At each wave length the observations were then averaged to yield mean drift-curves for the east and west limbs separately. The curves were then corrected for time delay and the results for the two limbs averaged. Finally, the corrections for diffusion and scattered light were applied in the manner described above.

The results for the region 3.5–10.2 μ are collected in Table 1 and plotted in Figure 4. The number in parentheses beside the wave-length region refers to the total number of runs made at each wave length. The second column of Table 1 gives the average value of the relative intensity corresponding to the values of $\cos\theta$ in the first column. Finally, the number of different values of $\cos\theta$ that were averaged into each normal point is indicated in the third column.

[11] J. U. White, *J. Opt. Soc. America*, **39**, 713, 1947.

Figure 4 shows that the degree of limb darkening decreases in the infrared from 3.5 to 10.2 μ. This result is qualitatively consistent with a systematic increase of the solar continuous opacity toward longer wave lengths in the infrared, as predicted by theoretical calculations of the absorption coefficient of the negative hydrogen ion.[12] The increase of opacity in the infrared, combined with the relatively high excitation potentials of infra-

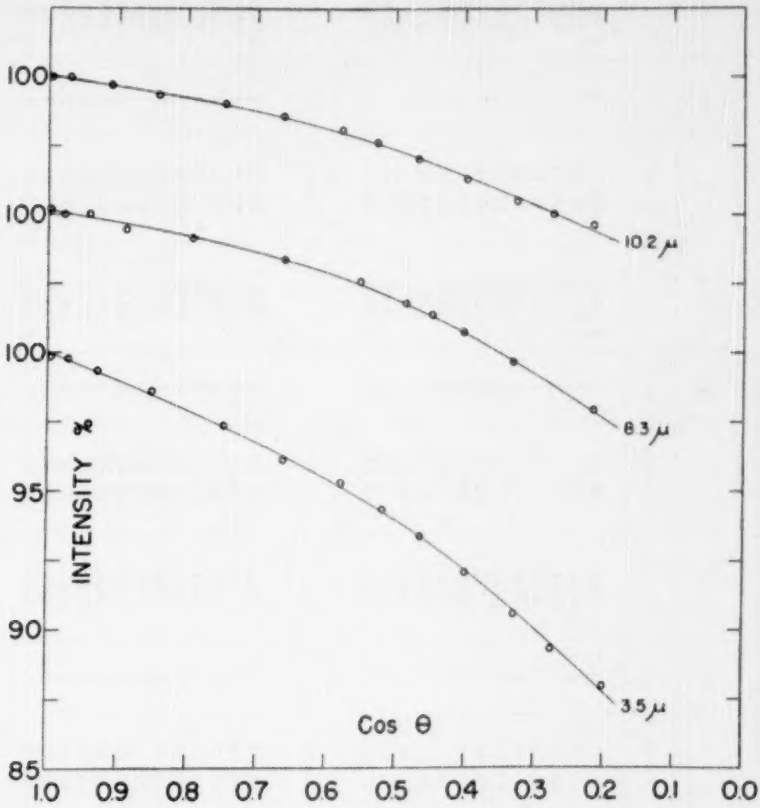

FIG. 4.—Solar limb-darkening-curves for the region 3.5–10.2 μ

red atomic lines, makes it probable that infrared solar absorption lines are relatively few and weak.[13] Hence they should have little or no effect on low-resolution limb-darkening observations that take in a broad spectral region.

Region 0.5–2.2 μ.—The response to radiation of the amplifying and recording system of the McGregor spectrometer departs from linearity for small values of the deflection. The drift-curves were therefore converted to a true intensity scale with the aid of the calibration-curve derived by McMath and Mohler.[6] The remainder of the reduction procedure was much less complex than that outlined in the preceding section. A determina-

[12] Chandrasekhar and Breen, *Ap. J.*, **104**, 430, 1946.

[13] McMath and Goldberg, *Proc. Amer. Phil. Soc.*, **93**, 362, 1949.

TABLE 2

SOLAR LIMB DARKENING FOR THE SPECTRAL REGION 0.5–2.2 μ

$\cos\theta$	I	Wt.	$\cos\theta$	I	Wt.	$\cos\theta$	I	Wt.	$\cos\theta$	I	Wt.	$\cos\theta$	I	Wt.
	λ 5485 (Wt. 2)			λ 6980 (Wt. 8)			λ 9920 (Wt. 9)			λ 15397 (Wt. 12)			λ 20664 (Wt. 8)	
0.9954	100.26	4	0.9965	99.52	3	0.9963	99.82	3	0.9964	100.01	4	0.9959	99.95	4
.9696	98.40	4	.9749	98.85	4	.9734	99.31	4	.9731	99.80	4	.9722	99.73	4
.9217	95.21	4	.9293	96.79	3	.9284	97.78	3	.9250	98.73	4	.9255	98.90	4
.8457	91.41	4	.8563	93.86	4	.8554	95.30	4	.8521	97.11	4	.8505	97.73	4
.7531	86.15	3	.7573	89.14	3	.7550	91.67	3	.7580	95.14	3	.7485	96.23	3
.6438	79.01	3	.6475	83.57	3	.6463	87.80	3	.6460	92.27	3	.6439	93.86	3
.5333	71.92	1	.5473	78.24	1	.5451	83.85	1	.5486	89.86	1	.5463	91.98	1
.4715	67.97	4	.4685	73.82	4	.4680	80.36	4	.4669	87.35	4	.4642	89.69	4
.4031	62.77	5	.3998	69.77	5	.3959	76.81	5	.3969	84.89	5	.3938	87.63	5
.3223	57.65	3	.3237	64.91	3	.3209	73.11	3	.3203	81.48	3	.3169	85.09	3
.2573	52.15	5	.2592	60.19	4	.2608	69.47	3	.2580	78.36	3	.2554	82.60	3
.2048	47.24	2	.2111	56.30	2	.2141	66.41	3	.2099	75.61	3	.2088	80.39	3
0.1631	43.06	2	0.1684	51.93	2	0.1690	62.81	2	0.1612	71.30	2	0.1598	77.30	2
	λ 6151 (Wt. 4)			λ 8384 (Wt. 8)			λ 11973 (Wt. 13)			λ 17093 (Wt. 15)			λ 22870 (Wt. 11)	
0.9967	99.48	3	0.9956	99.62	3	0.9964	99.82	4	0.9948	99.89	4	0.9960	100.05	4
.9725	98.67	4	.9723	98.74	4	.9733	99.21	4	.9727	99.71	4	.9732	99.68	4
.9270	96.49	3	.9272	97.40	3	.9279	98.23	4	.9263	98.92	4	.9263	99.07	4
.8585	92.83	4	.8548	94.59	4	.8544	96.11	4	.8514	97.56	4	.8514	97.74	4
.7613	87.66	3	.7539	90.65	3	.7597	93.21	4	.7575	95.90	2	.7520	96.02	3
.6592	81.80	2	.6495	86.59	2	.6438	89.60	3	.6448	93.57	3	.6447	94.13	3
.5462	75.87	2	.5431	81.45	2	.5458	85.85	3	.5473	91.15	1	.5472	91.98	1
.4723	71.02	3	.4716	78.17	4	.4675	82.83	4	.4650	88.73	4	.4649	89.93	4
.3993	65.75	5	.3971	74.34	5	.3960	79.67	5	.3947	86.38	5	.3952	87.98	5
.3206	60.48	3	.3233	69.96	2	.3190	76.21	3	.3176	83.32	3	.3175	85.21	3
.2613	55.64	4	.2619	66.36	4	.2565	72.36	3	.2562	80.37	3	.2561	83.05	3
.2094	51.51	2	.2137	63.31	2	.2093	69.39	3	.2098	77.93	3	.2097	80.70	3
0.1632	46.41	2	0.1732	59.78	2	0.1650	65.94	2	0.1608	73.93	2	0.1608	76.86	2

tion of the response-curve $K(t)$ of the combined cell, amplifier, and recorder showed a nearly exponential approach to the height of the step-intensity function with a time constant of 0.8 seconds. Since the time constant was short and the rate of scanning was slow, the effect of the time delay was a bodily displacement of each drift-curve along the time axis, without any appreciable alteration in shape. The only correction required for time delay was the above shift of origin, and the observations at the east and west limbs could therefore be averaged directly. The symmetry of the drift-curves is well illustrated in Figure 2, *b*.

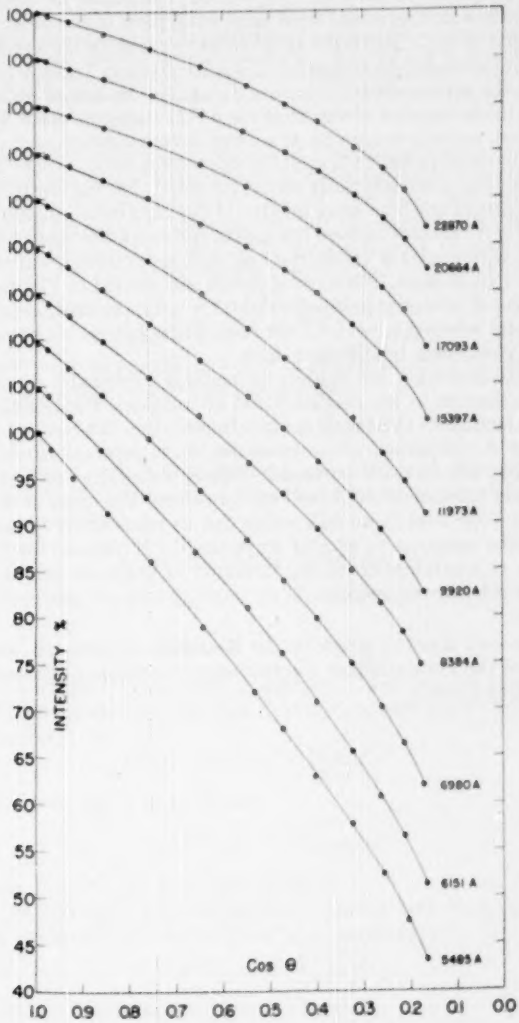

FIG. 5.—Solar limb-darkening-curves for the region 0.5–2.2 μ

As was pointed out in the previous section, the effects of scintillation, etc., blur the intensity profile into an **S**-shaped curve, and comparison of the observed curve with a theoretical family of curves serves to determine the scintillation constant, a. Owing to uncertainties in the calibration between intensity and recorder deflection for very small deflections, it was impossible to determine the scintillation constant with high precision and to correct the measurements at the extreme limb. Estimates of a, however, varied between 30,000 and 160,000, depending on the seeing. Since the error introduced at $\cos\theta = 0.16$ by a scintillation constant of 30,000 is 0.1 per cent, it was considered safe to carry out the measurements to $\cos\theta = 0.16$, without correction for diffusion. The zero point of the $\cos\theta$ scale was determined from large-scale plots of the intensity profile, and the point of inflection of each **S**-curve was taken as the limb or zero point.

The results for the wave-length region 0.5–2.2 μ are given in Table 2, where successive columns list $\overline{\cos\theta}$, the mean relative intensity I, and the weight of each normal point. The latter is equal to the number of values of $\cos\theta$ that comprise $\overline{\cos\theta}$. Usually three or four drift-curves were made in succession at a given wave length on each of 2-4 days. The weight assigned to each wave length is equal to the total number of runs and is indicated in parentheses beside the wave length. It should be noted that the wave lengths reported in Table 2 are averages of the true wave lengths of the runs distributed in a wave-length interval of about 100 A centered around the mean. Although the mean wave length may coincide in position with a solar or terrestrial line, each separate run was made in the continuum in a region free of lines. The normal points are plotted in Figure 5.

The probable error of a normal point of weight 3 is ± 0.2 per cent, except for the point closest to the limb, for which p.e. $= \pm 0.5$ per cent. These figures are based on deviations from the mean for runs made on different days.

Measures of limb darkening are subject to possible systematic errors from facular areas or other disturbances in the neighborhood of sunspots. For example, Figure 2, *a*, shows the effect of faculae in the sunspot zone. In addition, the center-to-limb contrast may vary with time. A comparison of our measures, by interpolation, with the extensive series of measures by Abbot shows systematic differences as large as 1 per cent for certain wave lengths and agreement to 0.1 per cent for others. The cause of the discrepancies is unknown, and we hope that these differences can be resolved by further observation.

An extension of the measures to shorter wave lengths is planned for the near future. In the meantime a redetermination of the structure of the solar atmosphere from the above observations is being undertaken.

We acknowledge with thanks a grant by the Research Corporation, which made possible the purchase of the Perkin-Elmer spectrometer, as well as continued grants-in-aid by McGregor Fund of Detroit.

DYNAMICS OF STAR STREAMING. II

P. STEHLE
University of Pittsburgh
Received April 10, 1950

ABSTRACT

Previous work on an extension of Chandrasekhar's treatment of stellar dynamics is continued. The potential energy of the star system is assumed to be subject to two first-order differential equations, and it is shown that, as a consequence, only systems with plane, cylindrical, or spherical symmetry are possible. The results are applied to a system whose mass is concentrated in a point nucleus, yielding a spherically symmetrical potential.

In a previous paper[1] some consequences of Chandrasekhar's postulates[2] for a stellar system were developed. It will be recalled that the quantities of interest in the theory are the coefficients a_{ij} of the Schwarzschild velocity ellipsoid, the components U_0^i of the average velocity of stars in a neighborhood, and the potential function V under whose influence the stars move. The quantity V is considered a smooth function of the co-ordinates. In Paper I it was shown that if V is regarded as subject to only one condition of the form

$$c^i V_{,i} = 0 ,$$

then the vector c^i must be parallel to a field of Euclidean motions, and the coefficients of the velocity ellipsoid may be expressed in the form

$$a_{ij} = A g_{ij} + B c_i c_j ,$$

where A is a constant and B is a constant, provided that the vector c^i actually is a Euclidean motion. It is the purpose of the present paper to consider more stringent conditions on the potential V.

I. SECOND-ORDER CONDITION ON V

A potential function can be subjected to, at most, two homogeneous first-order conditions,

$$c^{\alpha i} V_{,i} = 0 , \qquad \alpha = 1, 2 , \tag{1}$$

since, if the two vectors $c^{\alpha i}$ are linearly independent, this fixes the direction of ∇V at each point. The $c^{\alpha i}$ themselves are restricted by the condition that their vector product be parallel to a gradient:

$$c^1 \times c^2 = \lambda \nabla \phi .$$

Elimination of the scalars λ and ϕ yields

$$c^{2s} c^{1r}_{\ ,s} - c^{1s} c^{2r}_{\ ,s} = G_\alpha c^{\alpha r} , \tag{2}$$

where G_α is some function of the co-ordinates.

In addition to first-order conditions, the potential may be subject to second-order conditions. We assume one such condition to be imposed:

$$d^r V_{,r} + d^{rs} V_{,rs} = 0 . \tag{3}$$

[1] *Ap. J.*, **110**, 250, 1949, hereafter referred to as "Paper I."

[2] *Principles of Stellar Dynamics* (Chicago: University of Chicago Press, 1942).

We assume further that equations (1) and (3) are the only conditions imposed on V, and we then seek the possible forms for the velocity ellipsoid and the restrictions to be placed on the choice of the c_i^α. We shall show that in this case also c_i^α must be chosen parallel to a field of Euclidean motions. First, however, we show that the second-order condition (3) does not influence the form of the tensor a_{ij}.

The procedure is the same as in Paper I. Chandrasekhar's compatibility conditions are to be consequences of equations (1) and (3). From Paper I (eqs. [4.6] and [4.7]) we obtain

$$\epsilon^{pir} a_i^s + \epsilon^{pis} a_i^r = N_\alpha^{ps} c^{\alpha r} + N_\alpha^{pr} c^{\alpha s} + 2B^p d^{rs} , \tag{4}$$

$$\epsilon^{pij} a_{i,j}^r = M_\alpha^p c^{\alpha r} + N_\alpha^{ps} c_{,s}^{\alpha r} + B^p d^r . \tag{5}$$

These equations are solved for the B^p. To do this, define

$$A^{prs} = \epsilon^{pir} a_i^s + \epsilon^{pis} a_i^r - 2B^p d^{rs} . \tag{6}$$

Then

$$A^{prs} c_r^\alpha c_{\alpha s} = 2 N_\alpha^{ps} c_s^\alpha , \tag{7}$$

$$A^{prs} g_{rs} = 2 N_\alpha^{ps} c_s^\alpha = -2B^p d_s^s . \tag{8}$$

If we subtract equation (8) from equation (7), we obtain

$$2B^p d_s^s + A^{prs} c_r^\alpha c_{\alpha s} = 0 . \tag{9}$$

Defining

$$D = d^{rs} c_r^\alpha c_{\alpha s} - d_s^s \qquad \text{and} \qquad a_i^\alpha = a_i^r c_r^\alpha$$

equation (9) becomes

$$B^p = \frac{1}{D} \epsilon^{pir} a_i^\alpha c_{\alpha r} . \tag{10}$$

It will appear below that, in cases of interest, B^p vanishes.

The form of the a_{ij} may now be found. To do this, apply lemma 2 of Paper I, section 4, to the quantity A^{prs} of equation (6). Thus

$$\begin{aligned} \epsilon^{pir} a_i^s + \epsilon^{pis} a_i^r - 2B^p d^{rs} &= c^{\alpha r} c_{\alpha t} (\epsilon^{pis} a_i^t + \epsilon^{pit} a_i^s) + c^{\alpha s} c_{\alpha t} (\epsilon^{pir} a_i^t + \epsilon^{pit} a_i^r) \\ &- c^{\alpha r} c^{\beta s} c_{\alpha m} c_{\beta n} (\epsilon^{pim} a_i^n + \epsilon^{pin} a_i^m) - 2B^p (c^{\alpha r} c_{\alpha t} d^{st} + c^{\alpha s} c_{\alpha t} d^{rt} - c^{\alpha r} c^{\beta s} c_{\alpha m} c_{\beta n} d^{mn}) . \end{aligned} \tag{11}$$

Multiplication by E_{prs} and summation over p and s yields

$$a_k^r = (a_i^i - c^{\alpha s} a_{\alpha s}) \delta_k^r + 2 a^{\beta s} c_{\beta s} c^{\alpha r} c_{\alpha k} + c^{\alpha r} a_{\alpha k} - c_k^\alpha a_{\alpha r} - 2B^p \epsilon_{pks} D^{rs} , \tag{12}$$

where

$$D^{rs} = c^{\alpha r} c_{\alpha t} d^{st} + c^{\alpha s} c_{\alpha t} d^{rt} - c^{\alpha r} c^{\beta s} c_{\alpha m} c_{\beta n} d^{mn} - d^{rs} . \tag{13}$$

Finally, then,

$$a_{jk} = A g_{jk} + B_{\alpha\beta} c_j^\alpha c_k^\beta + c_j^\alpha a_{\alpha k} - c_k^\alpha a_{\alpha j} - 2B^p \epsilon_{pks} D_j^s , \tag{14}$$

where A and $B_{\alpha\beta}$ are scalars. The symmetry of a_{jk} yields

$$c_j^\alpha a_{\alpha k} - c_k^\alpha a_{\alpha j} = B^p (\epsilon_{pks} D_j^s - \epsilon_{pjs} D_k^s) . \tag{15}$$

The left side of equation (15) may be represented by $\Lambda^q \epsilon_{qjk}$ with

$$\begin{aligned} \Lambda^q &= \tfrac{1}{2}\epsilon^{qkj}(c^\alpha_j a_{\alpha k} - c^\alpha_k a_{\alpha j}) \\ &= \epsilon^{qkj} c^\alpha_j a_{\alpha k} \\ &= -DB^q , \end{aligned} \tag{16}$$

where the last step involves equation (10). However, equation (15) may be written

$$\begin{aligned} \Lambda^q &= B^p \epsilon^{qkj} \epsilon_{pks} D^s_j \\ &= (\delta^j_s \delta^q_p - \delta^q_p \delta^j_s) B^p D^s_j \\ &= B^j D^q_j - B^q D^s_s . \end{aligned} \tag{17}$$

Combining equations (17) and (16), we have

$$D^q_j B^j = (D^s_s - D) B^q . \tag{18}$$

But, from the definitions of D^q_j and D, $D^s_s = D$, and so

$$D^q_j B^j = 0 , \qquad B^j = 0 , \qquad \text{or} \qquad |D^q_j| = 0 . \tag{19}$$

Thus, provided that neither the determinant nor the trace of D^q_j vanishes, the quantities B^j are zero, and the second-order conditions on V do not influence the compatibility conditions. In cases of interest neither the determinant nor the trace vanishes.

The vanishing of B_p also implies the vanishing of the third and fourth terms in equation (14), owing to equation (15), and so we have

$$a_{jk} = A\, g_{jk} + B_{\alpha\beta} c^\alpha_j c^\beta_k . \tag{20}$$

The tensor a_{jk} is still subject to the fundamental equation of Chandrasekhar's theory, namely (Paper I, eq. [2.12]),

$$a_{ij,\,k} + a_{jk,\,i} + a_{ki,\,j} = 0 . \tag{21}$$

From this we now deduce that the quantity A above is constant. First, we show that ∇A is parallel to ∇V. Equation (4) becomes, on the use of equation (19),

$$\epsilon^{pqj} A_{,\,j} = [M^p_\alpha - (B_{\alpha\beta,\,j} c^\beta_i + B_{\alpha\beta} c^\beta_{i,\,j}) \epsilon^{pij}]\, c^{\alpha q} + [N^{ps} - \epsilon^{pis} B_{\alpha\beta} c^\beta_i]\, c^{\alpha q}_{\ \ ,s} . \tag{22}$$

The use of lemma 2 of Paper I and equation (2) of this paper reduces the last term to $N^p G_\alpha c^{\alpha q}$, so that equation (21) may be written

$$\epsilon^{pqj} A_{,\,j} = \tilde{M}^p_\alpha c^{\alpha q} . \tag{23}$$

Then

$$\tilde{M}^p_\alpha = \epsilon^{pqj} A_{,\,j} c_{\alpha q} .$$

Inserting this into equation (22) yields

$$A_{,\,j} c^{\alpha j} = 0 \tag{24}$$

which shows that A is subject to the same conditions as V.

Equation (21) can be written

$$A_{,k}g_{ij}+A_{,i}g_{jk}+A_{,j}g_{ki}+B_{\alpha\beta,k}c_i^\alpha c_j^\beta+B_{\alpha\beta,i}c_j^\alpha c_k^\beta + B_{\alpha\beta,j}c_k^\alpha c_i^\beta+c_i^\alpha\Gamma_{\alpha jk}+c_j^\alpha\Gamma_{\alpha ki}+c_k^\alpha\Gamma_{\alpha ij}=0 \tag{25}$$

where

$$\Gamma_{\alpha ij}=B_{\alpha\beta}\left(c^\beta_{i,j}+c^\beta_{j,i}\right). \tag{26}$$

Multiplication of equation (25) by g^{jk} yields

$$5A_{,i}+P^{\alpha\beta}B_{\alpha\beta,i}+2B_{\alpha\beta,j}c^{\alpha j}c_{\beta i}+c_i^\alpha\Gamma^j_{\alpha j}+2\Gamma_{\alpha ki}c^{\alpha k}=0\,. \tag{27}$$

Multiplication of equation (25) by $c^j_\gamma c^{\gamma k}$ yields

$$2A_{,i}+2A_{,j}c^{\gamma j}c_{\gamma i}+P^{\alpha\beta}B_{\alpha\beta,i}+2B_{\alpha\beta,j}c^{\alpha j}c_i^\beta+c_i^\alpha\left(\Gamma_{\alpha jk}c^j_\gamma c^{\gamma k}\right)+2\Gamma_{\alpha ki}c^{\alpha k}=0\,. \tag{28}$$

Subtraction of equation (28) from equation (27) gives

$$3A_{,i}-2A_{,j}c^{\gamma j}c_{\gamma i}+\left(\Gamma^j_{\alpha j}-\Gamma_{\alpha jk}c^j_\gamma c^{\gamma k}\right)c_i^\alpha=0\,. \tag{29}$$

The second term vanishes, and multiplication with $c^{\beta i}$ makes the first term vanish because of equation (24). Thus the bracket vanishes, and we are left with

$$A_{,i}=0\,,\qquad A=\text{Constant}\,. \tag{30}$$

We now turn our attention to the quantities $B_{\alpha\beta}$ and $c^{\alpha i}$. Multiplying equation (25) by $V^i_{,}V^j_{,}$ we obtain

$$c_k^\alpha\Gamma_{\alpha ij}V^i_{,}V^j_{,}=0\,. \tag{31}$$

The matrix $\|c_k^\alpha\|$ was assumed to be of rank 2, so that equation (31) implies

$$\Gamma_{\alpha ij}V^i_{,}V^j_{,}=2B_{\alpha\gamma}c^\gamma_{i,j}V^i_{,}V^j_{,}=0\,. \tag{32}$$

If $\|B_{\alpha\beta}\|$ is of rank 2, then

$$c^\gamma_{i,j}V^i_{,}V^j_{,}=0\,. \tag{33}$$

Hence

$$c^{\gamma i}\left(V^j_{,}V_{,j}\right)_{,i}=0\,, \tag{34}$$

which shows that $(V^j_{,}V_{,j})_{,i}$ has the same direction in space as does $V_{,i}$. The functions V and $V^i_{,}V_{,i}$ have the same surfaces of constant value, and hence

$$V^i_{,}V_{,i}=f(V)\,. \tag{35}$$

The fact that the length of the gradient of V depends only on V and not explicitly on the co-ordinates implies that the lines of ∇V are straight. To see this, proceed as follows: Construct normals to a surface σ of constant V, each of length ϵ. The locus of the endpoints of these lines is a surface to which these lines are normal.[3] This new surface is an equipotential surface to approximation ϵ^2. Proceeding N times in this way, we arrive at a surface with the same normals as the original equipotential, which is an equipotential to approximation $N\epsilon^2$. Since N is of the order of $1/\epsilon$ to make the separation of the two surfaces finite, the final surface is an equipotential to approximation ϵ and hence is an

[3] L. P. Eisenhart, *Introduction to Differential Geometry* (Princeton: Princeton University Press, 1940), p. 272.

equipotential. The family of equipotentials has a set of normals in common, and hence the lines of ∇V are straight.

It is intuitively obvious that the only types of equipotential surfaces which can form families with common normals are planes, cylinders, and spheres. This follows from the fact that the potential must be singular wherever two lines of ∇V intersect. A formal proof can easily be given in terms of the surfaces of center of the family of equipotentials.

The vectors $c^{\alpha i}$, which are perpendicular to the direction of ∇V, must lie in the equipotential planes, cylinders, or spheres and hence are expressible as Euclidean motions, two translations, a translation and a rotation, or a pair of rotations, respectively. Explicitly, then,

Planes perpendicular to z-axis: $c^{\alpha i} = \delta^{\alpha i}$,

Cylinders parallel to z-axis: $c^{1i} = \{0, 0, 1\}$,

$$c^{2i} = \{-y, x, 0\}, \tag{36}$$

Spheres: $c^{1i} = \{0, -z, y\}$,

$$c^{2i} = \{z, 0, -x\}.$$

(In the spherical case rotations about any two axes imply the one around the third, owing to the properties of the rotation group.)

Corresponding to each type of symmetry there exists a solution for the coefficients $B_{\alpha\beta}$ occurring in the velocity ellipsoid tensor. In general, from equation (25) we have

$$B_{\alpha\beta,\,k} c_i^\alpha c_j^\beta + B_{\alpha\beta,\,i} c_j^\alpha c_k^\beta + B_{\alpha\beta,\,j} c_k^\alpha c_i^\beta = 0 \tag{37}$$

because the c_i^α, being Euclidean motions, satisfy the Killing equation,

$$c_{i,\,j}^\alpha + c_{j,\,i}^\alpha = 0 .$$

If we define Λ by

$$\Lambda_{\beta k j} = B_{\alpha\beta,\,j} c_k^\alpha + \tfrac{1}{2} B_{\alpha\beta,\,k} c_j^\alpha ,$$

then equation (37) becomes

$$\Lambda_{\beta k j} c_i^\beta + \Lambda_{\beta k i} c_j^\beta = 0 . \tag{38}$$

The corollary to lemma 2 of Paper I may be applied to this. The corollary states that if

$$N_\alpha^p c^{\alpha q} + N_\alpha^q c^{\alpha p} = 0$$

then

$$N_\alpha^p = N \epsilon_{\alpha\beta} c^{\beta p} .$$

Thus

$$\Lambda_{\beta k j} = \tfrac{3}{2} \Lambda_k \epsilon_{\beta\gamma} c_j^\gamma$$

$$= B_{\alpha\beta,\,j} c_k^\alpha + \tfrac{1}{2} B_{\alpha\beta,\,k} c_j^\alpha .$$

Hence

$$B_{\alpha\beta,\,k} c_j^\alpha = 2 \Lambda_j \epsilon_{\beta\alpha} c_k^\alpha - \Lambda_k \epsilon_{\beta\alpha} c_j^\alpha .$$

Multiply by c_γ^j and sum over j:

$$B_{\gamma\beta,\,k} = 2 \Lambda_\gamma \epsilon_{\beta\alpha} c_k^\gamma - \Lambda_k \epsilon_{\beta\gamma} , \qquad \Lambda_\gamma = \Lambda_j c_\gamma^j .$$

Since $B_{\gamma\beta} = B_{\beta\gamma}$, we obtain

$$B_{\alpha\beta,\,k} = \Lambda_\alpha \epsilon_{\beta\gamma} c_k^\gamma + \Lambda_\beta \epsilon_{\alpha\gamma} c_k^\gamma . \tag{39}$$

This last equation may be integrated in the three cases as follows:

Planes:
$$B_{11} = \Lambda y^2 + 2\lambda_1 y + l_{11},$$
$$B_{22} = \Lambda x^2 + 2\lambda_2 x + l_{22},$$
$$B_{12} = -\Lambda xy - \lambda_1 x - \lambda_2 y + l_{12}.$$

Then
$$a_{ij} = \begin{pmatrix} A + \Lambda y^2 + 2\lambda_1 y + l_{11} & — & — \\ -\Lambda xy - \lambda_1 x - \lambda_2 y + l_{12} & A + \Lambda x^2 + 2\lambda_2 x + l_{22} & — \\ 0 & 0 & A \end{pmatrix}.$$

Cylinders:
$$B_{\alpha\beta} = \text{Constant} = l_{\alpha\beta},$$

so that
$$a_{ij} = \begin{pmatrix} A + l_{11} y^2 & — & — \\ l_{11} xy & A + l_{11} x^2 & — \\ -l_{12} y & l_{12} x & A + l_{22} \end{pmatrix}.$$

Spheres:
$$B_{\alpha\beta} = \frac{\Lambda x_\alpha x_\beta}{z^2} + \frac{\lambda_\alpha x_\beta + \lambda_\beta x_\alpha}{z} + l_{\alpha\beta}, \tag{40}$$

so that
$$a_{ij} = \begin{pmatrix} A + \Lambda y^2 + 2\lambda_2 y\, z + l_{22} z_2 & — & — \\ -\Lambda xy - (\lambda_2 x + \lambda_1 y)\, z - l_{12} z^2 & A + \Lambda x^2 + 2\lambda_1 x\, z + l_{11} z^2 & — \\ \lambda_1 y^2 - \lambda_2 xy - (l_{22} x - l_{12} y)\, z & -\lambda_1 xy + \lambda_2 x^2 + (l_{12} x - l_{11} y)\, z & A + l_{11} y^2 + l_{22} x^2 - 2 l_{12} xy \end{pmatrix}. \tag{41}$$

The spherical case is the only one of great physical or astronomical interest. It is the subject of the following section.

II. NUCLEAR STAR SYSTEMS

The steady state of a star system whose mass is concentrated chiefly in a heavy nucleus may be investigated by the methods just developed. With the mass so concentrated, the stars of the system may be considered to move in a spherically symmetrical potential V, which satisfies the Laplace equation; V is thus uniquely determined.

The distribution of velocities of the stars may be completely symmetrical. There is then no star streaming, and there will exist no differential motions. This is not necessarily so, however, and, on the basis of our previous results, we seek the most general velocity distribution.

Spherical symmetry requires the potential V to be invariant under independent rotations about any two axes intersecting at the center of symmetry. We choose these axes to be the x- and y-axes of a Cartesian co-ordinate system with origin at the nucleus. The conditions on V may then be written as follows:

$$c^{\alpha i} V_{,i} = 0, \qquad \alpha = 1, 2, \tag{42}$$

with the vectors $c^{\alpha i}$ given by

$$c^{1i} = \{0, -z, y\},$$
$$c^{2i} = \{z, 0, -x\}. \tag{43}$$

The results just derived for spherical symmetry may now be used. The coefficients a_{ij} of the distribution of the residual velocities of stars at any point are given by equation (41).

The tensor a_{ij} is invariant under reflection of the co-ordinates, since its elements are all homogeneous of the second degree. This means that the principal axes of the velocity ellipsoid at antipodal points are parallel. It will be shown below that one of these axes is radial, and hence the other two must be tangential to a sphere with origin as center. At each point of the sphere, then, two mutually orthogonal directions are defined, these directions being continuous functions of the co-ordinates on the sphere. However, no such orthogonal net exists on the surface of a sphere without there existing at least one singular point. In our case, because of the parallelism at antipodal points, there must be two such singular points. At these singular points, the eigen-values of the velocity ellipsoid tensor corresponding to tangential directions must be equal. This equality puts some restrictions on the coefficients occurring in the a_{ij}.

It is convenient to transform to spherical polar co-ordinates. To do this, we use the expression of equation (20) for the a_{ij} and equation (40) for the $B_{\alpha\beta}$, which are scalars. Let the new co-ordinates be

$$\bar{x}^1 = r\,, \qquad \bar{x}^2 = \theta\,, \qquad \bar{x}^3 = \varphi\,,$$

and

$$x^1 = r\cos\theta\,, \qquad x^2 = r\sin\theta\cos\varphi\,, \qquad x^3 = r\sin\theta\sin\varphi\,. \tag{44}$$

Then

$$\begin{aligned} B_{11} &= \Lambda\,\frac{\cot^2\theta}{\sin^2\varphi} + 2\lambda_1\,\frac{\cot\theta}{\sin\varphi} + l_{11}\,,\\ B_{22} &= \Lambda\cot^2\varphi + 2\lambda_2\cot\varphi + l_{22}\,,\\ B_{12} &= \Lambda\,\frac{\cot\theta\cot\varphi}{\sin\varphi} + \lambda_1\cot\varphi + \lambda_2\,\frac{\cot\theta}{\sin\varphi} + l_{12}\,. \end{aligned} \tag{45}$$

Also, since $\bar{c}^\alpha_i = c^\alpha_j(\partial x^j/\partial\bar{x}^i)$, we have

$$\begin{aligned} \bar{c}^1_i &= \{0,\ 0,\ r^2\sin^2\theta\}\,,\\ \bar{c}^2_i &= \{0,\ -r^2\sin\theta,\ -r^2\sin\theta\cos\theta\cos\varphi\}\,. \end{aligned} \tag{46}$$

The r component vanishes, since rotations leave r invariant.

The lack of l components for the c^α_i shows that the first row and first column of a_{ij} vanish except for the ll element, which is A. Thus one of the principal axes of the velocity ellipsoid is radial. The other two are, then, necessarily tangential. To find the directions of the tangential principal axes, we write

$$(A\,\bar{g}_{ij} + B_{\alpha\beta}\bar{c}^\alpha_i\bar{c}^\beta_j)\,\bar{u}^j = \mathfrak{a}\,\bar{g}_{ij}\bar{u}^j \tag{47}$$

or

$$B_{\alpha\beta}\bar{c}^\alpha_i\bar{c}^\beta_j\bar{u}^j = (\mathfrak{a} - A)\,\bar{g}_{ij}\bar{u}^j\,. \tag{48}$$

The tensor $B_{\alpha\beta}c^\alpha_i c^\beta_j$ is of rank 2 and has the following elements:

$$B_{\alpha\beta}\bar{c}^\alpha_2\bar{c}^\beta_2 = r^4(\Lambda\cos^2\varphi + 2\lambda_2\sin\varphi\cos\varphi + l_{22}\sin^2\varphi)\,;$$

$$\begin{aligned} B_{\alpha\beta}\bar{c}^\alpha_2\bar{c}^\beta_3 = r^4(&\Lambda\sin^2\theta\cos^2\theta\sin^2\varphi + 2\lambda_1\sin^3\theta\cos\theta\sin\varphi - 2\lambda_2\sin^2\theta\cos^2\theta\\ &\times\sin\varphi\cos\varphi + l_{11}\sin^4\theta - 2l_{12}\sin^3\theta\cos\theta\cos\varphi + l_{22}\sin^2\theta\cos^2\theta\cos^2\varphi)\,; \end{aligned} \tag{49}$$

$$\begin{aligned} B_{\alpha\beta}\bar{c}^\alpha_2\bar{c}^\beta_3 = r^4[&-\lambda_1\sin^2\theta\cos\varphi + \lambda_2\sin\theta\cos\phi\,(2\cos^2\varphi - 1)\\ &+ (l_{22} - \Lambda)\sin\theta\cos\theta\sin\varphi\cos\varphi - l_{12}\sin^2\theta\sin\varphi]\,. \end{aligned}$$

We take the poles of the spherical co-ordinate system to be the two singular points on the sphere. Then, as θ approaches zero, the two eigen-values of this tensor must become equal and independent of φ. Calling this eigen-value μ, we must have, near $\theta = 0$,

$$B_{\alpha\beta} c_i^\alpha c_j^\beta = \mu g_{ij} , \qquad i, j = 2, 3 . \tag{50}$$

The necessary and sufficient conditions for this are

$$\Lambda = l_{22} , \qquad \lambda_2 = 0 . \tag{51}$$

This yields

$$\begin{aligned} B_{\alpha\beta} c_2^\alpha c_2^\beta &= r^4 \Lambda , \\ B_{\alpha\beta} c_3^\alpha c_3^\beta &= r^4 [\Lambda \sin^2\theta \cos^2\theta + 2 \sin^3\theta \cos\theta (\lambda_1 \sin\varphi - l_{12} \cos\varphi) + l_{11} \sin^4\theta] , \\ B_{\alpha\beta} c_2^\alpha c_3^\beta &= - r^4 \sin^2\theta (\lambda_1 \cos\varphi + l_{12} \sin\varphi) . \end{aligned} \tag{52}$$

We investigate the variation of the direction of the principal axes with θ along a curve of constant φ, say, $\varphi = 0$. The eigen-value equation becomes

$$\begin{vmatrix} \Lambda - \mu & -\lambda_1 \sin^2\theta \\ -\lambda_1 \sin^2\theta & \Lambda \sin^2\theta \cos^2\theta + l_{11} \sin^4\theta - 2 l_{12} \sin^3\theta \cos\theta - \mu \end{vmatrix} = 0 . \tag{53}$$

Thus

$$\mu = \Lambda + \frac{f(\theta)}{2} \pm [f^2(\theta) - 4\lambda_1^2 \sin^4\theta]^{1/2} , \tag{54}$$

where

$$f(\theta) = -\Lambda (1 - \sin^2\theta \cos^2\theta) + l_{11} \sin^4\theta - 2 l_{12} \sin^3\theta \cos\theta .$$

Assuming $2\lambda_1 \sin^2\theta \ll f(\theta)$, we may write

$$\mu \approx \Lambda + f(\theta) \qquad \text{or} \qquad \Lambda + \frac{2\lambda_1^2 \sin^4\theta}{f^2(\theta)} . \tag{55}$$

The second root corresponds to a principal axis nearly in the θ-direction, while the first corresponds to one nearly in the φ-direction.

In general, the direction of the shortest principal axis, the axis of "star streaming," varies in a complicated way between the two poles. At the poles the velocity ellipsoid is a surface of revolution, with the unique axis, if any, in the radial direction.

SCATTERING BY A MOVING ELECTRON ATMOSPHERE AND ITS EFFECT ON SPECTRAL LINES. I. THE SCHUSTER PROBLEM

FRANK N. EDMONDS, JR.
Yerkes Observatory
Received June 16, 1950

ABSTRACT

The problem of the transfer of radiation in an atmosphere of free electrons undergoing differential expansion is solved in the first approximation under the conditions of the standard Schuster problem of line formation. It is further assumed that electron scattering is in accordance with the frequency-independent Thomson scattering coefficient, the Rayleigh phase function, and a Maxwellian distribution of thermal velocities. In the solution, account is taken of the noncoherent character of the scattering due to velocities arising from the thermal and mass motions of the electrons.

The solution for radiation emerging from the atmosphere contains terms for unscattered and scattered radiation. The latter contains a function which represents the spectral distribution of scattered radiation for incident monochromatic radiation. The shape of this function, which is due to the thermal motions of the electrons, produces broad spectral lines characterized by a shallow center and extended wings. Further, a shift of this spectral distribution function resulting from the differential expansion of the atmosphere produces asymmetries in spectral lines. Two numerical examples of these effects have been calculated.

I. INTRODUCTION

The importance of scattering of radiation by free electrons in high-temperature stellar atmospheres has been recognized more and more in recent years. The contribution of this type of scattering to the continuous opacity in stars of type O or early B and the effects which result from this contribution have been discussed by several authors.[1] In addition, this scattering produces a broadening and a shift in spectral lines because of the Compton effect and the Doppler effect arising from mass and thermal motions of the scattering electrons. An analysis of these resulting effects on the profiles of spectral lines leads to an interesting class of problems in radiative-transfer theory involving noncoherent scattering, i.e., scattering which redistributes the radiation in frequency. Such an analysis of the shifts effected by Compton scattering has been made by Chandrasekhar,[2] while Münch[3] has investigated the broadening due to thermal motions of the free electrons. However, there are definite indications that considerable mass motions, such as expansion, rotation, or turbulence, are present in the atmospheres of many high-temperature stars. In particular, differential expansion appears to exist in the atmospheres of Wolf-Rayet stars and supernovae. The term "differential expansion" is used to designate radial expansion of an atmosphere with a velocity that is a function of radial distance. Chandrasekhar[4] has shown that differential expansion with a velocity which varies linearly with optical depth will lead to the formation of absorption lines which are asymmetric and are shifted, effects which in planetary nebulae can produce a large reduction of the radiation pressure in Lyman-α. It would seem desirable, therefore, to study the changes in the contours of the emergent spectral lines produced by mass motions of the electrons.

In this paper the methods of radiative-transfer theory developed by Chandrasekhar[5]

[1] A. Unsöld, *Zs. f. Ap.*, **21**, 229, 1942; J. L. Greenstein, *Ap. J.*, **95**, 299, 1942; S. Chandrasekhar, *Ap. J.*, **103**, 351, 1946; M. Rudkjøbing, *Pub. mind. Medd. Københavns Obs.*, No. 145, 1947; Anne B. Underhill, *Ap. J.*, **107**, 349, 1948, **110**, 340, 1949, **111**, 203, 1950, and *M.N.*, **109**, 562, 1949.

[2] *Proc. R. Soc. London, A*, **192**, 508, 1948.

[3] *Ap. J.*, **108**, 116, 1948.

[4] *Rev. Mod. Phys.*, **17**, 138, 1948; *Ap. J.*, **102**, 402, 1945.

[5] *Radiative Transfer* (Oxford: Clarendon Press, 1950).

will be used to analyze the transfer of monochromatic radiation through a plane-parallel atmosphere of free electrons. These electrons will have thermal motions superposed on a mass motion arising from differential expansion. The Compton effect, which produces shifts of the order of magnitude of the Compton wave length (0.024 A), will be neglected in this discussion. A solution of the appropriate equation of radiative transfer subject to the boundary conditions of the Schuster problem will be obtained in the first approximation. The results will be used to illustrate the change produced in the profiles of spectral lines by the noncoherent electron scattering.

II. FORMULATION OF THE PROBLEM; EMISSION COEFFICIENT AND EQUATION OF TRANSFER

The radiative-transfer problem to be formulated is for an atmosphere undergoing differential expansion and consisting only of free electrons in thermal motion. As in the standard Schuster problem, it will be supposed that this electron atmosphere is a layer of finite optical thickness lying above an infinite plane surface radiating outward into the atmosphere. The radiation from this surface has a known intensity distribution in frequency and in direction. The problem is to determine the character of the emergent radiation. The differential expansion of the atmosphere will be along the outward normal (the z-axis) and will be described by a velocity which is a linear function of optical depth. The radiation field will be symmetric with respect to this axis. Finally, the thermal motions of the electrons will be described by a Maxwellian distribution of velocities associated with a kinetic temperature, T, which is constant throughout the atmosphere.

Scattering of radiation by the electrons will be considered as classical, in accordance with the frequency-independent Thomson scattering coefficient,

$$\sigma_e = \frac{8\pi}{3}\frac{e^4}{m^2c^4}, \tag{1}$$

and the Rayleigh phase function,

$$P(\Theta) = \tfrac{3}{4}(1+\cos^2\Theta). \tag{2}$$

In the foregoing equations m is the mass of the electron, e its charge, c the velocity of light, and Θ the angle of scattering. Optical depth within the atmosphere is defined by

$$d\tau = -N_e\sigma_e dz, \tag{3}$$

where N_e is the number of free electrons per cubic centimeter. The noncoherent nature of this scattering, as given by the Doppler principle, depends on the velocity of the scattering electron and the geometry of the scattering, as shown in Figure 1. The differential expansion of the atmosphere gives the electron's mass-motion velocity $W(\tau)$. The velocities, u, v, and w are the components of the electron's thermal velocity in a Cartesian co-ordinate system which is oriented so that v lies in the xy-plane of the atmosphere and u is the direction of the incident photon. The velocity U is the component of the electron's thermal velocity in the direction of the scattered photon and is given by

$$U = \beta_1 u + \beta_2 v + \beta_3 w, \tag{4}$$

where β_1, β_2, and β_3 are the direction cosines of U with respect to u, v, and w. In terms of the angles shown in Figure 1,

$$\beta_1 = \cos\Theta = \mu\mu' + [(1-\mu^2)(1-\mu'^2)]^{1/2}\cos\varphi, \tag{5}$$

$$\beta_2 = (1-\mu^2)^{1/2}\sin\varphi, \tag{6}$$

and

$$\beta_3 = \mu\,(1-\mu'^2)^{1/2} - \mu'\,(1-\mu^2)^{1/2}\cos\varphi\,, \tag{7}$$

using the notation

$$\mu = \cos\theta\,. \tag{8}$$

The relation between the frequency of the incident photon ν' and that of the scattered photon ν as given by the Doppler principle can be expressed quite simply in terms of the difference between the electron's velocity in the direction of the incident photon, $u + W\mu'$, and in the direction of the scattered photon, $U + W\mu$. This relation is

$$\nu' = \nu + \frac{\nu}{c}\left[\,U - u + W(\mu - \mu')\,\right]. \tag{9}$$

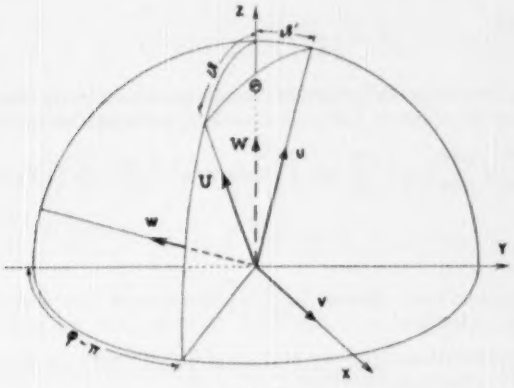

FIG. 1

The Maxwellian distribution function for thermal velocities (normalized to unity) is

$$f(u, v, w) = \left[\frac{m}{2\pi kT}\right]^{3/2} \exp\left\{-\frac{m}{2kT}(u^2 + v^2 + w^2)\right\}, \tag{10}$$

where k is Boltzmann's constant. In terms of this distribution function, the emission coefficient for electron scattering is given by

$$j(\nu, \tau, \mu) = N_e\sigma_e \int \frac{d\omega}{4\pi} \int_{-\infty}^{+\infty} du \int_{-\infty}^{+\infty} dv \int_{-\infty}^{+\infty} dw\, I(\nu', \tau, \mu')\, P(\Theta)\, f(u, v, w)\,, \tag{11}$$

where $d\omega$ is an increment of solid angle about the incident direction and $I(\nu', \tau, \mu')$ is the intensity of incident radiation. The integrations over u, v, and w indicated in equation (11) can be most easily performed by isolating the frequency variable,

$$\gamma = \nu' - \frac{\nu}{c} W(\mu - \mu') = \nu + \frac{\nu}{c}(U - u)\,, \tag{12}$$

as a variable of integration in place of v. By equations (4) and (12), we have

$$v = \frac{1}{\beta_2}\left[\,(1-\beta_1)\,u - \beta_3 w + \frac{c}{\nu}(\gamma - \nu)\,\right].$$

When this expression for v and equation (10) are substituted in equation (11), the emission coefficient may be expressed as[6]

$$j(\nu, \tau, \mu) = N_e\sigma_e \frac{c}{\nu}\left[\frac{m}{2\pi kT}\right]^{3/2} \int \frac{d\omega}{4\pi} \frac{P(\Theta)}{\beta_2} \int_{-\infty}^{+\infty} d\gamma I\left(\gamma + \frac{\nu}{c} W[\mu - \mu'], \tau, \mu'\right)$$
$$\times \int_{-\infty}^{+\infty} du \int_{-\infty}^{+\infty} dw \exp\left\{-\frac{m}{2kT}\left(u^2 + \left[\frac{(1-\beta_1)u - \beta_2 w + c(\gamma - \nu)/\nu}{\beta_2}\right]^2 + w^2\right)\right\}. \quad (14)$$

In further work it is convenient to express frequency in velocity units of $\sqrt{2}$ Doppler half-widths by the transformations

$$\alpha = \left[\frac{m}{4kT}\right]^{1/2} \frac{c}{\nu_0}(\nu - \nu_0) \quad (15)$$

and

$$\alpha' = \left[\frac{m}{4kT}\right]^{1/2} \frac{c}{\nu_0}(\gamma - \nu_0), \quad (16)$$

where ν_0 is a fixed frequency. When these transformations and the integrations over u and w are performed in equation (14), the emission coefficient becomes

$$j(\alpha, \tau, \mu) = \frac{N_e\sigma_e}{\sqrt{\pi}} \int \frac{d\omega}{4\pi} \frac{P(\Theta)}{(1-\beta_1)^{1/2}} \int_{-\infty}^{+\infty} d\alpha' I(\alpha' - \Omega[\mu - \mu'], \tau, \mu')$$
$$\times \exp\left\{-\frac{(\alpha' - \alpha)^2}{1-\beta_1}\right\}, \quad (17)$$

where

$$\Omega = -\left[\frac{m}{4kT}\right]^{1/2} W(\tau) \quad (18)$$

is the velocity of mass motion expressed in units of 0.7979 times the mean thermal velocity. In equation (17) the approximation

$$\alpha' - \alpha \simeq \left[\frac{m}{4kT}\right]^{1/2} \frac{c}{\nu}(\gamma - \nu), \quad (19)$$

in which c/ν is replaced by c/ν_0, has been made. This is allowable, since the integration over α' in equation (17) is restricted to a limited range by the exponential factor in the integrand.

Because σ_e is independent of frequency, the radiation scattered by the electrons is simply $N_e\sigma_e I(\alpha, \tau, \mu)$, and therefore the equation of radiative transfer for the electron atmosphere is

$$\mu \frac{dI(\alpha, \tau, \mu)}{d\tau} = I(\alpha, \tau, \mu) - \frac{j(\alpha, \tau, \mu)}{N_e\sigma_e}. \quad (20)$$

Under the conditions of the Schuster problem, solutions of this equation are required to satisfy the boundary conditions

$$\left.\begin{aligned} I(\alpha, \tau_1, \mu) &= \Im(\alpha, \mu), \\ I(\alpha, 0, -\mu) &\equiv 0 \end{aligned}\right\} \quad (\mu \geq 0), \quad (21)$$

where τ_1 is the total optical thickness of the atmosphere and $\Im(\alpha, \mu)$ represents the radiation field incident on the inner surface of the atmosphere.

[6] The infinite limits in the integration over ν should be replaced by the finite limits imposed by the limiting velocity of light. This leads to finite limits of integration over γ in eq. (14)—in fact, a range of integration over γ which is proportional to β_2. However, it can be shown that use of the infinite limits in eq. (14) is a valid approximation.

III. TRANSFORMATIONS OF THE EQUATION OF TRANSFER

The integration over a' in $j(a, \tau, \mu)$, as represented by equation (17), produces a mixing of frequencies which prevents solving equation (20) by the methods normally employed in radiative-transfer theory. However, this difficulty can be overcome by applying two transformations to equation (20). First, the transformation

$$\psi(a, \tau, \mu) = I(a + \Omega\mu, \tau, \mu), \tag{22}$$

which considers intensity at a frequency which varies continuously with Ω and hence with optical depth. By equation (22),

$$\begin{aligned}\frac{\partial \psi(a, \tau, \mu)}{\partial \tau} &= \frac{\partial I(a + \Omega\mu, \tau, \mu)}{\partial \tau} + \frac{\partial I(a + \Omega\mu, \tau, \mu)}{\partial (a + \Omega\mu)} \frac{d(a + \Omega\mu)}{d\tau} \\ &= \frac{\partial I(a + \Omega\mu, \tau, \mu)}{\partial \tau} + \frac{\partial \psi(a, \tau, \mu)}{\partial a} \mu \frac{d\Omega}{d\tau}.\end{aligned} \tag{23}$$

When equations (22) and (23) are substituted in equations (17) and (20) at the proper frequency, the latter two equations give

$$\begin{aligned}\mu \frac{\partial \psi(a, \tau, \mu)}{\partial \tau} - \mu^2 \frac{d\Omega}{d\tau} \frac{\partial \psi(a, \tau, \mu)}{\partial a} &= \psi(a, \tau, \mu) - \frac{1}{\sqrt{\pi}} \int \frac{d\omega}{4\pi} \frac{P(\Theta)}{(1 - \beta_1)^{1/2}} \\ &\times \int_{-\infty}^{+\infty} da' \psi(a', \tau, \mu') \exp\left\{ - \frac{(a' - a)^2}{1 - \beta_1} \right\}.\end{aligned} \tag{24}$$

Equation (24) is preferable to equation (20), in that the mass motion appears only as $d\Omega/d\tau$, which is a constant, since the velocity of differential expansion is a linear function of τ.

The second transformation uses the Fourier transform

$$\chi(\xi, \tau, \mu) = \frac{1}{\sqrt{(2\pi)}} \int_{-\infty}^{+\infty} e^{i\xi a} \psi(a, \tau, \mu)\, da. \tag{25}$$

In general, this transformation leads to a $\chi(\xi, \tau, \mu)$ which is complex. The fact that $\psi(a, \tau, \mu)$ is real requires that the real part of $\chi(\xi, \tau, \mu)$ be an even function of ξ, while the imaginary part must be an odd function. The application of transformation (25) is valid, and the inverse transform exists,[7] provided that $\psi(a, \tau, \mu)$ is integrable square over a for all values of τ and μ. It follows from this condition that $\chi(\xi, \tau, \mu)$ exists and is integrable square with respect to ξ and also that

$$\psi(\pm\infty, \tau, \mu) \equiv 0. \tag{26}$$

The second transformation involves multiplication of equation (24) by $e^{i\xi a}/\sqrt{(2\pi)}$ and integration over ξ, which gives

$$\begin{aligned}\mu \frac{\partial \chi(\xi, \tau, \mu)}{\partial \tau} - \mu^2 \frac{d\Omega}{d\tau} \frac{1}{\sqrt{(2\pi)}} \int_{-\infty}^{+\infty} e^{i\xi a} \frac{\partial \psi(a, \tau, \mu)}{\partial a}\, da &= \chi(\xi, \tau, \mu) \\ - \frac{1}{\sqrt{\pi}} \int \frac{d\omega}{4\pi} \frac{P(\Theta)}{(1 - \beta_1)^{1/2}} \frac{1}{\sqrt{(2\pi)}} \int_{-\infty}^{+\infty} da'\, e^{i\xi a'} \psi(a', \tau, \mu') \\ \times \int_{-\infty}^{+\infty} d(a' - a) \exp\left\{ - \frac{(a' - a)^2}{1 - \beta_1} - i\xi(a' - a) \right\}.\end{aligned} \tag{27}$$

[7] Cf. E. C. Titchmarsh, *Introduction to the Theory of Fourier Integrals* (Oxford: Clarendon Press, 1937), Theorem 48, p. 69.

Integrating the second term on the right-hand side by parts, with the use of condition (26), and integrating over $\alpha'-\alpha$ reduces this equation to the simpler form

$$\mu \frac{\partial \chi(\xi, \tau, \mu)}{\partial \tau} = \left(1 - i\mu^2 \xi \frac{d\Omega}{d\tau}\right) \chi(\xi, \tau, \mu) - \int \frac{d\omega}{4\pi} P(\Theta) \chi(\xi, \tau, \mu') e^{-(1-\beta_1)\xi^2/4} . \quad (28)$$

For $d\Omega/d\tau = 0$, corresponding to a uniform rather than a differential expansion of the atmosphere, equation (28) reduces to that obtained by Münch[8] in his investigation of the effects of thermal motions alone.

The boundary conditions (21) must be transformed in the same manner as the equation of transfer. The first transformation (22) gives

$$\left.\begin{aligned} \psi(\alpha, \tau_1, \mu) &= \Psi(\alpha, \mu) , \\ \psi(\alpha, 0, -\mu) &\equiv 0 \end{aligned}\right\} \quad (\mu \geq 0) , \quad (29)$$

where $\Psi(\alpha, \mu)$ is the transformed incident intensity. The second transformation gives

$$\left.\begin{aligned} \chi(\xi, \tau_1, \mu) &= X(\xi, \mu) , \\ \chi(\xi, 0, -\mu) &\equiv 0 \end{aligned}\right\} \quad (\mu \geq 0) , \quad (30)$$

where $X(\xi, \mu)$ is the Fourier transform of $\Psi(\alpha, \mu)$.

It is convenient to separate the real and imaginary parts of equation (28) by writing

$$\chi(\xi, \tau, \mu) = \chi^{(r)}(\xi, \tau, \mu) + i\chi^{(i)}(\xi, \tau, \mu) . \quad (31)$$

This allows equation (28) to be replaced by the two equations

$$\mu \frac{\partial \chi^{(r)}(\xi, \tau, \mu)}{\partial \tau} = \chi^{(r)}(\xi, \tau, \mu) + \mu^2 \xi \frac{d\Omega}{d\tau} \chi^{(i)}(\xi, \tau, \mu) - \frac{3}{8} \int_{-1}^{+1} \chi^{(r)}(\xi, \tau, \mu') p(\xi, \mu, \mu') d\mu' \quad (32)$$

and

$$\mu \frac{\partial \chi^{(i)}(\xi, \tau, \mu)}{\partial \tau} = \chi^{(i)}(\xi, \tau, \mu) - \mu^2 \xi \frac{d\Omega}{d\tau} \chi^{(r)}(\xi, \tau, \mu) - \frac{3}{8} \int_{-1}^{+1} \chi^{(i)}(\xi, \tau, \mu') p(\xi, \mu, \mu') d\mu' , \quad (33)$$

where

$$p(\xi, \mu, \mu') = \frac{1}{2\pi} \int_0^{2\pi} (1 + \cos^2 \Theta) e^{-(1-\cos\Theta)\xi^2/4} d\varphi \quad (34)$$

is a phase function obtained by substituting the expressions for $P(\Theta)$ and β_1, as given by equations (2) and (5), in equation (28) and integrating over the azimuthal angle. This integral has been evaluated by Münch,[9] who obtained the following expression for the phase function:

$$\begin{aligned} p(\xi, \mu, \mu') &= e^{-(1-\mu\mu')\xi^2/4} \\ &\times \{ [1 + \mu^2\mu'^2 + \tfrac{1}{2}(1-\mu^2)(1-\mu'^2)] I_0(\tfrac{1}{4}\xi^2 [1-\mu^2]^{1/2} [1-\mu'^2]^{1/2}) \\ &+ 2\mu\mu' [(1-\mu^2)(1-\mu'^2)]^{1/2} I_1(\tfrac{1}{4}\xi^2 [1-\mu^2]^{1/2} [1-\mu'^2]^{1/2}) \\ &+ \tfrac{1}{2}(1-\mu^2)(1-\mu'^2) I_2(\tfrac{1}{4}\xi^2 [1-\mu^2]^{1/2} [1-\mu'^2]^{1/2}) \}, \end{aligned} \quad (35)$$

where $I_n(\frac{1}{4}\xi^2[1-\mu^2]^{1/2}[1-\mu'^2]^{1/2})$ is a Bessel function of order n and with imaginary argument.

[8] *Op. cit.*, eqs. (16) and (24).

[9] *Ibid.*, eq. (27).

Equations (32) and (33) can now be solved by the standard approximate methods of radiative-transfer theory,[8] by which they are replaced by the system of linear differential equations

$$\left.\begin{aligned}\mu_j \frac{\partial \chi_j^{(r)}(\xi,\tau)}{\partial \tau} &= \chi_j^{(r)}(\xi,\tau) + \mu_j^2 \xi \frac{d\Omega}{d\tau}\chi_j^{(i)}(\xi,\tau) \\ &\quad - \frac{3}{8}\sum_{k=-n}^{+n} a_k \chi_k^{(r)}(\xi,\tau)\, p(\xi,\mu_j,\mu_k), \\ \mu_j \frac{\partial \chi_j^{(i)}(\xi,\tau)}{\partial \tau} &= \chi_j^{(i)}(\xi,\tau) - \mu_j^2 \xi \frac{d\Omega}{d\tau}\chi_j^{(r)}(\xi,\tau) \\ &\quad - \frac{3}{8}\sum_{k=-n}^{+n} a_k \chi_k^{(i)}(\xi,\tau)\, p(\xi,\mu_j,\mu_k)\end{aligned}\right\} \quad (j=\pm 1,\pm 2,\ldots,\pm n), \tag{36}$$

where the a_k's and μ_j's are the Gaussian weights and divisions and $\chi_j^{(\ )}(\xi,\tau) = \chi^{(\ )}(\xi,\tau,\mu_j)$. The boundary conditions (30), within the scheme of this approximation, are

$$\left.\begin{aligned}\chi_{+j}^{(r)}(\xi,\tau_1) &= X_{+j}^{(r)}(\xi), \qquad \chi_{+j}^{(i)}(\xi,\tau_1) = X_{+j}^{(i)}(\xi), \\ \chi_{-j}^{(r)}(\xi,0) &\equiv \chi_{-j}^{(i)}(\xi,0) \equiv 0\end{aligned}\right\} \quad (j=+1,+2,\ldots,+n). \tag{37}$$

IV. SOLUTION OF TRANSFORMED EQUATION OF TRANSFER IN FIRST APPROXIMATION

The solution of equations (36) for approximations higher than the first ($n = 1$) would be laborious, as the form of $p(\xi,\mu_j,\mu_k)$ prevents a general method for obtaining a solution in the nth approximation. Furthermore, accuracy greater than the right order of magnitude given by the first approximation is not desired, since the electron atmosphere described in the formulation of the problem is, at best, a first approximation of a high-temperature stellar atmosphere. Therefore, equations (36) will be solved in the first approximation, where

$$a_{+1} = a_{-1} = 1, \qquad \mu_{+1} = -\mu_{-1} = 1/\sqrt{3} \tag{38}$$

$$\begin{aligned}M(\xi) &= \tfrac{3}{8}p(\xi,1/\sqrt{3},1/\sqrt{3}) = \tfrac{3}{8}p(\xi,-1/\sqrt{3},-1/\sqrt{3}) \\ &= \tfrac{1}{2}e^{-\xi^2/6}[I_0(\xi^2/6) + \tfrac{1}{3}I_1(\xi^2/6) + \tfrac{1}{6}I_2(\xi^2/6)],\end{aligned} \tag{39}$$

and

$$\begin{aligned}N(\xi) &= \tfrac{3}{8}p(\xi,1/\sqrt{3},-1/\sqrt{3}) = \tfrac{3}{8}p(\xi,-1/\sqrt{3},1/\sqrt{3}) \\ &= \tfrac{1}{2}e^{-\xi^2/3}[I_0(\xi^2/6) - \tfrac{1}{3}I_1(\xi^2/6) + \tfrac{1}{6}I_2(\xi^2/6)].\end{aligned} \tag{40}$$

For this approximation, equations (36) become

$$\begin{aligned}\frac{1}{\sqrt{3}}\frac{\partial \chi_{+1}^{(r)}(\xi,\tau)}{\partial \tau} &= \chi_{+1}^{(r)}(\xi,\tau) + L(\xi)\chi_{+1}^{(i)}(\xi,\tau) \\ &\quad - M(\xi)\chi_{+1}^{(r)}(\xi,\tau) - N(\xi)\chi_{-1}^{(r)}(\xi,\tau);\end{aligned} \tag{41}$$

$$\begin{aligned}-\frac{1}{\sqrt{3}}\frac{\partial \chi_{-1}^{(r)}(\xi,\tau)}{\partial \tau} &= \chi_{-1}^{(r)}(\xi,\tau) + L(\xi)\chi_{-1}^{(i)}(\xi,\tau) \\ &\quad - M(\xi)\chi_{-1}^{(r)}(\xi,\tau) - N(\xi)\chi_{+1}^{(r)}(\xi,\tau);\end{aligned} \tag{42}$$

$$\begin{aligned}\frac{1}{\sqrt{3}}\frac{\partial \chi_{+1}^{(i)}(\xi,\tau)}{\partial \tau} &= \chi_{+1}^{(i)}(\xi,\tau) - L(\xi)\chi_{+1}^{(r)}(\xi,\tau) \\ &\quad - M(\xi)\chi_{+1}^{(i)}(\xi,\tau) - N(\xi)\chi_{-1}^{(i)}(\xi,\tau);\end{aligned} \tag{43}$$

and

$$-\frac{1}{\sqrt{3}}\frac{\partial \chi_{-1}^{(i)}(\xi,\tau)}{\partial \tau} = \chi_{-1}^{(i)}(\xi,\tau) - L(\xi)\chi_{-1}^{(r)}(\xi,\tau) - M(\xi)\chi_{-1}^{(i)}(\xi,\tau) - N(\xi)\chi_{+1}^{(i)}(\xi,\tau), \tag{44}$$

where

$$L(\xi) = \frac{\xi}{3}\frac{d\Omega}{d\tau}. \tag{45}$$

Equations (41)–(44) constitute a fourth-order set of linear, homogeneous, differential equations in τ with constant coefficients, since ξ may be considered a parameter. The general solution of these equations, as obtained by standard methods, is

$$\chi_{+1}^{(r)}(\xi,\tau) = [D_1\cos k''\tau - D_2\sin k''\tau]\,e^{k'\tau} + [D_3\cos k''\tau + D_4\sin k''\tau]\,e^{-k'\tau}; \tag{46}$$

$$\chi_{-1}^{(r)}(\xi,\tau) = -[(D_1E_1 - D_3E_2)\cos k''\tau - (D_1E_2 + D_2E_1)\sin k''\tau]\,e^{k'\tau} - [(D_3E_3 - D_4E_4)\cos k''\tau + (D_3E_4 + D_4E_3)\sin k''\tau]\,e^{-k'\tau}; \tag{47}$$

$$\chi_{+1}^{(i)}(\xi,\tau) = [D_2\cos k''\tau + D_1\sin k''\tau]\,e^{k'\tau} + [D_4\cos k''\tau - D_3\sin k''\tau]\,e^{-k'\tau}; \tag{48}$$

and

$$\chi_{-1}^{(i)}(\xi,\tau) = -[(D_1E_2 + D_2E_1)\cos k''\tau + (D_1E_1 - D_2E_2)\sin k''\tau]\,e^{k'\tau} - [(D_3E_4 + D_4E_3)\cos k''\tau - (D_3E_3 - D_4E_4)\sin k''\tau]\,e^{-k'\tau}, \tag{49}$$

where $k'(\xi)$ and $k''(\xi)$ are the characteristic roots defined by the relations

$$\tfrac{1}{3}(k'^2 - k''^2) = (M-1)^2 - N^2 - L^2, \qquad \tfrac{1}{3}k'k'' = L(M-1) \tag{50}$$

and

$$\begin{aligned} NE_1(\xi) &= M - 1 + k'/\sqrt{3}, & NE_2(\xi) &= L + k''/\sqrt{3}, \\ NE_3(\xi) &= M - 1 - k'/\sqrt{3}, & NE_4(\xi) &= L - k''/\sqrt{3}. \end{aligned} \tag{51}$$

Furthermore, equations (50) and (51) give

$$\begin{aligned} E_1 &= E_3(E_1^2 + E_2^2), & E_2 &= -E_4(E_1^2 + E_2^2), \\ E_3 &= E_1(E_3^2 + E_4^2), & E_4 &= -E_2(E_3^2 + E_4^2). \end{aligned} \tag{52}$$

Finally, the quantities D_1, D_2, D_3, and D_4 in equations (46)–(49) are arbitrary functions of ξ; they become determinate when the boundary conditions (37) are satisfied. In the first approximation these boundary conditions are

$$\begin{aligned} \chi_{+1}^{(r)}(\xi,\tau_1) &= X_{+1}^{(r)}(\xi), \qquad \chi_{+1}^{(i)}(\xi,\tau_1) = X_{+1}^{(i)}(\xi), \\ \chi_{-1}^{(r)}(\xi,0) &= \chi_{-1}^{(i)}(\xi,0) = 0; \end{aligned} \tag{53}$$

and, when solved for D_1, D_2, D_3, and D_4, they give

$$\eta D_1(\xi) = [X^{(r)}_{+1}F_1 + X^{(i)}_{+1}F_2](E_2^2+E_4^2) + [X^{(r)}_{+1}F_4 + X^{(i)}_{+1}F_3](E_1E_4 - E_2E_3) - [X^{(r)}_{+1}F_3 - X^{(i)}_{+1}F_4](E_1E_3 + E_2E_4), \tag{54}$$

$$\eta D_2(\xi) = -[X^{(r)}_{+1}F_2 - X^{(i)}_{+1}F_1](E_3^2+E_4^2) - [X^{(r)}_{+1}F_3 - X^{(i)}_{+1}F_4](E_1E_4 - E_2E_3) - [X^{(r)}_{+1}F_4 + X^{(i)}_{+1}F_3](E_1E_3 + E_2E_4), \tag{55}$$

$$\eta D_3(\xi) = [X^{(r)}_{+1}F_3 - X^{(i)}_{+1}F_4](E_1^2+E_2^2) + [X^{(r)}_{+1}F_2 - X^{(i)}_{+1}F_1](E_1E_4 - E_2E_3) - [X^{(r)}_{+1}F_1 + X^{(i)}_{+1}F_2](E_1E_3 + E_2E_4), \tag{56}$$

and

$$\eta D_4(\xi) = [X^{(r)}_{+1}F_4 + X^{(i)}_{+1}F_3](E_1^2+E_2^2) + [X^{(r)}_{+1}F_1 + X^{(i)}_{+1}F_2](E_1E_4 - E_2E_3) + [X^{(r)}_{+1}F_2 - X^{(i)}_{+1}F_1](E_1E_3 + E_2E_4), \tag{57}$$

where

$$\eta(\xi) = (F_1^2+F_2^2)(E_3^2+E_4^2) + (F_3^2+F_4^2)(E_1^2+E_2^2) + 2(F_1F_4+F_2F_3)(E_1E_4 - E_2E_3) - 2(F_1F_3 - F_2F_4)(E_1E_3 + E_2E_4) \tag{58}$$

and

$$F_1(\xi) = e^{k'\tau_1}\cos k''\tau_1, \qquad F_2(\xi) = e^{k'\tau_1}\sin k''\tau_1,$$
$$F_3(\xi) = e^{-k'\tau_1}\cos k''\tau_1, \qquad F_4(\xi) = e^{-k'\tau_1}\sin k''\tau_1. \tag{59}$$

Also the coefficients in equations (47) and (49) are

$$\eta(D_1E_1 - D_2E_2) = -[X^{(r)}_{+1}F_3 - X^{(i)}_{+1}F_4]E_1 - [X^{(r)}_{+1}F_4 + X^{(i)}_{+1}F_3]E_2 + [X^{(r)}_{+1}F_1 + X^{(i)}_{+1}F_2]E_3 - [X^{(r)}_{+1}F_2 - X^{(i)}_{+1}F_1]E_4, \tag{60}$$

$$\eta(D_1E_2 + D_2E_1) = -[X^{(r)}_{+1}F_4 + X^{(i)}_{+1}F_3]E_1 + (X^{(r)}_{+1}F_3 - X^{(i)}_{+1}F_4]E_2 - [X^{(r)}_{+1}F_2 - X^{(i)}_{+1}F_1]E_3 - [X^{(r)}_{+1}F_1 + X^{(i)}_{+1}F_2]E_4, \tag{61}$$

$$\eta(D_3E_3 - D_4E_4) = [X^{(r)}_{+1}F_3 - X^{(i)}_{+1}F_4]E_3 + [X^{(r)}_{+1}F_4 + X^{(i)}_{+1}F_3]E_2 - [X^{(r)}_{+1}F_1 + X^{(i)}_{+1}F_2]E_3 + [X^{(r)}_{+1}F_2 - X^{(i)}_{+1}F_1]E_4, \tag{62}$$

and

$$\eta(D_3E_4 + D_4E_3) = [X^{(r)}_{+1}F_4 + X^{(i)}_{+1}F_3]E_1 - [X^{(r)}_{+1}F_3 - X^{(i)}_{+1}F_4]E_2 + [X^{(r)}_{+1}F_2 - X^{(i)}_{+1}F_1]E_3 + [X^{(r)}_{+1}F_1 + X^{(i)}_{+1}F_2]E_4, \tag{63}$$

where use has been made of equations (52) and (54)–(57).

The question of the validity of the application of the Fourier transform (25) can be answered only within the scheme of the first approximation, using the solution obtained. To prove the existence of the inverse Fourier transform for this solution, $X^{(r)}_{+1}(\xi)$ and $X^{(i)}_{+1}(\xi)$ must be specified. However, examination of all coefficients of $X^{(r)}_{+1}(\xi)$ and $X^{(i)}_{+1}(\xi)$ in the solution as given by equations (46)–(51) and (54)–(63) shows that they are

bounded for all ξ except[10] $\xi = 0$ and for all τ. This allows the integrable-square requirement to be placed on $X_{+1}^{(r)}(\xi)$ and $X_{+1}^{(i)}(\xi)$. Furthermore, the solution has the required symmetry in ξ to insure that the inverse Fourier transform will give a real function.

V. THE EMERGENT RADIATION

Of greatest astrophysical interest is the nature of the radiation emerging from the electron atmosphere, as this is the radiation which is observed. For $\tau = 0$, equations (46), (48), (51), and (54)–(59) can be combined to give

$$\chi_{+1}^{(r)}(\xi, 0) = \Gamma_1 X_{+1}^{(r)} - \Gamma_2 X_{+1}^{(i)} \tag{64}$$

and

$$\chi_{+1}^{(i)}(\xi, 0) = \Gamma_2 X_{+1}^{(r)} + \Gamma_1 X_{+1}^{(i)}, \tag{65}$$

where

$$\begin{aligned} \tfrac{1}{4} N^2 \eta \Gamma_1(\xi) = {} & \tfrac{1}{3}(k'^2 + k''^2) \cosh k'\tau_1 \cos k''\tau_1 \\ & + (1/\sqrt{3})[Lk' - (M-1)k''] \cosh k'\tau_1 \sin k''\tau_1 \\ & - (1/\sqrt{3})[(M-1)k' + Lk''] \sinh k'\tau_1 \cos k''\tau_1, \end{aligned} \tag{66}$$

$$\begin{aligned} \tfrac{1}{4} N^2 \eta \Gamma_2(\xi) = {} & -\tfrac{1}{3}(k'^2 + k''^2) \sinh k'\tau_1 \sin k''\tau_1 \\ & + (1/\sqrt{3})[Lk' - (M-1)k''] \sinh k'\tau_1 \cos k''\tau_1 \\ & + (1/\sqrt{3})[(M-1)k' + Lk''] \cosh k'\tau_1 \sin k''\tau_1, \end{aligned} \tag{67}$$

and

$$\begin{aligned} \tfrac{1}{4} N^2 \eta(\xi) = {} & \tfrac{1}{2}[(M-1)^2 + L^2 + \tfrac{1}{3}(k'^2 + k''^2)] \cosh 2k'\tau_1 \\ & - (1/\sqrt{3})[(M-1)k' + Lk''] \sinh 2k'\tau_1 \\ & + (1/\sqrt{3})[Lk' - (M-1)k''] \sin 2k''\tau_1 \\ & - \tfrac{1}{2}[(M-1)^2 + L^2 - \tfrac{1}{3}(k'^2 + k''^2)] \cos 2k''\tau_1. \end{aligned} \tag{68}$$

From these equations it follows that

$$\left.\begin{aligned} \Gamma_1 &\to e^{-\tau_1\sqrt{3}} \cos(L\tau_1\sqrt{3}), \\ \Gamma_2 &\to e^{-\tau_1\sqrt{3}} \sin(L\tau_1\sqrt{3}) \end{aligned}\right\} \quad \text{as} \quad \xi \to \pm\infty. \tag{69}$$

Now the inverse Fourier transform for the solution for the emergent radiation is

$$\begin{aligned} \psi_{+1}(\alpha, 0) &= \frac{1}{\sqrt{(2\pi)}} \int_{-\infty}^{+\infty} e^{-i\xi\alpha} [\chi_{+1}^{(r)}(\xi, 0) + i\chi_{+1}^{(i)}(\xi, 0)] \, d\xi \\ &= \frac{1}{\sqrt{(2\pi)}} \int_{-\infty}^{+\infty} e^{-i\xi\alpha} (\Gamma_1 + i\Gamma_2)[X_{+1}^{(r)} + iX_{+1}^{(i)}] \, d\xi. \end{aligned} \tag{70}$$

By equations (45) and (69),

$$e^{-i\xi\alpha}(\Gamma_1 + i\Gamma_2) \to e^{-\tau_1\sqrt{3}} \exp\{-i(\alpha - \alpha_0)\xi\} \quad \text{as} \quad \xi \to \pm\infty, \tag{71}$$

where

$$\alpha_0 = \frac{\tau_1}{\sqrt{3}} \frac{d\Omega}{d\tau} = \frac{\tau_1}{\sqrt{3}} [\Omega(\tau_1) - \Omega(0)], \tag{72}$$

since $d\Omega/d\tau$ has been considered constant. It follows from equation (72) that α_0 represents the total change in the velocity of expansion over the atmosphere in the direction

[10] Actually, the solution becomes indeterminant for $\xi = 0$, but, as shown in Sec. VI, for $\tau = 0$, the solution remains bounded in passing to the limit $\xi = 0$.

$\mu_{+1} = 1/\sqrt{3}$. When the limiting value given by equation (71) is added and subtracted from the integrand in equation (70), $\psi_{+1}(a, 0)$ becomes

$$\psi_{+1}(a, 0) = e^{-\tau_1\sqrt{3}}\Psi_{+1}(a - a_0) + \frac{1}{\sqrt{(2\pi)}}\int_{-\infty}^{+\infty} e^{-i\xi a}\{[\Gamma_1 - e^{-\tau_1\sqrt{3}}\cos(L\tau_1\sqrt{3})] + i[\Gamma_2 - e^{-\tau_1\sqrt{3}}\sin(L\tau_1\sqrt{3})]\}[X_{+1}^{(r)} + iX_{+1}^{(i)}]\,d\xi\,, \tag{73}$$

where

$$\Psi_{+1}(a - a_0) = \frac{1}{\sqrt{(2\pi)}}\int_{-\infty}^{+\infty} e^{-i\xi(a-a_0)}[X_{+1}^{(r)} + iX_{+1}^{(i)}]\,d\xi \tag{74}$$

is the inverse Fourier transform of the incident radiation.

The integral in equation (73) may be rewritten in a form more convenient for numerical computations by using one of Parseval's formulae,[11]

$$\int_{-\infty}^{+\infty} F(t)\,G(t)\,e^{-ixt}dt = \int_{-\infty}^{+\infty} f(u)\,g(x-u)\,du\,, \tag{75}$$

where $F(t)$ and $G(t)$ are Fourier transforms of $f(x)$ and $g(x)$, respectively. This formula gives

$$\psi_{+1}(a, 0) = e^{-\tau_1\sqrt{3}}\Psi_{+1}(a - a_0) + \int_{-\infty}^{+\infty}\Psi_{+1}(\beta)\,\Delta\left(\tau_1, \frac{d\Omega}{d\tau};\ a - \beta\right)d\beta\,, \tag{76}$$

where

$$\Delta\left(\tau_1, \frac{d\Omega}{d\tau};\ x\right) = \frac{1}{2\pi}\int_{-\infty}^{+\infty} e^{-i\xi x}\{[\Gamma_1 - e^{-\tau_1\sqrt{3}}\cos(L\tau_1\sqrt{3})] + i[\Gamma_2 - e^{-\tau_1\sqrt{3}}\sin(L\tau_1\sqrt{3})]\}\,d\xi$$
$$= \frac{1}{\pi}\int_0^{\infty}\{[\Gamma_1 - e^{-\tau_1\sqrt{3}}\cos(L\tau_1\sqrt{3})]\cos\xi x + [\Gamma_2 - e^{-\tau_1\sqrt{3}}\sin(L\tau_1\sqrt{3})]\sin\xi x\}\,d\xi\,. \tag{77}$$

The application of equation (75) is valid, provided that the functions $\Delta(\tau_1, d\Omega/d\tau; a - \beta)$ and $X_{+1}^{(r)}(\xi) + iX_{+1}^{(i)}(\xi)$ are integrable with respect to their arguments. Since $X_{+1}^{(r)}(\xi)$ and $X_{+1}^{(i)}(\xi)$ are assumed to be integrable square, the latter condition is satisfied. The integrability of $\Delta(\tau_1, d\Omega/d\tau; a - \beta)$ will be discussed below in Section VI. In reducing $\Delta(\tau_1, d\Omega/d\tau; x)$ to the second form in equation (77), use has been made of the symmetry properties with respect to ξ of Γ_1 and Γ_2. The evaluation of this integral is possible, since the coefficients of $\cos\xi x$ and $\sin\xi x$ approach zero for large values of ξ. The obtaining of these coefficients was the purpose of the addition and subtraction performed in transforming equation (70) into equation (73). The function $\Delta(\tau_1, d\Omega/d\tau; x)$ depends on the two parameters of the atmosphere, τ_1 and $d\Omega/d\tau$. However, it is not easy to disentangle the manner in which each parameter influences $\Delta(\tau_1, d\Omega/d\tau; x)$, since the dependence of Γ_1 and Γ_2 on these parameters is a very complicated one. Now, by equations (22), (38), and (72), we obtain

$$\Psi_{+1}(a - a_0) = \Im_{+1}(a + \Omega[0]/\sqrt{3})\,, \tag{78}$$

since the incident radiation is at the level $\tau = \tau_1$. Finally, the substitution of equation (78) in equation (76) and the use of the transformation (22) for the frequency $a - \Omega(0)/\sqrt{3}$ (at the level $\tau = 0$) gives

$$I_{+1}(a, 0) = e^{-\tau_1\sqrt{3}}\Im_{+1}(a) + \int_{-\infty}^{+\infty}\Im_{+1}(a')\,\Delta\left(\tau_1, \frac{d\Omega}{d\tau};\ a - a'\right)da'\,, \tag{79}$$

which is the desired expression for the emergent radiation.

[11] Cf. Titchmarsh, *op. cit.*, eq. (2.1.8), p. 51.

The physical interpretation of equation (79) is quite simple. The first term on the right-hand side represents the contribution to the emergent radiation of the incident radiation which passes through the electron atmosphere without having suffered a single scattering process; the second term represents the contribution of the incident radiation which has suffered one or more scattering processes. The integral in the second term indicates the noncoherent nature of the scattering, the function $\Delta(\tau_1, d\Omega/d\tau; \alpha - \alpha')$ representing the spectral distribution of emergent scattered radiation arising from an incident monochromatic radiation at a frequency α' and of unit intensity.

VI. PROPERTIES OF $\Delta(\tau_1, d\Omega/d\tau; x)$

To determine the spectrum of electron scattering as represented by $\Delta(\tau_1, d\Omega/d\tau; x)$, the integral in equation (77) must be evaluated. Examination of this integral reveals that an appreciable contribution comes from large values of ξ. A further difficulty in performing this integration is that Γ_1 and Γ_2 are indeterminate at $\xi = 0$, the expressions given by equations (66), (67), and (68) becoming zero. This indeterminancy can be removed by expanding these expressions in powers of ξ, which gives the following result:

$$\Gamma_1 \to \frac{1 + \frac{1}{2}\tau_1\sqrt{3}}{1 + \tau_1\sqrt{3} + \frac{3}{4}\tau_1^2}, \qquad \Gamma_2 \to 0 \qquad \text{as} \qquad \xi \to 0. \tag{80}$$

For large values of ξ, numerical integration of the integral in equation (77) can be replaced by analytic integration, using an asymptotic expression for the integrand. Such an expression can be obtained from Münch's[12] asymptotic expansion of $M(\xi)$ in powers of $1/\xi$, namely,

$$M(\xi) \to \left(\frac{3}{\pi}\right)^{1/2}\left(\frac{3}{4}\frac{1}{\xi} - \frac{15}{16}\frac{1}{\xi^3} + \ldots\right) \qquad \text{as} \qquad \xi \to \infty. \tag{81}$$

The function $N(\xi)$ can be neglected, as it appears in the integrand as N^2 with the coefficient $\xi^{-2}e^{-\xi^3/3}$ in the dominant term of its asymptotic expansion. The substitution of equations (45) and (81) in equations (50) produces expansions in powers of ξ, which show that

$$k'/\sqrt{3} \to -(M - 1), \qquad k''/\sqrt{3} \to -L \qquad \text{as} \qquad \xi \to \infty. \tag{82}$$

These asymptotic behaviors give, in turn,

$$\left.\begin{aligned} \Gamma_1 - e^{-\tau_1\sqrt{3}}\cos(L\tau_1\sqrt{3}) &\to e^{-\tau_1\sqrt{3}}Q(\tau_1; 1/\xi)\cos\alpha_0\xi \\ \Gamma_2 - e^{-\tau_1\sqrt{3}}\sin(L\tau_1\sqrt{3}) &\to e^{-\tau_1\sqrt{3}}Q(\tau_1; 1/\xi)\sin\alpha_0\xi \end{aligned}\right\} \qquad \text{as} \qquad \xi \to \infty, \tag{83}$$

where

$$Q\left(\tau_1; \frac{1}{\xi}\right) = \frac{9\tau_1}{4\sqrt{\pi}}\frac{1}{\xi} + \left(\frac{9\tau_1}{4\sqrt{\pi}}\right)^2\frac{1}{\xi^2} + \left[\left(\frac{9\tau_1}{4\sqrt{\pi}}\right)^3 - \frac{5}{4}\left(\frac{9\tau_1}{4\sqrt{\pi}}\right)\right]\frac{1}{\xi^3} + \left[\left(\frac{9\tau_1}{4\sqrt{\pi}}\right)^4 - \frac{5}{2}\left(\frac{9\tau_1}{4\sqrt{\pi}}\right)^2\right]\frac{1}{\xi^4} + \ldots. \tag{84}$$

Except for small values of $d\Omega/d\tau$, the convergence indicated in equation (82) is quite rapid and offers a sensitive criterion for determining the value $\xi = a$ at which the analytic integration can be started. When the integration indicated in equation (77) is performed

[12] Unpublished.

analytically between the limits $\xi = a$ and infinity, using equations (83), the following contribution to $\Delta(\tau_1, d\Omega/d\tau; x)$ is obtained:

$$\Delta_a\left(\tau_1, \frac{d\Omega}{d\tau}; x\right) = \frac{e^{-\tau_1\sqrt{3}}}{\pi}\int_a^\infty Q\left(\tau_1, \frac{1}{\xi}\right)\cos(x-a_0)\,\xi\,d\xi$$

$$= \frac{9\tau_1 e^{-\tau_1\sqrt{3}}}{4\pi\sqrt{\pi}}\left\{-Ciab + b\left(\frac{9\tau_1}{4\sqrt{\pi}}\right)\left[\frac{\cos ab}{ab} - \frac{\pi}{2} + Siab\right]\right.$$

$$+\frac{b^2}{2}\left[\left(\frac{9\tau_1}{4\sqrt{\pi}}\right)^2 - \frac{5}{4}\right]\left[\frac{\cos ab}{(ab)^2} - \frac{\sin ab}{ab} + Ciab\right] \tag{85}$$

$$+\frac{b^3}{3}\left[\left(\frac{9\tau_1}{4\sqrt{\pi}}\right)^3 - \frac{5}{2}\left(\frac{9\tau_1}{4\sqrt{\pi}}\right)\right]\left[\frac{\cos ab}{(ab)^3} - \frac{\sin ab}{2(ab)^2} - \frac{\cos ab}{2ab}\right.$$

$$\left.\left.+\frac{\pi}{4} - \frac{1}{2}Siab\right] + \ldots\right\},$$

where

$$Siy = \int_0^y \frac{\sin t}{t}\,dt, \qquad Ciy = \int_\infty^y \frac{\cos t}{t}\,dt \tag{86}$$

are the sine and cosine exponential integrals and

$$b = |x - a_0|. \tag{87}$$

As seen from the series development,[13]

$$Ciab = \log_e ab + \gamma - \frac{(ab)^2}{2!2} + \frac{(ab)^4}{4!4} - \ldots \quad (\gamma = 0.57721\ldots), \tag{88}$$

the cosine exponential integral, and hence also $\Delta_a(\tau_1, d\Omega/d\tau; x)$ (cf. eq. [85]), have logarithmic singularities at $b = 0$ or $x = a_0$. The singularity in $\Delta_a(\tau_1, d\Omega/d\tau; x)$ presents difficulties in performing the integration indicated by equation (79), which may be overcome by defining the function

$$\Delta_0\left(\tau_1, \frac{d\Omega}{d\tau}; x\right) = \left\{\begin{array}{ll} \Delta\left(\tau_1, \frac{d\Omega}{d\tau}; x\right) & \text{for } x \geq x_1 > a_0 \\ \Delta\left(\tau_1, \frac{d\Omega}{d\tau}; x\right) + \frac{9\tau_1 e^{-\tau_1\sqrt{3}}}{4\pi\sqrt{\pi}}\log_e\left(\frac{b}{x_1 - a_0}\right) & \text{for } x_1 \geq x \geq a_0 \\ \Delta\left(\tau_1, \frac{d\Omega}{d\tau}; x\right) + \frac{9\tau_1 e^{-\tau_1\sqrt{3}}}{4\pi\sqrt{\pi}}\log_e\left(\frac{b}{a_0 - x_2}\right) & \text{for } a_0 \geq x \geq x_2 \\ \Delta\left(\tau_1, \frac{d\Omega}{d\tau}; x\right) & \text{for } a_0 > x_2 \geq x, \end{array}\right\} \tag{89}$$

where x_1 and x_2 are values of x for which $\Delta(\tau_1, d\Omega/d\tau; x)$ has been evaluated. Equation (89) shows that, except when

$$x_1 - a_0 = a_0 - x_2, \tag{90}$$

there will be a discontinuity in $\Delta_0(\tau_1, d\Omega/d\tau; x)$ at the point of singularity $x = a_0$. The magnitude of this discontinuity is given by

$$\frac{9\tau_1 e^{-\tau_1\sqrt{3}}}{4\pi\sqrt{\pi}}\log_e\left(\frac{a_0 - x_2}{x_1 - a_0}\right). \tag{91}$$

[13] Cf. E. Jahnke and F. Emde, *Tables of Functions* (New York: Dover Publications, 1945), p. 2.

To minimize the difficulties in integration over x arising from this discontinuity, it is desirable to choose x_1 and x_2 such that equation (90) is satisfied as closely as possible and also that $\Delta_0(\tau_1, d\Omega/d\tau; x)$ is a small quantity in the region of the discontinuity. In terms of $\Delta_0(\tau_1, d\Omega/d\tau; x)$ as defined by equation (89), equation (79) becomes

$$I_{+1}(a, 0) = e^{-\tau_1\sqrt{2}}\Im_{+1}(a) + \int_{-\infty}^{+\infty}\Im_{+1}(a')\,\Delta_0\left(\tau_1, \frac{d\Omega}{d\tau};\ a - a'\right)da' - \frac{9\tau_1 e^{-\tau_1\sqrt{2}}}{4\pi\sqrt{\pi}}\left\{\int_{a-x_1}^{a-a_0}\Im_{+1}(a')\log_e\left(\frac{a - a_0 - a'}{x_1 - a_0}\right)da' + \int_{a-a_0}^{a-x_2}\Im_{+1}(a')\log_e\left(\frac{a - a_0 - a'}{x_2 - a_0}\right)da'\right\}. \tag{92}$$

The first integral in equation (92) can be evaluated numerically, but the remaining two must be evaluated analytically because of the logarithmic singularity at the limits $a' = a - a_0$. This may require approximating $\Im_{+1}(a')$ in such a manner as to allow explicit integration. Since the singularity is logarithmic, convergence of the integrals is assured.

TABLE 1

THE FUNCTION $\Delta_0(\tau_1, d\Omega/d\tau; x)$ FOR $\tau_1 = 0.5$

x	$d\Omega/d\tau = 0.5$	$d\Omega/d\tau = 1.0$	x	$d\Omega/d\tau = 0.5$	$d\Omega/d\tau = 1.0$
−3.00		0.0004	0.25	0.122	0.0563
−2.00	0.004	.0039	0.50	.116	.0580
−1.50		.0079	0.75		.0576
−1.00	.030	.0221	1.00	.048	.0624
−0.75		.0352	1.50		.0282
−0.50	.067	.0533	2.00	0.012	.0113
−0.25	.106	.0484	3.00		0.0024
0.00	0.111	0.0472			
$\int_{-\infty}^{+\infty}\Delta dx$ computed	0.2178	0.14798	$\int_{-\infty}^{+\infty}\Delta dx$ from eq. (96)	0.2135	0.14975

The function $\Delta_0(\tau_1, d\Omega/d\tau; x)$ is tabulated in Table 1 for $\tau_1 = 0.5$ and $d\Omega/d\tau = 1.0$ and 0.5. The corresponding behavior of $\Delta(\tau_1, d\Omega/d\tau; x)$ is illustrated in Figure 2. The values of the two parameters describe an atmosphere in which the velocity of expansion increases outward, the increase over the atmosphere being 0.3990 and 0.1995 of the electron mean thermal velocity, respectively. The shape of the function $\Delta(\tau_1, d\Omega/d\tau; x)$ as shown in Figure 2 is similar to the spectrum of electron scattering, due to thermal motions only, as obtained by Münch.[14] It may be said, therefore, that the shape of $\Delta(\tau_1, d\Omega/d\tau; x)$ is produced essentially by the Maxwellian distribution of thermal velocities. The shift of the logarithmic singularity from $x = 0$ ($a = a'$) by the amount a_0, however, is due to the differential expansion of the atmosphere and is proportional to the product of the two parameters of the atmosphere, τ_1 and $d\Omega/d\tau$, according to equation (72).

An integral admitted by the original equation of transfer (20) and the boundary conditions (21) can be used to check these calculations of $\Delta_0(\tau_1, d\Omega/d\tau; x)$. Integration of equations (20) and (21) over a yields equations for the integrated intensity,

$$w(\tau, \mu) = \int_{-\infty}^{+\infty} I(a, \tau, \mu)\,da, \tag{93}$$

[14] *Op. cit.*, Fig. 1.

which are, in the first approximation, identical with the equations for the standard Schuster problem. The solution of these equations for the emergent integrated intensity is known to be

$$w_{+1}(0) = \frac{\mathfrak{W}_{+1}}{1 + \frac{1}{2}\tau_1\sqrt{3}}, \tag{94}$$

where $\mathfrak{W}_{+1}$ is the integrated incident intensity. Similar integration of equation (92) over $\mathfrak{a}$ gives

$$w_{+1}(0) = e^{-\tau_1\sqrt{3}}\mathfrak{W}_{+1} + \mathfrak{W}_{+1}\int_{-\infty}^{+\infty} \Delta_0\left(\tau_1, \frac{d\Omega}{d\tau};\ \mathfrak{a} - \mathfrak{a}'\right) d(\mathfrak{a} - \mathfrak{a}') + \frac{9\tau_1 e^{-\tau_1\sqrt{3}}}{4\pi\sqrt{\pi}}(x_1 - x_2). \tag{95}$$

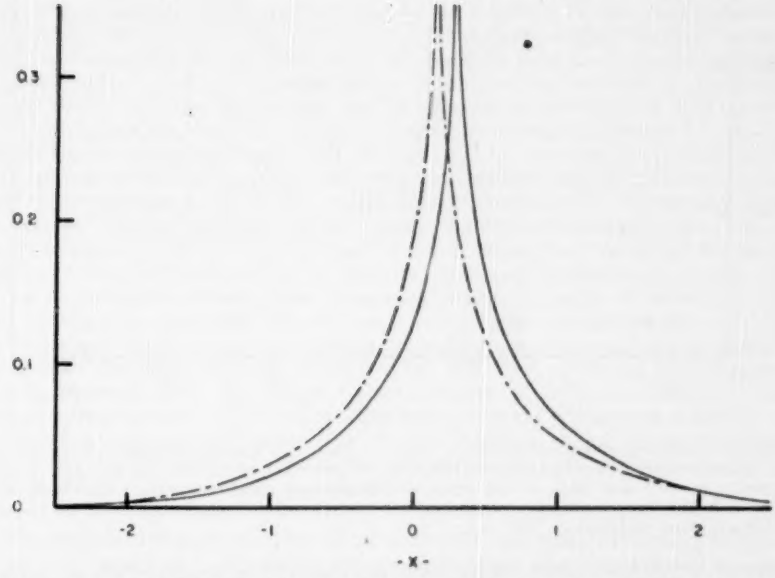

FIG. 2.—The spectral distribution $\Delta(\tau_1, d\Omega/d\tau; x)$ of emergent scattered intensity arising from incident monochromatic radiation of unit intensity. The argument x represents the difference between incident and scattered frequencies in units of $\sqrt{2}$ Doppler half-widths (cf. eq. [15]). The atmosphere parameters $\tau_1 = 0.5$ and $d\Omega/d\tau = 1.0$ give a spectral distribution (*full-line curve*) with a logarithmic singularity at $x = a_0 = 0.2887$ (cf. eq. [72]), while the spectral distribution for $\tau_1 = 0.5$, $d\Omega/d\tau = 0.5$ (*dot-and-dash curve*) has a similar singularity at $x = a_0 = 0.1444$.

Hence equations (94) and (95) give the following check on the computed function $\Delta_0(\tau_1, d\Omega/d\tau; x)$:

$$\int_{-\infty}^{+\infty} \Delta_0\left(\tau_1, \frac{d\Omega}{d\tau};\ x\right) dx = \frac{9\tau_1 e^{-\tau_1\sqrt{3}}}{4\pi\sqrt{\pi}}(x_2 - x_1) + \frac{1}{1 + \frac{1}{2}\tau_1\sqrt{3}} - e^{-\tau_1\sqrt{3}}. \tag{96}$$

Equation (96) indicates that $\Delta(\tau_1, d\Omega/d\tau; x)$ is integrable with respect to its argument, thereby validating the use of Parseval's formula (75) to obtain equation (76). Such checks for the functions $\Delta_0(\tau_1, d\Omega/d\tau; x)$ computed are included in Table 1.

VII. CHANGES PRODUCED IN PROFILES OF SPECTRAL LINES

An important application of the solution (92) for emergent radiation is the case in which the incident intensity is the residual intensity of a spectral line

$$r_{+1}(a) = \frac{\mathfrak{I}_{+1}(a)}{\mathfrak{I}_{+1}^{(c)}}. \tag{97}$$

The intensity of the incident continuum $\mathfrak{I}_{+1}^{(c)}$ may be considered a constant over the limited frequency range for which the approximation given by equation (19) is valid. This

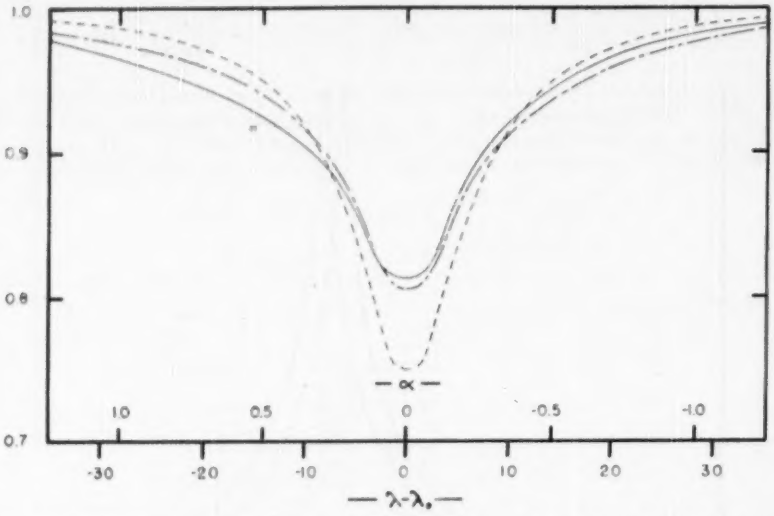

FIG. 3.—The emergent residual intensity $r_{+1}(a)$ of an absorption line whose incident residual intensity $r_{+1}(a)$ (*dashed curve*) is given by equation (100). The *full-line curve* represents $r_{+1}(a)$ for the atmosphere parameters $\tau_1 = 0.5$ and $d\Omega/d\tau = 1.0$, while the *dot-and-dash curve* represents $r_{+1}(a)$ for $\tau_1 = 0.5$, $d\Omega/d\tau = 0.5$. The conversion factor between the wave-length scale in angstrom units and the frequency variable a is given by equation (101).

constancy of $\mathfrak{I}_{+1}^{(c)}$ allows the substitution of equation (96) in equation (92) and gives for the emergent continuum the expression

$$I_{+1}^{(c)} = \frac{\mathfrak{I}_{+1}^{(c)}}{1 + \frac{1}{2}\tau_1\sqrt{3}}. \tag{98}$$

Hence the dividing of equation (92) by $\mathfrak{I}_{+1}^{(c)}$ gives, for the emergent residual intensity,

$$\begin{aligned} \frac{r_{+1}(a)}{1 + \frac{1}{2}\tau_1\sqrt{3}} = e^{-\tau_1\sqrt{3}} r_{+1}(a) + \int_{-\infty}^{+\infty} r_{+1}(a')\,\Delta_0\left(\tau_1, \frac{d\Omega}{d\tau};\ a - a'\right) da' \\ - \frac{9\tau_1 e^{-\tau_1\sqrt{3}}}{4\pi\sqrt{\pi}} \left\{ \int_{a-x_1}^{a-a_0} r_{+1}(a'') \log_e\left(\frac{a - a_0 - a'}{x_1 - a_0}\right) da' \right. \\ \left. + \int_{a-a_0}^{a-x_2} r_{+1}(a') \log_e\left(\frac{a - a_0 - a'}{x_2 - a_0}\right) da' \right\}. \end{aligned} \tag{99}$$

Integration of equation (99) over a shows that the equivalent width of the spectral line is unchanged by the electron scattering.

A good example to be considered is the dispersion-type profile for an absorption line,

$$r_{+1}(a) = 1 - (4 + 64a^2)^{-1}, \tag{100}$$

shown in Figure 3, since it may be considered typical of certain lines in high-temperature stellar atmospheres. For $T = 80{,}000°$ K and for the center of the line at $\lambda_0 = 3800$ A (cf. eq. [15]),

$$a = \frac{\lambda_0 - \lambda}{27.9}, \tag{101}$$

the corresponding half-width of the profile being 13.96 A and the equivalent width, 5.47 A. With the use of equations (99) and (100), profiles of the lines after scattering by the electron atmosphere have been computed for the two sets of atmosphere parameters. They are illustrated in Figure 3. It will be noticed that these emergent residual intensities differ from the incident residual intensity in two respects. First, the scattered line is shallower in the center and has extended wings. This is due to the shape of the function $\Delta(\tau_1, d\Omega/d\tau; x)$; it is therefore caused by the noncoherent scattering arising from the thermal motions of the electrons. Second, the profile is asymmetric toward the blue. This is caused by the shift of the logarithmic singularity in the function $\Delta(\tau_1, d\Omega/d\tau; x)$, and so this asymmetry is due to noncoherent scattering arising from the differential expansion of the atmosphere, being roughly proportional to the product of the two parameters, τ_1 and $d\Omega/d\tau$. The asymmetries shown in Figure 3 are characterized by the fact that the shift of the center of the lines is less than a tenth of the asymmetry at half-width. The smallness of this shift is caused by the term for unscattered radiation in equation (99), which reduces the shifts arising from electron scattering. For larger values of τ_1 the shift would become larger, since the terms for scattered radiation in equation (99) would become dominant. Furthermore, this dominance would produce a much broader and shallower profile, effectively reducing the asymmetry. For the temperature used in connection with equation (101), the values of the parameter $d\Omega/d\tau$ used to compute $r_{+1}(a)$ represent a total change in the velocity of expansion over the atmosphere of 620 km/sec for $d\Omega/d\tau = 1.0$ and 310 km/sec for $d\Omega/d\tau = 0.5$. Therefore, the asymmetries shown in Figure 3 may be considered large for high-temperature atmospheres. The same changes will be produced in the profile of an emission line.

It is a pleasure to express my appreciation to Dr. S. Chandrasekhar for suggesting this problem and for advice and guidance concerning it. I am also indebted to Dr. Guido Münch for furnishing his tabulation of the functions $M(\xi)$ and $N(\xi)$ used in the computations and for helpful discussions of these computations.

SCATTERING BY A MOVING ELECTRON ATMOSPHERE AND ITS EFFECT ON SPECTRAL LINES. II. THE PLANETARY NEBULA PROBLEM

FRANK N. EDMONDS, JR.
Yerkes Observatory
Received June 16, 1950

ABSTRACT

The problem of the transfer of radiation in a planetary nebula undergoing differential expansion and consisting of free electrons in thermal motion is solved in the first approximation for the emergent radiation. In the solution, account is taken of the noncoherent character of the scattering, which is due to the thermal and mass motions of the electrons.

The solution for the emergent radiation represents radiation of the incident flux from the central star, which has suffered scattering by electrons in the nebula. The solution contains a function which describes the spectral distribution of scattered intensity for incident monochromatic flux. The shape of this function produces in the solution a broadening of spectral lines characterized by a shallow center and extended wings. A shift of this function, due to the differential expansion of the nebula, produces shifts in the lines. A numerical example has been worked out.

I. INTRODUCTION

In the preceding paper[1] the transfer of radiation under the conditions of the standard Schuster problem in line formation has been considered for an atmosphere consisting of free electrons in thermal motion and undergoing differential expansion. The importance of scattering by free electrons in high-temperature stellar atmospheres is now generally recognized, and in many such atmospheres there are indications of considerable differential expansions. The term "differential expansion" is used to designate radial expansion of an atmosphere with a velocity that is a function of radial distance. In Paper I and in this discussion the velocity of expansion is considered to be a linear function of optical depth. However, in certain of the high-temperature stellar atmospheres in which differential expansion is believed to exist—for example, supernovae—the applicability of the Schuster problem boundary conditions is questionable. In these cases an electron atmosphere would be sufficiently far removed from the star to make the boundary conditions used in connection with radiative transfer in planetary nebulae seem more appropriate. It should be emphasized that the term "planetary nebula" is used in this paper not to designate a class of galactic objects but to describe a gaseous shell surrounding a star at a distance much larger than the stellar radius. In fact, the results of this paper are not applicable to the class of objects known as "planetary nebulae," since their optical thickness of free electrons is too small.

In this paper the transfer of radiation through a differentially expanding planetary nebula consisting of free electrons in thermal motion will be investigated in a manner analogous to the investigation of the Schuster problem in Paper I. The solution of the appropriate equation of transfer for the radiation emerging from the nebula will be obtained in the first approximation. In particular, this solution will be used to discuss the change produced in the profiles of spectral lines by the noncoherent character of the electron scattering. This noncoherency in the electron scattering is due to the Doppler effects arising from the thermal and mass motions of the electrons.

[1] F. N. Edmonds, Jr., *Ap. J.*, **112**, 307, 1950. This paper will be referred to as "Paper I," and equations in this paper will be designated by prefixing "I," e.g., "equation I (6)."

II. FORMULATION OF THE PROBLEM; EMISSION COEFFICIENT AND EQUATION OF TRANSFER

The curvature of the planetary nebula can be ignored in discussing the problem of radiative transfer, except when formulating the boundary conditions.[2] Therefore, the nebula can be considered as a plane-parallel atmosphere, and, except for the boundary conditions and the nature of the incident radiation at the inner surface, the description of the atmosphere given in Section II of Paper I will be used to describe the planetary nebula. Radiation incident at the inner surface of the nebula will consist of a flux $\pi F(\nu)$ from the central star and a diffuse radiation field from the inner surface of other portions of the nebula (using the picture of the planetary nebula as a spherical shell). In the plane-parallel representation of the nebula, the flux $\pi F(\nu)$ may be considered perpendicular to the plane of the nebulae, and the diffuse radiation field can be determined completely as to its intensity distribution in frequency and in direction in terms of the radiation emerging from the inner surface. This determination constitutes the boundary condition at the inner surface[2] (cf. eq. [6] below). Hence the incident diffuse radiation field may be considered to form a unified radiation field with the diffuse radiation field in the nebula, and only the flux from the central star is truly an incident radiation in the sense that its flux density distribution in frequency is arbitrary.

These differences between the electron atmospheres for the planetary nebula problem and for the Schuster problem affect the equation of radiative transfer only in that, for the planetary nebula problem, the source function contains an additional term. This additional term results from the scattering by the electrons within the nebula of the incident flux $\pi F(\nu)$. The expression for the corresponding emission coefficient is

$$j'(\nu, \tau, \mu) = \frac{N_e \sigma_e}{4} \int_{-\infty}^{+\infty} du \int_{-\infty}^{+\infty} dv \int_{-\infty}^{+\infty} dw F(\nu') e^{-(\tau_1 - \tau)} P(\Theta') f(u, v, w), \quad (1)$$

where N_e is the number of free electrons per cubic centimeter, σ_e the electron scattering coefficient (eq. I [1]), $P(\Theta')$ the Rayleigh phase function (eq. I [2]), and $f(u, v, w)$ the Maxwellian distribution function for electron thermal velocities (eq. I [10]). The exponential factor in the integrand of equation (1) indicates the reduction in the flux by electron scattering as it passes through the nebula. The optical depth τ is defined by equation I (3), and τ_1 is the optical depth at the inner surface. The angle of scattering Θ' satisfies the relation (eqs. I [5] and I [8])

$$\cos \Theta' = \beta_1' = \mu, \quad (2)$$

since the incident flux is normal to the plane of the nebula. This gives

$$P(\Theta') = \tfrac{3}{4}(1 + \mu^2). \quad (3)$$

The frequency ν' of the incident flux is related by the Doppler principle to the frequency ν of the scattered radiation, the relation being given by equation I (9). Finally, the variables of integration in equation (1), u, v, and w, are components of electron thermal velocity in directions indicated in Figure 1 of Paper I. The transformation of variables given by equations I (12), I (13), I (15), I (16), and I (19) and the integrations over u and w reduce equation (1) to the following form:

$$j(a, \tau, \mu) = \frac{3 N_e \sigma_e}{16 \sqrt{\pi}} \frac{(1 + \mu^2)}{(1 - \mu)^{1/2}} \int_{-\infty}^{+\infty} F(a' - \Omega[\mu - 1]) e^{-(\tau_1 - \tau)} \times \exp\left\{ -\frac{(a' - a)^2}{1 - \mu} \right\} da. \quad (4)$$

[2] Cf. E. A. Milne, *Zs. f. Ap.*, **1**, 98, 1930.

The expressions for $P(\Theta')$ and β_1', as given by equations (2) and (3), have been substituted in equation (4), and Ω, the electron velocity of differential expansion, is defined by equation I (18). Since Ω is a linear function of τ, $d\Omega/d\tau$ is a constant.

The equation of transfer for the nebula,

$$\mu \frac{dI(\alpha, \tau, \mu)}{d\tau} = I(\alpha, \tau, \mu) - \frac{1}{N_e \sigma_e} [\, j(\alpha, \tau, \mu) + j'(\alpha, \tau, \mu) \,], \tag{5}$$

is obtained by subtracting the emission coefficient (4) from the equation of transfer I (20). The emission coefficient $j(\alpha, \tau, \mu)$ in equation (5) is derived from the scattering by electrons of the diffuse radiation field within the nebula and is given by equation I (17). The emission coefficient $j'(\alpha, \tau, \mu)$ makes equation (5) an inhomogeneous equation in $I(\alpha, \tau, \mu)$, the homogeneous part of which is the equation of transfer for the Schuster problem.

The boundary conditions for the planetary nebula problem are

$$\left.\begin{aligned} I(\alpha, 0, -\mu) &\equiv 0\,, \\ I(\alpha, \tau_1, \mu) &= I(\alpha, \tau_1, -\mu) \end{aligned}\right\} \qquad (\mu \geq 0)\,. \tag{6}$$

The first condition merely states that no radiation is incident on the outer surface of the nebula. The second condition, as mentioned above, gives the incident intensity in terms of emergent intensity. It states a symmetry[2] which must exist in the diffuse radiation field at the inner surface, if it is assumed that no scattering occurs within the sphere surrounded by the nebula.

III. TRANSFORMATIONS OF EQUATION OF TRANSFER

As in the Schuster problem, the transformations indicated by equations I (22) and I (25) must be applied to equation (5) in order to remove the mixing of frequencies in the emission coefficients which prevents solving the equation by methods normally employed in radiative transfer theory.[3] For all terms in equation (5), excepting $j'(\alpha, \tau, \mu)$, the results obtained in the Schuster problem, as given by equation I (28), can be used. The two transformations to be applied to the emission coefficient $j'(\alpha, \tau, \mu)$ are the transformation which considers the incident flux at a frequency varying continuously with optical depth,

$$\tilde{\mathfrak{F}}(\alpha) = \tfrac{1}{4} F(\alpha + \Omega\mu)\,, \tag{7}$$

and the Fourier transform,

$$G(\xi) = \frac{1}{\sqrt{(2\pi)}} \int_{-\infty}^{+\infty} \tilde{\mathfrak{F}}(\alpha)\, e^{i\xi\alpha} d\alpha\,. \tag{8}$$

When applied to equation (4), these transformations give

$$\tfrac{3}{4}(1+\mu^2) G(\xi)\, e^{-(1-\mu)\xi^2/4} e^{-(\tau_1 - \tau)}\,. \tag{9}$$

Subtraction of this term from equation I (28) gives, as the transformed equation of transfer for the planetary nebula problem, the inhomogeneous equation,

$$\begin{aligned} \mu \frac{\partial \chi(\xi, \tau, \mu)}{\partial \tau} = \left(1 - i\mu^2 \xi \frac{d\Omega}{d\tau}\right) \chi(\xi, \tau, \mu) &- \int \frac{d\omega}{4\pi} P(\Theta)\, \chi(\xi, \tau, \mu')\, e^{-(1-\beta_1)\xi^2/4} \\ &- \tfrac{3}{4}(1+\mu^2) G(\xi)\, e^{-(1-\mu)\xi^2/4} e^{-(\tau_1 - \tau)}\,. \end{aligned} \tag{10}$$

When the transformations I (22) and I (25) are applied to the boundary conditions (6), they become

$$\left.\begin{aligned} \chi(\xi, 0, -\mu) &\equiv 0\,, \\ \chi(\xi, \tau_1, \mu) &= \chi(\xi, \tau_1, -\mu) \end{aligned}\right\} \qquad (\mu \geq 0)\,. \tag{11}$$

[2] Cf. S. Chandrasekhar, *Radiative Transfer* (Oxford: Clarendon Press, 1950).

The discussion of the validity of the application of the Fourier transform and the symmetry with respect to ξ of $\chi(\xi, \tau, \mu)$, as given in Section III of Paper I for the Schuster problem, is applicable to both $\chi(\xi, \tau, \mu)$ and $G(\xi)$ in equation (10). Since these quantities are complex, the use of equation I (31) and

$$G(\xi) = G^{(r)}(\xi) + iG^{(i)}(\xi) \tag{12}$$

allows the separation of equation (10) into its real and imaginary parts and gives

$$\begin{aligned}\mu \frac{\partial \chi^{(r)}(\xi, \tau, \mu)}{\partial \tau} &= \chi^{(r)}(\xi, \tau, \mu) + \mu^2 \xi \frac{d\Omega}{d\tau} \chi^{(i)}(\xi, \tau, \mu) \\ &\quad - \frac{3}{8} \int_{-1}^{+1} \chi^{(r)}(\xi, \tau, \mu') \, p(\xi, \mu, \mu') \, d\mu' \\ &\quad - \tfrac{3}{4}(1+\mu^2) G^{(r)}(\xi) \, e^{-(1-\mu)\xi^2/4} e^{-(\tau_1 - \tau)}\end{aligned} \tag{13}$$

and

$$\begin{aligned}\mu \frac{\partial \chi^{(i)}(\xi, \tau, \mu)}{\partial \tau} &= \chi^{(i)}(\xi, \tau, \mu) - \mu^2 \xi \frac{d\Omega}{d\tau} \chi^{(r)}(\xi, \tau, \mu) \\ &\quad - \frac{3}{8} \int_{-1}^{+1} \chi^{(i)}(\xi, \tau, \mu') \, p(\xi, \mu, \mu') \, d\mu' \\ &\quad - \tfrac{3}{4}(1+\mu^2) G^{(i)}(\xi) \, e^{-(1-\mu)\xi^2/4} e^{-(\tau_1 - \tau)} .\end{aligned} \tag{14}$$

The phase function $p(\xi, \mu, \mu')$, involving integration over the azimuthal angle, is given by equations I (34) and I (35). Equations (13) and (14) can now be solved by the standard approximate methods of radiative transfer theory,[3] by which they are replaced by the system of inhomogeneous linear differential equations,

$$\left.\begin{aligned}\mu_j \frac{\partial \chi_j^{(r)}(\xi, \tau)}{\partial \tau} &= \chi_j^{(r)}(\xi, \tau) + \mu_j^2 \xi \frac{d\Omega}{d\tau} \chi_j^{(i)}(\xi, \tau) \\ &\quad - \frac{3}{8} \sum_{k=-n}^{+n} a_k \chi_k^{(r)}(\xi, \tau) \, p(\xi, \mu_j, \mu_k) \\ &\quad - \tfrac{3}{4}(1+\mu_j^2) G^{(r)}(\xi) \, e^{-(1-\mu_j)\xi^2/4} e^{-(\tau_1 - \tau)} , \\ \mu_j \frac{\partial \chi_j^{(i)}(\xi, \tau)}{\partial \tau} &= \chi_j^{(i)}(\xi, \tau) - \mu_j^2 \xi \frac{d\Omega}{d\tau} \chi_j^{(r)}(\xi, \tau) \\ &\quad - \frac{3}{8} \sum_{k=-n}^{+n} a_k \chi_k^{(i)}(\xi, \tau) \, p(\xi, \mu_j, \mu_k) \\ &\quad - \tfrac{3}{4}(1+\mu_j^2) G^{(i)}(\xi) \, e^{-(1-\mu_j)\xi^2/4} e^{-(\tau_1 - \tau)}\end{aligned}\right\} \quad (j = \pm 1, \pm 2, \ldots, \pm n), \tag{15}$$

where the a_k's and μ_j's are Gaussian weights and divisions and $\chi_j^{(\ )}(\xi, \tau) = \chi^{(\ )}(\xi, \tau, \mu_j)$. As in equation (5), the homogeneous part of this system of equations constitutes the analogous set of equations I (36) for the Schuster problem. Within the scheme of this approximation, the boundary conditions (11) become

$$\left.\begin{aligned}\chi_{+j}^{(r)}(\xi, \tau_1) = \chi_{-j}^{(r)}(\xi, \tau_1), \quad \chi_{+j}^{(i)}(\xi, \tau_1) = \chi_{-j}^{(i)}(\xi, \tau_1), \\ \chi_{-j}^{(r)}(\xi, 0) \equiv \chi_{-j}^{(i)}(\xi, 0) \equiv 0\end{aligned}\right\} \quad (j = +1, +2, \ldots, +n). \tag{16}$$

IV. SOLUTION OF THE TRANSFORMED EQUATION OF TRANSFER IN THE FIRST APPROXIMATION

For reasons given in Section IV of Paper I, equations (15) will be solved in the first approximation, where they take the form

$$\frac{1}{\sqrt{3}}\frac{\partial \chi_{+1}^{(r)}(\xi,\tau)}{\partial\tau} = \chi_{+1}^{(r)}(\xi,\tau) + L(\xi)\chi_{+1}^{(i)}(\xi,\tau) - M(\xi)\chi_{+1}^{(r)}(\xi,\tau) - N(\xi)\chi_{-1}^{(r)}(\xi,\tau) - G^{(r)}(\xi)\, e^{-(1-1/\sqrt{3})\xi^2/4} e^{-(\tau_1-\tau)}, \tag{17}$$

$$-\frac{1}{\sqrt{3}}\frac{\partial \chi_{-1}^{(r)}(\xi,\tau)}{\partial\tau} = \chi_{-1}^{(r)}(\xi,\tau) + L(\xi)\chi_{-1}^{(i)}(\xi,\tau) - M(\xi)\chi_{-1}^{(r)}(\xi,\tau) - N(\xi)\chi_{+1}^{(r)}(\xi,\tau) - G^{(r)}(\xi)\, e^{-(1+1/\sqrt{3})\xi^2/4} e^{-(\tau_1-\tau)}, \tag{18}$$

$$\frac{1}{\sqrt{3}}\frac{\partial \chi_{+1}^{(i)}(\xi,\tau)}{\partial\tau} = \chi_{+1}^{(i)}(\xi,\tau) - L(\xi)\chi_{+1}^{(r)}(\xi,\tau) - M(\xi)\chi_{+1}^{(i)}(\xi,\tau) - N(\xi)\chi_{-1}^{(i)}(\xi,\tau) - G^{(i)}(\xi)\, e^{-(1-1/\sqrt{3})\xi^2/4} e^{-(\tau_1-\tau)}, \tag{19}$$

$$-\frac{1}{\sqrt{3}}\frac{\partial \chi_{-1}^{(i)}(\xi,\tau)}{\partial\tau} = \chi_{-1}^{(i)}(\xi,\tau) - L(\xi)\chi_{-1}^{(r)}(\xi,\tau) - M(\xi)\chi_{-1}^{(i)}(\xi,\tau) - N(\xi)\chi_{+1}^{(i)}(\xi,\tau) - G^{(i)}(\xi)\, e^{-(1+1/\sqrt{3})\xi^2/4} e^{-(\tau_1-\tau)}. \tag{20}$$

In the foregoing equations, use was made of equation I (38), and the functions $M(\xi)$, $N(\xi)$, and $L(\xi)$ are defined by equations I (39), I (40), and I (45), respectively. Equations (17)–(20) constitute a fourth-order set of linear inhomogeneous differential equations with coefficients which are constant, since ξ may be considered a parameter. The homogeneous parts of these equations are the analogous equations for the Schuster problem, equations I (41)–I (44). Therefore, the complementary solution to equations (17)–(20) is that found for the Schuster problem and given by equations I (46)–I (49). Hence only the particular solution remains to be determined. Substitution of the trial particular solution,

$$\begin{aligned} \chi_{+1}^{(r)}(\xi,\tau) &= \mathfrak{g}_{+1}^{(r)}(\xi)\, e^{-(\tau_1-\tau)}, \qquad \chi_{-1}^{(r)}(\xi,\tau) = \mathfrak{g}_{-1}^{(r)}(\xi)\, e^{-(\tau_1-\tau)}, \\ \chi_{+1}^{(i)}(\xi,\tau) &= \mathfrak{g}_{+1}^{(i)}(\xi)\, e^{-(\tau_1-\tau)}, \qquad \chi_{-1}^{(i)}(\xi,\tau) = \mathfrak{g}_{-1}^{(i)}(\xi)\, e^{-(\tau_1-\tau)}, \end{aligned} \tag{21}$$

into equations (17)–(20) gives a fourth-order set of linear inhomogeneous equations in $\mathfrak{g}_{+1}^{(r)}(\xi)$, $\mathfrak{g}_{-1}^{(r)}(\xi)$, $\mathfrak{g}_{+1}^{(i)}(\xi)$, and $\mathfrak{g}_{-1}^{(i)}(\xi)$ with the solution

$$\begin{aligned} \sigma\,\mathfrak{g}_{+1}^{(r)}(\xi) = {} & -\{(M-1-1/\sqrt{3})[(M-1)^2-N^2-\tfrac{1}{4}]+(M-1+1/\sqrt{3})L^2\}G^{(r)}(\xi)\, e^{-(1-1/\sqrt{3})\xi^2/4} \\ & -N[(M-1)^2-N^2-L^2-\tfrac{1}{4}]G^{(r)}(\xi)\, e^{-(1+1/\sqrt{3})\xi^2/4} \\ & -L[(M-1-1/\sqrt{3})^2+N^2+L^2]G^{(i)}(\xi)\, e^{-(1-1/\sqrt{3})\xi^2/4} \\ & +2NL(M-1)G^{(i)}(\xi)\, e^{-(1+1/\sqrt{3})\xi^2/4}, \end{aligned} \tag{22}$$

$$\begin{aligned} \sigma\,\mathfrak{g}_{-1}^{(r)}(\xi) = {} & N[(M-1)^2-N^2-L^2-\tfrac{1}{4}]G^{(r)}(\xi)\, e^{-(1-1/\sqrt{3})\xi^2/4} \\ & -\{(M-1+1/\sqrt{3})[(M-1)^2-N^2-\tfrac{1}{4}]+(M-1-1/\sqrt{3})L^2\}G^{(r)}(\xi)\, e^{-(1+1/\sqrt{3})\xi^2/4} \\ & +2NL(M-1)G^{(i)}\, e^{-(1-1/\sqrt{3})\xi^2/4} \\ & -L[(M-1+1/\sqrt{3})^2+N^2+L^2]G^{(i)}(\xi)\, e^{-(1+1/\sqrt{3})\xi^2/4}, \end{aligned} \tag{23}$$

$$\begin{aligned} \sigma\,\mathfrak{g}_{+1}^{(i)}(\xi) = {} & L[(M-1-1/\sqrt{3})^2+N^2+L^2]G^{(r)}(\xi)\, e^{-(1-1/\sqrt{3})\xi^2/4} \\ & -2NL(M-1)G^{(r)}(\xi)\, e^{-(1+1/\sqrt{3})\xi^2/4} \\ & -\{(M-1-1/\sqrt{3})[(M-1)^2-N^2-\tfrac{1}{4}]+(M-1+1/\sqrt{3})L^2\}G^{(i)}(\xi)\, e^{-(1-1/\sqrt{3})\xi^2/4} \\ & +N[(M-1)^2-N^2-L^2-\tfrac{1}{4}]G^{(i)}(\xi)\, e^{-(1+1/\sqrt{3})\xi^2/4}, \end{aligned} \tag{24}$$

and

$$\begin{aligned}
&\sigma \mathfrak{g}_{-1}^{(i)}(\xi) = \\
&-2NL(M-1)G^{(r)}(\xi)\, e^{-(1-1/\sqrt{3})\xi^2/4} \\
&+L[(M-1+1/\sqrt{3})^2+N^2+L^2]G^{(r)}(\xi)\, e^{-(1+1/\sqrt{3})\xi^2/4} \\
&+N[(M-1)^2-N^2-L^2-\tfrac{1}{3}]G^{(i)}(\xi)\, e^{-(1-1/\sqrt{3})\xi^2/4} \\
&-\{(M-1+1/\sqrt{3})[(M-1)^2-N^2-\tfrac{1}{3}]+(M-1-1/\sqrt{3})L^2\}G^{(i)}(\xi)\, e^{-(1+1/\sqrt{3})\xi^2/4},
\end{aligned} \tag{25}$$

where

$$\sigma(\xi) = [(M-1)^2 - N^2 - L^2 - \tfrac{1}{3}]^2 + 4L^2(M-1)^2. \tag{26}$$

Substitution of equations (22)–(25) in equations (21) gives the particular solution which, in combination with the complementary solution, gives, as the most general solution to equations (17)–(20),

$$\begin{aligned}
\chi_{+1}^{(r)}(\xi, \tau) = {} & (D_1 \cos k''\tau - D_2 \sin k''\tau)\, e^{k'\tau} \\
& + (D_3 \cos k''\tau + D_4 \sin k''\tau)\, e^{-k'\tau} + \mathfrak{g}_{+1}^{(r)}(\xi)\, e^{-(\tau_1-\tau)},
\end{aligned} \tag{27}$$

$$\begin{aligned}
\chi_{-1}^{(r)}(\xi, \tau) = {} & -[(D_1E_1 - D_2E_2)\cos k''\tau - (D_1E_2 + D_2E_1)\sin k''\tau]\, e^{k'\tau} \\
& -[(D_3E_3 - D_4E_4)\cos k''\tau + (D_3E_4 + D_4E_3)\sin k''\tau]\, e^{-k'\tau} \\
& + \mathfrak{g}_{-1}^{(r)}(\xi)\, e^{-(\tau_1-\tau)},
\end{aligned} \tag{28}$$

$$\begin{aligned}
\chi_{+1}^{(i)}(\xi, \tau) = {} & (D_2 \cos k''\tau + D_1 \sin k''\tau)\, e^{k'\tau} \\
& + (D_4 \cos k''\tau - D_3 \sin k''\tau)\, e^{-k'\tau} + \mathfrak{g}_{+1}^{(i)}(\xi)\, e^{-(\tau_1-\tau)},
\end{aligned} \tag{29}$$

and

$$\begin{aligned}
\chi_{-1}^{(i)}(\xi, \tau) = {} & -[(D_1E_2 + D_2E_1)\cos k''\tau + (D_1E_1 - D_2E_2)\sin k''\tau]\, e^{k'\tau} \\
& -[(D_3E_4 + D_4E_3)\cos k''\tau - (D_3E_3 - D_4E_4)\sin k''\tau]\, e^{-k'\tau} \\
& + \mathfrak{g}_{-1}^{(i)} e^{-(\tau_1-\tau)}.
\end{aligned} \tag{30}$$

The characteristic roots $k'(\xi)$ and $k''(\xi)$ and the functions $E_1(\xi)$, $E_2(\xi)$, $E_3(\xi)$, and $E_4(\xi)$ are defined by equations I (50) and I (51), respectively.

The coefficients D_1, D_2, D_3, and D_4 in equations (27)–(30) are arbitrary functions of ξ. They are determined by the boundary conditions (16), which, in the first approximation, take the form

$$\begin{gathered}
\chi_{+1}^{(r)}(\xi, \tau_1) = \chi_{-1}^{(r)}(\xi, \tau_1), \qquad \chi_{+1}^{(i)}(\xi, \tau_1) = \chi_{-1}^{(i)}(\xi, \tau_1), \\
\chi_{-1}^{(r)}(\xi, 0) \equiv \chi_{-1}^{(i)}(\xi, 0) \equiv 0.
\end{gathered} \tag{31}$$

These four equations can be solved for D_1, D_2, D_3, and D_4, the solution being

$$\begin{aligned}
\eta' D_1 = {} & (g_1H_1 + g_2H_2)(E_3^2 + E_4^2) + (g_1H_4 + g_2H_3)(E_1E_4 - E_2E_3) \\
& - (g_1H_3 - g_2H_4)(E_1E_3 + E_2E_4) + (g_3E_1 + g_4E_2)(H_3^2 + H_4^2) \\
& + (g_3E_4 - g_4E_3)(H_1H_4 + H_2H_3) - (g_3E_3 + g_4E_4)(H_1H_3 - H_2H_4),
\end{aligned} \tag{32}$$

$$\begin{aligned}
\eta' D_2 = {} & -(g_1H_2 - g_2H_1)(E_3^2 + E_4^2) - (g_1H_3 - g_2H_4)(E_1E_4 - E_2E_3) \\
& - (g_1H_4 + g_2H_3)(E_1E_3 + E_2E_4) - (g_3E_2 - g_4E_1)(H_3^2 + H_4^2) \\
& + (g_2E_3 + g_4E_4)(H_1H_4 + H_2H_3) + (g_3E_4 - g_4E_3)(H_1H_3 - H_2H_4),
\end{aligned} \tag{33}$$

$$\begin{aligned}
\eta' D_3 = {} & (g_1H_3 - g_2H_4)(E_1^2 + E_2^2) + (g_1H_2 - g_2H_1)(E_1E_4 - E_2E_3) \\
& - (g_1H_1 + g_2H_2)(E_1E_3 + E_2E_4) + (g_3E_3 + g_4E_4)(H_1^2 + H_2^2) \\
& - (g_3E_2 - g_4E_1)(H_1H_4 + H_2H_3) - (g_3E_1 + g_4E_2)(H_1H_3 - H_2H_4),
\end{aligned} \tag{34}$$

and

$$\begin{aligned}\eta' D_4 = {} & (g_1H_4 + g_2H_2)(E_1^2 + E_2^2) + (g_1H_1 + g_2H_2)(E_1E_4 - E_2E_3) \\ & + (g_1H_2 - g_2H_1)(E_1E_3 + E_2E_4) - (g_3E_4 - g_4E_3)(H_1^2 + H_2^2) \\ & - (g_3E_1 + g_4E_2)(H_1H_4 + H_2H_3) + (g_3E_2 - g_4E_1)(H_1H_3 - H_2H_4)\,,\end{aligned} \tag{35}$$

where

$$\begin{aligned}\eta'(\xi) = {} & (H_1^2 + H_2^2)(E_3^2 + E_4^2) + (H_3^2 + H_4^2)(E_1^2 + E_2^2) \\ & + 2(H_1H_4 + H_2H_3)(E_1E_4 - E_2E_3) - 2(H_1H_3 - H_2H_4)(E_2E_4 + E_1E_3)\,,\end{aligned} \tag{36}$$

$$\begin{aligned} g_1(\xi) &= \mathfrak{g}_{-1}^{(r)}(\xi) - \mathfrak{g}_{+1}^{(r)}(\xi)\,, & g_2(\xi) &= \mathfrak{g}_{-1}^{(i)}(\xi) - \mathfrak{g}_{+1}^{(i)}(\xi)\,, \\ g_3(\xi) &= \mathfrak{g}_{-1}^{(r)}(\xi)\, e^{-\tau_1}\,, & g_4(\xi) &= \mathfrak{g}_{-1}^{(i)}(\xi)\, e^{-\tau_1}\,, \end{aligned} \tag{37}$$

and

$$\begin{aligned} H_1(\xi) &= F_1 + E_1F_1 - E_2F_2\,, & H_2(\xi) &= F_2 + E_1F_2 + E_2F_1\,, \\ H_3(\xi) &= F_3 + E_3F_3 + E_4F_4\,, & H_4(\xi) &= F_4 + E_3F_4 - E_4F_3\,. \end{aligned} \tag{38}$$

The quantities $F_1(\xi)$, $F_2(\xi)$, $F_3(\xi)$, and $F_4(\xi)$ appearing in equations (38) are defined by equations I (59). Also, equation I (52) and (32)–(35) give, for the coefficients in equations (28) and (30),

$$\begin{aligned}\eta'(D_1E_1 - D_2E_2) = {} & -(g_1H_3 - g_2H_4)E_1 - (g_1H_4 + g_2H_3)E_2 + (g_1H_1 + g_2H_2)E_3 \\ & - (g_1H_2 + g_2H_1)E_4 + g_3(H_3^2 + H_4^2)(E_1^2 + E_2^2) \\ & + [g_3(E_1E_4 - E_2E_3) - g_4(E_1E_3 + E_2E_4)](H_1H_4 + H_2H_3) \\ & - [g_3(E_1E_3 + E_2E_4) + g_4(E_1E_4 - E_2E_3)](H_1H_3 - H_2H_4)\,,\end{aligned} \tag{39}$$

$$\begin{aligned}\eta'(D_1E_2 + D_2E_1) = {} & -(g_1H_4 + g_2H_3)E_1 + (g_1H_3 - g_2H_4)E_2 - (g_1H_2 - g_2H_1)E_3 \\ & - (g_1H_1 + g_2H_2)E_4 + g_4(H_3^2 + H_4^2)(E_1^2 + E_2^2) \\ & + [g_3(E_1E_3 + E_2E_4) + g_4(E_1E_4 - E_2E_3)](H_1H_4 + H_2H_3) \\ & + [g_3(E_1E_4 - E_2E_3) - g_4(E_1E_3 + E_2E_4)](H_1H_3 - H_2H_4)\,,\end{aligned} \tag{40}$$

$$\begin{aligned}\eta'(D_3E_3 - D_4E_4) = {} & (g_1H_3 - g_2H_4)E_1 + (g_1H_4 + g_2H_3)E_2 - (g_1H_1 + g_2H_2)E_3 \\ & + (g_1H_2 - g_2H_1)E_4 + g_3(H_1^2 + H_2^2)(E_3^2 + E_4^2) \\ & + [g_3(E_1E_4 - E_2E_3) + g_4(E_1E_3 + E_2E_4)](H_1H_4 + H_2H_3) \\ & - [g_3(E_1E_3 + E_2E_4) - g_4(E_1E_4 - E_2E_3)](H_1H_3 - H_2H_4)\,,\end{aligned} \tag{41}$$

and

$$\begin{aligned}\eta'(D_3E_4 + D_4E_3) = {} & (g_1H_4 + g_2H_3)E_1 - (g_1H_3 - g_2H_4)E_2 + (g_1H_2 - g_2H_1)E_3 \\ & + (g_1H_1 + g_2H_2)E_4 + g_4(H_1^2 + H_2^2)(E_3^2 + E_4^2) \\ & - [g_3(E_1E_3 + E_2E_4) - g_4(E_1E_4 - E_2E_3)](H_1H_4 + H_2H_3) \\ & - [g_3(E_1E_4 - E_2E_3) + g_4(E_1E_3 + E_2E_4)](H_1H_3 - H_2H_4)\,.\end{aligned} \tag{42}$$

Examination of the solution given by equations (22)–(30) and (32)–(42) shows that all coefficients of $G^{(r)}(\xi)$ and $G^{(i)}(\xi)$ are bounded for all values of τ and for all values of ξ

except $\xi = 0$.[4] Hence, within the scheme of the first approximation, the integrable-square condition for the validity of the application of the Fourier transform (cf. Sec. III, Paper I) can be transferred to $G^{(r)}(\xi)$ and $G^{(i)}(\xi)$. Furthermore, the solution in the first approximation has the correct symmetry in ξ to insure that its inverse Fourier transform will be a real function.

V. THE EMERGENT RADIATION

For $\tau = 0$, equations (27) and (29) give the solution for the emergent radiation. When equations (22)–(26) and (32)–(38) are substituted in these equations, they can be reduced to the form

$$\chi_{+1}^{(r)}(\xi, 0) = \Lambda_1 G^{(r)}(\xi) - \Lambda_2 G^{(i)}(\xi) \tag{43}$$

and

$$\chi_{+1}^{(i)}(\xi, 0) = \Lambda_2 G^{(r)}(\xi) + \Lambda_1 G^{(i)}(\xi), \tag{44}$$

where

$$\eta' \sigma \Lambda_1 = A_1(k_1 + k_2) - A_2(k_3 + k_4) + e^{-\tau_1}(A_3 k_1 - A_4 k_3 - \eta' k_2), \tag{45}$$

$$\eta' \sigma \Lambda_2 = -A_1(k_3 + k_4) - A_2(k_1 + k_2) - e^{-\tau_1}(A_3 k_3 - A_4 k_1 - \eta' k_4), \tag{46}$$

$$\begin{aligned} k_1 = {} & N[(M-1)^2 - N^2 - L^2 - \tfrac{1}{3}] e^{-(1-1/\sqrt{3})\xi^2/4} \\ & - \{(M-1+1/\sqrt{3})[(M-1)^2 - N^2 - \tfrac{1}{3}] + (M-1-1/\sqrt{3}) L^2\} \\ & \times e^{-(1+1/\sqrt{3})\xi^2/4}, \end{aligned} \tag{47}$$

$$\begin{aligned} k_2 = {} & \{(M-1-1/\sqrt{3})[(M-1)^2 - N^2 - \tfrac{1}{3}] + (M-1+1/\sqrt{3}) L^2\} \\ & \times e^{-(1-1/\sqrt{3})\xi^2/4} - N[(M-1)^2 - N^2 - L^2 - \tfrac{1}{3}] e^{-(1+1/\sqrt{3})\xi^2/4}, \end{aligned} \tag{48}$$

$$\begin{aligned} k_3 = {} & NL(M-1) e^{-(1-1/\sqrt{3})\xi^2/4} \\ & - L[(M-1+1/\sqrt{3})^2 + N^2 + L^2] e^{-(1+1/\sqrt{3})\xi^2/4}, \end{aligned} \tag{49}$$

$$\begin{aligned} k^4 = {} & L[(M-1-1/\sqrt{3})^2 + N^2 + L^2] e^{-(1-1/\sqrt{3})\xi^2/4} \\ & - NL(M-1) e^{-(1+1/\sqrt{3})\xi^2/4}, \end{aligned} \tag{50}$$

$$\begin{aligned} \tfrac{1}{4} N^2 A_1 = {} & \tfrac{1}{4} N^2 \eta \Gamma_1 - (1/\sqrt{3}) N k'' \cosh k' \tau_1 \sin k'' \tau_1 \\ & - (1/\sqrt{3}) N k' \sinh k' \tau_1 \cos k'' \tau_1, \end{aligned} \tag{51}$$

$$\begin{aligned} \tfrac{1}{4} N^2 A_2 = {} & -\tfrac{1}{4} N^2 \eta \Gamma_2 + (1/\sqrt{3}) N k'' \sinh k' \tau_1 \cos k'' \tau_1 \\ & - (1/\sqrt{3}) N k' \cosh k' \tau_1 \sin k'' \tau_1, \end{aligned} \tag{52}$$

$$\begin{aligned} \tfrac{1}{4} N^2 A_3 = {} & [(M-1)^2 + N(M-1) - \tfrac{1}{3} k'^2] \cosh 2k' \tau_1 \\ & - [(M-1)^2 + N(M-1) + \tfrac{1}{3} k''^2] \cos 2k'' \tau_1, \end{aligned} \tag{53}$$

$$\begin{aligned} \tfrac{1}{4} N^2 A_4 = {} & (1/\sqrt{3})[Lk' - (M-1) k'' - N k''] \sinh 2k' \tau_1 \\ & + (1/\sqrt{3})[(M-1) k' + N k' + L k''] \sin 2k'' \tau_1, \end{aligned} \tag{54}$$

and

$$\begin{aligned} \tfrac{1}{4} N^2 \eta' = {} & \tfrac{1}{4} N^2 \eta + [N(M-1) + \tfrac{1}{2} N^2](\cosh 2k' \tau_1 - \cos 2k'' \tau_1) \\ & - (1/\sqrt{3}) N k' \sinh 2k' \tau_1 - (1/\sqrt{3}) N k'' \sin 2k'' \tau_1. \end{aligned} \tag{55}$$

[4] As in the Schuster problem, the solution becomes indeterminate at $\xi = 0$, but it remains bounded in passing to the limit $\xi = 0$.

The functions Γ_1, Γ_2, and η appearing in equations (51), (52), and (55), respectively, are given by equations I (66), I (67), and I (68), respectively. All terms in equations (47)–(50) contain negative exponentials in ξ^2, and so the functions k_1, k_2, k_3, and k_4 and hence, by equations (45) and (46), Λ_1 and Λ_2 go to zero as $\pm\xi$ goes to infinity.

Now the inverse Fourier transform of the solution for emergent radiation is (cf. eqs. I [25] and I [70])

$$\psi_{+1}(a, 0) = \frac{1}{\sqrt{(2\pi)}}\int_{-\infty}^{+\infty} e^{-ix\xi}\left[\chi_{+1}^{(r)}(\xi, 0) + i\chi_{+1}^{(i)}(\xi, 0)\right] d\xi$$

$$= \frac{1}{\sqrt{(2\pi)}}\int_{-\infty}^{+\infty} e^{-ix\xi}(\Lambda_1 + i\Lambda_2)\left[G^{(r)}(\xi) + iG^{(i)}(\xi)\right] d\xi \tag{56}$$

by equations (43) and (44). Use of a Parseval formula, given by equation I (75), reduces equation (56) to the form[5]

$$\psi_{+1}(a, 0) = \int_{-\infty}^{+\infty} \tilde{\vartheta}(\beta)\,\Delta'\left(\tau_1, \frac{d\Omega}{d\tau};\ a - \beta\right) d\beta\,, \tag{57}$$

where

$$\Delta'\left(\tau_1, \frac{d\Omega}{d\tau};\ x\right) = \frac{1}{2\pi}\int_{-\infty}^{+\infty} e^{ix\xi}(\Lambda_1 + i\Lambda_2)\, d\xi$$

$$= \frac{1}{\pi}\int_0^{\infty} (\Lambda_1 \cos x\xi + \Lambda_2 \sin x\xi)\, d\xi\,. \tag{58}$$

The symmetry of Λ_1 and Λ_2 with respect to ξ was used in obtaining the second representation of $\Delta'(\tau_1, d\Omega/d\tau; x)$ in equation (58). This function depends on the parameters of the nebula, τ_1 and $d\Omega/d\tau$; but, as in the Schuster problem, it is not easy to disentangle the manner in which each parameter influences $\Delta'(\tau_1, d\Omega/d\tau; x)$, since Λ_1 and Λ_2 depend on these parameters in a very complicated manner. Finally, the transformations (7) and I (22), when applied to equation (57) for the frequencies $a + \Omega(0)$ and $\beta + \Omega(0)$ (at the level $\tau = 0$), give, as the desired expression, the emergent radiation,

$$I_{+1}(a) = \frac{1}{4}\int_{-\infty}^{+\infty} F(a')\,\Delta'\left(\tau_1, \frac{d\Omega}{d\tau};\ a - a'\right) da'\,. \tag{59}$$

Physically, the right-hand side of equation (59) represents that portion of the incident flux $\pi F(a)$ from the central star which has suffered at least one scattering in passing through the nebula. The integral indicates the noncoherent nature of the electron scattering. Unlike the Schuster problem, the unscattered portion of the flux is not represented in equation (59), since it is in the direction of the normal to the atmosphere ($\mu = 1$). The function $\Delta'(\tau_1, d\Omega/d\tau; a - a')$ represents the spectral distribution of emergent scattered radiation arising from incident monochromatic flux at a frequency a' and of unit flux density.

VI. PROPERTIES OF $\Delta'(\tau_1, d\Omega/d\tau; x)$

Since Λ_1 and Λ_2 decrease exponentially to zero for large ξ, the integration indicated in equation (58) need not be performed beyond values of ξ, which are not large. Furthermore, the convergence of the integral is assured. The only difficulty encountered in this integration is that Λ_1 and Λ_2 become indeterminate at $\xi = 0$, since the expressions given by equations (45), (46), and (55) become zero. This indeterminacy can be removed by expanding these expressions in ξ and passing to the limit, with the result that

$$\Lambda_1 \to \frac{k_1 + k_2}{\sigma}(1 - e^{-\tau_1})\,, \qquad \Lambda_2 \to 0 \qquad \text{as} \qquad \xi \to 0\,. \tag{60}$$

[5] The conditions for use of the Parseval formula, discussed in Sec. V of Paper I, are satisfied since $G^{(r)}(\xi)$ and $G^{(i)}(\xi)$ are assumed to be integrable square and $\Delta'(\tau_1, d\Omega/d\tau; a - \beta)$ is integrable in its argument as shown in Sec. VI, below.

The function $\Delta'(\tau_1, d\Omega/d\tau; x)$ has been evaluated for the parameter values $\tau_1 = 0.5$ and $d\Omega/d\tau = 1.0$, and the results are tabulated in Table 1 and illustrated in Figure 1. This function differs in several respects from the analogous function for the Schuster problem, $\Delta(\tau_1, d\Omega/d\tau; x)$, as defined by equation I (77) and shown for the same values of

TABLE 1

THE FUNCTION $\Delta'(\tau_1, d\Omega/d\tau; x)$ FOR $\tau_1 = 0.5$ AND $d\Omega/d\tau = 1.0$

x	$\Delta'(\tau_1, d\Omega/d\tau; x)$	x	$\Delta'(\tau_1, d\Omega/d\tau; x)$
−2.00	0.044	0.25	0.681
−1.00	.157	0.50	.585
−0.50	.376	1.00	.313
−0.25	.538	2.00	0.098
0.00	0.664		
$\int_{-\infty}^{+\infty} \Delta' d\tau$ computed	1.306	$\int_{-\infty}^{+\infty} \Delta' dx$ from equation (68)	1.363

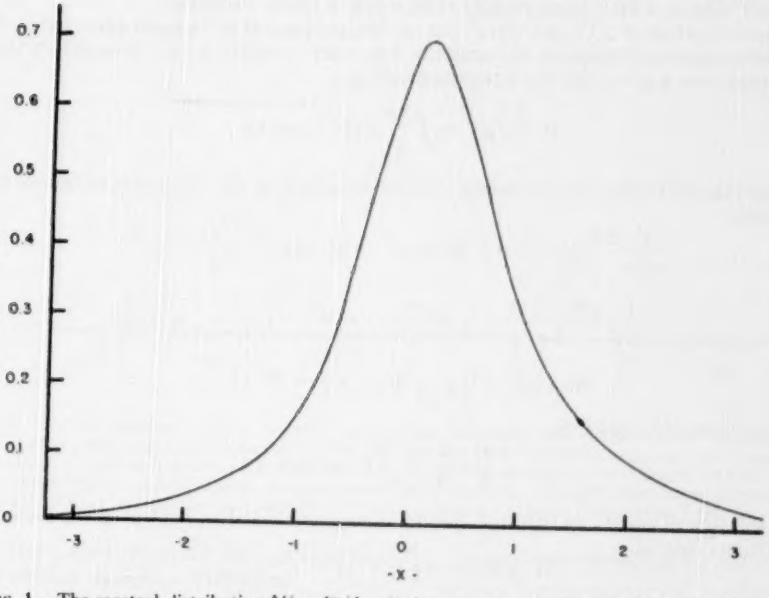

FIG. 1.—The spectral distribution $\Delta'(\tau_1, d\Omega/d\tau; x)$ of emergent scattered intensity arising from incident monochromatic flux of unit flux density. The argument x represents the difference between incident and scattered frequencies in units of $\sqrt{2}$ Doppler half-widths (cf. eq. I [15]). The curve shown is for the atmosphere parameters $\tau_1 = 0.5$ and $d\Omega/d\tau = 1.0$.

the parameters in Figure 2 of Paper I. The most noticeable difference is that, while $\Delta(\tau_1, d\Omega/d\tau; x)$ has a logarithmic singularity at $x = \alpha_0$, where α_0 is defined by equation I (72), $\Delta'(\tau_1, d\Omega/d\tau; x)$ does not. The explanation for this is essentially that the incident flux is pointing in a direction different from that for the emergent intensity, whereas in the Schuster problem the incident and emergent intensities are for the same direction. Also $\Delta'(\tau_1, d\Omega/d\tau; x)$ has its maximum shifted by an amount less than α_0; it shows a slight asymmetry not evident in $\Delta(\tau_1, d\Omega/d\tau; x)$; and it is broader than the similar func-

tion for the Schuster problem. These three differences have a common explanation. When radiation of the incident flux is scattered at a given level τ' in the planetary nebula, the effects of differential expansion on the transfer of this radiation to the outer surface will be essentially for the optical depth τ'. Hence the spectral distribution of scattered emergent radiation for this radiation initially scattered at τ' will have a shift similar to that found in the Schuster problem for $\Delta(\tau_1, d\Omega/d\tau; x)$, but by an amount less than a_0, since the effective optical depth is less. Now the function $\Delta'(\tau_1, d\Omega/d\tau; x)$ may be considered as the superposition for all τ' of these spectral distribution functions weighted by the factor $e^{-(\tau_1-\tau')}$ appearing in the flux. This superposition would produce the three differences between $\Delta(\tau_1, d\Omega/d\tau; x)$ and $\Delta'(\tau_1, d\Omega/d\tau; x)$.

It is more difficult, therefore, to explain the characteristics of $\Delta'(\tau_1, d\Omega/d\tau; x)$ in terms of thermal and mass motions of the electrons in a manner similar to that in Section VI of Paper I for the Schuster problem. The thermal motions give $\Delta'(\tau_1, d\Omega/d\tau; x)$ its general shape, while the differential expansion of the planetary nebula produces the shift in its maximum. But the superposition discussed in the preceding paragraph also affects both these features. Since the shift of the maximum is less than a_0, the strict proportionality of this shift to the product of the parameters τ_1 and $d\Omega/d\tau$, obtained for the Schuster problem, cannot be shown. It is reasonable to assume that the shift is still proportional to $d\Omega/d\tau$, but the weighting factor in the superposition, $e^{-(\tau_1-\tau')}$, would tend to increase the shift with τ_1 a little more rapidly than would a linear variation.

The calculation of $\Delta'(\tau_1, d\Omega/d\tau; x)$ can be checked against an integral admitted by the original equation of transfer (5) and the boundary conditions (6). Integrating these equations over a gives, for the integrated intensity,

$$W(\tau, \mu) = \int_{-\infty}^{+\infty} I(a, \tau, \mu)\, da\,, \tag{61}$$

an equation of transfer and boundary conditions, which, in the first approximation, take the form

$$\frac{1}{\sqrt{3}} \frac{dW_{+1}(\tau)}{d\tau} = \tfrac{1}{2}\,[W_{+1}(\tau) - W_{-1}(\tau)\,] - \frac{f}{4}\, e^{-(\tau_1-\tau)}\,, \tag{62}$$

$$-\frac{1}{\sqrt{3}} \frac{dW_{-1}(\tau)}{d\tau} = \tfrac{1}{2}\,[W_{-1}(\tau) - W_{+1}(\tau)\,] - \frac{f}{4}\, e^{-(\tau_1-\tau)}\,, \tag{63}$$

and

$$W_{-1}(0) = 0\,, \qquad W_{+1}(\tau_1) = W_{-1}(\tau_1)\,. \tag{64}$$

In equations (62) and (63),

$$\frac{f}{4} = \frac{1}{4} \int_{-\infty}^{+\infty} F(a)\, da\,. \tag{65}$$

The solution of equations (62) and (63) for emergent radiation, subject to the boundary conditions (64), is

$$W_{+1}(0) = (\tfrac{1}{2}\sqrt{3})\,(1 - e^{-\tau_1})\, f\,. \tag{66}$$

Also, integrating equation (59) over a gives

$$W_{+1}(0) = \frac{f}{4} \int_{-\infty}^{+\infty} \Delta'\left(\tau_1, \frac{d\Omega}{d\tau};\ a - a'\right) d\,(a - a')\,; \tag{67}$$

and so equations (66) and (67) may be combined to give

$$\int_{-\infty}^{+\infty} \Delta'\left(\tau_1, \frac{d\Omega}{d\tau};\ x\right) dx = (2\sqrt{3})\,(1 - e^{-\tau_1})\,. \tag{68}$$

which shows that $\Delta'(\tau_1, d\Omega/d\tau; x)$ is integrable in its argument. This check on $\Delta'(\tau_1, d\Omega/d\tau; x)$ is included in Table 1.

VII. CHANGES PRODUCED IN THE PROFILES OF SPECTRAL LINES

It is important to consider the solution for emergent radiation when the incident flux is the residual flux of a spectral line,

$$R(\mathfrak{a}) = \frac{F(\mathfrak{a})}{F^{(c)}}, \tag{69}$$

where $\pi F^{(c)}$, the flux of the continuum, may be considered constant, as in the Schuster problem (cf. Sec. VII, Paper I). This constancy in $\pi F^{(c)}$ allows the substitution of equation (68) in equation (59), giving, for the emergent intensity of the continuum,

$$I_{+1}^{(c)}(\mathfrak{a}) = (\tfrac{1}{2}\sqrt{3})(1 - e^{-\tau_1}) F^{(c)}. \tag{70}$$

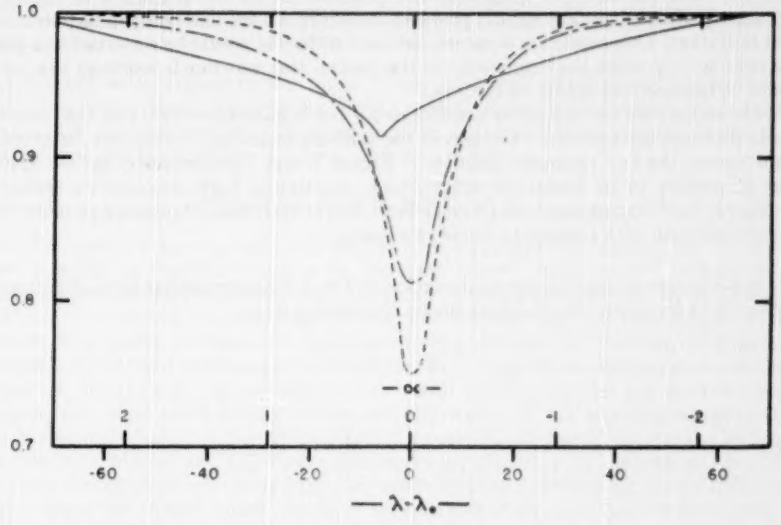

FIG. 2.—The emergent residual intensity $r_{+1}(\mathfrak{a})$ of an absorption line whose incident residual flux $R(\mathfrak{a})$ (*dashed curve*) is given by equation I (100). The *full-line curve* represents $r_{+1}(\mathfrak{a})$ for the atmosphere parameters $\tau_1 = 0.5$ and $d\Omega/d\tau = 1.0$. The *dot-and-dash curve* represents $r_{+1}(\mathfrak{a})$ as obtained for the Schuster problem in Paper I for the same parameters and incident profile. The conversion factor between the wave-length scale in angstrom units and the frequency variable $\mathfrak{a}$ is given by equation I (101).

Therefore, when equation (59) is divided by $\frac{1}{4}F^{(c)}$, the following expression for the emergent residual intensity is obtained:

$$(2\sqrt{3})(1 - e^{-\tau_1})\, r_{+1}(\mathfrak{a}) = \int_{-\infty}^{+\infty} R(\mathfrak{a}')\, \Delta'\left(\tau_1, \frac{d\Omega}{d\tau};\ \mathfrak{a} - \mathfrak{a}'\right) d\mathfrak{a}'. \tag{71}$$

Integration of equation (71) over $\mathfrak{a}$ shows that the equivalent width of a spectral line is unchanged by the electron scattering.

Equation (71) and $\Delta'(\tau_1, d\Omega/d\tau; x)$ as evaluated above have been used to determine the profile, after scattering by the nebula, of an absorption line with an incident profile given by equations I (100) and I (101). These profiles are shown in Figure 2. As in the Schuster problem, the shallower center and extended wings of the emergent residual

intensity are caused primarily by the thermal motion of the electrons, while the shift of the center of the line and the asymmetry are caused by the differential expansion within the nebula and are roughly proportional to the product of the parameters τ_1 and $d\Omega/d\tau$. As discussed in Section VII of Paper I, the parameter values used correspond to an increase in velocity of expansion over the nebula of 620 km/sec, which represents considerable differential expansion. Therefore, the shift of the center of the emergent profile in Figure 2 is rather large. The same changes would be produced in the profile of an emission line.

For purposes of comparison, the profile for emergent radiation calculated in the Schuster problem for the same parameters and the same profile of incident radiation is included in Figure 2. This profile is less broadened than the profile calculated for the planetary nebula, and its center is shifted less to the blue. The principal reason for these differences is that the emergent radiation in the Schuster problem consists not only of the radiation which has been scattered by the electron atmosphere but also of the radiation which has not been scattered, as shown by equation I (99). This unscattered radiation tends to reduce the effects arising from the noncoherent nature of the scattering by the electrons. For the planetary nebula problem, however, all the emergent radiation is scattered radiation. This condition of no unscattered radiation would be observed in a planetary nebula only when the luminosity of the central star was much less than that of the nebula in the spectral region of the line.

In the sense that the boundary conditions for the Schuster problem and the planetary nebula problem are opposite extremes of the possible boundary conditions for extended atmospheres, the two emergent profiles in Figure 2 may be considered as two limiting cases of profiles to be found for differentially expanding high-temperature stellar atmospheres. Such atmospheres as those of Wolf-Rayet stars should produce profiles which are intermediate with respect to these two cases.

It is a pleasure to express my appreciation to Dr. S. Chandrasekhar for suggesting this problem and for many helpful discussions concerning it.

THE THERMODYNAMIC STRUCTURE OF THE OUTER SOLAR ATMOSPHERE. II. COMMENT ON EMPIRICAL DETERMINATIONS OF b_n AND T_e*

RICHARD N. THOMAS
University of Utah
Received May 9, 1950

ABSTRACT

An apparent discrepancy between several empirical determinations of b_n and T_e is investigated. The former is resolved, while the latter is only partially so. It appears that scattered "photospheric" radiation contributes nonnegligibly to the chromospheric eclipse Balmer continuum and that there is consequently a slight polarization to be expected throughout the chromosphere.

In the preceding papers of the series "Superthermic Phenomena in Stellar Atmospheres," our remarks on the deviation from thermodynamic equilibrium in high-kinetic-temperature atmospheres have been made from a theoretical standpoint. That is, we have written, for the number of atoms in quantum level n,

$$N_n = \text{Constant} \cdot N_i N_e T_e^{-3/2} e^{X_n \varpi_n} b_n , \tag{1}$$

where the symbols are conventional, and b_n thus measures the ratio of the number of atoms actually in the state to that in the state under conditions of thermodynamic equilibrium at the same T_e, N_i, and N_e. Then we have calculated the b_n by applying the condition of a spectroscopically steady state. For the case in which atmospheric kinetic temperature exceeds the radiation temperature characteristic of the star, as illustrated by the solar hydrogen chromosphere, we obtain $b_n > 1$ and b_n decreasing monotonically toward the series limit.[1] In an independent set of calculations for the solar hydrogen chromosphere, Giovanelli obtains this same behavior for b_n.[2] In an earlier set of calculations,[3] essentially based on the assumption of a pure capture spectrum for the hydrogen chromosphere, Menzel and Cillié have obtained a set of $b_n < 1$. It has been shown,[1] however, that the assumptions underlying this treatment are not valid for the solar chromosphere; hence we should expect the later calculations of Thomas[1] and of Giovanelli[2] to be nearer the truth.

The Menzel-Cillié treatment was developed for an interpretation of the 1932 eclipse observations, however, for which an empirical determination[3] of the b_n values apparently gave $b_n < 1$. Hence one apparently had the wrong methods predicting the correct behavior for the b_n, and vice versa. (It should be noted, however, that the theoretical $b_n < 1$ showed an irreconcilable disagreement with the empirical b_n as regards an agreement over the whole set of observed lines.) Some time ago I convinced myself that this empirical set of $b_n < 1$ arose from a misleading interpretation of the data. The argument was marginal, and it seemed best to hold it in abeyance for the time being, at least until more detailed theoretical calculations could be carried out. However, a recent critical analysis[4] of the observed chromospheric Balmer decrement as a function of height pre-

* Publication supported by the University of Utah Research Fund.

[1] R. N. Thomas, *Ap. J.*, **108**, 142, 1948; **109**, 480, 1949 (hereafter cited as "Paper III").

[2] *Australian J. Sci. Res.*, **1**, 360, 1948.

[3] *Ap. J.*, **85**, 88, 1937.

[4] R. N. Thomas, *Ap. J.*, **111**, 165, 1950.

sented what I believe to be essentially conclusive empirical evidence that the b_n in the chromosphere exceed unity—in agreement with the theoretical expectation.

The above problem on an apparent empirical indication of $b_n < 1$ therefore becomes more pressing; for the same basic eclipse observations, analyzed from two different aspects, apparently give contradictory results. It therefore seems worth while to go through this earlier argument that casts doubt on the empirical determination leading to $b_n < 1$.

It should be remarked that one has a strong a priori reason to doubt these earlier, $b_n < 1$, results; for the same analysis presented a value for the kinetic temperature near 6000°–10,000°, while it seems generally established[4, 5] that the value is nearer 25,000°–35,000°. We shall then consider this rather low-value temperature determination also.

Finally, the following discussion is of some interest from the standpoint of polarization in the continuous radiation obtained from the chromosphere. If the following suggested interpretation is correct, we should expect polarization in the Balmer continuum.

I. THE EMPIRICAL ANOMALY

a) SUMMARY OF EMPIRICAL RESULTS REQUIRING $b_n > b_{n+k} > 1$

We briefly summarize the argument[4] which leads to the empirical $b_n > 1$. Consider two methods commonly used in obtaining the height gradient of hydrogen in the solar atmosphere. In the first method we compare the emission from a given Balmer line at two eclipse heights. With the exception of an error resulting from the neglect of self-absorption effects, the emission height gradient may be interpreted directly as the height gradient of the number of atoms in the upper level of the line. The neglected self-absorption effects clearly make this inferred value a lower limit to the true value. In the second method we attempt to eliminate self-absorption effects by observing the height at which the various Balmer lines just vanish. Presumably, the various lines reach the same intensity at their respective vanishing points, and the emission is so small that self-absorption effects drop out. By correcting for the difference in transition probability, the comparison of vanishing points for the two lines gives the ratio of the populations of the two levels at the two heights. The problem is to convert this population ratio into a height gradient for the population of either level. From equation (1) we see that, if the b_n values were the same for the two levels at a given height, the figure just obtained would, when corrected for the Boltzmann factor $\exp(X_n)$, give the height gradient of either level. If, however, $b_n > b_{n+k}$, then the emission at a given height for Balmer line H_n would be greater than it would in the case of $b_n = b_{n+k}$; the line H_n would persist to a greater height relative to H_{n+k}; and we would underestimate the height gradient if we used the observational material with no b_n correction. If $b_n < b_{n+k}$, the reverse situation would hold. We can then compare the density gradients obtained by the first and second methods, in the hope of obtaining the behavior of b_n. We note, of course, that a result showing the density gradient from the first method to be less than that from the second would be somewhat inconclusive because of the neglected self-absorption effect. Fortunately, however, we find the first-method gradient to exceed the second. The situation is not peculiar to data from one eclipse, nor is the difference so small as to be masked by observational error. (The difference is almost a factor of 2.) Hence it would appear that, from this comparison of two methods of estimating the hydrogen density gradient, we have a conclusive demonstration of the direction of deviation of the chromosphere from thermodynamic equilibrium; that is, $b_n > b_{n+k} > 1$.

A similar analysis of the change with height of the Balmer decrement demonstrates the importance, and permits the quantitative measure, of self-absorption in the Balmer lines. Combining the several results, we obtain quantitative values for the kinetic temperature and the height gradient of kinetic temperature and hydrogen density. The

[5] R. O. Redman, *M.N.*, **102**, 140, 1942.

temperature comes close to the 30,000°–35,000° value measured by Redman[5] from line profiles, and the temperature gradient is positive. Thus, since the theoretical predictions of the behavior of the b_n, based on these high T_e values, agree with the empirical behavior, it would seem that we have a self-consistent physical picture of the chromosphere. Consider, however, the earlier[3] empirical determination of T_e and b_n.

b) TEMPERATURE DETERMINATION

From the formulae of Paper III we may write the sum of free-bound and free-free emission in the Balmer continuum in all directions as follows:

$$E_\nu d\nu = E_{\kappa 2} d\nu \frac{1}{2 b_e} \left(\frac{2\pi r}{b_e}\right)^{1/2} \left[1 - \frac{Na}{2.1!} + \frac{(Na)^2}{3.2!} \cdots\right], \tag{2}$$

$$E_{\kappa 2} = N_e^2 T_e^{-3/2} K h e^{-h\nu/kT_e} \left[\sum_2^\infty \frac{e^{X_n}}{n^3} + \frac{kT_e}{2hR}\right], \tag{3}$$

$$X_n = \frac{R}{n^2} \frac{h}{kT_e},$$

where K is a constant, b_e the logarithmic density gradient, r the solar radius, and R the Rydberg constant. The other symbols are conventional. Equation (2) represents the total emission along the line of sight above a given height, with the integration carried out under the assumption of an isothermal atmosphere. The bracket in equation (2) represents the self-absorption effect, which is small for the Balmer continuum. Equation (3) represents the emission per cubic centimeter in all directions. In Menzel and Cillié's calculations[3] the absorption effects have been ignored, and the emission per unit frequency at λ 3640 is compared with that at λ 3500. From equations (2) and (3) it is apparent that the emission ratio depends only upon T_e. Then, if we interpret the observed chromospheric radiation in the Balmer continuum as bound-free and free-free chromospheric emission, we have a measure of T_e. Making this interpretation and using the 1932 eclipse data,[6] Menzel and Cillié obtain[3] a value of some 5000° for T_e at an eclipse height of 670 km. (Their original results give 12,000°, but a factor ln_e 10 was omitted in the original computations.) It is clear that inclusion of the differential absorption term would, though small in effect, further reduce the T_e value and thus increase the discrepancy between this 5000° value and the much higher values that our other analyses indicate exist at this level.

c) EMPIRICAL b_n VALUES

Combining the expressions for line emission and continuous emission (per unit frequency interval), we may write from the results of Paper III (or the Menzel-Cillié analysis):

$$b_n = \frac{E_{n2}}{E_{\kappa 2}} \frac{1}{2R} \frac{e^{X_n}}{P_n} \frac{e^{-h\nu/kT_e}}{g_{n2}} \left[1 + \left(\sum_{n'>2} P_{n'} + \frac{kT_e}{2hR}\right) P_2^{-1}\right] \frac{\text{Abs}(\kappa)}{\text{Abs}(n)}; \tag{4}$$

$$P_n = \frac{e^{X_n}}{n^3}; \qquad g_{n2} = \text{Gaunt factor} \sim 1,$$

where the last terms refer to the absorption terms, i.e., the factor by which the emission is diminished by the absorption effects. Using earlier data,[6] Menzel and Cillié obtain values for b_n from the observed values of E_{n2} and $E_{\kappa 2}$ and assumed values for T_e. We reproduce their results for $T_e = 5000°$ and add a set of results for $T_e = 35{,}000°$, in Table 1, both sets of calculations made by ignoring the absorption term in equation (4). The values of

[6] *Harvard Obs. Circ.*, No. 410, 1935.

b_n past $n = 25$ or so oscillate to some degree and are therefore not too reliable. For the 5000° T_e—the value that must be used if a self-consistent application of the method of analysis is to be made—we have $b_n < 1$. If we introduce the self-absorption into the determination, the b_n values rise. We note, however, that there is no reason to expect self-absorption to be of importance for these later series members if the chromospheric region has indeed this low value of T_e. Furthermore, the empirical demonstration of the presence of self-absorption, given by the author,[4] loses its rigor if we admit $b_n < 1$.

Thus the contradiction in the two sets of analysis of the eclipse data is clearly stated in the results of sections *b* and *c* and in the summary of section *a*. Unless some error is found in one of the two methods of interpretation, we have a very serious contradiction in the empirical results from the eclipse data. It is difficult to see how the conclusion drawn in section *a* from the two kinds of eclipse emission gradient can be voided. If it stands, we must have $b_n > b_{n+4}$; and then self-absorption must be important if the Balmer decrement is to be explained. And, granting this last, the empirical b_n in Table 1, even for $T_e = 5000°$, rise above the value 1. Then the empirical $T_e = 5000°$ remains as the stumbling block. Granted that the author's T_e determination[4] is highly uncertain, one still cannot explain away Redman's results[6] from line profiles. Let us then consider the suggestion already mentioned of a possible error in the interpretation of Menzel and Cillié's results.[3]

TABLE 1

EMPIRICAL b_n VALUES

	n				
	10	15	20	25	30
b_n $T_e = 5000°$	0.32	0.66	0.85	1.00	~1.1
b_n $T_e = 35{,}000°$	0.73	1.23	1.51	1.74	1.90

II. A POSSIBLE RESOLUTION OF THE EMPIRICAL ANOMALY

It is apparent that, once one makes the interpretation of the source of the chromospheric continuum to be the chromospheric free-bound and free-free emission, the results of sections *b* and *c* above follow inescapably. The question arises, How justified is this interpretation? The other source for the chromospheric continuum is scattered light from the "photosphere." (We have earlier shown the chromospheric continuous emission to be negligible compared with the "normal" solar field, save in the Lyman continuum. We now compare, however, the direct chromospheric emission with the scattered photospheric radiation.) Dividing equation (3) by 4π, we have the intensity emitted per cubic centimeter per unit solid angle. Taking the general solar "photospheric" field to be a black-body region at temperature T_r, we have, for the intensity of scattered light per cubic centimeter per unit solid angle,

$$I_\nu d\nu = \frac{2h\nu^3}{c^2}\left(e^{h\nu/kT_r} - 1\right)^{-1} W. \tag{5}$$

Here W contains two factors, the electron scattering term, W_1, and the geometrical "dilution" factor, W_2. The effect of this last is to restrict the angular integration over W_1 to the inner hemisphere. We have, therefore,

$$W = \frac{1}{2}\left(\frac{e^2}{mc^2}\right)^2 N_e \int (1 + \cos^2\theta)\, d\omega = \left(\frac{e^2}{mc^2}\right)^2 \frac{4\pi}{3} N_e, \tag{6}$$

where θ is the scattering angle and the integration is over one hemisphere. From this we obtain, for the ratio of chromospheric emission (eq. [2] corrected by $1/4\pi$ to reduce to unit solid angle) to chromospheric scattering of "photospheric" radiation (eqs. [5] and [6]),

$$\frac{I_\nu)_E}{I_\nu)_S} = \frac{3KN_e}{32\pi^2}\left(\frac{mc^3}{e^2}\right)^2 \frac{e^{(T_r^{-1}-T_e^{-1})h\nu/k}}{\nu^3 T_e^{3/2}}\left[\sum_2^\infty P_n + \frac{kT_e}{2hR}\right]. \tag{7}$$

Hence for $T_e = 35{,}000°$, $T_r = 6000°$, $N_e = 2\cdot 10^{11}$; and at λ 3640 we obtain

$$\frac{I_\nu)_E}{I_\nu)_S} = 2.4\,. \tag{8}$$

We note, however, that this ratio 2.4 holds for 1 cc at the eclipse height in question, whereas the observed radiation comes from an integration along the line of sight and perpendicular to it. Since the emission varies as N_e^2 and the scattering as N_e, we must multiply equation (8) by $2^{-3/2}$ to take account of the integration. This factor is an upper estimate; for the temperature increases upward, further reducing the emission relative to the scattering. Thus we obtain

$$\frac{I_\nu)_E}{I_\nu)_S} \simeq 0.8\,.$$

Hence the scattered radiation should be about half the observed emission at the Balmer limit.

This conclusion has two consequences. First, the denominator in equation (4) involves E_{n2}; but in the numerical work the observed emission was used. According to equation (9), only about half of it should have been used; therefore, the b_n in Table 1—for both sets of T_e values—should be about doubled. Such a doubling brings the $b_n > 1$, for $n > 15$ at least. We note, however, that the b_n then appear to diverge from 1 for the higher n values—a result certainly unacceptable physically. We then have two choices: either (1) we must further reduce T_e, if we wish to retain $b_n < b_{n+k}$, or (2), we recognize $b_n > b_{n+k}$ and introduce the self-absorption correction, which raises the earlier b_n over the later ones. Procedure 1 seems hardly realistic, for *no* observations support lower values of T_e. We then have alternative 2, and the b_n anomaly is thus resolved. We note that a consideration of the amount of self-absorption necessary for procedure 2 forms the essential gist of the author's[4] considerations on self-absorption. Only a minimum estimate results, however, as there we essentially neglected the b_n in the self-absorption discussion. (The emission in the continuum, of course, plays no role in these self-absorption arguments.)

The second consequence has to do with the empirical T_e determination. Half the radiation corresponds to scattered radiation, which we have taken to correspond to $T_r = 6000°$. Hence, the *direction* of the discrepancy is understood. Numerically, however, the empirical anomaly still remains; for, even if all the observed radiation at the Balmer limit came from scattered radiation, equation (5) implies that a T_r of some 4000° would be required. It is well known that the solar emission at λ 3640 drops below the 6000° black-body-curve. If we adopt the 4000° value at this height, the scattered radiation forms a smaller portion of the observed radiation from the chromosphere. It would seem that only a more careful study of the decrement in the continuum as a function of height could resolve the anomaly. As already indicated, we should expect the scattered radiation to increase in relative importance with height, and the effect should be detectable observationally. Unfortunately, although they are the most complete thus far, the Menzel-Cillié results contain data at only one height for this continuum decrement. At the next eclipse, therefore, particular attention should be paid the emission in the Balmer continuum as a function of height in the chromosphere.

In regard to such eclipse observations, a further criterion of the relative importance of scattered and emitted light should be provided by polarization effects; for, if our suggestion is correct, part of the Balmer continuum—being scattered light—should be polarized. Taking Baumbach's result[7] that some 20 per cent of the scattered light at the limb is polarized, we should expect, from the preceding remarks, about 10 per cent polarization at the Balmer limit and at the low eclipse heights. An attempt to measure such polarization should then provide another test of the present interpretation of the source of the eclipse Balmer continuum. Both the relative amount of scattered light and the percentage of polarization increase with height; hence the polarization effect should become measurably pronounced with height and provide additional information for the considerations of the preceding paragraph.

III. SUMMARY

In summary, we conclude that the empirical $b_n < 1$ are erroneous, resulting from an interpretation of the Balmer continuum as coming wholly from free-bound and free-free chromospheric emission and neglecting scattered "photospheric" light. The present calculations have assumed a "photospheric" emission corresponding to a 6000° Planck function; and, while this is probably an overestimate in the Balmer continuum, the scattering term would seem to be nonnegligible. While the correction introduced by the inclusion of the scattering term acts in the correct direction to lessen the discrepancy in the empirical T_e determined from measures in the continuum, the quantitative correction is not sufficient to remove it. We obtain, however, two observational approaches to the problem, which should be attempted at the next eclipse. The ratio of scattered to emitted radiation increases with height in the chromosphere; hence the emission at several wave lengths in the Balmer continuum should be measured as a function of chromospheric height. Second, the presence of scattering introduces a polarization term, which also increases with chromospheric height.

I am deeply indebted to Dr. Walter O. Roberts and Dr. John Evans, of the High Altitude Observatory, for extended discussions over the present problem. The early stages of the investigation were carried out in a number of discussions with Dr. Donald Menzel, of the Harvard Observatory. While he cannot be held responsible for the final results presented here, the contribution by him is obvious.

[7] *A.N.*, **267**, 273, 1938.

SUPERTHERMIC PHENOMENA IN STELLAR ATMOSPHERES. VI. COMMENT ON REGIONS OF EMISSION FLUCTUATION IN THE SOLAR ATMOSPHERE*

RICHARD N. THOMAS
University of Utah
Received June 2, 1950

ABSTRACT

Regions of fluctuating emission in the solar atmosphere must involve density fluctuations, independently of whether there is a simultaneous change in excitation. Such density fluctuation must be discussed in terms of a nonstatic model. One such model may be a supersonic jet, and a quantitative description of such a jet is provided by an extension, to the case including a gravitational field, of an early theory by Prandtl. The theory is applied to the Menzel-Cillié "hot-spot" region observed at the 1932 eclipse.

I. THE GENERAL PROBLEM

It seems well established that the spectroscopic state of the solar chromosphere and corona deviates considerably from any condition of thermodynamic equilibrium, and certainly from any such state inferred from the classical boundary temperature of the sun. In particular, at an eclipse height of some 1000 km, the chromospheric hydrogen is 99.5 per cent ionized.[1] The ionization and spectroscopic state of the remaining elements can be only estimated until some detailed investigation occurs. The implications of this uncertainty for the interpretation of eclipse data on the emission gradients of the various chromospheric and coronal lines are obvious. We note also, however, that the same kind of uncertainty enters into an interpretation of other regions of altered emission. An example lies in the old problem of whether the apparent chromospheric ejections are actually mass motion or whether they simply represent the spreading of regions of increased excitation. Here a decision in favor of actual mass motion appears to have been generally reached in at least the majority of cases. The chromospheric spicules, introduced and discussed by Roberts,[2] form another case in which a decision must be made between actual mass motion and the motion of an excitation "front." Another example of interest comes from eclipse observations of the so-called "hot-spot" regions, first discussed by Menzel and Cillié[3] in connection with the 1932 eclipse data (and since observed and discussed for the 1936 eclipse also).[4] Here there were no data on any kinematic properties, the essential distinguishing feature of the region being the emission characteristics. All spectral lines strengthened. Menzel and Cillié lay greatest stress on the increased helium emission and the pronounced strengthening of the coronal spectrum above the hot spot. These features led them to attribute the phenomenon to a temperature rise—hence the label "hot-spot."

It is of some interest to examine critically the notion that a rise in emission from some

* The work reported was carried out with the support of Harvard University Contract W19-122ac-17 with the Air Materiel Command, and in collaboration with personnel of that contract at the High Altitude Observatory in Boulder, Colorado.

[1] R. N. Thomas, *Ap. J.*, **108**, 142, 1948.

[2] *Ap. J.*, **101**, 136, 1945.

[3] *Harvard Obs. Circ.*, No. 410, 1935.

[4] Menzel, private communication; Shibata, Araki, Kakinuma, Kawaguchi, *Memoirs of Astrophysics* (Japan) **1**, 1, 1948.

particular region indicates uniquely a rise in the temperature of the region. (Because of the absence of thermodynamic equilibrium, we mean, of course, the kinetic temperature when we mention temperature.) As mentioned, a set of detailed calculations for the departures from thermodynamic equilibrium exists only for hydrogen; hence a quantitative discussion must be based on the hydrogen data. Fortunately, the hydrogen emission mimics that from the other elements in the various examples cited above. Furthermore, since the solar atmosphere is effectively all hydrogen, the procedure will certainly indicate the essential thermodynamic features of whatever phenomenon is studied. Then we note that we can write the expression for the line emission, per unit volume, from the chromosphere as

$$E_{nn'} = \text{Constant} \cdot b_n N_e^2 \frac{e^{X_n}}{T_e^{3/2}} A_{nn'} \varpi_n , \tag{1}$$

where the symbols have their conventional meaning. We note that the expression in the above form implies the high degree of ionization earlier mentioned; so that we may replace the number of ions by the number of electrons in the more usual form of the Boltzmann-Saha relation and so obtain equation (1). Thus we see that a rise in T_e alone causes a decrease, rather than an increase, in the hydrogen emission, unless b_n increases faster than $T_e^{3/2}$. The rate of change of b_n with temperature has not been sufficiently accurately calculated, with the complete inclusion of the chromospheric radiation field, to make any absolutely reliable statement of results. However, several sets of approximate calculations[5, 6] indicate that the change is not so rapid as $T_e^{3/2}$. It would seem, then, that a density, rather than a temperature, increase—or at least a density increase in addition to a temperature increase—must be invoked to account for the hydrogen observations.

We must, of course, immediately make two qualifications to this statement. First, an observed rise in the hydrogen emission does not preclude a temperature rise, it simply requires a correspondingly greater rise in density. Second, the hydrogen situation may not be an exact duplicate for the helium situation (and that of other high-excitation ions), where the ionization may be far from complete. In these latter cases a temperature rise may cause a greater rise in the ion density; hence we now must use N_iN_e rather than N_eN_e in equation (1). The essential point, however, comes with our earlier observation—a density rise must occur to match the hydrogen observations. Hence, whatever our model for the region of increased emission, it would seem that one primary phenomenon must be the density fluctuation.

In an earlier paper[7] we tentatively explored one model that gives such a density variation—a supersonic jet. The discussion was pictorial. It would seem useful to present some kind of quantitative jet model that might be compared with observations. In the following we consider such a model, which we obtain by extending some early work by Prandtl to include the case of a gravitational field. We neglect electromagnetic phenomena not because of a belief in their unimportance but because of a wish to investigate the extent to which we may interpret the observations on the jet picture alone. As a tentative application of the results, we briefly consider the hot-spot phenomenon in the last section. This application is rather natural when we note that data exist on the emission as a function of height. These data lend more interest to the application when we note that the hot-spot emission falls off more rapidly with height than that in the surrounding atmosphere does—and, indeed, actually falls below the atmospheric value. If we interpret the phenomenon as being wholly a density fluctuation, the analogy with the supersonic jet stands out. We return to the point in the last section.

[5] Giovanelli, *Australian J. Sci. Res.*, **1**, 289, 1948.

[6] R. N. Thomas, *Ap. J.*, **109**, 480, 1949.

[7] R. N. Thomas, *ibid.*, **108**, 130, 1948.

II. AN APPROXIMATE MODEL FOR A SUPERSONIC JET IN A GRAVITATIONAL FIELD

The modern theories[8] of supersonic jets have demonstrated, in agreement with observation, that eventually a shock wave forms somewhere in the jet; hence the original shock-free, completely periodic model of a jet constructed by Prandtl[9] does not actually occur in practice. However, for jets in which the original pressure excess over the atmospheric value is small, we may have very small-amplitude shock waves—essentially sound waves—and the Prandtl description is a reasonably good one. In several of the astronomical phenomena the emission—hence the density—does not fluctuate by more than a factor of 2 or so times the atmospheric value. Hence there is a reasonable hope that the Prandtl approximation may nearly describe the physical situation. An application of the complete modern theory of jets would involve the numerical solution of the differential equations governing the flow. Such a procedure in the astronomical case would require a set of solutions, covering a variety of initial conditions—labor hardly warranted by the usual astronomical data.

A more serious difficulty arises when we recall that Prandtl's solution applies to a jet discharging into a uniform atmosphere. Here in the astronomical case we have a jet discharging into an atmosphere whose density decreases outward along the jet axis. The problems attending such a jet have not, to the author's knowledge, been solved, either to the extent of the Prandtl approximation or in the general case. In the hot-spot case, for example, the perturbation is not trivial; for we have observations covering a range of 1600 km in height. From previous work[10] on the steady state of the chromosphere, the density variation over this range is a factor of 3.3. Thus the change in the picture caused by the density gradient is certainly not to be ignored. We proceed to consider the problem.

We may review briefly Prandtl's picture of the phenomenon. First, the periodic nature of the jet is a fairly obvious conclusion; for the initial expansion angle of the moving column of gas (i.e., the angular aspect of the expansion cone) is fixed uniquely by the ratio of initial pressure in the jet to that in the atmosphere. If the jet continues to diverge, it will clearly overexpand. The velocity profile across the jet is not uniform, however; therefore, when the outer boundary of the jet has been bent back parallel to the jet axis, there is an underpressure along the axis. Hence the jet narrows down again, and the flow is recompressed. Prandtl attempts to describe the flow by the velocity potential (cylindrical co-ordinates r and z), thus:

$$\phi = wz - A \sin \beta z f(r), \tag{2}$$

where w is the mean flow velocity. Whence, if u and v are the velocity components corresponding to z and r,

$$u = w - A\beta \cos \beta z f(r), \tag{3}$$

$$v = -A \sin \beta z f'(r). \tag{4}$$

The function $f(r)$ is determined by substituting equations (2) and (3) in the combined dynamical equation and equation of continuity, with boundary conditions that $f(0)$ shall be unity, $f'(0) = 0$, and $f(d/2) = 0$ if d is the jet orifice diameter. The function f is readily shown to be the Bessel function, $J_0(\alpha r)$, for the (cylindrical symmetry) three-dimensional case, where

$$\alpha = \beta \sqrt{\left(\frac{w}{a}\right)^2 - 1}, \tag{5}$$

[8] Courant and Friedrichs, *Supersonic Flow and Shock-Waves* (New York: Interscience Publishers, 1948).

[9] *Phys. Zs.*, **5**, 599, 1904.

[10] R. N. Thomas, *Ap. J.*, **111**, 165, 1950.

with a the sound velocity. For the two-dimensional case f is cos αr. For our purposes, however, we are interested only in the flow on the axis, and it suffices to know $f(0) = 1$. Then we have the energy equation along the axis:

$$\frac{u^2}{2} + \frac{\gamma}{\gamma - 1}\frac{p}{\rho} = \text{Constant}. \tag{6}$$

If we adopt the subscript o to denote conditions in which the velocity is w and adopt the adiabatic relation, we have, for the streamline along the axis,

$$\frac{w^2}{a_o^2} - \frac{u^2}{a_o^2} = \frac{2}{\gamma - 1}\left[\left(\frac{\rho}{\rho_o}\right)^{\gamma - 1} - 1\right], \tag{7}$$

where γ is the specific heat ratio. Then, using equation (2), we obtain (using $f[0] = 1$)

$$\frac{2}{\gamma - 1}\left[\left(\frac{\rho}{\rho_o}\right)^{\gamma - 1} - 1\right] = \left[\frac{2wA\beta}{a_o^2}\right]\cos\beta z - \left[\frac{\beta A}{a_o}\right]^2 \cos^2 \beta z. \tag{8}$$

Now in the Prandtl solution the ratio of initial to atmospheric pressure; the Mach number, M; jet diameter, d; and location of jet orifice were assumed known. Hence, since

$$\alpha = \frac{2x_1}{d}, \qquad \text{3-dimensional flow } (x_1 \text{ first root of } J_0),$$

$$\alpha = \frac{\pi}{d}, \qquad \text{2-dimensional flow},$$

the axial wave length, $2\pi/\beta$, follows from equation (4), and the density ratio in equation (7) may be predicted. In the present case, however, the ratio of axial density to atmospheric density is assumed known, and the relation between the eclipse height and the location of the jet mouth is unknown. If it could be assumed that the temperature in the jet at the point $\beta z = \pi/2$ were the same as that in the atmosphere, then from equations (2) and (3) we see that the atmospheric density would be ρ_o. Then the ρ/ρ_o in equation (7) might be used as atmospheric density, and the equation could be solved directly in terms of the observations. Since the variation of a, the velocity of sound, is neglected in the solution, the assumption is perhaps not unreasonable for cases in which the initial overpressure is not large.

Consider, now, the modification of the problem introduced by the presence of the gravitational field. The energy equation (5) becomes, along the axis of the jet,

$$\frac{u^2}{2} + \frac{\gamma}{\gamma - 1}\frac{p}{\rho} + g z = \text{Constant}; \tag{9}$$

hence equation (7) becomes (subscript o refers now to conditions in the jet at a particular height)

$$\frac{u_o^2}{a_o^2} - \frac{u^2}{a_o^2} - \frac{2g(z - z_o)}{a_o^2} = \frac{2}{\gamma - 1}\left[\left(\frac{\rho}{\rho_o}\right)^{\gamma - 1} - 1\right]. \tag{10}$$

We now recognize two main effects of a gravitational field. First, a moving stream of gas, apart from its interaction with the atmosphere, must be decelerated, owing to the exchange of kinetic for potential energy. Second, the static atmosphere must exhibit a density gradient. The existence of the density gradient causes a further modification of the velocity of the moving stream of gas if the temperature gradient is not large enough positively to balance exactly the negative density gradient because of expansion effects. We

make these obvious remarks in an attempt to obtain an approximate solution that covers the essential physical details of the problem. Consider, first, the density variation along the axis of the jet, or the right side of equation (10).

Because of the density gradient in the atmosphere, we should not expect to refer the variation of the thermodynamic parameters to some initial condition; for we should then expect a systematic, as well as an oscillatory, variation with z. Rather, it would seem that a scheme which would at least take out first-order systematic effects would be to refer the density within the jet to the atmospheric density at the same height. Thus we write the right-hand side of equation (10) as

$$\frac{2}{\gamma-1}\left[\left(\frac{\rho}{\rho_o}\right)^{\gamma-1}-1\right]=\frac{2}{\gamma-1}\left[\left(\frac{\rho}{\rho_a}\right)^{\gamma-1}\frac{T_a}{T_\infty}-\frac{T_o}{T_\infty}\right]\frac{T_\infty}{T_o}, \tag{11}$$

where we replace $(\rho_i/\rho_j)^{\gamma-1}$ by $a_i^2/a_j^2 = T_i/T_j$, and by the additional subscript a we indicate conditions in the atmosphere. The subscript o refers to some fixed height. We obtain T_a/T_∞ from the atmospheric temperature gradient determined in another article.[10] Table 1 contains ρ/ρ_a.

Consider, now, the expressions for the velocity components that replace equations (2) and (3). We have already mentioned the two expected variations in the velocity over the case without gravity—the gravitational deceleration and the expansion acceleration. It can be shown that, for the case of high Mach number and small initial pressure amplitude, the first term in equation (2), representing the undisturbed flow, contains the expansion effect as a second-order term (i.e., the expansion term having $1/M$ as a coefficient). The first-order term is the initial velocity before expansion. The second term in equation (2), the perturbation term, contains, however, the expansion term as the first-order term. Thus it would seem reasonable, for our approximate treatment here, to set

$$w^2 = w_i^2 - 2gz = w_o^2 - 2g(z - z_o), \tag{12}$$

and

$$u = w - A\beta\cos\beta z f(r, z), \tag{13}$$

$$v = -A\sin\beta z f_r'(r, z), \tag{14}$$

where the subscript i refers to conditions at $z = 0$. That is, we throw all the effect of atmospheric density gradient into the periodic term and treat the undisturbed flow velocity as though it were modified by the gravitational term only. We note thus that above the height $w_i^2/2g = z_c$ the solution contains only the periodic terms, and so no longer corresponds to a net motion of matter into the atmosphere. The data on hand refer to a portion of the atmosphere well below z_c; hence this result is not of interest here other than perhaps indicating the limitations imposed by our assumptions. It is clear, however, that a jet extending only to a limited height must be the source of some disturbance even at its maximum height; therefore, this last consequence of our approximation is not completely absurd from a physical standpoint. The other approximations, in the solution for $f(r, z)$, will cause the solution to break down before this height z_c, however.

Then, we obtain $f(r, z)$ by substituting equations (13) and (14) in the general hydrodynamical equations. We have for these last, under the assumption of steady-state flow and denoting the total velocity by q,

$$q\cdot\nabla q = -\frac{\nabla p}{\rho} - g_{iz}$$
$$\nabla\cdot(\rho q) = 0, \tag{15}$$

whence

$$\left(\frac{u^2}{a^2}-1\right)\frac{\partial u}{\partial z}+\frac{uv}{a^2}\left(\frac{\partial u}{\partial r}+\frac{\partial v}{\partial z}\right)+\left(\frac{v^2}{a^2}-1\right)\frac{\partial v}{\partial r}+\frac{ug}{a^2}-\frac{v}{r}=0. \tag{16}$$

If we make the same approximations as in the Prandtl development, we treat the perturbations as second-order terms and neglect their products. Thus we have, as the defining equation for the problem,

$$\left(\frac{u^2}{a^2}-1\right)\frac{\partial u}{\partial z}+\frac{u g}{a^2}-\frac{\partial v}{\partial r}-\frac{v}{r}=0\,. \tag{17}$$

Using expressions (13) and (14), we obtain, after some algebra,

$$\left[f''_{rr}+\frac{f'_r}{r}+\mathfrak{a}^2 f\right]A\,\sin\beta z-\left[\frac{\mathfrak{a}^2}{\beta}\,f'_z-\frac{g\beta}{a^2}\,f\right]A\,\cos\beta z+\frac{g}{w}=0\,, \tag{18}$$

where

$$\mathfrak{a}^2=\beta^2\left(\frac{w^2}{a^2}-1\right). \tag{19}$$

The term g/w is of the same order of magnitude as those already ignored; so, dropping it, treating the w in equation (19) as constant, and writing

$$f=R(r)\,Z(z)\,, \tag{20}$$

we readily obtain

$$R''+\frac{R'}{r}+(\mathfrak{a}^2-\gamma_1^2)R=0\,, \tag{21}$$

$$Z'-\left(\frac{\beta^2 g}{\mathfrak{a}^2 a^2}+\frac{\beta\gamma_1^2}{\mathfrak{a}^2}\tan\beta z\right)Z=0\,, \tag{22}$$

where we have introduced γ_1^2 as the constant accompanying the separation of variables in the usual manner. Thus we have for solutions:

$$R=J_0(\eta r)\,, \tag{23}$$

$$Z=\exp\left(\frac{\beta^2 g}{\mathfrak{a}^2 a^2}\,z\right)\sec^{\gamma_1^2/\mathfrak{a}^2}\beta z\,, \tag{24}$$

where

$$\eta^2=\mathfrak{a}^2-\gamma_1^2 \tag{25}$$

and J_0 is the Bessel function of zero order. We see that γ_1^2 must be positive, for the maximum width, d, of the jet is fixed by

$$J_0\left(\eta\,\frac{d}{2}\right)=0\quad\rightarrow\quad d=\frac{2x_1}{\sqrt{\mathfrak{a}^2-\gamma_1^2}}, \tag{26}$$

where x_1 is the first root, 2.405, of J_0. Then we note that $\gamma_1=0$ corresponds to the case of no atmospheric density gradient. Since the jet must be wider in the presence of the density gradient, γ_1^2 must be positive.

Thus, for the flow along the axis, we have, from equations (13) and (24),

$$\frac{w^2}{a_\infty^2}-\frac{u^2}{a_\infty^2}=\frac{2A\beta}{a_\infty^2}\,w\exp\left(\frac{\beta^2 g}{\mathfrak{a}^2 a^2}\,z\right)\cos^{(1-\gamma_1^2/\mathfrak{a}^2)}\beta z -\left(\frac{A\beta}{a_\infty}\right)^2\exp\left(\frac{2\beta^2 g}{\mathfrak{a}^2 a^2}\,z\right)\cos^{2(1-\gamma_1^2/\mathfrak{a}^2)}\beta z\,. \tag{27}$$

Hence from equations (10), (11), (12), and (27) we have, for the equation to be compared with observations, if we choose z_∞ as the height at which $\beta z=\pi/2$,

$$\left(\frac{\rho}{\rho_\infty}\right)^{\gamma-1}\frac{T_\infty}{T_{\infty\infty}}=h+k\,c_1(z)\cos^6\beta z-l\,c_2(z)\cos^{2\mathfrak{p}}\beta z\,, \tag{28}$$

where

$$h = \frac{T_o}{T_\infty}, \qquad \theta = 1 - \frac{\gamma_1^2}{a^2},$$

$$k = \frac{\gamma - 1}{2} \frac{T_o}{T_\infty} \frac{2A\beta}{a_o} \frac{w_o}{a_o} \exp\left(\frac{\beta^2 g}{a^2 a_o^2} z_o\right),$$

$$l = \frac{\gamma - 1}{2} \left(\frac{A\beta}{a_o}\right)^2 \exp\left(\frac{2\beta^2 g}{a^2 a_o^2} z_o\right) \frac{T_o}{T_\infty},$$

$$\epsilon_1(z) = \frac{w(z)}{w_o} \exp\left[\frac{\beta^2 g}{a^2 a_o^2}(z - z_o)\right],$$

$$\epsilon_2(z) = \exp\left[\frac{2\beta^2 g}{a^2 a_o^2}(z - z_o)\right],$$

where z_o is some arbitrary reference height. We note, of course, that the zero point of z is unknown in the astronomical case. Hence, we write

$$z = \Delta + H, \tag{29}$$

where H is the height used in the astronomical measures, and Δ is thus to be determined. Thus the solution involves six parameters—h, k, l, θ, β, Δ—to be determined from the observations. We therefore require density measures at a minimum of six points to obtain the parameters of the theory—and at several more points if we are to have much of a test of the validity of the jet interpretation. Let us consider briefly an application of the results.

III. THE HOT SPOT

We have already mentioned that the reason for particular interest in the hot spot stems from the existence of numerical (eclipse) data on the height variation of the emission (such data do not yet exist, e.g., for the spicules). This variation shows that the emission in the hot spot first exceeds and then falls below the emission in the surrounding atmosphere as we proceed along the "axis" of the hot spot. We would expect such behavior from a supersonic jet, according to the theory just developed. It is, however, somewhat misleading to speak of the "surrounding atmosphere," for our view of the phenomenon is two-dimensional. Thus, if the hot spot is not on the solar limb, any given region of the hot spot actually corresponds to a greater height than the apparent surrounding atmosphere on the limb. We see, however, that this situation will actually cause us to underestimate the emission fluctuation if we refer it to the apparent surrounding atmosphere on the limb. Hence the precise numerical results of the following analysis cannot be taken to have much significance; but the rough physical picture is probably correct. If the hot spot were on the limb, the numerical results would also be significant.

Table 1 contains the observed data. The density ratio follows from the assumption that the emission fluctuation results from a density fluctuation alone. From what has been said earlier on this point, we see that the tabular values again provide only lower limits to the fluctuation. A further difficulty arises from an inspection of the data. There exist observations at just three points, while we have seen the theory to require six. We can, however, ask after the plausibility of the present interpretation by the following argument.

Consider the value of h. If we had atmospheric temperature equal to axial jet temperature at the height z_o, we could obtain a solution; for such a condition would set

$h = 1$. Then, by interpolation in the observed set of data, we readily find that the left side of equation (26) has the value unity at $h = 1785$ km. Hence

$$\beta(\Delta + 1785) = \frac{\pi}{2}. \tag{30}$$

Thus we have a determinate problem. Solving the equations by successive approximation, we obtain the results given in Table 2. The free parameter in the set of solutions is d, the width of the jet. From the sample spectrum given by Menzel and Cillié[1] it would

TABLE 1

CHANGE OF EMISSION WITH HEIGHT

	Height (Km)		
	900	1730	2570
$\log \frac{E \text{ (region } b)}{E \text{ (normal)}}$	0.28	0.02	−0.46
$\frac{\rho}{\rho_0}$	1.91	1.05	+0.35

TABLE 2

RESULTS OF THE SOLUTION OF EQUATION (26) WITH $h = 1$; $\gamma = \frac{5}{3}$

γ_1^2/a^2	0	0.025
β^{-1} (degrees)	22	60
λ_0 (km)	7920	21,600
d (km)	3030	8700
Δ (km)	195	3615
w_0/a_0	2.24	2.17
w_0 (km/sec)	83	91
w_h/a_0	2.43	2.67
$A\beta/a_0$	0.38	0.65

appear that d is some 10^4 km. Thus, for this case $h = 1$, we find very small values of γ_1/a to be necessary in fitting the observations. We find initial velocities of 80–100 km/sec required for the jet model. These velocities are reasonable, particularly in view of the velocities of this same order reported recently[11] for the larger spicules. Consider, however, the value of Δ—the distance below the eclipse zero point where the "jet" originates on this model. We note that, in order to obtain the larger values for d, the jet diameter, we must have quite large values for Δ. And it would be somewhat more satisfactory if this jet were not to originate at such a distance below the chromosphere. Hence, as near as we can judge from Table 2, any improvement desired would be one bringing the origin of the jet higher in the solar atmosphere. If we are to keep d large, it is apparent that this aim is to be accomplished only by increasing z_0. And, from equation (26), we can increase z_0 only by taking $h < 1$. But this is the most reasonable direction of change for h; for we expect the temperature of the jet to decrease as it expands, while we know that the temperature of the atmosphere increases with height. Hence, if the initial temperature of jet and

[11] W. O. Roberts, Paper at AAS, Tucson, December, 1949, meeting.

atmosphere were anywhere near the same, we would expect $h < 1$. A previous discussion[7] of this point of comparative conditions in jet and atmosphere indicates that similar conditions are the more likely. Thus, while the observations are not sufficient in number to provide an adequate test of the theory, the foregoing considerations indicate that the jet suggestion is at least in harmony with the existing data.

Such a situation as the foregoing leads, of course, to the hope that at the next eclipse there may be at least six observations of intensity at different heights in the atmosphere. The necessity of such an extended study—probably by Menzel's jumping-film technique—has already been indicated in connection with the state of the undisturbed atmosphere.[10] We should note here that a more complete set of observations would require a more refined interpretation than the present; for it is apparent that the observed density ratios between jet region and the atmospheric region underestimate the fluctuation, because of the limited area along the line of sight occupied by the jet (e.g., we could never observe emission ratio zero, even if there were zero emission from the jet region). Once we have obtained the state of the background atmosphere, however, a correction for this effect is straightforward. Next, if we do have a difference in kinetic temperature between jet and atmosphere, we cannot interpret the difference in emission simply as a density effect but must use some such relation as equation (1). This procedure is, of course, also straightforward.

In summary, we have noted that, for the various types of phenomena involving an emission fluctuation in the solar chromosphere and corona, the essentially complete ionization of hydrogen in the "normal" chromosphere requires the phenomenon to involve a density fluctuation. One possibility for such a density fluctuation is a supersonic jet. We have attempted to provide a quantitative model for such a jet in the astronomical case by extending Prandtl's approximate theory to the case of a jet moving in a gravitational field. A brief application of the theory to the case of the eclipse hot-spot region provides an illustration. An excess in number of parameters (of the jet theory) over number of observations prohibits a complete test of the jet picture for the hot-spot case, but a few plausibility arguments indicate that the interpretation is at least not incompatible with the observations. If such a hot-spot phenomenon occurs at the next eclipse, the proposed program of investigation of the background atmosphere should simultaneously provide an adequate supply of data for a more complete test of the jet model.

I am deeply grateful to Dr. Walter O. Roberts and Dr. John W. Evans, of the High Altitude Observatory, and to Dr. Donald H. Menzel, of the Harvard Observatory, for extended discussions and suggestions over the material and problem treated here.

THEORETICAL COMPUTATIONS OF TRANSITION PROBABILITIES FOR ELECTRONIC SPECTRA OF C_2 AND N_2^+

HARRISON SHULL*
Physics Department, University of Chicago
Received May 4, 1950

ABSTRACT

The oscillator strengths for the transitions $^3\Pi_g \leftrightarrow {}^3\Pi_u$ (Swan bands) and $^1\Pi_g \leftrightarrow {}^1\Pi_u$ of C_2 and $^2\Sigma_u^+ \leftrightarrow {}^2\Sigma_g^+$ first negative bands) of N_2^+ are computed. The transitions are treated as one-electron transitions $x\sigma_g \leftrightarrow y\sigma_u$, in which the MO's are taken as linear combinations of AO's of either the Slater form or the self-consistent field functions fitted by exponentials of the Slater form. The *f*-numbers are computed as a function of the atomic orbital form and as a function of hybridization of $2s$ and $2p\sigma$ orbitals. The oscillator strengths are found to be insensitive to the forms used for the AO's but relatively sensitive to hybridization in the region of low hybridization. The most probable *f*-number for the C_2 Swan bands is considered to be 0.13. This value is considerably higher than those used previously in astronomical calculations.

I. INTRODUCTION

Transition probabilities for the spectra of C_2 and N_2^+ are of considerable interest, especially for astronomical calculations. The C_2 emission bands are well known in cometary spectra, in the sun, and in some of the stars, and the N_2^+ spectra have been found in the auroral discharge, in cometary spectra, and in the light of the night sky.[1] Furthermore, the C_2 Swan band system has been used recently by Brewer, Gilles, and Jenkins[2] as a measure of the partial pressure of C_2 vapor necessary for their determination of the heat of sublimation of carbon. Inasmuch as this work leads indirectly to a value for the *f*-number of this transition and since work is in progress to determine the transition probability for C_2 directly,[3] it was felt that there was unusual interest in detailed theoretical calculations of these values. Finally, it seemed appropriate to consider in detail the use of molecular orbital (MO) theory in the LCAO (linear combination of atomic orbitals) approximation for the calculation of transition probabilities for the type of valence-shell transition of interest here. Previously published work[4] has been largely confined to valence-shell transitions of types $N \rightarrow V$ or $N \rightarrow Q$.[5]

The transitions of interest for this paper are the following: C_2, $^3\Pi_g \leftrightarrow {}^3\Pi_u$ (Swan bands) and $^1\Pi_g \leftrightarrow {}^1\Pi_u$ (Deslandres-D'Azambuja bands), and N_2^+, $^2\Sigma_u^+ \leftrightarrow {}^2\Sigma_g^+$ (first negative bands). We may write, following Mulliken,[6] for the electron configuration of the lower states of the transitions in C_2,

$$(K)\,(K)\,(z\sigma_g)^2(y\sigma_u)^2(w\pi_u)^3(x\sigma_g), \qquad {}^3,{}^1\Pi_u,$$

* National Research Council Post-Doctoral Fellow in the Natural Sciences. Present address: Department of Chemistry, Iowa State College, Ames, Iowa.

[1] E.g., G. Herzberg, *Molecular Spectra and Molecular Structure*, Vol. 1: *Diatomic Molecules* (New York: Prentice-Hall, 1939), pp. 522–531.

[2] *J. Chem. Phys.*, **16**, 797–807, 1948.

[3] Private communication from L. Brewer.

[4] See especially R. S. Mulliken and C. A. Rieke, *Phys. Soc. Rep. Prog. Phys.*, **8**, 231–273, 1941, for a review of methods, previous calculations, and references.

[5] From the MO point of view, *N*, *V* transitions involve the transfer of an electron between corresponding bonding and antibonding orbitals; *N*, *Q* transitions, the transfer between a nonbonding π orbital and a bonding or antibonding σ-type orbital. The valence-shell transitions of interest in this paper approach the *N*, *V* type with increasing hybridization but do not directly fall into this category (see n. 4 for further discussion of *N*, *V* and *N*, Q transitions).

[6] *Rev. Mod. Phys.*, **4**, 1–86, 1932.

and, for the upper states,

$$(K)(K)(z\sigma_g)^2(y\sigma_u)(w\pi_u)^2(x\sigma_g)^2, \qquad {}^3,{}^1\Pi_g .$$

Similar configurations may be written for the lower and upper states of the first negative bands of N_2^+, viz.,

Lower: $(K)(K)(z\sigma_g)^2(y\sigma_u)^2(w\pi_u)^4(x\sigma_g)$, $\quad {}^2\Sigma_g^+$,

Upper: $(K)(K)(z\sigma_g)^2(y\sigma_u)(w\pi_u)^4(x\sigma_g)^2$, $\quad {}^2\Sigma_u^+$.

Similar transitions, involving the transfer of an electron from a $y\sigma$ orbital to an $x\sigma$ orbital have been found in CN, CO^+, and BO and between two excited states of N_2. The calculations of this paper may be carried over directly to the last-mentioned N_2 case, but to these transitions in CN, CO^+, and BO only after taking careful consideration of the effect of polarity upon the MO. It is likely that polarity will be very important for CO^+ and BO, but perhaps may be neglected in the calculations for CN.

The assumption is made that the orbitals not directly involved in the transition are unchanged by the transition. Under these conditions the calculation of transition probabilities is reduced to that for the jump $(y\sigma_u)^2(x\sigma_g) \rightarrow (y\sigma_u)(x\sigma_g)^2$, since the effects of the remaining electrons in the orbital configuration cancel out if their orbitals do not change appreciably. This further reduces to a one-electron problem, since only that one of the two $y\sigma_u$ electrons can jump whose spin is different from that of the one $x\sigma_g$ electron initially present.

Lyddane, Rogers, and Roach[7] published a note on the abundance of molecules in the solar reversing layer in which f-values for C_2 were calculated with the "most reasonable standard wave functions," considering both AO and MO approximations. Unfortunately, they give no details of their calculations, and apparently the f-value reported for C_2 is a figure adjusted through the use of an empirical factor determined from the ratio of calculated to observed f-values for CN. It is not stated to what extent (if any) mixing of $2s$ and $2p\sigma$ atomic functions was considered in obtaining the best form for the $y\sigma$ and $x\sigma$ orbitals for either C_2 or CN, or how the question of polarity in CN was taken into account.

Recently Bates[8] has considered the N_2^+ problem in some detail, using for the nitrogen atom (*a*) Slater-type wave functions and (*b*) a self-consistent field (SCF) wave function, as published tabularly by Brown, Bartlett, and Dunn,[9] fitted by exponentials. These calculations, however, assume no hybridization; but, since it seems very likely (see below) that there is an important degree of hybridization in the orbitals under consideration, this assumption must be examined with care.

II. LCAO FORMS OF THE MOLECULAR ORBITALS

The most convenient type of approximation to the MO for use in the computations is a linear combination of atomic orbitals (LCAO) of the appropriate symmetry. In the absence of hybridization, the electron configuration for the lower state of C_2 may be written

$$(K)(K)(s+s)^2(s-s)^2(p\pi+p\pi)^3(p\sigma+p\sigma), \qquad {}^3,{}^1\Pi_u .$$

Here $(s+s)$ means that the MO is approximated by the (normalized) linear combination of a $2s$ carbon AO on atom a and a corresponding AO, taken with like sign, on atom b. The symbols for the other three orbitals have a similar meaning in terms of $2s$, $2p\pi$, and $2p\sigma$ AO, respectively.[10]

[7] *Phys. Rev.*, **60**, 281, 1941.

[8] *Proc. R. Soc. London, A*, **196**, 562–591, 1949.

[9] *Phys. Rev.*, **44**, 296, 1933.

[10] It should be noted that, throughout this paper, $2p\sigma$ AO on each atom are chosen so that the positive lobe points toward the other atom.

It is almost certain, however, that there is a significant amount of hybridization of $2s$ and $2p\sigma$ AO in the LCAO forms of the MO needed for this calculation. The question of the amount of this hybridization is considered later in this paper. Including a variable amount of hybridization, the LCAO MO in normalized form may be written:

$$\psi_{\sigma_g} = \frac{(-\beta_1 2s_a + \alpha_1 2p\sigma_a) + (-\beta_1 2s_b + \alpha_1 2p\sigma_b)}{\sqrt{2(1+S_g)}},$$

$$\psi_{\sigma_u} = \frac{(\alpha_2 2s_a - \beta_2 2p\sigma_a) - (\alpha_2 2s_b - \beta_2 2p\sigma_b)}{\sqrt{2(1-S_u)}}.$$

The α's and β's (each of which is to be taken as positive) are connected by normalization relations, $\alpha_1^2 + \beta_1^2 = 1$ and $\alpha_2^2 + \beta_2^2 = 1$, so that each hybrid AO of the form $a,2s + b,2p\sigma$ is separately normalized. Because of the nonorthogonality of the orbitals on atoms a and b, respectively, the normalization factors S_g and S_u are required:

$$S_g = \alpha_1^2 \int (2p\sigma)_a (2p\sigma)_b d\tau + \beta_1^2 \int (2s)_a (2s)_b d\tau - 2\alpha_1\beta_1 \int (2s)_a (2p\sigma)_b d\tau,$$

$$S_u = \alpha_2^2 \int (2s)_a (2s)_b d\tau + \beta_2^2 \int (2p\sigma)_a (2p\sigma)_b d\tau - 2\alpha_2\beta_2 \int (2s)_a (2p\sigma)_b d\tau.$$

In these formulae, of course, by $2s$ is meant a normalized atomic $2s$ wave function, and similarly for $2p\sigma$.

In the expressions for ψ_{σ_g} and ψ_{σ_u}, the $2s$ and $2p\sigma$ wave functions on each atom are chosen with opposite sign. In the absence of hybridization ($\beta_2 = 0$), the ψ_{σ_u} MO would become $s - s$. This would be expected to be strongly antibonding because of the large overlap of the two s AO. Further, a mixture of $p\sigma$ with the same or opposite sign to that of s in each AO would respectively increase or decrease the amount of antibonding character. From the known change in internuclear distance r_e when a $y\sigma_u$ electron is removed from N_2(r_e = 1.096 A) to give N_2^+(r_e = 1.07 A), it appears that the $y\sigma_u$ MO is slightly, but only slightly, antibonding. Hence the range of hybridization in which s and $p\sigma$ functions enter with opposite signs was chosen. Similar considerations based on the fact that removal of an $x\sigma_g$ electron from N_2 gives N_2^+ with r_e = 1.117 A, indicating that $x\sigma_g$ is slightly, but only slightly, bonding, again led to the use of hybrid AO with opposite signs for s and $p\sigma$ in the case of $x\sigma_g$. For this paper, calculations were then made for the following ranges:

$$0 \leq \beta_1^2 \leq 0.5, \qquad 1.0 \geq \alpha_1^2 \geq 0.5 \qquad 0 \leq \beta_2^2 \leq 0.5, \qquad 1.0 \geq \alpha_2^2 \geq 0.5.$$

Three distinct approximations were made concerning the form of the s and $p\sigma$ AO to be used in these MO: (1) The usual Slater type of nodeless AO[11, 12] was used with $\mu = Z/n$ = 1.625 for C, and 1.95 for N. Here Z is the Slater effective nuclear charge and n is the principal quantum number, here equal to 2. (2) Slater functions with altered μ were used for C_2, with an increased μ for the bonding $x\sigma_g$ MO and a decreased μ for the antibonding $y\sigma_u$ MO. (3) Use was made of SCF carbon and nitrogen atomic wave functions calculated with exchange by the Hartree-Fock method.[13] The radial functions, given tabularly in the literature, were here fitted by analytic functions of the Slater form. For the $2s$ AO, a sufficiently good fit was obtained by using the Slater $2s$ AO made orthogonal

[11] *Phys. Rev.*, **36**, 57, 1930.

[12] See Mulliken, Rieke, Orloff, and Orloff, *J. Chem. Phys.*, **17**, 1248, 1949. In the present paper, for carbon $2s$ the very slightly different function $-0.244 \times (1s;\ 5.4) + 1.030 \times (2s;\ 1.625)$ was used.

[13] For carbon: Jucys, *Proc. R. Soc. London, A*, **173**, 59, 1939. For nitrogen: Hartree and Hartree, *Proc. R. Soc. London, A*, **193**, 299, 1948.

to the Slater $1s$ AO,[12] but for the $2p\sigma$ AO it was found necessary to use two terms to give a moderately good fit. The analytical fits used were as follows:

For carbon: $\psi_{2p}^{\text{SCF}} = 0.514\chi\,(2p;\,2.00) + 0.556\chi\,(2p;\,1.00)$;

For nitrogen: $\psi_{2p}^{\text{SCF}} = 0.579\chi\,(2p;\,2.58) + 0.502\chi\,(2p;\,1.22)$.

Here $\chi(2p;\,2.00)$ represents a normalized Slater $2p\sigma$ AO with $\mu = Z/n = 2.00$.

III. METHOD OF CALCULATION

Semitheoretical f-numbers[4] have been calculated in this paper, that is to say, with

$$f = \frac{8\pi^2 m c}{3h}\nu D .$$

Here ν is taken as the *observed* frequency of maximum intensity, while D is calculated theoretically from the following equations:

$$D = GQ^2 , \qquad Q = \int \psi_{\sigma_g} z \psi_{\sigma_u} d\tau .$$

For the transitions discussed in this paper, only one electron is free to jump, and hence $G = 1$. The quantity D is, of course, a function of the internuclear distance, and for this parameter the observed r_e for the lower of the two electronic states was used. The origin of z is taken as halfway between the nuclei.

The foregoing calculations have been performed with the electric dipole operator as indicated by the equation for Q. In addition, it would be interesting to see the effect upon the results of using the matrix element of the momentum instead of the dipole moment.[14] Calculations using this alternative method are contemplated for a further publication.

For C_2, $^3\Pi_g \leftrightarrow {}^3\Pi_u$, the parameters[15] used were $r_e = 1.31$ A and $\nu = 19{,}400$ cm^{-1}. The f-number for emission will not differ appreciably from that for absorption calculated here because of the small change in r_e during the transition. The results quoted for C_2 are all for the Swan bands (triplet system). If the intensity of the corresponding singlet transition is desired, the appropriate figure for the triplet system should be multiplied by 1.34, which is the ratio of the frequencies in the two cases. For N_2^+, ν was taken as 25,500 cm^{-1} and $r_e = 1.117$ A.[16]

For computation of the integrals, the usual transformation into spheroidal co-ordinates μ, ν, and ϕ is made. In these co-ordinates the variables are separable, and the problem reduces to a series of standard integrations which are very similar to those occurring in the evaluation of overlap integrals from Slater functions.[17] These are

$$A_n(p) = \int_1^\infty \mu^n e^{-p\mu} d\mu \qquad \text{and} \qquad B_n(pt) = \int_{-1}^{+1} \nu^n e^{-pt\nu} d\nu .$$

The arguments p and pt of these functions are the parameters defined by Mulliken *et al.*[12]

If the hybrid orbitals given above are used, the desired transition integrals are obtained as linear combinations of moment integrals involving simple Slater functions

[14] The author is indebted to Professor S. Chandrasekhar for this suggestion. For applications of this method see, e.g., *Ap. J.*, **102**, 223 and 395, 1945; **108**, 354, 1948.

[15] Phillips, *Ap. J.*, **107**, 389, 1948, and **108**, 434, 1948.

[16] Herzberg, *op. cit.*, p. 490.

[17] Details of these A and B integrals and references to tables and recursion formulas may be found in the paper cited in n. 12.

times a function of certain overlap integrals. In the general case the effective charges for the $(x\sigma_a)$ and $(y\sigma_a)$ orbitals are different. We then obtain, for Q,

$$Q = \frac{1}{\sqrt{(1+S_a)(1-S_a')}}\{ -(\beta_1\alpha_2+\alpha_1\beta_2)\int (2s)_a z\,(2s)_a' d\tau + (\beta_1\beta_2+\alpha_1\alpha_2)\int (2s)_a z\,(2p\sigma)_a' d\tau + \beta_1\alpha_2\int (2s)_a z\,(2s)_b' d\tau + \alpha_1\beta_2\int (2p\sigma)_a z\,(2p\sigma)_b' d\tau - \beta_1\beta_2\int (2s)_a z\,(2p\sigma)_b' d\tau - \alpha_1\alpha_2\int (2p\sigma)_a z\,(2s)_b' d\tau\},$$

where S_a and S_a' are defined as above, but here in the general case with different μ, denoted by the use of a prime. The formulae for the transition moment integrals involving simple Slater functions are tabulated in Table 1 for the case of unequal μ and in Table 2

TABLE 1

TRANSITION MOMENT INTEGRALS FOR SLATER FUNCTIONS OF UNEQUAL CHARGE*

$$\int 2s_a z\,2p\sigma_a' d\tau = -\int 2s_b z\,2p\sigma_b' d\tau = \frac{160}{\sqrt{3}}\frac{(\mu'\mu)^{5/2}}{(\mu+\mu')^6}.$$

$$\int 2s_a z\,2s_a' d\tau = -\int 2s_b z\,2s_b' d\tau = \int 2p\sigma_a z\,2p\sigma_a' d\tau = -\int 2p\sigma_b z\,2p\sigma_b' d\tau = -\frac{16(\mu\mu')^{5/2}R}{(\mu+\mu')^5}.$$

$$\int 2s_a z\,2s_b' d\tau = -\int 2s_b z\,2s_a' d\tau = \frac{(\mu\mu')^{5/2}R^6}{96}(A_5B_1 - 2A_3B_3 + A_1B_5).$$

$$\int 2p\sigma_a z\,2p\sigma_b' d\tau = -\int 2p\sigma_b z\,2p\sigma_a' d\tau = \frac{(\mu\mu')^{5/2}R^6}{32}[A_3(B_1+B_5) - B_3(A_1+A_5)].$$

$$\int 2s_a z\,2p\sigma_b' d\tau = -\int 2s_b z\,2p\sigma_a' d\tau = \frac{(\mu\mu')^{5/2}R^6}{32\sqrt{3}}[B_4(A_3-A_1) + B_2(A_3-A_5) + A_2(B_5-B_3) + A_4(B_1-B_3)].$$

$$\int 2p\sigma_a z\,2s_b' d\tau = -\int 2p\sigma_b z\,2s_a' d\tau = \frac{(\mu\mu')^{5/2}R^6}{32\sqrt{3}}[B_4(A_1-A_3) + B_2(A_5-A_3) + A_2(B_5-B_3) + A_4(B_1-B_3)].$$

* The quantities p and t are defined as in the paper of Mulliken *et al.* (*J. Chem. Phys.*, **17**, 1248, 1949). In the following, the A's are functions of the argument p, and the B's are functions of the argument pt. Atomic units are used throughout. By "$2s_a$" is meant a normalized Slater $2s$ wave function on atom a. R is the internuclear distance.

TABLE 2

TRANSITION MOMENT INTEGRALS FOR SLATER FUNCTIONS OF LIKE CHARGE*

$$\int 2s_a z\,2s_a d\tau = \int 2p\sigma_a z\,2p\sigma_a d\tau = -\int 2s_b z\,2s_b d\tau = -\int 2p\sigma_b z\,2p\sigma_b d\tau = -\frac{R}{2}.$$

$$\int 2s_a z\,2p\sigma_a d\tau = -\int 2s_b z\,2p\sigma_b d\tau = \frac{5}{2\mu\sqrt{3}}.$$

$$\int 2s_a z\,2p\sigma_b d\tau = -\int 2s_b z\,2p\sigma_a d\tau = \frac{Re^{-p}}{60\sqrt{3}}\left[\frac{150}{p} + 150 + 63p + 13p^2 + p^3\right].$$

$$\int 2s_a z\,2s_b d\tau = \int 2p\sigma_a z\,2p\sigma_b d\tau = 0.$$

* See Table 1 for definitions of symbols.

for the case of equal μ. In the latter case and for all integrals involving two functions on the same atom, it was found that the computations were simplified if the A's and B's were written out explicitly. For the remaining cases it was easier to evaluate the A's and B's and use these values in the appropriate formula. Table 3 lists the numerical values of integrals used in this paper.

IV. RESULTS OF CALCULATIONS

The results of the computations may be most easily expressed graphically. The f-number as ordinate is plotted against the degree of hybridization β_1^2 of the $x\sigma_g$ orbital as abscissa, where the hybrid AO on each atom is represented by $(-\beta_1 2s + \alpha_1 2p)$. In view of the fact that the internuclear distance for the ground state of N_2, 1.096 A, changes to 1.117 A in N_2^+ upon ionization of the $x\sigma_g$ electron, and to 1.07 A in N_2^+ upon ionization of the $y\sigma_u$ electron, the assumption was made that the degree of hybridization is about the same in the two orbitals, that is to say, that there is about as much s character in the $x\sigma_g$ orbital as there is p character in the $y\sigma_u$.

In Figure 1 three curves have been drawn. The top curve represents the locus of points where the degree of hybridization, in terms of the coefficient squared, is 0.1 greater in the $y\sigma_u$ than in the $x\sigma_g$ orbital. The middle curve is for equal hybridization ratios, and the lower curve represents the case of 0.1 more hybridization in the $x\sigma_g$ orbital than in the $y\sigma_u$

To save space, only the graphs for C_2 are presented, since those for N_2^+ (partly by chance, partly because of the very similar MO's involved in the transition) are almost identical. Table 4 lists results of computations for some particular points permitting a comparison between C_2 and N_2^+. Figure 1 shows the curves, using Slater functions, of f-numbers versus degree of hybridization. Curves for the SCF function are almost identical with these (see Table 4). Figure 2 presents the results for the case of altered effective Q.

V. DISCUSSION

Experimentally, absolute f-numbers are difficult to determine accurately, especially for molecules unstable under ordinary conditions. In general, one may reasonably set a factor of 2 as the likely degree of uncertainty in an experimental determination for such a molecule. Under these conditions, it is quite possible that the theoretical determination of f-numbers may be as good as, or better than, the experimental determination, provided, of course, that the theoretically computed f-values are not unusually sensitive to the approximations made.

The smallness of the differences obtained above between the computed f-numbers for all hybrid ratios is encouraging with respect to the effect of hybridization. This, however, does not test the approximation involved in the use of LCAO forms. Previous computations by Mulliken and Rieke[4] for $N \rightarrow V$ transitions showed a tendency for semi-theoretical LCAO f-values based on ordinary Z-values to be two- or threefold too large, when compared with available experimental results. Mulliken and Rieke found, however, that the discrepancy could be eliminated in the case of, for example, the N, V transition of H_2, by altering the Slater Z upward for the bonding orbital and downward for the antibonding orbital. A similar modification was tried here in the case of C_2, and the results are presented in Figure 2. In this case the change in effective Z was made proportionately as large as was found necessary for H_2. The curves are seen to diverge somewhat in the region of high hybridization but are almost identical in the region of zero hybridization. It is obvious, however, that there has been only a very small change in the f-number as a result of this alteration—certainly, far from the factor of about 3 found by Mulliken and Rieke for N, V transitions. One may therefore hope from this result that the calculated f-numbers in the type of transition discussed here are relatively insensitive, for a given degree of hybridization, to the various approximations (use of LCAO, MO, and forms of AO), and therefore may be accepted as being close to the correct values.

TABLE 3

VALUES OF TRANSITION MOMENT INTEGRALS USED IN THIS PAPER (IN ATOMIC UNITS)

	FOR SLATER FUNCTIONS FOR $n=2$						FOR SCF FUNCTION FOR C				FOR SCF FUNCTION FOR N			
$R/2$	+1.24	+1.24	+1.24	+1.24	+1.25	+1.06	+1.24	+1.24	+1.24	+1.24	+1.06	+1.06	+1.06	+1.06
μ	+1.625	+1.66	+1.95	+1.95	+1.95	+1.95	+2.00(2p)	+1.625(2s)	+5.4(1s)	+5.4(1s)	+2.58(2p)	+1.95(2s)	+6.7(1s)	+6.7(1s)
μ'	+1.625	+1.66	+1.95	+1.625	+1.30	+1.95	+1.625(2s)	+1.00(2p)	+1.00(2p)	+2.00(2p)	+1.95(2s)	+1.22(2p)	+1.22(2p)	+2.58(2p)
p	+4.04	+4.12	+4.84	+4.44	+4.04	+4.12	+4.50	+3.26	+7.95	+9.19	+4.78	+3.35	+8.36	+9.80
$p\mu$	0	0	0	+0.403	+0.807	0	+0.465	+0.776	+5.46	+4.22	+0.665	+0.771	+5.79	+4.35
$\int 2s_a z\, 2s'_a d\tau$	−1.24	−1.24	−1.24	−1.22	−1.12	−1.06								
$\int ns_a z\, 2p\sigma'_a d\tau$	+0.888	+0.876	+0.740	+0.791	+0.802	+0.745	+0.775	+0.950	+0.0374	+0.102	+0.607	+0.794	+0.0293	+0.0862
$\int 2s_a z\, 2s'_b d\tau$	0	0	0	−0.072	−0.177	0								
$\int 2p\sigma_a z\, 2p\sigma'_b d\tau$	0	0	0	+0.032	+0.112	0								
$\int ns_a z\, 2p\sigma'_b d\tau$	−0.304	−0.286	−0.171	−0.281	−0.433	−0.243		−0.672	−0.148	−0.0675		−0.534	−0.118	−0.0420
$\int 2p\sigma_a z\, ns'_b d\tau$	+0.304	+0.286	+0.171	+0.186	+0.221	+0.243	+0.172				+0.106			

The major remaining uncertainty lies in the precise amount of hybridization actually present in the $x\sigma_g$ and $y\sigma_u$ orbitals. From Figures 1 and 2 it is evident that the *f*-number resulting from the present computations is strongly dependent upon the degree of hybridization only in the region of low hybridization. If there is *any considerable amount* of hybridization—as is fairly certain—the value is definite to within perhaps 25 per cent.

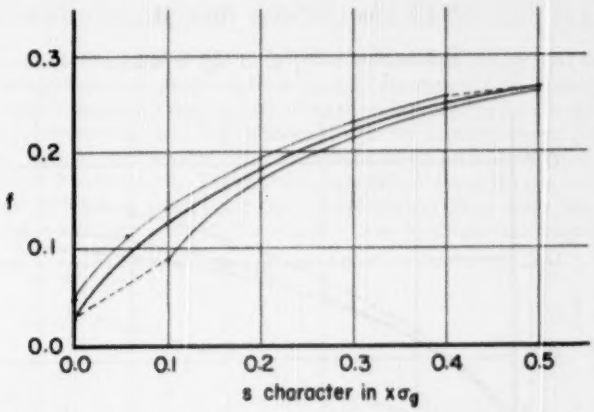

FIG. 1.—Calculated *f*-number for C_2, $^3\Pi_g \rightarrow {}^3\Pi_u$ plotted against degree of hybridization of the $x\sigma_g$ orbital (amount of *s* character in the $x\sigma_g$ orbital). The three curves from top to bottom are, respectively, for the cases in which the degree of hybridization of the $y\sigma_u$ is 0.1 greater than, is equal to, and is 0.1 less than that of the $x\sigma_g$ orbital.

TABLE 4

f-NUMBERS FOR C_2, $^3\Pi_u \rightarrow {}^3\Pi_g$ AND N_2^+, $^2\Sigma_g^+ \rightarrow {}^2\Sigma_u^+$ TRANSITIONS AS A FUNCTION OF HYBRIDIZATIONS AND THE NATURE OF THE LCAO WAVE FUNCTION

Hybridization:[a]				
Per cent $2p$ in $y\sigma_u$	0	17	30	50
Per cent $2s$ in $x\sigma_g$	0	8	30	50
Wave-function approximation:				
C_2 ($Z=3.25$)	0.028	0.13	0.22	0.27
C_2 ($Z_{\sigma_g}=3.90$, $Z_{\sigma_u}=3.25$)	.030	.12	.20	.24
C_2 ($Z_{\sigma_g}=3.90$, $Z_{\sigma_u}=2.60$)	.037	.12	.19	.22
C_2 (SCF)	.021	.13	.24	.29
N_2^+ ($Z=3.90$)	.026	.12	.21	.25
N_2^+ (SCF)	0.025	0.13	0.23	0.27

[a] "Per cent hybridization" means $100\beta_1^2$ for $x\sigma_g$, $100\beta^2$ for $y\sigma_u$.

Professor R. S. Mulliken has considered this problem in some detail in connection with other work, and, by minimizing the energy in a semiempirical manner, he arrives at the following preliminary estimated hybridizations for N_2^+:[18] for $z\sigma_g$: 100 per cent *s* (very close); for $y\sigma_u$: 17 per cent *p*; for $x\sigma_g$: 8 per cent *s*. These percentages are expressed in terms of squares of coefficients. The values found for C_2 are essentially the same.

[18] Further details of these calculations will be published elsewhere. The author is indebted to Professor Mulliken for furnishing these data prior to publication.

Using these hybridization values, "best" values may be obtained for the f-numbers by interpolation between the curves given in the figures. The f-numbers for the pertinent hybridizations are included in Table 4 for the different approximate wave functions. We may consider as "best" semitheoretical values the following:

0.13 for C_2: $^3\Pi_g \leftarrow {}^3\Pi_u$,

0.17 for C_2: $^1\Pi_g \leftarrow {}^1\Pi_u$,

0.12 for N_2^+: $^2\Sigma_u^+ \leftarrow {}^2\Sigma_g^+$.

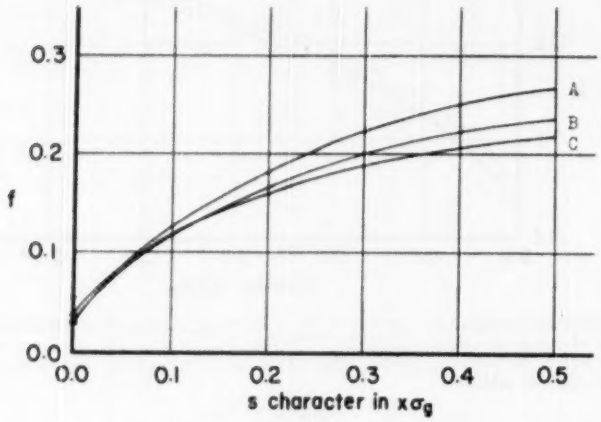

FIG. 2.—f-number for C_2, $^3\Pi_g \rightarrow {}^3\Pi_u$ as a function of effective Z and degree of hybridization. All three curves are for equal hybridization in $x\sigma_g$ and $y\sigma_u$. Curve A is for $Z_{\sigma_g} = Z_{\sigma_u} = 3.25$; B for $Z_{\sigma_g} = 3.90$, $Z_{\sigma_u} = 3.25$; C for $Z_{\sigma_g} = 3.90$, $Z_{\sigma_u} = 2.60$.

Experimentally, only the values of White[19] for the $^2\Sigma \rightarrow {}^2\Sigma$ transition of CN, analogous to that here considered for N_2^+, may be compared with this value. White found about 0.1 as the most probable value, with 0.026 as a lower limit and 1 as an upper limit. If one assumes polarity to have little effect in this case because of the similarity of C and N, there is very good agreement between experiment and the present theoretical results.

It should be pointed out that the present values are somewhat higher than have previously been assumed in astronomical calculations, and consequently the concentrations of these diatomic molecules are proportionately lower.

The author is greatly indebted to Professor R. S. Mulliken, who suggested this problem and without whose continued helpful guidance the computations could not have reached the present form. The author also thanks the National Research Council for a fellowship making this study possible.

[19] *J. Chem. Phys.*, **8**, 79, 459, 1940.

NOTES

THE BALMER SERIES AND THE PARALLAX OF THE PLEIADES

The number of visible lines of the Balmer series has been recognized as a practical criterion for the spectroscopic determination of absolute magnitudes of early-type stars. Struve and Unsöld[1] presented a diagram showing the relation between the quantum number of the last hydrogen line and the luminosity for the spectral range O5–A3. Linear formulae of the criterion for four spectral intervals between B0 and A8 were given by the author[2] and for F0–F5 stars by U. Becker.[3] In using field stars of B type for standardization, well-known difficulties arise; since the luminosities of these stars are often rather doubtful, the scope and zero point of the relations may be somewhat uncertain. Moving

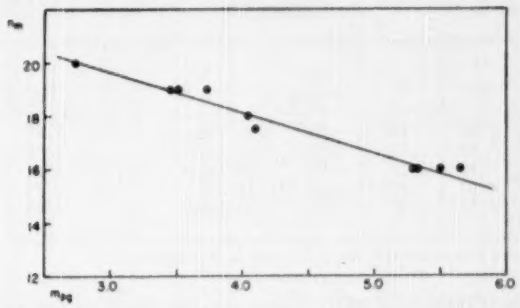

FIG. 1.—Relation between quantum number n_m of last visible Balmer line and apparent photographic magnitude of the Pleiades.

and open clusters containing enough early-type stars may be preferred for the standardization, though the possibility must be considered that the Balmer series operates in a different way from cluster to cluster. Different behavior in this respect is not totally excluded, since total absorption, central depth, and line width differ between B stars belonging to separated groups in the sky.

Among the Pleiades there are enough apparently bright stars in the range of our optical equipment to discuss the relation between the quantum number n_m of the last line of the Balmer series and the luminosity of late B stars. The spectrograms were taken with the UV spectrograph attached to the 72-cm reflector of the Heidelberg Observatory, giving a dispersion of about 51 A/mm at $H\gamma$ and 29 A/mm at λ 3700. The setting of the spectrograph, especially the slit-width, was the same for all exposures on Perutz-Persenso plates.

28 Tauri (Pleione) has been omitted from the discussion, since its photospheric Balmer series is overlain by a sharp series produced by a shell (see Table 1).

[1] *Ap. J.*, **91**, 365, 1940.

[2] *Zs. f. Ap.*, **25**, 72, 1948 (*Mitt. Sternw. Heidelberg*, No. 54); *Zs. f. Ap.*, **25**, 268, 1948 (*Mitt. Sternw. Heidelberg*, No. 61).

[3] *Zs. f. Ap.*, **26**, 7, 1949 (*Mitt. Sternw. Heidelberg*, No. 68).

The apparent magnitudes m_{pg} and the spectral types were taken from Binnendijk's[4] paper; the spectral types have been determined by Morgan. A least-squares solution gave

$$m_{pg} = -0^m.65\,(n_m - 10) + 9^m.27\,. \quad (1)$$

For B4–B9 stars distributed over nearly the whole northern sky,

$$M_v = -0^m.64\,(n_m - 10) + 4^m.28 \quad (2)$$

has been found.[2] The scope of both curves is the same, the difference $m - M = +5^m.10$ (corrected with the mean color index $-0^m.11$ of the 10 stars) allows us either to correct the zero point of equation (2) or to find a spectroscopic parallax of the Pleiades. Taken as a distance modulus, it yields $\pi = 0''.010$. Binnendijk has found from a discussion of all available parallax determinations (trigonometric, dynamical, proper-motion, dark-material, spectrum-magnitude) that $\pi = 0''.010 \pm 0''.003$, and Gratton,[5] from a similar discussion, adopted $\pi = 0''.0098 \pm 0''.0007$. These are the same values as result from our $m - M$. The good agreement is considered as a confirmation of the zero point of equation (2).

TABLE 1

Star	m_{pg}	Sp.	Last *H* Line	Star	m_{pg}	Sp.	Last *H* Line
16 Tauri	5.33	B8	*H*16	21 Tauri	5.65	B8	*H*16
17 Tauri	3.52	B6	*H*19	23 Tauri	4.04	B6	*H*18
18 Tauri	5.50	B8	*H*16	25 Tauri	2.74	B7	*H*20
19 Tauri	4.10	B6	*H*17.5*	He 722	5.29	B8	*H*16
20 Tauri	3.73	B7	*H*19	27 Tauri	3.46	B8	*H*19

* Since the existence of *H*18 is doubtful, *H*17.5 was used in the calculation.

The influence of line broadening by rotation on the quantum number of the last line has been neglected. Formerly, no certain influence could be discovered.[2] It seems to be certain that stellar rotation of about 100 or 200 km/sec results in a reduction of the quantum number of considerably less than 1 for stars with not extraordinarily high last-line numbers.

G. R. Miczaika

Heidelberg Observatory
April 14, 1950

REVISED STANDARDS FOR SUPERGIANTS ON THE SYSTEM OF THE YERKES SPECTRAL ATLAS

In order to define with precision an empirical system such as the Yerkes spectral classification,[1] it is necessary to give types for a considerable number of stars; in fact, the accuracy of such a system can be said to depend on the number of standards available.

[4] *Ann. Sterrew. Leiden*, **19**, 2, 1946.

[5] *Zs. f. Ap.*, **15**, 46, 1938.

[1] W. W. Morgan, P. C. Keenan, and Edith Kellman, *An Atlas of Stellar Spectra* (Chicago: University of Chicago Press, 1943).

TABLE 1

STANDARD STARS

Star	α (1900)	δ (1900)	Sp.	m_{vis}	Star	α (1900)	δ (1900)	Sp.	m_{vis}
195592	20h 27m 2	+43° 59′	O9 I	7.15	13 Mon	6h 27m 5	+ 7° 24′	A0 Ib	4.50
218915	23 6.7	+52 31	O9 I	7.06	η Leo	10 1.9	+17 15	A0 Ib	3.58
ι Ori	5 30.5	− 5 59	O9 III	2.87	HR 618	2 1.7	+57 57	A1 Ia	5.90
α Cam	4 44.1	+66 10	O9.5 Ia	4.38	14433	2 14.8	+56 47	A1 Ia	6.54
ζ Ori	5 35.7	− 2 0	O9.5 Ib	2.05	16778	2 36.3	+59 24	A2 Ia	7.71
19 Cep	22 2.1	+61 48	O9.5 Ib	5.17	HR 7573	19 47.8	+24 44	A2 Ia	5.67
47432	6 33.5	+ 1 42	O9.5 III	6.13	α Cyg	20 38.0	+44 55	A2 Ia	1.33
ε Ori	5 31.1	− 1 16	B0 Ia	1.75	ν Cep	21 42.6	+60 40	A2 Ia	4.46
15 Sgr	18 9.3	−20 45	B0 Ia	5.42	9 Per	2 15.4	+55 23	A2 Ib	5.22
194839	20 22.8	+41 3	B0 Ia	7.45	HR 8345	21 45.6	+40 41	A2 Ib	6.49
205196	21 28.6	+57 4	B0 Ib	7.36	213470-1	22 26.5	+56 43	A3 Ia	6.73
48434	6 38.3	+ 4 2	B0 III	5.78	HR 641	2 6.6	+58 6	A3 Ib	6.50
κ Ori	5 43.0	− 9 42	B0.5 Ia	2.20	HR 8443	22 3.7	+52 49	A3 Ib	6.50
6675	1 2.4	+69 10	B0.5 Ib	7.1	HR 825	2 42.1	+56 40	A5 Ia	6.53
187459	19 45.0	+33 12	B0.5 Ib	6.35	164514	17 56.4	−22 54	A5 Ia	7.28
κ Aql	19 31.5	− 7 15	B0.5 III	5.04	HR 2874	7 25.6	−22 49	A5 Ib	4.80
κ Cas	0 27.3	+62 23	B1 Ia	4.24	19 Aur	5 13.4	+33 51	A5 II	5.16
216411	22 47.6	+58 28	B1 Ia	7.16	φ Cas	1 13.8	+57 42	F0 Ia	5.25
ζ Per	3 47.8	+31 35	B1 Ib	2.91	α Lep	5 28.3	−17 54	F0 Ib	2.69
ρ Leo	10 27.5	+ 9 49	B1 Ib	3.85	ι¹ Sco	17 40.6	−40 5	F2 Ia	3.14
ο Per	3 38.0	+31 58	B1 III	3.94	89 Her	17 51.4	+26 4	F2 Ia	5.48
10 Per	2 18.2	+56 9	B2 Ia	6.24	ν Aql	19 21.4	+ 0 8	F2 Ib	4.86
χ² Ori	5 58.0	+20 8	B2 Ia	4.71	HR 7055	18 41.2	−10 14	F2 Ib–II	5.81
9 Cep	21 35.2	+61 38	B2 Ib	4.87	22 And	0 5.1	+45 31	F2 II	5.08
ε CMa	6 54.7	−28 50	B2 II	1.63	ν Her	17 54.7	+30 12	F2 II	4.48
14134	2 12.1	+56 40	B3 Ia	6.66	44 Cyg	20 27.2	+36 36	F5 Ia	6.30
σ² CMa	6 58.8	−23 41	B3 Ia	3.12	α Per	3 17.2	+49 30	F5 Ib	1.90
55 Cyg	20 45.5	+45 45	B3 Ia	4.89	35 Cyg	20 14.8	+34 40	F5 Ib	5.18
χ Aur	5 26.2	+32 7	B3 Ib	4.88	ν Per	3 38.4	+42 16	F5 II	3.93
9 Gem	6 10.9	+23 46	B3 Ib	6.26	41 Cyg	20 25.3	+30 2	F5 II	4.09
ι CMa	6 51.7	−16 55	B3 II	4.39	HR 690	2 16.9	+54 55	F7 Ib	6.46
5 Per	2 4.5	+57 10	B5 Ia	6.36	45 Dra	18 30.9	+56 58	F7 Ib	4.95
η CMa	7 20.1	−29 6	B5 Ia	2.43	δ CMa	7 4.3	−26 14	F8 Ia	1.98
167838	18 11.9	−15 28	B5 Ia	6.64	γ Cyg	20 18.6	+39 56	F8 Ib	2.32
67 Oph	17 55.6	+ 2 56	B5 Ib	3.92	HR 2974	7 37.0	−31 26	G0 Ia	6.64
15497	2 24.6	+57 15	B6 Ia	7.20	HR 8752	22 55.9	+56 25	G0 Ia	5.48
183143	19 23.0	+18 5	B7 Ia	6.93	HR 207	0 40.9	+59 2	G0 Ib	6.49
14322	2 13.8	+55 27	B8 Ia	6.84	μ Per	4 7.6	+48 9	G0 Ib	4.28
14542	2 15.9	+56 56	B8 Ia	6.95	β Cam	4 54.5	+60 18	G0 Ib	4.22
β Ori	5 9.7	− 8 19	B8 Ia	0.34	β Aqr	21 26.3	− 6 1	G0 Ib	3.07
53 Cas	1 55.6	+63 54	B8 Ib	5.62	ε Leo	9 40.2	+24 14	G0 II	3.12
13 Cep	21 51.5	+56 8	B8 Ib	6.01	83 Vir	13 39.1	−15 41	G0 II	5.71
HR 1035	3 21.0	+59 36	B9 Ia	4.42	α Sge	19 35.6	+17 47	G0 II	4.37
σ Cyg	21 13.5	+38 59	B9 Ia	4.28	104 Aqr	23 36.6	−18 22	G0 II	4.95
4 Lac	22 20.5	+48 58	B9 Iab	4.64	ζ Mon	8 3.6	− 2 42	G2 Ib	4.41
HR 1804	5 20.7	+30 7	B9 Ib	5.72	HR 3459	8 38.8	− 6 52	G2 Ib	4.70
172324	18 34.5	+37 21	B9 Ib	8.0	22 Vul	20 11.2	+23 12	G2 Ib	5.38
43836	6 13.3	+23 19	B9 II	7.03	α Aqr	22 0.7	− 0 48	G2 Ib	3.19
HR 964	3 8.1	+56 46	A0 Ia	5.92	ξ Pup	7 45.1	−24 37	G3 Ib	3.47
HR 1040	3 21.9	+58 32	A0 Ia	4.76	α¹ Cap	20 12.1	−12 49	G3 Ib	4.55

TABLE 1—*Continued*

Star	α (1900)	δ (1900)	Sp	m_{vis}	Star	α (1900)	δ (1900)	Sp	m_{vis}
HR 8692	22h45m9	+50° 9′	G4 Ib	6.43	π^6 Ori	4h53m4	+ 1° 34′	K2 II	4.73
25 Gem	6 35 0	+28 17	G5 Ib	6.54	56 Ori	5 47 2	+ 1 50	K2 II	5.01
9 Peg	21 39 8	+16 53	G5 Ib	4.52	σ^1 CMa	6 50 0	− 24 4	K3 Iab	4.12
ω Gem	6 56 3	+24 21	G5 II	5.21	η Per	2 43 4	+55 29	K3 Ib	3.93
β Sct	18 41 9	− 4 51	G5 II	4.47	ι Aur	4 50 5	+33 0	K3 II	2.90
AX Sgr	18 2 6	−18 34	G8 Ia	8.0–9.0*	π Her	17 11 6	+36 55	K3 II	3.36
RW Cep	22 19 4	+55 28	G8 Ia	6.8–7.5	γ Aql	19 41 5	+10 22	K3 II	2.80
ϵ Gem	6 37 8	+25 14	G8 Ib	3.18	ψ^1 Aur	6 17 2	+49 20	K5 Iab	5.10
56 UMa	11 17 3	+44 2	G8 II	5.06	ξ Cyg	21 1 3	+43 32	K5 Ib	3.92
ζ Cyg	21 8 7	+29 49	G8 II	3.40	HR 8726	22 52 1	+49 12	K5 Ib	5.10
θ Lyr	19 12 9	+37 57	K0 II	4.46	6 Gem†	6 6 3	+22 56	M1 Ia	6.30
ζ Cep	22 7 4	+57 42	K1 Ib	3.62	μ Cep†	21 40 4	+58 19	M2 Ia	4.0–4.8
HR 2334	6 22 1	+ 0 22	K1 II	5.29	α Ori†	5 49 8	+ 7 23	M2 Iab	0.1–1.2
θ Her	17 52 8	+37 16	K1 II	3.99	119 Tau†	5 26 3	+18 31	M2 Ib	4.73
ϵ Peg	21 39 3	+ 9 25	K2 Ib	2.54					

* Photographic magnitude.

† Spectral types of the M supergiants may vary slightly.

In this respect the Yerkes spectral atlas leaves something to be desired, since at certain seasons of the year it is not always possible to find suitable standards. In addition, there has been a gain in accuracy effected during the last seven years; in the case of the supergiants especially, the number of significant subdivisions recognizable has increased considerably; for example, the B stars of luminosity class I can now be separated with ease into groups of higher and lower luminosity.

The revised standards are listed in Table 1. Numbers without prefixes are from the *Henry Draper Catalogue*. The description of the luminosity classes is similar to that given in the spectral atlas.

The only star for which a considerable change in type has been made is RW Cep. The type is uncertain because of the extreme range in excitation of the lines present. We have placed it and the similar spectrum of AX Sgr at G8 Ia; there are certain criteria which suggest a type of K rather than G, and Dr. Philip Keenan is of the opinion that class K is to be preferred; the star is definitely not of class M, as given in the spectral atlas.

Omissions from the present list include ϵ Aur, ρ Cas, and ζ Cap, all of which have been omitted because of spectral peculiarities, and α Sco, whose spectrum can be seriously affected by its blue companion in the region of H and K.

We are greatly indebted to Dr. W. P. Bidelman for placing a number of excellent spectrograms at our disposal and for allowing us to include in the table several stars now being discussed by him. We have also had the advantage of a number of discussions with Dr. Keenan.

W. W. Morgan
Nancy G. Roman

Yerkes Observatory
July 2, 1950